

Development of Ruthenium-based Heterogeneous Catalysts for Hydrogen Production from Polyols

Ph.D. Thesis

by

Ankit Kumar

(Roll No. 1801231003)



DEPARTMENT OF CHEMISTRY

INDIAN INSTITUTE OF TECHNOLOGY INDORE

November 2023

Development of Ruthenium-based Heterogeneous Catalysts for Hydrogen Production from Polyols

A THESIS

*Submitted in partial fulfilment of the
requirements for the award of the degree*

of

DOCTOR OF PHILOSOPHY

by

Ankit Kumar



DEPARTMENT OF CHEMISTRY

INDIAN INSTITUTE OF TECHNOLOGY INDORE

November 2023



INDIAN INSTITUTE OF TECHNOLOGY INDORE

CANDIDATE'S DECLARATION

I hereby certify that the work which is being presented in the thesis entitled “**Development of Ruthenium-based Heterogeneous Catalysts for Hydrogen Production from Polyols**” in the partial fulfilment of the requirements for the award of the degree of **DOCTOR OF PHILOSOPHY** and submitted in the **DEPARTMENT OF CHEMISTRY, Indian Institute of Technology Indore**, is an authentic record of my own work carried out during the time period from December 2018 to November 2023 under the supervision of Dr. Sanjay Kumar Singh, Professor, Department of Chemistry, IIT Indore.

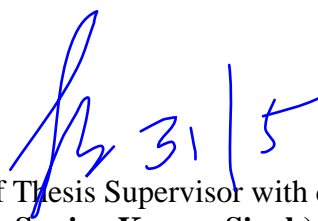
The matter presented in this thesis has not been submitted by me for the award of any other degree of this or any other institute.

Signature of the student with date
(ANKIT KUMAR)

This is to certify that the above statement made by the candidate is correct to the best of my knowledge.


Signature of Thesis Supervisor with date
(Dr. Sanjay Kumar Singh)

Ankit Kumar has successfully given his Ph.D. Oral Examination was held on May 31, 2024.


Signature of Thesis Supervisor with date
(Dr. Sanjay Kumar Singh)

Acknowledgements

Positive developments in our lives are often the result of our own hard work and dedication, but they are also greatly influenced by the assistance, motivation, guidance, support, and love we receive from various individuals at different points along our journey. I want to seize this moment to express my gratitude to all those who have played pivotal roles in helping me reach my goals.

First and foremost, I would like to express my sincere gratitude to my respected **Ph.D. thesis supervisor, Prof. Sanjay Kumar Singh**, who gave me the opportunity to join his research group at the Department of Chemistry, Indian Institute of Technology (IIT) Indore, in December 2018. I will always be grateful to him for his enormous help, support, guidance, insightful scientific discussions, critical comments, and suggestions throughout my doctoral studies, which helped me to improve my skills at different levels. His extensive knowledge, scientific mindset, innovative ideas, ethical principles, and exceptional management abilities have consistently served as a source of inspiration for me. Thanks to his mentorship, I have been able to develop into the researcher I am today. His advice and constant encouragement were of immense help in enabling me to take up challenging tasks. I am thankful to him for his precious time and suggestions for my thesis corrections. Without his generous support and constant motivation, bringing this thesis work towards completion would have been impossible. He is an ideal supervisor and a complete human being, and I could not have imagined a better mentor for my doctoral study.

I am thankful to my PSPC members, **Prof. Rajesh Kumar and Dr. Amrendra Kumar Singh**, for their insightful and valuable suggestions at every comprehensive research progress seminar. I am thankful to **Convenor DPGC, Department of Chemistry**, for his help during my doctoral study. I would like to acknowledge the **Head, Department of Chemistry IIT Indore**, for providing infrastructure and lab facilities. I would like to thank the **DST-FIST 500 MHz NMR facility of the Department of Chemistry, IIT Indore**.

I would like to express my deep sense of gratitude to **Prof. Suhas S. Joshi (Director, IIT Indore)**, **Prof. Neelesh Kumar Jain (Former Officiating Director, IIT Indore)** and **Prof. Pradeep Mathur (Former Director, IIT Indore)** for providing me with the opportunity to be a part of one of the most premiere institute of India. I am grateful to them for providing all the support and best research facilities at IIT Indore.

I would also like to thank all faculty members, **Prof. Rajneesh Misra, Prof. Suman Mukhopadhyay, Prof. Apurba K. Das, Prof. Sampak Samanta, Prof. Biswarup Pathak, Dr. Tridib K. Sarma, Prof. Anjan Chakraborty, Prof. Tushar Kanti Mukherjee, Prof. Shaikh M. Mobin, Dr. Satya S. Bulusu, Dr. C. Venkatesh, Dr. Debayan Sarkar, Dr. Abhinav Raghuvanshi, Dr. Selvakumar Sermadurai, Dr. Umesh A. Kshirsagar, Dr. Dipak Kumar Roy, and Dr. Pravarthana Dhanpal** for their guidance and help during various activities in the Department of Chemistry, IIT Indore.

I am grateful to my institute, **IIT Indore**, for providing the best infrastructure and **SIC facilities**. I am also thankful to the **Council of Scientific & Industrial Research (CSIR)**, the **Government of India**, for providing research scholarships (**JRF and SRF grants**) for my doctoral studies.

I wish to thank the technical staff from Sophisticated Instrumentation Center (SIC), IIT Indore, Mr. Kinny Pandey, Mr. Ghanshyam Bhavsar, Mr. Nitin Upadhyay, Mr. Atul Singh, Mr. Ravinder, Mrs. Mitali Dave, Ms. Kajal Chaudhari, and Mr. Ranjeet Raghuvanshi for their timely technical support without which it would never have been possible to complete my work. I am also thankful to Mr. Rahul Srivas for his timely help. I would like to acknowledge Mr. Manish Kushwaha for all his help throughout the five years. I am thankful to Mrs. Vinita Kothari, Mr. Rameshwar Dohare, Mr. Parthiban, Mr. Mayur Dhake, Mr. Shubham Verma, Mr. Shailesh, Mr. Jugal Kishore, Mr. Lokesh, Mr. Lalit, Mr. Dayaram, Mr. Manoj, Mr. Pinkesh, Mr. Aditya, Mr. Santosh, Mr. Ram and other technical and non-technical staff for all their help during my stay at IIT Indore.

I am very much thankful to my former labmates cum seniors Dr. Rohit Kumar Rai, Dr. Ambikesh Dhar Dwivedi, Dr. Hemanta Deka, Dr. Chinky Binnani, Dr. Dharmendra Kumar Panchariya, Dr. Debashis Panda, Dr. Mahendra Kumar Awasthi, Dr. Soumyadip Patra, and Vinod Kumar Sahu, from whom I have learnt a lot and received enormous support and guidance. Coming to my present labmates, I would like to express my deep gratitude to Ms. Bhanu Priya for her unwavering support and encouragement during the challenging years of my Ph.D. Our friendship has been a constant source of inspiration, motivation, and solace. In times of doubt and stress, her presence provided much-needed respite, reminding me that life exists beyond academia. She was always there to listen, to offer a kind word, or simply to share a laugh, making the arduous research process more enjoyable. Her belief in me and my abilities bolstered my confidence, and I am immensely thankful for her enduring friendship. I extend my acknowledgement to all my other lab mates Mr. Rahul Raman Chaudhari, Mr. Sanjeev Kushwaha, Mr. Tushar Kharde, Ms. Jayashree Parthiban, Mr. Khanindra Kalita, Ms. Vaishnavi Kulkarni, and Ms. Poojarani Sahu for their help and pleasant company. I also wish to acknowledge present and past M.Sc. students and interns from our group: Mr. Nazmul, Ms. Vanitha, Ms. Nivedha, Ms. Chanchal, Ms. Nirupama Sheet, Mr. Pranav Pathak, Ms. Ankita Mondal, Mr. Manoj Joshi, Ms. Shubh Jhavar, Mr. Pranjal Gupta, and Ms. Sneha Rathwa with whom I spent a pleasant time.

I would like to sincerely thank all my seniors, juniors, and friends at IIT Indore, Dr. Indresh Singh Yadav, Dr. Faizal Khan, Dr. Radhe Shyam Ji, Dr. Shobhan Chatterjee, Dr. Kuldeep Gogoi, Dr. Kuber Rawat, Dr. Pramod Gavel, Dr. Siddhartha, Dr. Rohit Jadhav, Dr. Amit Pandit, Dr. Soumya Kanti De, Dr. Devraj Singh, Dr. Pravin Kumar, Dr. Anupam Kumar, Dr. Vivek Rana, Dr. Prashant Mishra, Dr. Bhawna, Dr. Reena, Dr. Meenal, Mr. Shambhu Nath, Mr. Navdeep, Mr. Rahul Kumar Singh, Mr. Shanmugam, Mr. Abhishek Ojha, Mr. Shivendra Singh, Mr. Rahul Yadav, Mr. Dilip Pandey, Mr. Bhanuprakash, Mr. Rajesh, Mr. Abhinay Chillal, Mr. Devashish Chorey, Mr. Sarathkumar, Mr. Vishal Jagdale, Mr. Rajnish, Mr. Arpit, Mr. Rajendra Goud, Mr. Brahmaddutt, Mr. Vikas, Mr. Kailash, Mr. Omkar, Mr. Manish, and Mr. Nitin Rajesh for their company and help.

I would like to express my gratitude to all my teachers who have taught me and guided me in my life, starting from my school days.

*I would like to sincerely thank the most amazing people in my life, **my family!** Words cannot express my gratitude towards my respected father, **Mr. Ramkhilavan Chaurasia**, and my loving mother, **Mrs. Guddi Chaurasia**, for all their sacrifice in bringing me up. Their faith and affection for me and support in all forms encouraged me to achieve this success, which would make them feel proud. I would like to thank my beloved sisters, **Mrs. Shalini Chaurasia and Mrs. Sonali Chaurasia**, for all our beautiful memories since childhood. My special thanks go to my all-loving brothers, especially **Mr. Manoj Chaurasia**, for their constant help, love, and support. I am also thankful to all my other family members and friends for supporting me at every stage of my life and in my dreams.*

I am filled with gratitude towards the divine for consistently bringing incredible individuals into my life and granting me the resilience and perseverance needed to overcome formidable obstacles.

While words may fall short in conveying the depth of my appreciation, as I reach the culmination of this journey, I take immense pleasure in extending my heartfelt thanks to everyone who played a significant role in my achievements, transforming them into an unforgettable and cherished experience.

Thank You!!!

-Ankit

This thesis is dedicated to

**“MY
PARENTS”**

SYNOPSIS

The ever-increasing demand for sustainable resources to support clean energy production and chemical needs has surged due to the ongoing depletion of fossil fuels, population growth, and the booming industrial sector worldwide. The global consumption of fossil fuels and the release of greenhouse gases like carbon dioxide (CO₂), methane (CH₄), and other pollutants are accelerating climate change, ultimately resulting in global warming. It is imperative to reduce our dependence on fossil fuels like coal, petroleum, and natural gas and seek out renewable and sustainable fuel sources. In this context, hydrogen has emerged as a clean energy carrier, yet its production and storage present formidable challenges due to the unique physical properties of hydrogen gas. In this regard, liquid hydrogen storage material (LHSM) such as formic acid, formaldehyde, methanol, ethylene glycol, glycerol and other polyols are attractive candidates for on-demand hydrogen production, as they are liquid in nature and hence safe to handle and transport. Herein, an attempt has been made to design and develop efficient catalytic systems for generating hydrogen gas from abundantly available biomass-derived polyols e.g., ethylene glycol (EG) and glycerol (GLY). Efforts have also been devoted to achieving high selectivity of H₂ along with the production of value-added platform chemicals during the transformation of these polyols. This thesis consists of six chapters; the first chapter provides a concise overview of the importance of hydrogen, its applications, and the challenges associated with its storage and production, along with a detailed literature review of hydrogen production from polyols (ethylene glycol and glycerol) over heterogeneous catalysts. The following chapters (2-5), provide detailed results and discussion on the development of various ruthenium-based heterogeneous catalytic systems designed for generating hydrogen gas from ethylene glycol and glycerol. The primary goal of this thesis is to develop a highly effective and efficient catalytic system in producing environmentally friendly hydrogen (green hydrogen) from sustainable sources. Additionally, the research aims to gain insights into the catalytic pathways involved in hydrogen production through carefully controlled experiments. The concluding chapter summarizes the key findings of this thesis and provides a brief overview of potential future directions for this

research work. The content of each of the chapters included in the thesis is summarized as follows:

Chapter 1. Introduction: General Overview of Hydrogen Storage and Production from Renewable Resources over Heterogeneous Catalysts

Chapter 1 describes the current scenario of the increasing global energy demand and worsening environmental conditions, which endorse that there is an urgent requirement for a sustainable and highly efficient energy solution. Addressing this challenge necessitates a shift towards cleaner and more potent energy sources. In this context, hydrogen energy is seen as a promising alternative and renewable energy source due to several key factors. Although there is significant literature available for hydrogen production from biomass-derived oxygenated compounds over the heterogeneous catalysts, several challenges related to the development of efficient catalysts for pure hydrogen gas production along with some valuable products, performing catalytic reactions at lower temperatures, and low-cost catalytic systems for practical and industrial applications, need to be addressed properly. Noble-metal and non-noble metal-based catalysts have proven to be promising and effective in hydrogen production from biomass-derived oxygenated compounds through reforming processes. However, non-noble metals such as Ni-based catalysts face severe problems of sintering of the catalyst due to carbon deposition in the reforming reactions, which decreases the catalytic activity. To overcome these issues, noble metal-based catalysts have been explored widely in hydrogen production reactions. The choice of support plays a crucial role in tuning the catalytic activity in dehydrogenation reactions by strong metal support interaction, which enhances the activity, selectivity and stability of the catalyst. In this direction, this thesis describes the development of ruthenium-based heterogeneous catalysts and their catalytic activities towards hydrogen production from biomass-derived polyols such as glycerol and ethylene glycol, along with the production of value-added platform chemicals in an aqueous medium. Moreover, detailed investigations are also performed based on controlled experiments to provide mechanistic aspects of these transformations.

Based on the research gaps identified from the available literature reports, the prime objectives of the present research work are:

- To develop and investigate ruthenium-based heterogeneous catalysts for the selective production of hydrogen gas from glycerol in water.
- To design and develop supported ruthenium-based catalytic system to investigate the role of support in the transformation of glycerol to hydrogen gas and lactic acid.
- To develop ruthenium-based heterogeneous catalyst for hydrogen gas production from ethylene glycol in water.
- To employ ruthenium catalyst for hydrogen production from ethylene glycol through upcycling of PET-based plastic waste.

Chapter 2. Catalytic Transformation of Glycerol to Hydrogen Gas and Lactic Acid over Ruthenium Catalyst in Water

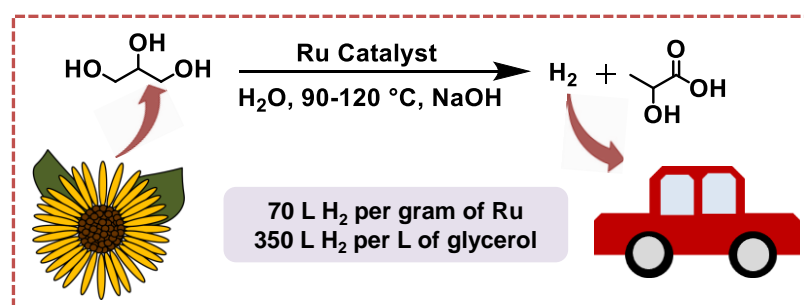


Figure 1. Selective hydrogen production from glycerol over ruthenium catalyst in water.

This chapter describes the synthesis of ruthenium-based heterogeneous catalyst and its characterization by various spectroscopic techniques such as P-XRD, FE-SEM, TEM, and XPS analysis. Further, ruthenium catalyst was explored for the dehydrogenation of glycerol in water at 90-120 °C in the presence of NaOH (2.0 equiv.). Various reaction parameters, such as the effect of water concentration, the effect of base concentration, different types of bases and temperature, were employed to achieve a high yield of hydrogen gas and a valuable byproduct, lactic acid. Water and base concentration played a crucial role in achieving the complete conversion of glycerol with a high yield of hydrogen gas. Notably, a high yield of hydrogen gas (1.6 equiv. per mol of

glycerol) and lactic acid (70%) with complete conversion of glycerol (>99%) was achieved at 110 °C. The composition of gas was confirmed by GC-TCD analysis and observed complete selectivity of hydrogen gas without any contaminations of other gases (CO, CO₂ and CH₄). Controlled experiments were performed to elucidate the reaction pathway of catalytic dehydrogenation of glycerol under optimized reaction conditions. Advantageously, the studied ruthenium catalyst also exhibited high long-term stability and generated 70 L H₂ per gram of Ru and 350 L H₂ per L of glycerol in the presence of NaOH (2.0 equiv.) at 110 °C.

Chapter 3. Investigating the Role of Support in the Catalytic Transformation of Glycerol to Hydrogen Gas and Lactic Acid over the Ru/support Catalysts

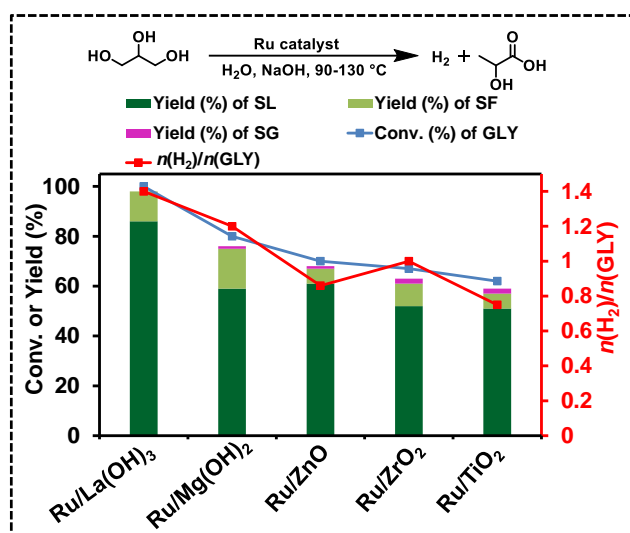


Figure 2. Selective catalytic transformation of aqueous glycerol to hydrogen gas and lactic acid over supported ruthenium catalysts.

This chapter describes the development of ruthenium nanoparticles stabilized over various supports (La(OH)₃, Mg(OH)₂, ZnO, ZrO₂, TiO₂) and to explore these catalytic systems to produce hydrogen gas and lactic acid (LA) from glycerol in water under mild reaction conditions. By tuning the reaction conditions such as temperature, base concentration, water concentration, and choice of appropriate support materials, the yield and selectivity of both H₂ gas and LA were substantially increased. Notably, a high yield of H₂ gas

($n(\text{H}_2)/n(\text{GLY}) \sim 1.4$) and LA (86%) from glycerol was achieved in the presence of NaOH (2.0 equiv.) with complete conversion of glycerol over the Ru/La(OH)₃ catalyst at 130 °C. The effect of different supports in the catalytic dehydrogenation of glycerol was also tested, where Ru/La(OH)₃ outperformed the others. The high activity of the catalyst was attributed to probably due to the high dispersion of metal nanoparticles over supports and strong metal-support interaction (SMSI) between Ru metal and La(OH)₃ support. Several controlled experiments were carried out under optimized reaction conditions to validate the catalytic dehydrogenation pathway of glycerol. Notably, Ru/La(OH)₃ catalyst showed remarkable performance in bulk-scale reactions with a productivity of 12 L H₂/gRu/h at 130 °C and could be recyclable up to six catalytic runs without any significant loss in the catalytic activity. This catalytic system provides new insights into exploring terminal diols (ethylene glycol, 1,3-propanediol, 1,4-butanediol, and 1,5-pentanediol) as important substrates to produce purified hydrogen gas under optimized reaction conditions.

Chapter 4. Selective Hydrogen Gas Production from Ethylene Glycol over Ruthenium Catalyst in Water

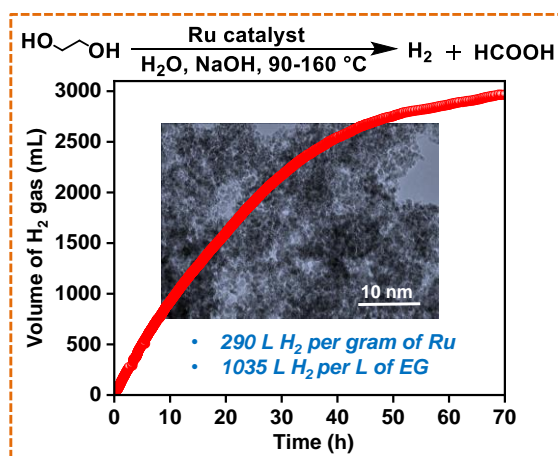


Figure 3. Hydrogen gas production from ethylene glycol to formic acid over ruthenium catalyst in water.

This chapter describes the synthesis of ruthenium-based heterogeneous catalyst by aqueous phase reduction method for the dehydrogenation of ethylene glycol in water. The chemical and morphological properties of the synthesized ruthenium catalyst were established using P-XRD, TEM, XPS, and other

techniques. Further, hydrogen production from ethylene glycol was carried out in water at 90-160 °C. The composition of the gas produced during the catalytic dehydrogenation of ethylene glycol was confirmed by GC-TCD analysis. Under optimized reaction conditions, 3.0 equivalents of hydrogen gas and 85% yield of formic acid from ethylene glycol were achieved in water using NaOH (3.5 equiv.) at 110 °C. Several reaction parameters, such as NaOH concentration, reaction temperature, and water concentration, were extensively investigated to achieve high catalytic activity. Notably, the base concentration and reaction temperature greatly influenced the catalytic dehydrogenation reaction, and it was observed that at low concentrations of base (2.1 equiv. of NaOH) and high reaction temperature (at 160 °C), a high yield of H₂ gas and formic acid was achieved. Moreover, efforts were made to investigate the reaction pathway during the catalytic dehydrogenation process by performing controlled reactions under optimized reaction conditions. Advantageously, the ruthenium catalyst exhibited appreciably high long-term stability over 70 h, generating ca. 290 L of H₂ per gram of Ru with a yield of 1035 L of H₂ per L of ethylene glycol.

Chapter 5. Hydrogen Production from Ethylene Glycol through Upcycling of PET-based Plastic Waste over Ruthenium Catalyst in Water

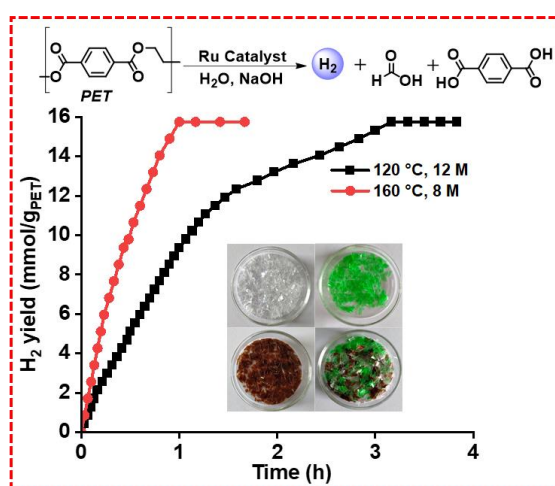


Figure 4. Hydrogen gas production from PET-based plastic waste over ruthenium catalyst in water.

In this chapter, ruthenium catalyst is explored for the catalytic upgradation of PET-based plastic waste into hydrogen gas in water at low-temperature. Firstly, depolymerization of PET-based plastic waste was carried out in aqueous alkaline solution (4 M-12 M) at 110-160 °C in the absence of the catalyst. Complete depolymerization of PET into terephthalic acid and ethylene glycol was achieved, as confirmed by ¹H NMR spectroscopy. Further, one-pot catalytic depolymerization and dehydrogenation of PET waste was performed over the ruthenium catalyst into hydrogen gas and formic acid in an alkaline aqueous condition (4 M-12 M) in the temperature range of 110-160 °C. The volume of produced gas was measured by water displacement set-up, and the purity of the gas was confirmed by GC-TCD analysis. The purity of terephthalic acid, produced during catalytic dehydrogenation of PET (after acidification), was confirmed by P-XRD, FT-IR and NMR analysis. The developed catalytic system is applicable to gram-scale H₂ gas production from PET-based plastic waste with a high yield of H₂ gas (~38,000 mL H₂/gRu) without contamination of other gases (CO, CO₂ and CH₄), highlighting the potential application of the developed catalytic system. The developed catalytic system performed equally well for hydrogen production from different colored PET-based plastics (transparent, green, brown, and mixed PET).

Chapter 6. Summary and future scope

- We developed various ruthenium-based heterogeneous catalysts that are characterized by various spectroscopic techniques such as P-XRD, FE-SEM, TEM, XPS and others.
- Synthesized ruthenium catalyst was explored for the selective hydrogen production from glycerol and ethylene glycol in water at a lower temperature in the presence of a base.
- Experimental findings revealed that water and base played a crucial role in achieving a high yield of hydrogen gas (1.6 equiv.) and lactic acid (70%) from glycerol (conversion >99%) at 110 °C.
- Our studied catalyst also exhibited high long-term stability and generated ~2 L H₂/gRu/h from glycerol at 110 °C.

- Notably, a high yield of H₂ gas ($n(\text{H}_2)/n(\text{GLY})$ ratio of 1.4) and lactic acid (86% yield) from glycerol was achieved over the Ru/La(OH)₃ catalyst.
- Ru/La(OH)₃ catalyst displayed remarkable performance in bulk-scale reactions with a productivity of ~12 L H₂/gRu/h at 130 °C.
- We developed an efficient catalytic process to produce hydrogen gas from aqueous ethylene glycol at 90-160 °C over the ruthenium catalyst.
- We achieved $n(\text{H}_2)/n(\text{EG})$ ratio of ~3.0 and FA (85% yield) from ethylene glycol in aqueous alkaline medium at 110 °C. Advantageously, the ruthenium catalyst exhibited appreciably high long-term stability with a productivity of ~4 L H₂/gRu/h at 110 °C.
- We reported an integrated process for one-pot upcycling of PET-based plastic waste and yielded selective hydrogen gas under alkaline aqueous conditions at 110-160 °C over the ruthenium catalyst.
- The developed catalytic system is applicable to gram-scale H₂ gas production from PET-based plastic waste with a high yield of gas (~38,000 mL H₂/gRu) without any contaminations of other gases (CO, CO₂ and CH₄), highlighting the potential application of the developed catalytic system.
- The developed catalytic system performed equally well for hydrogen production from different types of PET-based plastic waste (transparent, green, brown, and mixed PET).
- Controlled experiments and time-dependent studies were carried out to elucidate the plausible reaction pathway of catalytic dehydrogenation of polyols (GLY and EG) under optimized reaction conditions.

Hydrogen energy is widely recognized as a promising renewable energy alternative. Although it is naturally abundant, it doesn't exist in a free state and can be derived from sustainable sources such as biomass or water in the presence of a suitable catalyst. It serves as a clean energy carrier, generating only water as a byproduct when used in fuel cells. The majority of hydrogen is

currently produced from the reforming of non-renewable resources (coal, petroleum, and natural gas). Reforming is an energy-intensive process which requires high temperatures ($>250\text{ }^{\circ}\text{C}$), and the produced H_2 gas often has contamination of CO_2 and other gases (CO and alkanes). In this thesis, attempts have been made to develop efficient catalytic systems to generate pure H_2 gas under milder reaction conditions so that pure H_2 gas can be directly utilized in fuel cell applications. The developed catalytic system may also be utilized for selective H_2 gas production from biomass-derived xylitol (C-5), sorbitol (C-6) or glucose (C-6) at lower temperatures compared to the reforming process. The choice of appropriate support materials plays an important role in tuning the catalytic activity to achieve high productivity for H_2 gas production from biomass-derived polyols. Bimetallic nanoparticles stabilized over various basic supports (layered double hydroxides or mixed-metal oxides) need to be explored in the dehydrogenation of polyols at low temperatures for the selective production of H_2 gas. However, low-cost catalytic systems for hydrogen production are highly desirable for practical and industrial applications.

List of publications included in the thesis

1. **Kumar A.**, Awasthi M. K., Priya B., Singh S. K. (2022), Selective Hydrogen Production from Glycerol over Ruthenium Catalyst, *ChemCatChem*, 14, e202101951 (DOI: 10.1002/cctc.202101951). (Impact Factor: 4.5)
2. **Kumar A.**, Priya B., Singh S. K. (2023), Ruthenium Catalyzed Transformation of Ethylene Glycol for Selective Hydrogen Gas Production in Water, *ACS Sustain. Chem. Eng.*, 11, 3999-4008 (DOI: 10.1021/acssuschemeng.2c04521). (Impact Factor: 8.4)
3. **Kumar A.**, Awasthi M. K., Sheet N., Kharde T. A., Singh S. K. (2023), One-pot Upcycling of Waste Plastics for Selective Hydrogen Production at Low-Temperature, *ChemCatChem*, 15, e202300574 (DOI: 10.1002/cctc.202300574). (Impact Factor: 4.5)
4. **Kumar A.**, Priya B., Rai R. K., Garg P., Deshpande U., Singh S. K. (2023), Selective Catalytic Transformation of Aqueous Glycerol to Hydrogen Gas and Lactic Acid over the Ruthenium Catalyst. (*Manuscript Submitted*)

List of publications other than included in thesis

1. Dostagir SK N. H. Md., Awasthi M. K., **Kumar A.**, Gupta K., Behrens S., Shrotri A., Singh S. K. (2019), Selective Catalysis for Room-temperature Hydrogenation of Biomass-derived Compounds over Supported NiPd Catalysts in Water, *ACS Sustain. Chem. Eng.*, 7, 9352-9359 (DOI: 10.1021/acssuschemeng.9b00486). (Impact Factor: 8.4)
2. Deka H., **Kumar A.**, Patra S., Awasthi M. K., Singh, S. K. (2020), Synthesis, Structure and Catalytic Activity of Manganese(II) Complexes derived from Bis(imidazole)methane-based Ligands, *Dalton Trans.*, 49, 757-763 (DOI: 10.1039/c9dt03886h). (Impact Factor: 4.0)
3. Patra S., **Kumar A.**, Singh S. K. (2022), Hydrogen Production from Formaldehyde and Paraformaldehyde in Water under Additive-Free Conditions: Catalytic Reactions and Mechanistic Insights, *Inorg. Chem.*, 61, 4618-4626 (DOI: 10.1021/acs.inorgchem.1c03529). (Impact Factor: 4.6)

4. Priya B., **Kumar A.**, Dostagir S. K. N. H. Md., Shrotri A., Singh S. K. (2022), Catalytic Hydrogenation of Biomass-derived furoic Acid to Tetrahydrofuroic Acid derivatives over Pd/CoO_x Catalyst in Water, ChemCatChem, 14, e202200590 (DOI: 10.1002/cctc.202200590). (Impact Factor: 4.5)

5. Priya B., **Kumar A.**, Garg P., Deshpande U., Singh S. K. (2023), Pd/HAP Catalyzed Synthesis of Adipic Acid from 1,6-hexanediol under Aerial Base Free Conditions, ChemCatChem, e202300863 (DOI: 10.1002/cctc.202300863). (Impact Factor: 4.6)

Conferences

1. Poster presentation at “**3rd National Symposium on Shaping the Energy Future: Challenges & Opportunities SEFCO-2019**” at CSIR-Indian Institute of Petroleum Dehradun (Dehradun, U. K.), India, (May 2019). Kumar A., Sahu V. K., Singh, S. K., Selective Catalysis for Room Temperature Hydrogenation of Biomass-derived Compounds over Supported NiPd Catalysts in Water.

2. Attended “**International Conference on Emerging Trends in Chemistry**” at IIT Indore (Indore, M. P.), India (July 2019).

3. Attended “**International Conference on Material Chemistry and Catalysis**” at Tezpur University, Assam, India (March 2021).

4. Poster presentation at “**29th CRSI-NSC**” in association with the Chemical Research Society of India (CRSI) & American Chemical Society (ACS) at IISER Mohali (Punjab), India (July 2022). Kumar A., Singh S. K., Selective Hydrogen Production from Glycerol over Ruthenium Catalyst.

5. Poster presentation at “**International Conference on Modern Trends in Inorganic Chemistry-XVIII**” (**MTIC-XIX 2022**), at Institute of Science, Banaras Hindu University, Varanasi, India (December 2022). Kumar A., Singh S. K., Selective Hydrogen Production from Glycerol over Ruthenium Catalyst.

6. Poster presentation at “**International Conference on Sustainable Chemistry-2023**” at IIT Indore, India (February 2023). Kumar A., Kharde T. A., Singh S. K., Ruthenium Catalyzed Hydrogen Production from Alcohols in Water.

TABLE OF CONTENTS

1.	List of Figures	XVII
2.	List of Schemes	XXXIII
3.	List of Tables	XXXVI
4.	Nomenclature	XXXIX
5.	Acronyms	XL
<i>Chapter 1.</i>	<i>Introduction: General Overview of Hydrogen Storage and Production from Renewable Resources over Heterogeneous Catalysts</i>	1-42
1.1	Introduction and background	1-3
1.2	Hydrogen production: challenges and opportunities	3-9
1.2.1	Hydrogen production from non-renewable resources	4-6
1.2.2	Hydrogen production from renewable resources	6-9
1.3	Hydrogen storage	9-13
1.3.1	Physical methods	10
1.3.2	Chemical methods	11-13
1.3.2.1	Solid-state storage	11-12
1.3.2.2	Chemical storage	12-13
1.4	Polyols as a renewable source of hydrogen	13-26
1.4.1	Ethylene glycol as a liquid hydrogen storage material	14-20
1.4.1.1	Hydrogen production through steam reforming of ethylene glycol	15-17
1.4.1.2	Hydrogen production through aqueous phase reforming of ethylene glycol	17-20
1.4.2	Glycerol as a liquid hydrogen storage material	20-26
1.4.2.1	Hydrogen production through steam reforming of glycerol	21-24
1.4.2.2	Hydrogen production through aqueous phase	24-26

	reforming of glycerol	
1.5	Catalytic transformation of glycerol to hydrogen gas and lactic acid	26-27
1.6	Research gaps for hydrogen production from polyols	28
1.7	Objectives of the thesis	28
1.8	Organization of the thesis	29
1.9	References	29-42
Chapter 2.	<i>Catalytic Transformation of Glycerol to Hydrogen Gas and Lactic Acid over Ruthenium Catalyst in Water</i>	43-82
2.1	Introduction	43-46
2.2	Experimental section	46-50
2.2.1	Materials and instrumentation	46-47
2.2.2	Procedure for the synthesis of ruthenium catalyst	48
2.2.3	Procedure for catalytic conversion of GLY to H ₂ gas	48-49
2.2.4	Heterogeneity test of ruthenium catalyst	49
2.2.5	Recyclability experiment for the catalytic conversion of GLY to H ₂ gas over ruthenium catalyst	49
2.2.6	Bulk-scale hydrogen production from GLY over ruthenium catalyst	49
2.2.7	Gas composition analysis	50
2.3	Results and discussion	50-
2.3.1	Synthesis and characterization of ruthenium catalyst	50-52
2.3.2	Catalytic reaction for hydrogen production from glycerol	53-73
2.4	Conclusions	74
2.5	References	74-82

Chapter 3.	<i>Investigating the Role of Support in the Catalytic Transformation of Glycerol to Hydrogen Gas and Lactic Acid over the Ru/support Catalyst</i>	83-124
3.1	Introduction	83-86
3.2	Experimental section	86-89
3.2.1	Materials and instrumentation	86-88
3.2.2	Catalyst synthesis	88
3.2.3	Catalytic test	88-89
3.2.4	Heterogeneity test	89
3.2.5	Recyclability experiment	89
3.2.6	Bulk-scale reaction	89
3.3	Results and discussion	90-116
3.3.1	Synthesis, characterization, and screening of catalysts for the transformation of GLY to H ₂ gas and SL	90-97
3.3.2	Catalytic transformation of GLY to H ₂ and SL over the Ru/La(OH) ₃	97-106
3.3.3	Scope of Ru/La(OH) ₃ catalyst for H ₂ production from various terminal diols	106-111
3.3.4	Catalyst stability and recyclability	111-116
3.4	Conclusions	116-117
3.5	References	117-124
Chapter 4.	<i>Selective Hydrogen Gas Production from Ethylene Glycol over Ruthenium Catalyst in Water</i>	125-157
4.1	Introduction	125-127
4.2	Experimental section	127-130
4.2.1	Materials and instrumentation	127-128
4.2.2	Synthesis of the ruthenium catalyst	129
4.2.3	Catalytic hydrogen production from EG over the ruthenium catalyst	129
4.2.4	Recyclability experiment	129

4.2.5	Bulk-scale hydrogen production from EG over the ruthenium catalyst	130
4.2.6	Heterogeneity test for the ruthenium catalyst	130
4.2.7	Gas composition analysis	130
4.3	Results and discussion	130-150
4.3.1	Catalyst characterization	130-133
4.3.2	Catalytic hydrogen production from EG	133-145
4.3.3	Catalyst stability and recyclability	146-150
4.4	Conclusions	150
4.5	References	151-157
<i>Chapter 5.</i>	<i>Hydrogen Production from Ethylene Glycol through Upcycling of PET-based Plastics Waste over Ruthenium Catalyst in Water</i>	159-194
5.1	Introduction	159-161
5.2	Experimental section	161-164
5.2.1	Materials and instrumentation	161-162
5.2.2	Synthesis of the ruthenium catalyst	163
5.2.3	Catalytic reaction for one-pot depolarization and dehydrogenation of PET	163
5.2.4	Recyclability experiment	163-164
5.2.5	Bulk scale reaction	164
5.2.6	Mercury poisoning experiment	164
5.2.7	Gas composition analysis	164
5.3	Results and discussion	165-188
5.3.1	Synthesis and characterization of the ruthenium catalyst	165-166
5.3.2	Catalytic one-pot depolarization and dehydrogenation of PET-based plastic waste	166-178
5.3.3	Catalytic hydrogen production from different types of PET	179-186
5.3.4	Bulk scale transformation of PET and reusability of the ruthenium catalyst	187-188
5.4	Conclusions	189

5.5	References	189-194
<i>Chapter 6.</i>	<i>Summary and Future Scope</i>	195-199
6.1	Summary of this thesis	195-198
6.2	Future scope	198-199

List of Figures

<i>Chapter 1.</i>	<i>Introduction: General Overview of Hydrogen Storage and Production from Renewable Resources over Heterogeneous Catalysts</i>	
Figure 1.1	World total energy consumption by source in (a) 1973 and (b) 2022. World total energy supply by source in (c) 1973 and (d) 2022	2
Figure 1.2	World total CO ₂ emission by source in (a) 1973 and (b) 2022	2
Figure 1.3	Distribution of primary energy sources for hydrogen production	4
Figure 1.4	Various methods for hydrogen storage	10
<i>Chapter 2.</i>	<i>Catalytic Transformation of Glycerol to Hydrogen Gas and Lactic Acid over Ruthenium Catalyst in Water</i>	
Figure 2.1	(a) SEM image and corresponding (b) EDX spectra of fresh ruthenium catalyst	51
Figure 2.2	(a) SEM image and corresponding (b) elemental mapping of fresh ruthenium catalyst	51
Figure 2.3	(a) TEM image and corresponding (b) particle size distribution, (c) P-XRD pattern, and (d) XPS profile of Ru 3p region of fresh ruthenium catalyst	52
Figure 2.4	N ₂ adsorption-desorption isotherm of fresh ruthenium catalyst	52
Figure 2.5	Time course plot for the production of hydrogen gas from GLY over the ruthenium	54

	catalyst (inset: GC-TCD analysis of gas evolved during the catalytic reaction). Reaction conditions: Ruthenium catalyst (0.1 mmol), GLY (6.84 mmol), NaOH (7.52 mmol and 13.68 mmol), water (20.52 mmol), and 110 °C	
Figure 2.6	GC-TCD analysis of the (a) gas produced from GLY over the ruthenium catalyst and (b) standard mixture of gases with the composition of CO (24.965%), CO ₂ (24.962%), CH ₄ (25.012%) and H ₂ (25.061%). Reaction conditions: Ruthenium catalyst (0.1 mmol), GLY (6.84 mmol), NaOH (7.52 mmol), water (20.52 mmol), and 110 °C	54
Figure 2.7	Effect of water concentration on hydrogen production from GLY over the ruthenium catalyst. Reaction conditions: Ruthenium catalyst (0.1 mmol), GLY (6.84 mmol), NaOH (7.52 mmol), water (0-5 equiv.), and 110 °C	55
Figure 2.8	(a) Temperature-dependent study for hydrogen production from GLY over the ruthenium catalyst at 90-120 °C. (b) Arrhenius plot of initial TOF values to calculate activation energy. Reaction conditions: Ruthenium catalyst (0.1mmol), GLY (6.84 mmol), NaOH (7.52 mmol), water (20.52 mmol), and 110 °C	57
Figure 2.9	Effect of base concentration on hydrogen production from GLY over the ruthenium catalyst. Reaction conditions: Ruthenium catalyst (0.1 mmol), GLY (6.84 mmol), NaOH (0.5- 2.0 equiv.), water (20.52 mmol), and 110 °C	59
Figure 2.10	Time course plot for the distribution of GLY and various products in the presence of (a) 1.1	60

equiv. and (b) 2.0 equiv. of NaOH during the hydrogen production from GLY over the ruthenium catalyst. Reaction conditions: Ruthenium catalyst (0.1 mmol), GLY (6.84 mmol), NaOH (7.52 mmol and 13.68 mmol), water (20.52 mmol), 110 °C. GLY (glycerol), SL (sodium lactate), PD (1,2-propanediol), SG (sodium glycolate), and SF (sodium formate)

- Figure 2.11** ^1H NMR spectra of the crude reaction mixture of the catalytic reaction in $\text{D}_2\text{O}:\text{H}_2\text{O}$ (1:9) for hydrogen production from GLY over the ruthenium catalyst. Reaction conditions: Ruthenium catalyst (0.1 mmol), GLY (6.84 mmol), NaOH (10.26 mmol), water (20.52 mmol), and 110 °C 62
- Figure 2.12** ^1H NMR spectra of the crude reaction mixture of the catalytic reaction in $\text{D}_2\text{O}:\text{H}_2\text{O}$ (1:9) for hydrogen production from GLY over the ruthenium catalyst. Reaction conditions: Ruthenium catalyst (0.1 mmol), GLY (6.84 mmol), NaOH (13.68 mmol), water (20.52 mmol), and 110 °C 62
- Figure 2.13** ^{13}C NMR spectra of the crude reaction mixture of the catalytic reaction in $\text{D}_2\text{O}:\text{H}_2\text{O}$ (1:9) for hydrogen production from GLY over the ruthenium catalyst. Reaction conditions: Ruthenium catalyst (0.1 mmol), GLY (6.84 mmol), NaOH (13.68 mmol), water (20.52 mmol), and 110 °C 63
- Figure 2.14** ^1H NMR spectra of the crude reaction mixture of glyoxal treated with the base under catalyst-free conditions. Reaction conditions: Glyoxal (6.84 mmol), NaOH (13.68 mmol), water 65

(20.52 mmol), and 110 °C

- Figure 2.15** ¹H NMR spectra of the crude reaction mixture of glyoxal treated with the base in the presence of ruthenium catalyst. Reaction conditions: Ruthenium catalyst (0.1 mmol), glyoxal (6.84 mmol), NaOH (13.68 mmol), water (20.52 mmol), and 110 °C 65
- Figure 2.16** ¹H NMR spectra of the crude reaction mixture of glycolic acid treated with the base in the presence of ruthenium catalyst. Reaction conditions: Ruthenium catalyst (0.1 mmol), glycolic acid (6.84 mmol), NaOH (13.68 mmol), water (20.52 mmol), and 110 °C 66
- Figure 2.17** ¹H NMR spectra of the crude reaction mixture of formic acid treated with the base in the presence of ruthenium catalyst. Reaction conditions: Ruthenium catalyst (0.1 mmol), formic acid (6.84 mmol), NaOH (13.68 mmol), water (20.52 mmol), and 110 °C 66
- Figure 2.18** ¹H NMR spectra of the crude reaction mixture of lactic acid treated with the base in the presence of ruthenium catalyst. Reaction conditions: Ruthenium catalyst (0.1 mmol), lactic acid (6.84 mmol), NaOH (13.68 mmol), water (20.52 mmol), and 110 °C 67
- Figure 2.19** (a) Mercury poisoning test for the hydrogen production from GLY over the ruthenium catalyst. Reaction conditions: Ruthenium catalyst (0.1 mmol), Hg, GLY (6.84 mmol), NaOH (13.68 mmol), water (20.52 mmol), and 110 °C, and (b) Recyclability experiments for hydrogen production from GLY over the ruthenium catalyst. Reaction conditions: 68

	Ruthenium catalyst (0.1 mmol), GLY (6.84 mmol), NaOH (13.68 mmol), water (20.52 mmol), and 110 °C	
Figure 2.20	(a) TEM image, and corresponding (b) particle size distribution curve for the spent ruthenium catalyst	69
Figure 2.21	XPS profile of Ru 3p region of the spent ruthenium catalyst	70
Figure 2.22	P-XRD pattern of the spent ruthenium catalyst	70
Figure 2.23	¹ H NMR spectra of (a) PVP (polyvinyl pyrrolidone) under optimized reaction conditions and (b) pure PVP in D ₂ O:H ₂ O (1:9)	71
Figure 2.24	Time course plot for the bulk-scale production of hydrogen gas from GLY over the ruthenium catalyst. Reaction conditions: Ruthenium catalyst (0.1 mmol), GLY (2 mL), NaOH (54.72 mmol), water (1.48 mL), and 110 °C	72
Figure 2.25	¹ H NMR spectra of purified lactic acid in D ₂ O	72
Figure 2.26	¹³ C NMR spectra of purified lactic acid in D ₂ O	73
Chapter 3.	<i>Investigating the Role of Support in the Catalytic Transformation of Glycerol to Hydrogen Gas and Lactic Acid over the Ru/support Catalyst</i>	
Figure 3.1	P-XRD pattern of the ruthenium-based supported catalysts	90
Figure 3.2	Effect of different supports on the dehydrogenation of GLY to H ₂ gas and SL. Reaction Conditions: Ru/support (100 mg), GLY (13.68 mmol), NaOH (27.36 mmol), water (41.04 mmol), 130 °C, 4.5 h, and 600 rpm	93
Figure 3.3	N ₂ adsorption-desorption isotherm of supported ruthenium catalysts	93
Figure 3.4	XPS spectra (a) wide scan, (b) Ru 3p region, (c)	95

	La 3d region, (d) O 1s region, (e) TEM image, and corresponding (f) particle size distribution curve for Ru/La(OH) ₃ catalyst	
Figure 3.5	TEM image and corresponding particle size distribution (inset) for (a) Ru/Mg(OH) ₂ , (b) Ru/ZnO, (c) Ru/ZrO ₂ and (d) Ru/TiO ₂ catalysts	96
Figure 3.6	(a-b) SEM images and corresponding (c) EDX spectra for the Ru/La(OH) ₃ catalyst	96
Figure 3.7	(a) SEM image and corresponding (b) elemental mapping showing the presence of (c) Ru (cyan), (d) La (red), and (e) O (green) in the Ru/La(OH) ₃ catalyst	97
Figure 3.8	Time course plot for hydrogen gas production from GLY over the Ru/La(OH) ₃ catalyst. Reaction conditions: Ru/La(OH) ₃ (100 mg), GLY (13.68 mmol), NaOH (27.36 mmol), water (41.04 mmol), 130 °C, and 600 rpm	98
Figure 3.9	Effect of (a) $n(\text{GLY})/n(\text{H}_2\text{O})$ ratio, (b) NaOH concentration, and (c) temperature on the catalytic dehydrogenation of GLY over Ru/La(OH) ₃ catalyst. Reaction condition: Ru/La(OH) ₃ (100 mg), GLY (13.68 mmol), NaOH (0.5-2.0 equiv.), water (0-20 equiv.), 90-130 °C, and 600 rpm. (d) Time-dependent catalytic dehydrogenation of GLY over the Ru/La(OH) ₃ catalyst. Reaction condition: Ru/La(OH) ₃ (100 mg), GLY (13.68 mmol), NaOH (27.36 mmol), water (41.04 mmol), 130 °C, and 600 rpm	100
Figure 3.10	Effect of water content on hydrogen production from GLY over the Ru/La(OH) ₃ catalyst. Reaction conditions: Ru/La(OH) ₃ (100 mg), GLY (13.68 mmol), NaOH (27.36 mmol),	101

	water (0-20 equiv.), 130 °C, and 600 rpm	
Figure 3.11	Effect of base concentration on hydrogen production from GLY over the Ru/La(OH) ₃ catalyst. Reaction conditions: Ru/La(OH) ₃ (100 mg), GLY (13.68 mmol), NaOH (0.5-2.0 equiv.), water (41.04 mmol), 130 °C, and 600 rpm	101
Figure 3.12	(a) Temperature-dependent study for hydrogen production from GLY over the Ru/La(OH) ₃ catalyst (b) Arrhenius plot of initial TOF values to calculate activation energy	104
Figure 3.13	¹ H NMR spectra of purified lactic acid in D ₂ O	105
Figure 3.14	¹³ C NMR spectra of purified lactic acid in D ₂ O	106
Figure 3.15	¹ H NMR spectra of the crude reaction mixture of the catalytic reaction for hydrogen production from glyoxal without catalyst. Reaction conditions: glyoxal (13.68 mmol), NaOH (27.36 mmol), water (41.04 mmol), 130 °C, and 600 rpm	108
Figure 3.16	¹ H NMR spectra of the crude reaction mixture of the catalytic reaction for hydrogen production from glyoxal over the Ru/La(OH) ₃ catalyst. Reaction conditions: Ru/La(OH) ₃ (100 mg), glyoxal (13.68 mmol), NaOH (27.36 mmol), water (41.04 mmol), 130 °C, and 600 rpm	109
Figure 3.17	¹ H NMR spectra of the crude reaction mixture of the catalytic reaction for hydrogen production from glycolic acid over the Ru/La(OH) ₃ catalyst. Reaction conditions: Ru/La(OH) ₃ (100 mg), glycolic acid (13.68 mmol), NaOH (27.36 mmol), water (41.04 mmol), 130 °C, and 600 rpm	109

Figure 3.18	¹ H NMR spectra of the crude reaction mixture of the catalytic reaction for hydrogen production from lactic acid over the Ru/La(OH) ₃ catalyst. Reaction conditions: Ru/La(OH) ₃ (100 mg), lactic acid (13.68 mmol), NaOH (27.36 mmol), water (41.04 mmol), 130 °C, and 600 rpm	110
Figure 3.19	¹ H NMR spectra of the crude reaction mixture of the catalytic reaction for hydrogen production from formic acid over the Ru/La(OH) ₃ catalyst. Reaction conditions: Ru/La(OH) ₃ (100 mg), formic acid (13.68 mmol), NaOH (27.36 mmol), water (41.04 mmol), 130 °C, and 600 rpm	110
Figure 3.20	Hg poisoning experiment to validate the heterogeneous nature of the Ru/La(OH) ₃ catalyst	112
Figure 3.21	Time course plot for the bulk-scale production of hydrogen gas from GLY over the Ru/La(OH) ₃ catalyst. Reaction conditions: Ru/La(OH) ₃ (100 mg), GLY (68.4 mmol), NaOH (136.8 mmol), water (205.2 mmol), 130 °C, and 600 rpm	113
Figure 3.22	Recyclability experiment for hydrogen production from GLY over the Ru/La(OH) ₃ catalyst. Reaction conditions: Ru/La(OH) ₃ (100 mg), GLY (13.68 mmol), NaOH (27.36 mmol), water (41.04 mmol), 130 °C, and 600 rpm	113
Figure 3.23	Time course plot for the bulk-scale production of hydrogen gas from EG over the Ru/La(OH) ₃ catalyst. Reaction conditions: Ru/La(OH) ₃ (100 mg), EG (68.4 mmol), NaOH, water (205.2 mmol), 130 °C, and 600 rpm	114

Figure 3.24	P-XRD pattern of the spent Ru/La(OH) ₃ catalyst	114
Figure 3.25	(a) TEM image, and corresponding (b) particle size distribution graph of the spent Ru/La(OH) ₃ catalyst	115
Chapter 4.	<i>Selective Hydrogen Gas Production from Ethylene Glycol over Ruthenium Catalyst in Water</i>	
Figure 4.1	(a-b) TEM images, and corresponding (c) Particle size distribution curve, and (d) P-XRD pattern of the fresh ruthenium catalyst	131
Figure 4.2	(a) SEM image, corresponding (b) elemental mapping, and (c) EDX spectra of fresh ruthenium catalyst	132
Figure 4.3	N ₂ adsorption-desorption isotherm of fresh ruthenium catalyst	132
Figure 4.4	(a) XPS spectra of Ru 3p region and (b) Ru 3d region of fresh ruthenium catalyst	133
Figure 4.5	Time course plot (GC-TCD data in inset) for hydrogen gas production from EG over the ruthenium catalyst at 110 °C. Reaction conditions: Ruthenium catalyst (0.1 mmol), EG (5 mmol), NaOH (10.5 mmol), and water (20 mmol)	134
Figure 4.6	GC-TCD analysis of the (a) standard mixture of gases with the composition of CO (24.965%), CO ₂ (24.962%), CH ₄ (25.012%) and H ₂ (25.061%), and (b-d) gas produced from EG dehydrogenation over the ruthenium catalyst at (b) 110 °C, (c) 130 °C, and (d) 160 °C. Reaction Conditions: Ruthenium catalyst (0.1 mmol), EG (5 mmol), NaOH (10.5 mmol), water (20 mmol), 110 °C, 130 °C, and 160 °C	134

Figure 4.7	Effect of water concentration on hydrogen production from EG over the ruthenium catalyst. Reaction conditions: Ruthenium catalyst (0.1 mmol), EG (5 mmol), NaOH (10.5 mmol), water (0–10 equiv.), and 110 °C	135
Figure 4.8	(a) TEM image, and the corresponding (b) particle size distribution curve of the ruthenium catalyst synthesized without PVP	136
Figure 4.9	(a) Effect of base concentration on hydrogen production from EG over the ruthenium catalyst, (b) Initial reaction rate and product formation rate-NaOH concentration profile. Reaction conditions: Ruthenium catalyst (0.1 mmol), EG (5 mmol), water (20 mmol), NaOH (0.5-3.5 equiv., 3.9 M-27.34 M), 110 °C, and 600 rpm	138
Figure 4.10	Dependence of ruthenium catalyst concentration on the reaction rate for hydrogen production from EG	139
Figure 4.11	Time course plot for (a) temperature-dependent hydrogen production from EG over the ruthenium catalyst at 90-160 °C. (b) the distribution of EG, SF and SG during the catalytic dehydrogenation of EG over the ruthenium catalyst at 110 °C. Reaction conditions: Ruthenium catalyst (0.1 mmol), EG (5 mmol), NaOH (10.5 mmol), and water (20 mmol)	141
Figure 4.12	(a) Temperature-dependent study for hydrogen production from EG over the ruthenium catalyst at 90-120 °C. (b) Arrhenius plot of initial TOF values. Reaction conditions: Ruthenium catalyst (0.1 mmol), EG (5 mmol), NaOH (10.5	143

	mmol), and water (20 mmol)	
Figure 4.13	Kinetic studies for dehydrogenation of ethylene glycol over the ruthenium catalyst using Eyring analysis	143
Figure 4.14	GC-TCD analysis of the (a) standard mixture of gases with the composition of CO (24.965%), CO ₂ (24.962%), CH ₄ (25.012%), and H ₂ (25.061%), and (b-d) gas produced (if any) from formic acid dehydrogenation over ruthenium catalyst at (b) 110 °C, (c) 130 °C, and (d) 160 °C. Reaction Conditions: Ruthenium catalyst (0.1 mmol), formic acid (5 mmol), NaOH (10.5 mmol), water (20 mmol), 110 °C, 130 °C, and 160 °C	144
Figure 4.15	(a) Mercury poisoning test, and (b) Recyclability experiment for hydrogen production from ethylene glycol over the ruthenium catalyst. Reaction conditions: Ruthenium catalyst (0.1 mmol), EG (5 mmol), NaOH (10.5 mmol), water (20 mmol), and 110 °C	147
Figure 4.16	Time course plot for the bulk-scale production of hydrogen gas from EG over the ruthenium catalyst. Reaction conditions: Ruthenium catalyst (0.1 mmol), EG (50 mmol), NaOH (17.5 mmol), water (200 mmol), and 110 °C	147
Figure 4.17	(a) P-XRD pattern, and (b) XPS spectra of the spent ruthenium catalyst	148
Figure 4.18	TEM image, and corresponding (b) particle size distribution curve of the spent ruthenium catalyst	149

Chapter 5. Hydrogen Production from Ethylene Glycol through

Upcycling of PET-based Plastics Waste over Ruthenium Catalyst in Water

- Figure 5.1** (a) TEM image, (b) the corresponding particle size distribution curve, (c) P-XRD pattern, and (d) the XPS spectra of the fresh ruthenium catalyst 165
- Figure 5.2** (a-b) SEM images, (c) corresponding elemental mapping, and (d) EDX spectra of fresh ruthenium catalyst 167
- Figure 5.3** Illustrative scheme and time course plot for the one-pot depolymerization and hydrogen production from *t*-PET over the ruthenium catalyst. Reaction conditions: ruthenium catalyst (0.1 mmol), *t*-PET (0.192 g), NaOH (12 M), H₂O (2 mL), and 120 °C 167
- Figure 5.4** GC-TCD analysis of the gas produced from one-pot dehydrogenation of (a) *t*-PET, (b) *g*-PET, (c) *b*-PET, and (d) *m*-PET over the ruthenium catalyst along with the (e) standard mixture of gases with the composition of CO (24.965%), CO₂ (24.962%), CH₄ (25.012%) and H₂ (25.061%). Reaction conditions: Ruthenium catalyst (0.1 mmol), PET (0.192 g), NaOH (12 M), water (2 mL), and 120 °C 168
- Figure 5.5** ¹H NMR spectra (in D₂O:H₂O (v/v 1:9)) of the crude reaction mixture of the catalytic depolymerization of *t*-PET. Reaction conditions: Ruthenium catalyst (0.1 mmol), *t*-PET (0.192 g), NaOH (12 M), water (2 mL), and 110 °C 169
- Figure 5.6** ¹H NMR spectra of the crude reaction mixture of the catalytic reaction in D₂O:H₂O (1:9) depolymerization of *t*-PET. Reaction 170

	conditions: PET (0.192 g), NaOH (12 M), water (2 mL), and 120 °C	
Figure 5.7	Time-dependent distribution of Na ₂ TPA, EG, SG, and SF for the catalytic dehydrogenation of <i>t</i> -PET over the ruthenium catalyst. Reaction conditions: Ruthenium catalyst (0.1 mmol), PET (0.192 g), NaOH (12 M), H ₂ O (2 mL), and 120 °C	170
Figure 5.8	¹ H NMR spectra of bis(hydroxyethyl)terephthalate in methanol-d ⁴	173
Figure 5.9	¹³ C NMR spectra of bis(hydroxyethyl)terephthalate in methanol-d ⁴	174
Figure 5.10	¹ H NMR spectra (in D ₂ O:H ₂ O (v/v 1:9)) of the crude reaction mixture of the depolymerization of BHET (without catalyst). Reaction conditions: BHET (1.0 mmol), NaOH (12 M), water (2 mL), 120 °C, and 2 h	174
Figure 5.11	¹ H NMR spectra (in D ₂ O:H ₂ O (v/v 1:9)) of the crude reaction mixture of the catalytic dehydrogenation of BHET over the ruthenium catalyst. Reaction conditions: Ruthenium catalyst (0.1 mmol), BHET (1.0 mmol), NaOH (12 M), water (2 mL), 120 °C, and 3.5 h	175
Figure 5.12	(a) Temperature-dependent plot for hydrogen gas generation from <i>t</i> -PET over the ruthenium catalyst, and the corresponding (b) Arrhenius plot of initial TOF values to calculate activation energy. Reaction conditions: Ruthenium catalyst (0.1 mmol), <i>t</i> -PET (0.192 g), NaOH (12 M), H ₂ O (2 mL), and 120-140 °C	176
Figure 5.13	Effect of base concentration on hydrogen gas generation from <i>t</i> -PET over the ruthenium catalyst. Reaction conditions: Ruthenium	177

	catalyst (0.1 mmol), <i>t</i> -PET (0.192 g), NaOH (8 M -12 M), H ₂ O (2 mL), and 120 °C	
Figure 5.14	Effect of base concentration on hydrogen gas generation from <i>t</i> -PET over the ruthenium catalyst. Reaction conditions: Ruthenium catalyst (0.1 mmol), <i>t</i> -PET (0.192 g), NaOH (4 M-8 M), H ₂ O (2 mL), and 160 °C	177
Figure 5.15	Effect of different bases: time course plot for hydrogen gas generation from <i>t</i> -PET over the ruthenium catalyst. Reaction conditions: Ruthenium catalyst (0.1 mmol), <i>t</i> -PET (0.192 g), base (12 M), H ₂ O (2 mL), and 120 °C	178
Figure 5.16	Catalytic one-pot dehydrogenation of <i>t</i> -PET, <i>g</i> -PET, <i>b</i> -PET, and <i>m</i> -PET over the ruthenium catalyst. Reaction conditions: Ruthenium catalyst (0.1 mmol), PET (0.192 g), NaOH (12 M), H ₂ O (2 mL), and 120 °C	180
Figure 5.17	Product distribution for the catalytic one-pot dehydrogenation of <i>t</i> -PET, <i>g</i> -PET, <i>b</i> -PET, and <i>m</i> -PET over the ruthenium catalyst. Reaction conditions: Ruthenium catalyst (0.1 mmol), PET (0.192 g), NaOH (12 M), H ₂ O (2 mL), and 120 °C	181
Figure 5.18	P-XRD pattern of <i>c</i> -TPA, along with the TPA, was produced during the catalytic dehydrogenation of <i>t</i> -PET, <i>g</i> -PET, <i>b</i> -PET, and <i>m</i> -PET. Reaction conditions: Ruthenium catalyst (0.1 mmol), PET (0.192 g), NaOH (12 M), water (2 mL), and 120 °C. (<i>t</i> , <i>b</i> , <i>g</i> , <i>m</i> , and <i>c</i> stands for transparent, brown, green, mixed, and commercial, respectively)	182
Figure 5.19	FT-IR spectra of <i>c</i> -TPA along with the TPA as produced during the catalytic dehydrogenation	183

of *t*-PET, *b*-PET, *g*-PET, and *m*-PET. Reaction conditions: Ruthenium catalyst (0.1 mmol), PET (0.192 g), NaOH (12 M), water (2 mL), and 120 °C. (*t*, *b*, *g*, *m*, and *c* stands for transparent, brown, green, mixed, and commercial, respectively)

Figure 5.20 ¹H NMR spectra of (a) *c*-TPA along with the 184

(b-e) TPA as produced during the catalytic dehydrogenation of (a) *t*-PET, (b) *g*-PET, (c) *b*-PET, and (d) *m*-PET. Reaction conditions: Ruthenium catalyst (0.1 mmol), PET (0.192 g), NaOH (12 M), water (2 mL), and 120 °C. (*t*, *b*, *g*, *m*, and *c* stands for transparent, brown, green, mixed, and commercial, respectively)

Figure 5.21 ¹³C NMR spectra of (a) *c*-TPA along with the 185

(b-e) TPA as produced during the catalytic dehydrogenation of (a) *t*-PET, (b) *g*-PET, (c) *b*-PET, and (d) *m*-PET. Reaction conditions: Ruthenium catalyst (0.1 mmol), PET (0.192 g), NaOH (12 M), water (2 mL), and 120 °C. (*t*, *b*, *g*, *m*, and *c* stands for transparent, brown, green, mixed, and commercial, respectively)

Figure 5.22 TGA analysis of the commercial (*c*-TPA) and 186

synthesized TPA (*t*-TPA, *g*-TPA, and *b*-TPA) by one-pot depolymerization and dehydrogenation of respective PET over ruthenium catalyst. Reaction conditions: Ruthenium catalyst (0.1 mmol), PET (0.192 g), NaOH (12 M), water (2 mL), and 120 °C

Figure 5.23 Bulk scale reaction for hydrogen production 186

from *t*-PET over the ruthenium catalyst. Reaction conditions: ruthenium catalyst (0.1 mmol), *t*-PET (1.0 g), NaOH (12M and 8M),

120 °C and 160 °C, and H₂O (10 mL)

Figure 5.24 Recyclability experiment for hydrogen production from *t*-PET over the ruthenium catalyst. Reaction conditions: ruthenium catalyst (0.1 mmol), *t*-PET (0.192 g), NaOH (8 M), 160 °C, and H₂O (2 mL) 188

Figure 5.25 Mercury poisoning experiment performed for one-pot dehydrogenation of *t*-PET over ruthenium catalyst. Reaction conditions: Ruthenium catalyst (0.1 mmol), elemental Hg (0.3 g), PET (0.192 g), NaOH (12 M), water (2 mL), and 120 °C 188

List of Schemes

Chapter 1. Introduction: General Overview of Hydrogen Storage and Production from Renewable Resources over Heterogeneous Catalysts

Scheme 1.1	Key reactions involved in the steam reforming of methane	4
Scheme 1.2	Key reaction involved in the partial oxidation of hydrocarbons	5
Scheme 1.3	Key reactions involved in the pyrolysis of hydrocarbons	5
Scheme 1.4	Key reactions involved in the electrolysis of water	7
Scheme 1.5	Key reaction involved in the pyrolysis of biomass	9
Scheme 1.6	Key reactions involved in the steam reforming of ethylene glycol	15
Scheme 1.7	Catalytic reaction pathway for steam reforming of EG. Adapted with permission from ref [63] of Springer Nature.	17
Scheme 1.8	Key reactions involved in the aqueous phase reforming of EG	18
Scheme 1.9	Key reactions involved in the steam reforming of glycerol	21
Scheme 1.10	Catalytic reaction pathway for steam reforming of GLY. Reprinted with permission from ref [97] of the Royal Society of Chemistry	23
Scheme 1.11	Plausible pathways for the catalytic conversion of GLY to H ₂ gas and valuable co-products	27

Chapter 2. Catalytic Transformation of Glycerol to Hydrogen Gas and Lactic Acid over Ruthenium Catalyst in Water

Scheme 2.1	Key reactions involved in the transformation of GLY to H ₂ gas	45
-------------------	---	----

Scheme 2.2	Controlled reactions to investigate the pathway of hydrogen production from glycerol over the ruthenium catalyst	64
Scheme 2.3	Plausible reaction pathway for hydrogen production from glycerol over the ruthenium catalyst	68
 <i>Chapter 3. Investigating the Role of Support in the Catalytic Transformation of Glycerol to Hydrogen Gas and Lactic Acid over the Ru/support Catalyst</i>		
Scheme 3.1	Control experiments to elucidate the reaction intermediates in the catalytic transformation of GLY to H ₂ and SL	111
Scheme 3.2	Plausible reaction pathways for hydrogen production from GLY over the Ru/La(OH) ₃ catalyst	111
 <i>Chapter 4. Selective Hydrogen Gas Production from Ethylene Glycol over Ruthenium Catalyst in Water</i>		
Scheme 4.1	Catalytic hydrogen production from ethylene glycol over various catalysts	126
Scheme 4.2	Control experiments to elucidate the reaction pathway for EG transformation to H ₂ gas	145
Scheme 4.3	Plausible pathway for the dehydrogenation of EG into formate	145
 <i>Chapter 5. Hydrogen Production from Ethylene Glycol through Upcycling of PET-based Plastics Waste over Ruthenium Catalyst in Water</i>		
Scheme 5.1	Control experiments to elucidate the plausible reaction pathway for one-pot dehydrogenation of PET	172
Scheme 5.2	Plausible pathway for the one-pot	173

depolymerization and catalytic dehydrogenation of PET-based plastic on the control experiments conducted (i) with and (ii) without ruthenium catalyst in the presence of NaOH (12 M), water (2.0 mL) at 120 °C

Scheme 5.3 Control experiments (a) depolymerization of BHET without ruthenium catalyst, (b) dehydrogenation of BHET over ruthenium catalyst. Reaction conditions: Ruthenium catalyst (0.1 mmol), BHET (1.0 mmol), NaOH (12 M), H₂O (2.0 mL), and 120 °C 175

List of Tables

Chapter 1. *Introduction: General Overview of Hydrogen Storage and Production from Renewable Resources over Heterogeneous Catalysts*

Table 1.1	Comparative table for the energy contents of different fuels	3
Table 1.2	Hydrogen storage capacity of different metal hydrides	12
Table 1.3	Comparative table for the different wt% of liquid hydrogen storage system	13
Table 1.4	Catalysts reported for hydrogen production through steam reforming of EG	17
Table 1.5	Catalysts reported for hydrogen production through aqueous phase reforming of EG	20
Table 1.6	Catalysts reported for hydrogen production through steam reforming of GLY	24
Table 1.7	Catalysts reported for hydrogen production through aqueous phase reforming of GLY	26

Chapter 2. *Catalytic Transformation of Glycerol to Hydrogen Gas and Lactic Acid over Ruthenium Catalyst in Water*

Table 2.1	Reaction optimization for hydrogen production from glycerol over the ruthenium catalyst	56
Table 2.2	Effect of the base and temperature on hydrogen production from GLY over the ruthenium catalyst	58
Table 2.3	Hydrogen Production from glycerol using varying loading of ruthenium catalyst	59

Chapter 3. *Investigating the Role of Support in the Catalytic Transformation of Glycerol to Hydrogen Gas and Lactic Acid over the Ru/support Catalyst*

Table 3.1	Optimization of reaction condition for	91
------------------	--	----

	hydrogen production from glycerol over the ruthenium catalyst	
Table 3.2	Textural properties of Ru-based supported catalysts	94
Table 3.3	Optimization of reaction conditions for hydrogen production from glycerol over Ru/La(OH) ₃ catalyst	99
Table 3.4	Effect of stirring speed on the dehydrogenation of GLY over the Ru/La(OH) ₃ catalyst	102
Table 3.5	Effect of different types of bases in hydrogen production from glycerol over the Ru/La(OH) ₃ catalyst	103
Table 3.6	Optimization of reaction condition for hydrogen production from glycerol over the Ru/La(OH) ₃ catalyst	105
Table 3.7	Hydrogen production from other terminal diols over the Ru/La(OH) ₃ catalyst	107
Chapter 4.	<i>Selective Hydrogen Gas Production from Ethylene Glycol over Ruthenium Catalyst in Water</i>	
Table 4.1	Optimization of the reaction condition for hydrogen production from EG over ruthenium catalyst	136
Table 4.2	Optimization of the reaction conditions for hydrogen production from EG over ruthenium catalyst	140
Table 4.3	Hydrogen production from EG using varying loading of ruthenium catalyst	140
Table 4.4	Effect of stirring speed on the dehydrogenation of EG at different reaction temperatures	149

Chapter 5. *Hydrogen Production from Ethylene Glycol through Upcycling of PET-based Plastics Waste over Ruthenium Catalyst in Water*

Table 5.1	Reaction optimization for the one-pot depolymerization and dehydrogenation of PET-based plastic wastes over the ruthenium catalyst	171
------------------	--	-----

Nomenclature

MHz	Mega hertz
MPa	Mega pascal
wt%	Weight percent
λ	Wavelength
μ	Micro
K	Kelvin
°	Degree
°C	Degree Celsius
θ	Theta
nm	Nanometer
M	Molar
mL	Millilitre
μ L	Microlitre
L	Litre
a. u.	Arbitrary unit
min	Minute
EJ	Exajoule
Mt	Million metric ton
g	Gram
kg	Kilogram
h	Hour

Acronyms

EG	Ethylene glycol
GLY	Glycerol
SR	Steam reforming
APR	Aqueous phase reforming
ATR	Autothermal reforming
LHSM	Liquid hydrogen storage material
WGS	Water-gas shift
CGH ₂	Compressed gaseous hydrogen
CCH ₂	Cryo-compressed hydrogen
SRM	Steam reforming of methane
SREG	Steam reforming of ethylene glycol
SRG	Steam reforming of glycerol
STP	Standard temperature and pressure
DOE	Department of Energy
PET	Polyethylene terephthalate
TPA	Terephthalic acid
Na ₂ TPA	Disodium terephthalate
HAP	Hydroxyapatite
HT	Hydrotalcite
CNF	Carbon nanofiber
Sel.	Selectivity
Conv.	Conversion
SMSI	Strong metal-support interaction
LA	Lactic acid
SL	Sodium lactate
SF	Sodium formate
SG	Sodium glycolate
PD	1,2-propanediol
equiv.	Equivalent
NMR	Nuclear magnetic resonance
XPS	X-ray photoelectron spectroscopy

TEM	Transmission electron microscopy
FE-SEM	Field emission scanning electron microscopy
P-XRD	Powder X-ray diffraction
ICP-AES	Inductively coupled plasma atomic emission spectroscopy
FTIR	Fourier transform infrared spectroscopy
TGA	Thermal gravimetric analysis
D ₂ O	Deuterium oxide
MeOH-d ⁴	Deuterated methanol
TMS	Tetramethyl silane
Ar	Argon
H ₂	Hydrogen
CO	Carbon monoxide
CO ₂	Carbon dioxide
CH ₄	Methane
CB	Carbon balance
ppm	Parts per million
TOF	Turnover frequency
Aq.	Aqueous

Chapter 1

Introduction: General Overview of Hydrogen Storage and Production from Renewable Resources over Heterogeneous Catalysts

1.1. Introduction and background

The continuous consumption of fossil fuels and the escalating greenhouse gas emissions are adversely affecting air quality and contributing to global climate change, leading to the phenomenon of global warming.^[1] In this regard, the scientific community is highly motivated to find alternative pathways to mitigate climate change and the development of clean energy technologies in line with a clean chemistry industry will be a major driver to stop fossil fuel consumption. According to the International Energy Agency (IEA) World Energy Outlook 2023, it was reported that global energy consumption experienced a significant increase, growing 2.5 times from 194 EJ in 1973 to 442 EJ by 2022. Concurrently, the total primary energy supply also surged, increasing by 2.4 times worldwide, from 254 EJ in 1973 to 632 EJ in 2022 (Figure 1.1).^[2] However, it is noteworthy that more than 80% of this energy supply continued to be sourced from fossil fuels, encompassing coal, oil, and natural gas.^[3] This heavy reliance on fossil fuels has a detrimental impact on the environment, primarily due to the excessive emission of carbon dioxide (CO₂). These emissions have seen a substantial increase, rising from 15,641 million metric tons (Mt) of CO₂ in 1973 to a staggering 36,930 Mt CO₂ in 2022 (Figure 1.2).^[2] This alarming trend underscores the urgent need to address the global challenge of reducing CO₂ emissions. Therefore, it is crucial to explore and identify sustainable fuel options that can play a significant role in the transition towards cleaner global energy solutions. These efforts are expected to accelerate progress towards achieving the objectives set forth in the Paris Agreement 2015, particularly in the context of limiting global temperature increases to well below 2 °C in the 21st century.^[4]

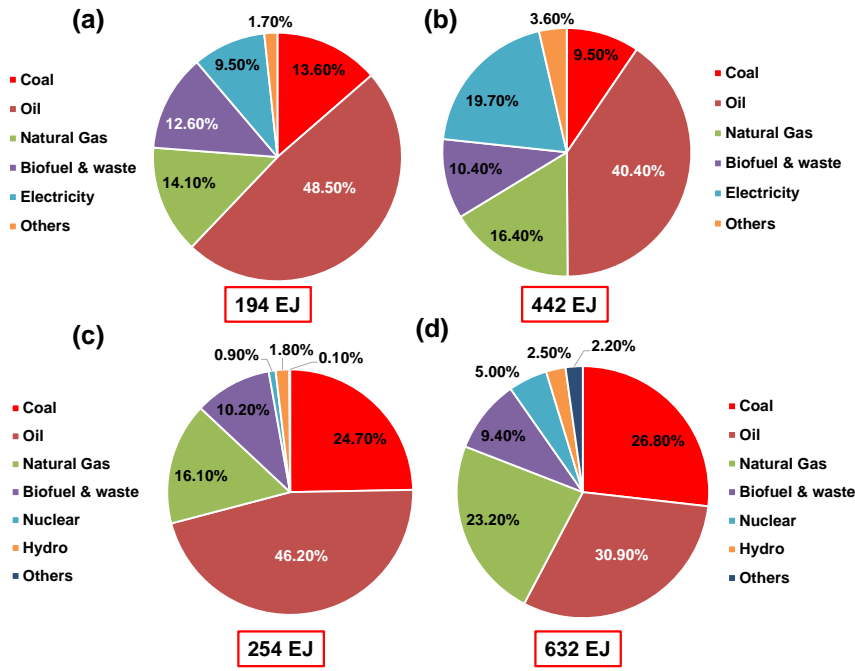


Figure 1.1. World total energy consumption by source in (a) 1973 and (b) 2022. World total energy supply by source in (c) 1973 and (d) 2022. Source: IEA, World Energy Outlook 2023.^[2]

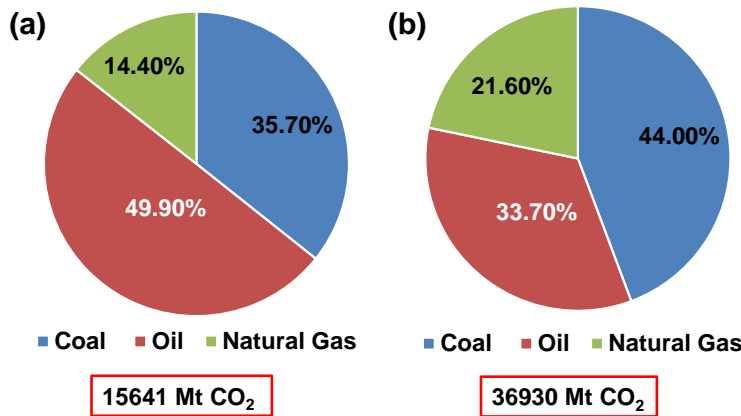


Figure 1.2. World total CO₂ emission by source in (a) 1973 and (b) 2022. Source: IEA, World Energy Outlook 2023.^[2]

In this regard, hydrogen can be considered a promising alternative energy resource due to several key factors. H₂ is abundantly available on Earth, primarily in the form of water. It possesses the characteristic of being highly flammable, requiring only a small amount of energy and oxygen to ignite. When used in fuel cells, it produces energy and only water as a by-product, emitting no carbon in the process.^[5-7] Moreover, hydrogen offers the advantage of a high energy storage capacity (120 MJ/kg), making it a cleaner-burning

option compared to conventional fossil fuels (Table 1.1).^[8] This makes hydrogen an excellent energy carrier for various applications, such as fuel cells, which are used in stationary energy supply, energy transportation, and hydrogen-powered vehicles. Hydrogen energy faces a major hurdle due to its extremely low energy density of 0.01 MJ/L at STP, in stark contrast to gasoline's 32 MJ/L.^[9] This low volumetric energy density poses difficulties in efficiently storing hydrogen as a fuel under ambient conditions.

Table 1.1. Comparative table for the energy contents of different fuels.^[8]

Entry	Fuel	Gravimetric energy density (MJ/kg)	Energy density (MJ/L)
1	H ₂	120	0.01
2	Liquified natural gas	54.4	22.2
3	Propane	49.6	25.3
4	Biodiesel	42.2	33
5	Automotive gasoline	46.4	32
6	Automotive diesel	45.6	38.6
7	Ethanol	29.6	24
8	Methanol	19.7	15.6
9	Butanol	36.6	29.2
10	Wood (dry)	16.2	-

1.2. Hydrogen production: challenges and opportunities

H₂ gas can be generated from renewable sources like biomass and water, as well as non-renewable ones such as fossil fuels. However, to ensure sustainable hydrogen production, it is imperative that a continuous and substantial supply of energy be obtained from renewable sources like solar, wind, and ocean waves. This shift towards renewable energy inputs is essential for environmentally friendly hydrogen production.^[10-11] Historically, hydrogen gas has been primarily produced through various methods, with 48% derived from natural gas, 30% from oil/naphtha reforming, 18% from coal gasification, and 4% from electrolysis (Figure 1.3).^[12]

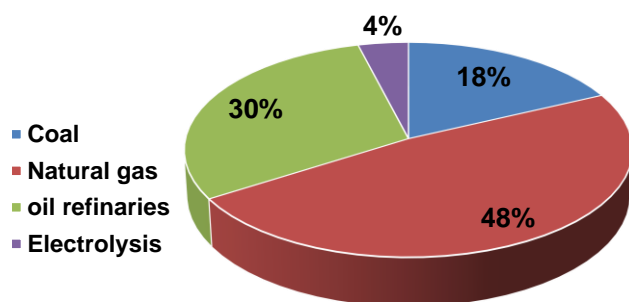


Figure 1.3. Distribution of primary energy sources for hydrogen production.^[12]

1.2.1. Hydrogen production from non-renewable resources

The primary global source for hydrogen production currently relies heavily on fossil fuels. The predominant technologies used to meet the demand for hydrogen involve processes like hydrocarbon reforming and pyrolysis.^[13] These methods require not only hydrocarbons but also additional reactants, such as steam and oxygen, which are essential for hydrogen production. H₂ gas production from non-renewable resources receives criticism for its environmental impact, mainly due to greenhouse gas emissions.^[14] Various methods for the generation of hydrogen gas from fossil fuels include steam reforming, partial oxidation, autothermal reforming, etc.

1.2.1.1. Steam reforming

Currently, hydrogen gas (H₂) is being produced by steam reforming of methane (SRM) at higher temperatures (700-1000 °C) and higher pressure (3-25 bar) using a suitable catalyst along with co-production of CO and CO₂ (eq. 1.1). To achieve high methane conversion and high H₂ selectivity, SR reaction must be followed by water-gas shift reaction (WGSR) where CO and H₂O react to produce H₂ and CO₂ gases (eq. 1.2).^[15]



Scheme 1.1. Key reactions involved in the steam reforming of methane.^[15]

1.2.1.2. Partial oxidation

Partial oxidation is an alternative approach to SR reactions that transforms hydrocarbons into a mixture of carbon monoxide and other partially oxidized products. This method is versatile and can utilize various feedstocks, such as heavy fuel oil, methane, and coal, for H₂ gas production.^[13] Non-noble metal-based catalysts are employed for partial oxidation reactions due to their ability to accommodate variable oxidation states and the adsorption of reactants and intermediates on their surfaces.^[16] The partial oxidation reaction of hydrocarbons is shown in eq. 1.3.



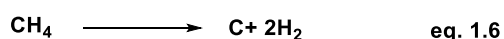
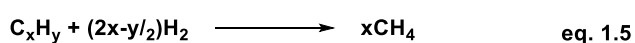
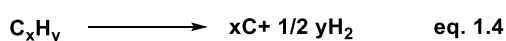
Scheme 1.2. Key reaction involved in the partial oxidation of hydrocarbons.

1.2.1.3. Auto-thermal reforming

Auto-thermal reforming (ATR) is a process that combines exothermic partial oxidation with O₂, which releases energy, and then this released energy can be used for the endothermic steam reforming reaction.^[17] In this method, steam and oxygen gas are fed into the reformer, where both SR and partial oxidation reactions occur at the same time, achieving a thermodynamically neutral reaction state.^[18]

1.2.1.4. Pyrolysis of hydrocarbons

Pyrolysis is a process of thermal decomposition to break down lighter hydrocarbons into carbon and H₂ in the absence of oxygen (eq. 1.4).^[19] When the thermal decomposition initiates with heavy fractions (having a boiling point higher than 350 °C), it can produce hydrogen following two steps. These two steps are hydrogasification (eq. 1.5) and subsequent methane cracking (eq. 1.6). Methane pyrolysis is widely used to produce hydrogen gas because no CO₂ is produced in this process, and carbon is recovered as a solid.^[20]



Scheme 1.3. Key reactions involved in the pyrolysis of hydrocarbons.^[20]

1.2.1.5. Coal gasification

Coal gasification is a thermochemical transformation process where coal is converted into hydrogen and carbon monoxide. Coal can be transformed into synthesis gas using steam or air at high temperatures and pressures.^[21] Also, in this process, coal reacts with CO₂ and undergoes a Boudouard reaction to produce additional carbon monoxide.

1.2.2. Hydrogen production from renewable resources

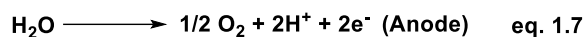
Green hydrogen has become a pivotal focal point in the quest for sustainable energy solutions, driven by the prevalent utilization of non-renewable resources in the production of hydrogen gas.^[22] This shift towards green hydrogen production holds significant promise for substantially reducing carbon emissions linked to energy generation and contributing to the effort to limit global temperature increases to 2 °C.^[4] Green hydrogen can be produced through the electrolysis of water or from biomass or biomass-derived components.

1.2.2.1. Hydrogen production from water

Water serves as an abundant source for producing hydrogen gas through its separation into hydrogen and oxygen without the release of any harmful gases, provided that there is an ample supply of energy.^[23] Hydrogen gas can be produced from water through various methods, including electrolysis powered by electric current, thermolysis utilizing thermal energy, photoelectrolysis harnessing photonic energy, and biophotolysis facilitated by microorganisms.^[24]

1.2.2.1.1. Electrolysis

A straightforward method for producing H₂ and O₂ from water involves the application of an electric current. Electricity can be converted into chemical energy, such as hydrogen and oxygen gases, through different reactions at the anode and cathode electrodes. (Scheme 1.4).^[25]



Scheme 1.4. Key reactions involved in the electrolysis of water.^[25]

Various technologies exist for water electrolysis, including alkaline water electrolysis, solid oxide electrolysis, and proton exchange membrane (PEM) electrolysis.^[26] Alkaline water electrolysis employs a concentrated lye solution as an electrolyte and non-noble metal catalysts like nickel (Ni) as electrodes. It also necessitates the use of a gas separator to collect hydrogen (H₂) and oxygen (O₂) separately.^[27] In contrast, PEM electrolysis relies on a humidified polymer membrane as an electrolyte and employs noble metals such as platinum (Pt) and iridium oxide as electrodes. Both technologies operate effectively at temperatures ranging from 50-80°C and can withstand pressures of up to 30 bar. In contrast, solid oxide electrolysis requires significantly higher temperatures, typically between 700-900°C, to dissociate water into H₂ and O₂. Consequently, alkaline water and PEM electrolysis are considered promising approaches for large-scale hydrogen production due to their cost-effectiveness.^[26] Nevertheless, for on-site generation of high-purity H₂ gas without CO₂ emissions via water electrolysis, a crucial prerequisite is the utilization of energy from renewable sources such as wind, solar, sea waves, and biomass.^[27]

1.2.2.1.2. Thermolysis

The thermochemical processes involve the decomposition of H₂O into hydrogen and oxygen gases at elevated temperatures exceeding 2500 °C.^[28] It is a reversible reaction and presents significant challenges when it comes to separating H₂ and O₂ due to the risk of their recombination, which could lead to an explosion. Additionally, a substantial obstacle in this process is the development of materials capable of withstanding the high temperatures required for thermolysis.

1.2.2.1.3. Photoelectrocatalysis

The process of photoelectrolysis involves harnessing both solar energy absorption and electrolysis within a unified system to enhance the sustainability of energy generation. In this method, not only does solar energy play a pivotal role, but electricity is also required to facilitate the process. Consequently, the combination of photonic and electrical energies is converted into chemical energy, specifically in the form of hydrogen.^[40] This transformation is achieved by absorbing photons with energy levels exceeding the band gap of photoelectrodes. This, in turn, generates electron-hole pairs within photoelectrochemical cells, thereby aiding in the dissociation of water into hydrogen (H₂) and oxygen (O₂).^[41]

1.2.2.2. Hydrogen production from biomass

Biomass primarily consists of raw materials such as agricultural residues, plant waste, municipal solid waste, and industrial byproducts. It represents a highly promising and sustainable alternative source of renewable energy.^[31] Hydrogen production from biomass-derived components is both economically and technically feasible. Unlike fossil fuels, the transformation of biomass into hydrogen gas reduces CO₂ emissions and facilitates the absorption of CO₂ from the atmosphere, resulting in a carbon-neutral system.^[32] From biomass hydrogen can be produced by two primary methods: thermochemical and biological processes.

1.2.2.2.1. Thermochemical processes

H₂ can be produced efficiently from biomass through a thermochemical process encompassing pyrolysis, gasification, and hydrothermal liquefaction.^[33] Biomass can be converted into hydrogen gas using pyrolysis and gasification processes. Pyrolysis is a method used to transform various forms of biomass into solid, liquid, or gaseous products in the absence of oxygen in temperatures ranging from 300-1000 °C and results in the production of bio-oil, bio-char, and other gases like H₂, CH₄, CO_x, or hydrocarbons.^[34] Hydrogen can be produced from pyrolysis by following the equation below.



Scheme 1.5. The key reaction involved in the pyrolysis of biomass.

In a separate approach, biomass can be transformed into a combustible gas mixture via biomass gasification at 800-900 °C and produces the mixture of CO and H₂ gas along with CO₂, H₂O and CH₄.^[31] For the conversion of moist biomass, a hydrothermal liquefaction technique becomes essential. This method operates under high pressure (40-220 bar) and temperatures (250-370 °C), resulting in the production of liquid bio-crude, gaseous steam, and solid byproducts.^[35]

1.2.2.2. Biological processes

In the realm of sustainability, there has been a growing interest in harnessing hydrogen from biomass through biological processes. Two prominent methods for generating hydrogen gas from biomass are dark fermentative and photo fermentative processes. In dark fermentative processes, anaerobic bacteria play a pivotal role in the production of H₂ gas, organic acids, and CO₂. Conversely, in the photo fermentative process, photosynthetic bacteria are employed to yield H₂ and CO₂ from a diverse range of substrates.^[36]

1.3. Hydrogen storage

Storing hydrogen gas in its natural state poses significant challenges due to its low volumetric energy density (0.0108 MJ/L). Hydrogen can be stored physically or chemically using various technologies (Figure 1.4). For physical storage, two common methods have been employed: compression under high pressure (ranging from 350 to 700 bar) and cryogenic storage at extremely low temperatures (-253 °C).^[37] However, both approaches have some inefficiencies and require substantial energy inputs, especially during long-term transportation. Consequently, it is strongly advisable to explore alternative hydrogen carriers that can facilitate the effective storage, transportation, and efficient on-site dispensing of hydrogen gas.^[38] Hydrogen can be chemically stored in a high-density form known as a liquid hydrogen storage material (LHSM). LHSMs are getting noticed for their potential to solve challenges

linked to using hydrogen for clean energy in storage and transportation.^[39]

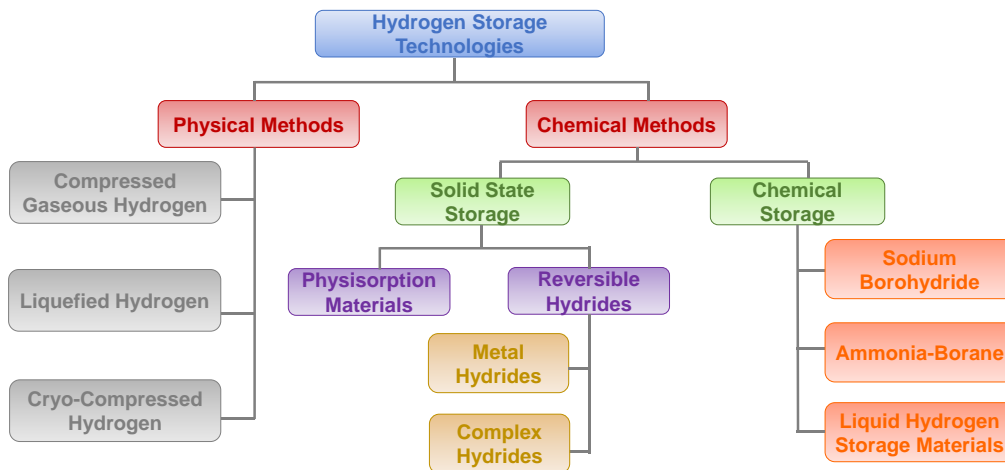


Figure 1.4. Various methods for hydrogen storage.^[40]

1.3.1. Physical methods

H₂ gas can be stored as liquid hydrogen (LH₂), compressed gas (CGH₂), or cryo-compressed hydrogen (CCH₂).

Compressed H₂ gas typically can be stored within high-pressure tanks or cylinders, where it is maintained under high pressures (350 to 700 bar). This pressurization serves to enhance its energy density (gravimetric energy density) while simultaneously minimizing its storage volume, facilitating ease of transportation and storage.^[40] Liquid hydrogen, which is formed when hydrogen gas is chilled to a low temperature of -253 °C, is a transparent, colorless liquid renowned for its high energy density under these frigid conditions.^[37] Safety is a significant concern due to the potential risks associated with leaks, which could result in explosive incidents. In comparison to the storage of CGH₂ (i.e., 350 or 700 bar), pressure in LH₂ storage tanks is much less (<1 MPa), which further eliminates the high costs associated with the composite material used which are being used for CCH₂ storage.^[41] Cryo-compressed hydrogen, a cryogenic gas with a supercritical temperature, offers a solution for storage and safety. Gaseous hydrogen undergoes compression at approximately -233 °C, preventing liquefaction. This approach exhibits favorable volumetric and gravimetric capacities, but challenges such as boil-off issues, heat transfer, long-term storage, and energy expenses related to liquefaction necessitate further investigation.^[42]

1.3.2. Chemical methods

The preceding discussion highlights the limitations of physical hydrogen storage methods that prompted a global quest for more effective storage techniques. Chemical hydrogen storage methods involve the interaction between H_2 and storage materials. The strength of these interactions may vary, ranging from weak van der Waal forces to strong, ionic and covalent bonds.^[43] Chemical hydrogen storage methods can be categorized into two types: (I) chemical storage and (II) solid-state storage.

1.3.2.1. Solid-state storage

Solid-state hydrogen storage involves storing H_2 gas within a solid material instead of as a compressed H_2 gas or liquid H_2 . This method aims to overcome storage challenges, offering improved stability, handling, and transport capabilities for hydrogen. Depending on the strength of the interaction between H_2 and the storage material, it can be categorized into two types: (i) reversible hydrides and (ii) physisorption materials. The addition of a small amount of Ti (specifically, 2 mol%) allowed for reversible regeneration of the $NaAlH_4$ complex hydride system through the application of hydrogen pressure, demonstrated by Bogdanovic and colleagues on Ti-doped $NaAlH_4$.^[44] The bonding within complex hydrides exhibits a combination of both ionic and covalent characteristics. For example, in $LiNH_2$, the N–H bond within the NH_2^- anion is primarily covalent in nature, while the Li–N bond displays a blend of ionic and covalent attributes.^[45-47] Complex hydrides boast impressive theoretical gravimetric densities: $NaAlH_4$ (7.5 wt.%), $LiAlH_4$ (10.6 wt.%), $LiBH_4$ (18.4 wt.%), and Li_3N (11.5 wt.%).^[46] However, their practical reversible gravimetric capacities typically fall within the range of 4-5 wt% under typical operating temperatures and pressures. Metal hydride formation involves the disintegration of H_2 molecules over the metal surface, enabling hydrogen atoms to infiltrate the crystal lattice. The primary challenges associated with metal hydrides are their low gravimetric energy density, elevated operating temperatures, and the expensive nature of rare earth metals. Among the various metal hydrides listed in Table 1.2, MgH_2 has garnered substantial interest due to its high gravimetric energy density of 7.6 wt%.^[47]

Table 1.2. Hydrogen storage capacity of different metal hydrides.^[48]

Entry	Metals	Hydrides	H ₂ storage (wt%)	Operating T (°C) at 1 bar H ₂
1	LaNi ₅	LaNi ₅ H ₆	1.37	12
2	FeTi	FeTiH ₂	1.89	-8
3	Mg ₂ Ti	Mg ₂ TiH ₄	3.59	255
4	ZrMn ₂	ZrMn ₂ H ₂	1.77	440
5	Mg	MgH ₂	7.60	279

Physisorption storage involves weakly binding hydrogen molecules to a material's surface using London dispersive forces.^[48] This technology stores hydrogen affordably at room temperature and low pressures. Porous materials like zeolites, MOFs, COFs, and carbon materials (fullerenes, nanotubes, graphene) are extensively researched for this purpose.^[49]

1.3.2.2. Chemical storage

Chemical hydrogen storage surpasses physical hydrogen storage in terms of efficiency due to its ability to store a substantial amount of hydrogen and release it effectively as required. Hydrogen can be effectively stored using diverse chemical storage methods, including hydrides (NaBH₄, AlH₃),^[50] amine borane adducts,^[51] and liquid hydrogen storage material (LHSM).

While significant strides have been made in hydrogen production, challenges persist in the realms of hydrogen storage and transportation. These challenges encompass a low volumetric energy density (0.01 MJ/L), safety concerns, and the expenses associated with cryogenic or high-pressure compression cylinders and tanks.^[8] Therefore, there is a pressing need to explore innovative approaches for the convenient storage and transportation of hydrogen gas. In recent decades, numerous hydrogen storage technologies have undergone investigation. These include hydrogen adsorption in metal hydrides, utilization of metal-organic frameworks (MOFs), and nanostructured materials.^[42] Nevertheless, these methods are constrained by their limited hydrogen storage capacities (HSCs), demanding operational conditions, high costs, and suboptimal energy efficiency. Storing hydrogen within the chemical bonds of small organic compounds, especially within organic liquids, presents

an attractive path for the development of future hydrogen transportation systems. In recent years, liquid hydrogen storage materials (LHSM) such as methanol (12 wt%),^[52] formic acid (4.4 wt%),^[53] formaldehyde (8.4 wt%),^[53] hydrazine (8 wt%),^[54] ammonia,^[55] ethylene glycol (6.5 wt%),^[56] etc. have garnered significant interest (Table 1.3). Moreover, many of these liquid hydrogen storage substances exhibit a notably high gravimetric hydrogen density, are cost-effective, readily available, and can be sourced from renewable materials.

Table 1.3. Comparative table for the different wt% of Chemical hydrogen storage system.

Entry	Substrate	Reaction equation	wt%
1	Methane	$\text{CH}_4 + \text{H}_2\text{O} \longrightarrow \text{CO} + 3\text{H}_2$	17.6
2	Ammonia	$2\text{NH}_3 \longrightarrow \text{N}_2 + 3\text{H}_2$	17.6
3	Hydrazine	$\text{N}_2\text{H}_4 \cdot \text{H}_2\text{O} \longrightarrow \text{N}_2 + 2\text{H}_2 + \text{H}_2\text{O}$	8.0
4	Methanol	$\text{CH}_3\text{OH} + \text{H}_2\text{O} \longrightarrow \text{CO}_2 + 3\text{H}_2$	12.0
5	Formaldehyde	$\text{HCHO} + \text{H}_2\text{O} \longrightarrow \text{CO}_2 + 2\text{H}_2$	8.4
6	Formic acid	$\text{HCOOH} \longrightarrow \text{CO}_2 + \text{H}_2$	4.4
7	Ethanol	$\text{C}_2\text{H}_5\text{OH} + \text{H}_2\text{O} \longrightarrow \text{CH}_3\text{COOH} + 2\text{H}_2$	6.2
8	Ethylene glycol	$\text{C}_2\text{H}_6\text{O}_2 + \text{H}_2\text{O} \longrightarrow \text{C}_2\text{H}_4\text{O}_3 + 2\text{H}_2$	5.0
		$\text{C}_2\text{H}_6\text{O}_2 + 2\text{H}_2\text{O} \longrightarrow 2\text{HCOOH} + 3\text{H}_2$	6.1
9	Glycerol	$\text{C}_3\text{H}_8\text{O}_3 \longrightarrow \text{C}_3\text{H}_6\text{O}_3 + \text{H}_2$	2.2

1.4. Polyols as a renewable source of hydrogen

Biomass-derived polyols like glycerol (C3), xylitol (C5), mannitol (C6), and sorbitol (C6) are among the top twelve platform chemicals identified by the Department of Energy (DOE). They share analogous chemical structures, with each carbon linked to a hydroxyl group (-OH), making them readily obtainable from plentiful sugar sources.^[57] Biomass-based polyols can be derived from cellulose and hemicellulose hydrolysis and have higher oxygen content, enhancing water solubility and reducing volatility. This makes them more suitable for hydrogen production through APR at milder reaction conditions, unlike steam reforming.^[58] During catalytic reforming processes, polyols undergo dehydrogenation to produce valuable products (organic acids) that are difficult to reform, causing deactivation of the catalyst as well as corrosion of the reaction vessel. Therefore, it is highly desirable to design catalysts that have

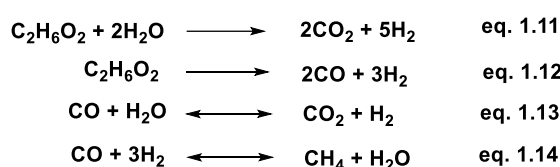
the ability to cleave the C-C bond to promote water-gas shift and methanation reaction.^[59] Acidity and basicity have significant effects on catalytic activity in hydrogen production through reforming processes. Acidic support favors alkane formation in reforming reactions, while basic and neutral supports help in the WGS reactions.^[60] Different processes like chemical looping, steam reforming, and in-situ carbon capture are used to produce high-purity H₂ gas from hydrocarbons, alcohols, and biomass-derived compounds. Steam reforming reactions have been carried out at >250 °C and 5-25 bar using Ni and Pt-based supported catalysts.^[61] Under these reaction conditions, the catalyst gets deactivated at high temperatures due to carbon deposition, catalyst poisoning and sintering.^[62] In 2002, Dumesic et al., first time reported the hydrogen gas production through APR of biomass-derived oxygenated compounds and other valuable fine chemicals using various catalysts at 200-250 °C under 15-50 bar.^[63] During the APR process, both gaseous (CO₂, H₂, CO, CH₄ and light alkanes) and liquid products are formed.^[64] In a similar direction, various catalytic systems for the production of hydrogen gas have been widely studied from biomass-derived oxygenated compounds (ethylene glycol and glycerol) via SR and APR processes.

1.4.1. Ethylene glycol as a liquid hydrogen storage material

Ethylene glycol (EG) is a colorless, odorless, and simplest vicinal diol. Notably, EG serves as a key ingredient in automotive antifreeze and coolant systems, as well as de-icing solutions for both windshields and aircraft. Furthermore, it finds extensive use in the production of polyester fibers and resins, notably in the form of polyethylene terephthalate (PET).^[65] EG can be obtained through the hydrogenolysis of polyols derived from biomass or, alternatively, by hydrating ethylene oxide derived from petrochemical sources as well as the depolymerization of PET.^[65-66] EG can also be explored as a promising candidate for liquid hydrogen storage materials with its cost-effectiveness, renewable sourcing options, and existing industrial application.

1.4.1.1. Hydrogen production through steam reforming of ethylene glycol

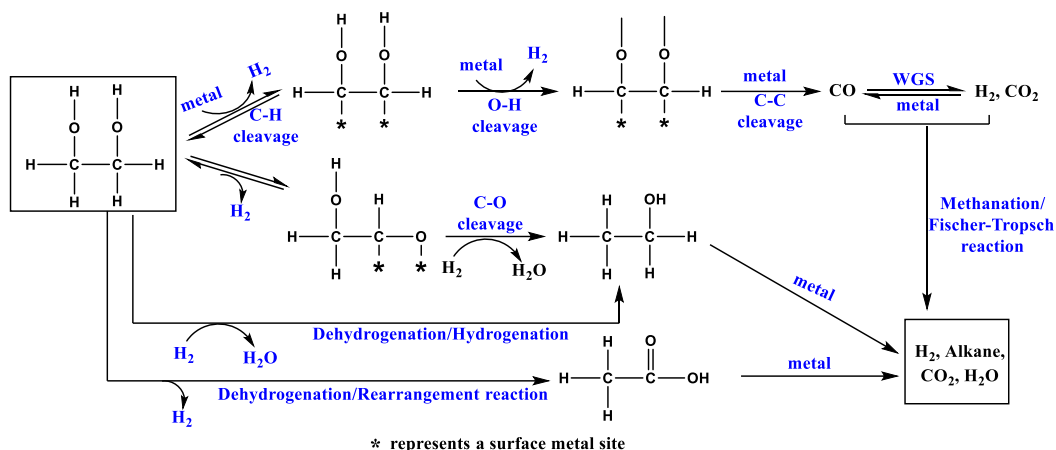
The steam reforming of oxygenates derived from biomass is acknowledged as an economically viable process for efficiently harnessing renewable energy resources by hydrogen production.^[63] During steam reforming of ethylene glycol (SREG), various chemical reactions take place (Scheme 1.6). The primary reaction involves the SREG (eq.1.11). Additionally, secondary reactions may occur, including decomposition reactions (eq. 1.12), water-gas shift reactions (WGS) (eq. 1.13), and methanation reactions (eq. 1.14). The given reactions indicate that the WGS reaction can improve the selectivity for H₂ production, whereas methanation is less desirable for H₂ generation.^[63]



Scheme 1.6. Key reactions involved in the steam reforming of ethylene glycol.^[63]

An effective steam-reforming catalyst should exhibit activity for both the WGS reaction and the cleavage of C-C or C-H bonds. Additionally, the catalyst should not promote any concurrent or subsequent reactions that compete with eq. 1.11 and 1.13, as this would reduce the overall yield of H₂. Various metals, such as Ni, Pt, Pd, Rh, and Ru, have garnered attention as promising catalysts for hydrogen production through the reforming of oxygenated compounds. While Ni offers advantages in terms of availability and cost, Pt exhibits superior activity and selectivity to produce H₂ gas from EG. Hydrogen production through steam reforming of EG has been explored over a variety of catalysts (Table 1.4).^[58,67-74] Gong et al. explored various Ni-based catalysts (Ni/ γ -Al₂O₃, Ni/MgO, Ni/CeO₂ and Ni/ZrO₂) for steam reforming of EG and achieved 93% EG conversion with H₂ yield of 47-64% at 400 °C.^[58] Zhang et al. explored Ni-based catalysts synthesized by co-precipitation and impregnation methods. They checked the effect of Ni loading, reaction temperature and support modification in the catalytic SREG reaction. They modified the Ni/CeO₂ catalyst by the addition of Al₂O₃, TiO₂ and ZrO₂ and found that the Ni/CeO₂-Al₂O₃ catalyst exhibited high catalytic performance to

achieve 94% EG conversion with 67% yield of H₂ gas at 250 °C in 24 h.^[67] Taghizadeh et al. studied catalytic performance and kinetic modelling in the SREG over Pd-Ni/KIT and obtained 99.8% conversion of EG with 71.3% yield of H₂ gas at 500 °C in 4 h.^[68] Cao et al. investigated steam reforming of EG over Ni-based catalyst supported over attapulgite. It showed conversion of EG (97.2%) and 71.2% of H₂ yield with the co-production of CH₄, CO and CO₂ over Ni/ATP_{GS} at 600 °C in 4 h. However, in 8 h a high yield of H₂ gas (80.8%) was achieved with 89.8 % conversion of EG over Ni/ATP_{GS} catalyst.^[69] Taghizadeh et al. reported Ni and Pt-based supported catalysts over γ -Al₂O₃. Results showed that 3%Pt-12%Ni/ γ - Al₂O₃ gave 96% EG conversion with 76.6% yield of H₂ gas at 450 °C in 1 h.^[70] Nichio and co-workers performed reforming reaction of EG over NiPt bimetallic catalyst supported over hydrotalcite (HT) and demonstrated that NiPt/HT catalyst is more active and selective towards H₂ than Ni/HT catalyst. They obtained 94% conversion of EG with 90.3% selectivity of H₂ gas at 600 °C in 2 h.^[71] Vaidya et al. explored Ru/Al₂O₃ catalyst for the SREG to produce H₂ gas and obtained only 13.6% conversion of EG and 36.4% selectivity of H₂ gas at 400 °C in 1 h.^[72] Yadav et al. explored Ni-Cu/mixed metal oxides (Ni-Cu/M-MgO, where M was CeO₂, La₂O₃, ZrO₂) for the reforming of EG. Out of these, the Ni-Cu/La₂O₃-MgO catalyst performed well over others and was found to be the most active and robust catalyst. They achieved 96% conversion of EG with 63.3% yield of H₂ gas at 500 °C in 2 h.^[73] Dagle et al. investigated 15 wt% Ni, 5 wt% Rh, and 15 wt% Co supported over MgAl₂O₄ for steam reforming of EG at 500 °C. Ni and Rh-based catalysts exhibited complete conversion of EG. However, only 42% conversion of EG was found in the case of Co/MgAl₂O₄ catalyst, but methane selectivity was found to be low (8%) as compared to Ni and Rh-based catalysts (~24%). This inferred that the Co/MgAl₂O₄ catalyst was a promising catalyst for the SREG reaction to produce a high yield of H₂ gas.^[74] The reaction pathway for the APR process of polyols is shown in Scheme 1.7. Firstly, reactant molecules adsorb and dehydrogenate over the catalyst active site, followed by C-C and C-O bond breaking to yield organic molecules, which are reformed into gaseous products that are finally desorbed from the catalytic active sites.



Scheme 1.7. Catalytic reaction pathway for steam reforming of EG. Adapted with permission from ref [63] of Springer Nature.

Table 1.4. Catalysts reported for hydrogen production through steam reforming of EG.

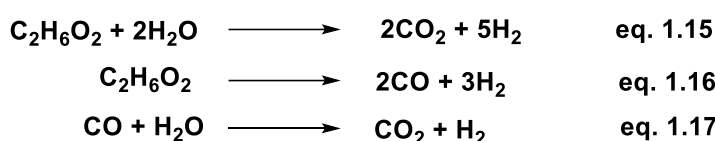
Entry	Catalyst	T(°C)/t(h)	Conv. (%)	H ₂ Yield/Sel. (%)	Reference
1	Ni/ γ -Al ₂ O ₃	400/2	96.5	47.1/-	58
2	Ni/CeO ₂ -Al ₂ O ₃	250/24	94	67/-	67
3	Pd-Ni/KIT-6	500/4	99.8	71.3/-	68
4	Ni/ATP _{JS}	600/8	89.8	80.8/-	69
5	3%Pt-12%Ni/ γ -Al ₂ O ₃	450/1	96	76.6/-	70
6	PtNi/HT	600/2	94	-/90.3	71
7	Ru/ γ -Al ₂ O ₃	400/1	13.6	-/36.4	72
8	NiCu/La ₂ O ₃ -MgO	500/2	96	63.3/-	73
9	Co/MgAl ₂ O ₄	500/-	42	-	74

1.4.1.2. Hydrogen production through aqueous phase reforming of ethylene glycol

Aqueous-phase reforming (APR) stands out as an energy-efficient process (>200 °C) for converting biomass-derived oxygenated compounds into hydrogen gas as compared to steam reforming and gasification reactions (requires high temperatures), which often entail numerous unwanted side reactions. Unlike these methods, APR doesn't require the vaporization of water and effectively reduces undesired decomposition reactions. Moreover, APR takes advantage of WGS reaction at lower temperatures, allowing for the simultaneous generation

of H₂ and CO₂ while minimizing the production of CO.^[75]

Several biomass-derived oxygenated compounds, including methanol, ethanol, sorbitol, glycerol, and ethylene glycol, have found utility in the APR process for hydrogen production.^[76] APR process not only involves the breaking of C–C bonds but also encompasses C–H bond scission to generate molecules for adsorption over the catalyst surface, notably the CO molecule, which subsequently undergoes WGS reaction to produce CO₂ and H₂ as shown in Scheme 1.8.^[77]



Scheme 1.8. Key reactions involved in the aqueous phase reforming of EG.^[76]

Therefore, selecting an appropriate catalyst for this reaction necessitates a preference for promoting C-C cleavage and WGS reactions while simultaneously inhibiting C-O bond scission and methanation reactions. A wide range of catalysts has been developed for APR of EG for the production of H₂ gas (Table 1.5). For example, Dumesic and co-workers reported Pt/Al₂O₃ catalyst for reforming of EG to achieve almost complete conversion of EG (99%) with 88% H₂ selectivity along with other gaseous products (CO₂ and alkanes) at 225 °C in 24 h.^[63] Further, Dumesic et al. also investigated the Raney Ni-Sn catalyst to produce H₂ gas from EG at 265 °C. They observed that the Raney Ni-Sn catalyst exhibited high selectivity for H₂ gas (96%) as compared to earlier reported Pt/Al₂O₃ catalyst (88% H₂ selectivity).^[78] They also explored Ni, Pd, Pt, Ru, Rh and Ir metal-based catalysts supported over silica for APR of EG at 210 °C and 225 °C and observed the production of different gaseous products (H₂, CO, CO₂, CH₄, ethane and higher paraffin). Rh, Ru, and Ni catalysts showed more inclination towards producing alkanes over generating hydrogen, displaying lower selectivity for the latter. Moreover, the Ni/SiO₂ catalyst underwent deactivation at 225 °C. Pt and Pd-based silica-supported catalysts showed high selectivity for H₂ gas and low selectivity for alkanes and were found to be promising catalysts for APR of EG.^[64] Nichio et al. also explored the APR of EG at 250 °C under 44 bar and obtained 58% conversion of EG and 56.1% selectivity for H₂ gas with the simultaneous

production of other gases such as CO, CO₂ and CH₄.^[71] Li et al. developed Ni/Zn/Al-derived hydrotalcite catalyst for APR of EG and achieved complete selectivity for H₂ gas with complete conversion of EG.^[75] Fan et al. synthesized Co/ZnO catalysts with varying ratios of Co and Zn and performed APR of EG. They observed that with the increase in Co/Zn ratio from 1:3 to 2:1, the selectivity of H₂ gas decreased from 89% to 52%, and selectivity towards hydrocarbons increased from 29% to 46%, while EG conversion also increased from 5.2% to 8.6%.^[79] Lin et al. explored the NiFe catalyst and checked the effect of Co addition for hydrogen production through APR of EG. They observed that NiFe catalyst exhibited better catalytic activity than Ni and Fe monometallic catalysts. However, the addition of Co into the NiFe catalyst enhanced the catalytic activity and achieved 95.1% EG conversion with 99.8% selectivity for H₂ gas at 225 °C in 3 h.^[80] Kim et al. developed Pt-Mn supported catalyst (Pt-Mn/CMK-3) for APR of EG and observed that alloying of Mn into the Pt/CMK-3 catalyst showed good H₂ yield (40%) compared to monometallic catalyst.^[81] Bitter et al. reported Ni, Co, Cu and Pt nanoparticles stabilized over carbon nanofiber (CNF) and performed aqueous phase reforming of EG at 230 °C. They observed that the H₂ selectivity was found to be decreased in the following order: Pt/CNF (53%)>Co/CNF (21%)>Ni/CNF (15%). In the case of Ni and Co, H₂ selectivity was low due to the methanation process. The formation of H₂ gas through the reforming process is associated with the co-production of liquid products such as glycolic acid, glycolaldehyde, acetic acid, formic acid, methanol, and ethanol. The Co/CNF catalyst was deactivated rapidly due to the formation of acid products.^[82]

Table 1.5. Catalysts reported for hydrogen production through aqueous phase reforming of EG.

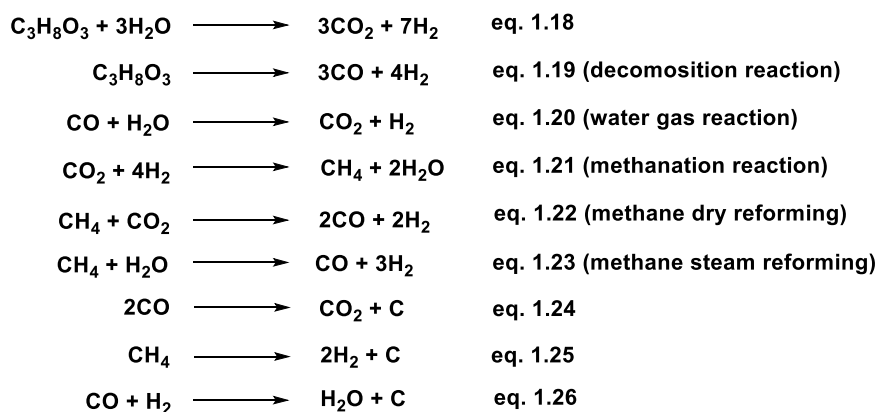
Entry	Catalyst	T(°C)/t(h)	Conv. (%)	H ₂ Yield/Sel. (%)	Reference
1	Pt/Al ₂ O ₃	265/24	99	-/88	63
2	Pd/SiO ₂	225/-	3.0	-/98.5	64
3	Ni-Pt/HT	250/4	58	-/56.1	71
4	Ni/Zn/Al-HT	225/2.5	99	-/100	75
5	Raney-NiSn	265/-	97	-/96	78
6	Co/ZnO	225/8	5.2	-/89	79
7	NiFeCo	225/3	95.1	-/99.8	80
8	Pt-Mn/CMK	250/-	40	40/-	81
9	Pt/CNF	230/24	45.7	-/53	82

1.4.2. Glycerol as a liquid hydrogen storage material

Industrial production of biodiesel through the transesterification of different oils and fats has become a vital strategy to enhance society's energy security and promote sustainability. During biodiesel production, a major by-product, glycerol, is formed, which is 10 wt% of biodiesel.^[83] Currently, the predominant method for disposing of excess glycerol from biodiesel production is incineration, which results in a substantial environmental impact on both biodiesel manufacturing and the biofuel supply chain, particularly in Europe, where millions of metric tons are incinerated annually. Therefore, there is a pressing need to explore alternative, more environmentally friendly solutions for handling surplus glycerol. These alternative approaches not only aim to mitigate the environmental consequences associated with incineration but also seek to enhance the economic viability of biodiesel production. To address this challenge, researchers have proposed various catalytic pathways, including reforming process, dehydrogenation, oxidation, dehydration, and esterification.^[84]

1.4.2.1. Hydrogen production through steam reforming of glycerol

Steam reforming of methane (SRM) is a prevailing technology in the industry for hydrogen production. However, an appealing alternative route for generating hydrogen-rich synthesis gas (a mixture of H₂ and CO) involves the steam reforming of glycerol (SRG).^[85] Conversely, SRG is a thermochemical process capable of producing various product compositions, whether in gaseous or liquid phases. This versatility depends on the careful selection of catalyst composition, support type, and the specific reaction conditions used for transforming glycerol (GLY) into the desired products. In the SRG reaction, each mole of GLY holds the theoretical capability to yield seven moles of hydrogen (9.6 wt%). Steam reforming of GLY involves a complex interplay of reactions (as shown in eq. 1.18). It encompasses the decomposition of GLY (eq. 1.19) and the WGS reaction (eq. 1.20). Nevertheless, this existing process is intricate due to the occurrence of several concurrent reactions. These also include the methanation reaction (eq. 1.21), methane dry and steam reforming reactions (eq. 1.22 and 1.23) under specific operating conditions, and various carbon formation reactions (eq. 1.24-1.26) may also take place.^[86-87]



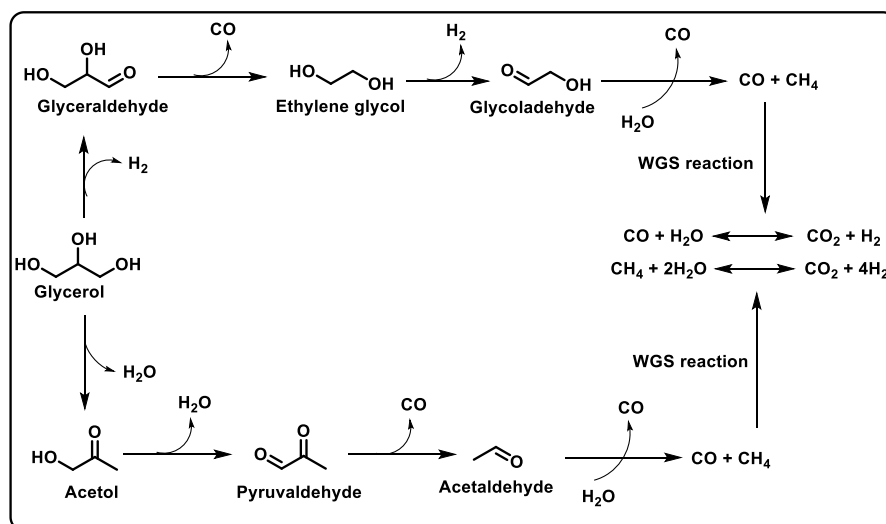
Scheme 1.9. Key reactions involved in the steam reforming of glycerol.^[86-87]

H₂ gas production through SRG is significantly affected by two key factors: reaction temperature and the ratio of water to GLY. It is very crucial to design and synthesize the catalysts to possess the capability of breaking C-C, O-H, and C-H bonds and facilitating the WGS reaction in the SRG. The performance and durability of a catalyst depend not just on the active metal used but also on the support material chosen. In most cases, achieving a high

dispersion of the active metal is desirable, and this is facilitated by using support material having a high surface area and the ability to possess strong metal-support interactions (SMSI).

In literature, most of the catalytic reactions for the transformation of GLY through reforming processes have primarily concentrated on Ru,^[88-91] Pt,^[92-94] Ir,^[95] and Pd-based catalysts (Table 1.6).^[96] For instance, Hirai et al. developed Ru/Y₂O₃ catalyst and observed complete conversion of GLY with 90% H₂ yield at 600 °C along with other gases (CO, CO₂ and CH₄).^[88] Adhikari et al. explored Ru/Al₂O₃ catalyst for the SR of GLY at 900 °C and observed only 58% conversion of GLY with 42% yield of H₂ gas.^[89] Vaidya et al. reported the kinetics of steam reforming of GLY over the Ru/Al₂O₃ catalyst at 350-500 °C. They performed reaction at 500 °C for 2 h and obtained 50% GLY conversion with the H₂ yield of 58.3% with co-production of CO (7.2%), CO₂ (34.2%), and CH₄ (0.3%).^[90] In the similar direction, Kousi et al. explored modified Ru/Al₂O₃ catalysts for GLY reforming and observed 93%, 85%, and 57% conversion of GLY over Ru/Al₂O₃, Ru/B₂O₃-Al₂O₃ and Ru/MgO-Al₂O₃ catalysts at 600 °C respectively with the H₂ yield of ~68% along with other gases (CO, CO₂ and CH₄).^[91] Santo and co-workers investigated the promotional effect of Mn in the Pt/C catalyst for SRG reaction. Firstly, they carried out a catalytic reaction over Pt/C catalyst and observed only 26% conversion of GLY with 36.9% selectivity of H₂ gas at 225 °C in 1 h. Further, introducing Mn into the Pt/C catalyst, significant enhancement in the GLY conversion (78.2%) and decrease in the H₂ selectivity (25.2%) was observed along with the generation of various gaseous (CO, CO₂ or CH₄) and liquid products (EG, acetaldehyde, acetol, and other alcohols).^[92] Buffoni et al. explored Pt catalyst supported over SiO₂-C composite material for the steam reforming of GLY. They carried out reforming reaction at 450 °C for 2 h and obtained 83% conversion of GLY with 51% selectivity of H₂ gas.^[93] Fraga et al. developed a Pt catalyst supported over layered double hydroxide for SRG and achieved complete conversion of GLY with 68% selectivity of H₂ gas at 350 °C in 40 h.^[94] Pompeo and co-workers reported Pt and Ni-based catalysts supported over SiO₂ with various metal loading for SRG reaction at 350-450 °C. They found that the Pt/SiO₂ catalyst gave a complete conversion of GLY(>99%) with 70% selectivity of H₂ gas than the Ni/SiO₂ catalyst.^[71] Shen

et al. investigated Ir/CeO₂ catalyst for SRG to produce H₂ gas at 400-550 °C and achieved >99% GLY conversion even at 400 °C with 85% H₂ gas selectivity.^[95] Shaibani et al. reported the SRG reaction for hydrogen gas production over Pd/Al₂O₃ catalyst and obtained 78.9% GLY conversion with 78.7% H₂ selectivity at 600 °C in 2 h.^[96] Highly effective noble metal-based catalysts, although known for their superior catalytic activity and carbon reduction in steam reforming reactions, are often limited in use due to their high cost. On the other hand, Ni-based catalytic systems have been explored with various supports such as Al₂O₃, La₂O₃, SiO₂, CeO₂, and ZrO₂.^[97-100] Ni-based catalysts exhibit proficiency in the breaking of C-C, O-H, and C-H bonds, as well as facilitating dehydrogenation and hydrogenation reactions. However, a significant challenge arises due to the high reaction temperatures, leading to carbon deposition, coking, and sintering of Ni metal, ultimately resulting in the deactivation of the catalytic system.^[95-96]



Scheme 1.10. Catalytic reaction pathway for steam reforming of GLY. Reprinted with permission from ref [97] of Royal Society of Chemistry.

Table 1.6. Catalysts reported for hydrogen production through steam reforming of GLY.

Entry	Catalyst	T(°C)/t(h)	Conv. (%)	H ₂ Yield/Sel. (%)	Reference
1	Ru/Y ₂ O ₃	600/24	>99	-/90	88
2	Ru/Al ₂ O ₃	900/-	58	42/-	89
3	Ru/Al ₂ O ₃	500/2	50	58.3/-	90
4	Ru/Al ₂ O ₃	600/-	93	68/-	91
5	Pt-Mn/C	225/1	78.2	25.2/-	92
6	Pt/SiO ₂ -C	450/2	83	51/-	93
7	Pt/LDH (Mg/Al)	350/40	>99	-/68	94
8	Pt/SiO ₂	450/2	>99	-/70	71
9	Ir/CeO ₂	400-550/-	>99	-/>85	95
10	Pd/Al ₂ O ₃	600/2	78.9	-/78.7	96

1.4.2.2. Hydrogen production through aqueous phase reforming of glycerol

Despite its promising features, the APR process also has several limitations, such as uncontrolled methanation on metal catalysts, which is a significant challenge for achieving high H₂ selectivity. Among the various monometallic catalysts considered, Pt-based catalysts stand out as a preferable choice for APR reactions due to their remarkable ability to facilitate C–C bond cleavage.^[101] Various Pt-based catalysts, including Pt/Al₂O₃,^[63] Pt-Re/C,^[101] Pt/MgO,^[102] Pt-Mo/C,^[103] Pt-Cu/Mg(Al)O,^[104] Pt-KHT/28,^[105] Pt-Ni/MWCNT,^[106] and PtFe/γ-Al₂O₃,^[107] already have been explored by various research teams for the APR of glycerol in the temperature ranging from 200-250 °C (Table 1.7). For instance, Dumesic et al. explored Pt/Al₂O₃ catalyst for APR of GLY and obtained 83% conversion of GLY with 75% H₂ selectivity along with other gaseous products (CO₂ and alkanes) at 225 °C in 24 h.^[63] Wang et al. studied the hydrogen generation from APR of GLY over Pt-Re/C using KOH or without KOH. The Pt/C was found to be very selective for H₂ gas, but activity was very low. Further, the addition of Re in the Pt/C catalyst resulted in significant enhancement of the catalytic activity with 58.5% GLY conversion and 24.5% H₂ selectivity at 225 °C over 3%Pt-3%Re/C using KOH.^[101] Tian and co-workers investigated the effect of various Pt-supported catalysts for hydrogen

production through APR of GLY. It was observed that Pt-based supported catalysts followed the order in terms of catalytic activity, Pt/Al₂O₃ > Pt/MgO > Pt/SiO₂ > Pt/HUSY > Pt/AC > Pt/SAPO-11. Neutral and acidic supports favored alkane formation, while basic supports showed high catalytic activity and hydrogen production rates. Pt/MgO demonstrated superior hydrogen selectivity, achieving a 13.8% GLY conversion with 79.9% selectivity for H₂.^[102] Basic supports exhibited high catalytic activity and higher hydrogen production rate, while acidic and neutral supports helped the alkane formation. Out of these, Pt/MgO performed well in terms of hydrogen selectivity over others and observed 13.8% GLY conversion with 79.9% H₂ selectivity.^[102] Nozawa and co-workers carried out ethanol reforming over different supported catalysts and found an increase in the catalytic activity in the order of Ir < Pt < Rh < Ru.^[108] This observation has sparked interest in exploring ruthenium-based catalysts for APR of biomass-derived oxygenated hydrocarbons. Ruthenium stands out among noble metals for its cost-effectiveness and excellent capability to cleave C–C bonds. Despite these qualities, its use in APR reactions is restricted due to its lower catalytic performance compared to platinum-based catalysts. Recently, Raja et al. developed Ru catalysts supported over N-doped mesoporous carbon (Ru-NMC-3 and RuPt-NMC-3) for APR of GLY and achieved 92% conversion of GLY with 88.5% H₂ selectivity at 250 °C.^[109] Similarly, they also explored Ru/NaY catalyst for APR of GLY at 250 °C under N₂ pressure (600 psi), exhibiting 88.1% GLY conversion with 74% H₂ selectivity along with high CO₂ contamination up to 24%.^[110]

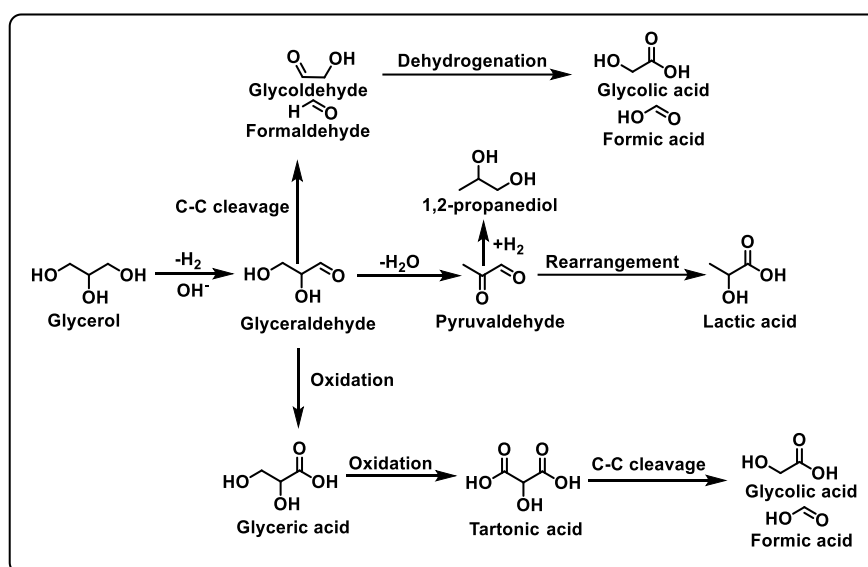
Table 1.7. Catalysts reported for hydrogen production through aqueous phase reforming of GLY.

Entry	Catalyst	T(°C)/t(h)	Conv. (%)	Sel. of H ₂ (%)	Reference
1	Pt/Al ₂ O ₃	225/24	83	75	63
2	Pt-Re/C	225/2	58.5	24.5	101
3	Pt/MgO	230/4	13.8	79.9	102
4	Pt-Mo/C	230/720	26	55.3	103
5	Pt-Cu/Mg(Al)O	200/5	98	55.3	104
6	Pt-KHT/28	250/4	83	67.4	105
7	Pt-Ni/MWCNT	250/-	99	90.9	106
8	Pt-Fe/ γ - Al ₂ O ₃	225/-	66	45.8	109
9	Ru-NMC-3	250/12	92	88.5	109
10	RuPt-NMC-3	250/12	87.9	82.2	109
11	Ru/NaY	250/12	88.1	68.1	110

1.5. Catalytic transformation of glycerol to hydrogen gas and lactic acid

GLY has the potential to undergo various valuable chemical transformations to produce glyceric acid, ethylene glycol, glyceraldehyde, lactic acid, propanediol, acrolein, glycolic acid, etc.^[84] Among these, lactic acid holds significant importance in industries, functioning as an acidulant and preservative in the food sector, finding applications in cosmetics and pharmaceuticals, and serving as a fundamental building block for the biodegradable plastic known as polylactic acid (PLA).^[111] LA is industrially manufactured through two primary methods: anaerobic fermentation of carbohydrates and chemical synthesis. However, the fermentation process has several disadvantages, including extended reaction times and complex separation and purification procedures. On the other hand, chemical synthesis involving HCN and CH₃CHO can be used to produce lactic acid, but its ecological impact has led to reduced interest in this method.^[112] Even though the dehydrogenative method for converting GLY to LA is an appealing choice to generate both H₂ gas and LA, most of the research focuses on the oxidative conversion of GLY to LA employing Cu, Ni, Au, or Pd-based catalysts.^[113-114] During the former process, excessive oxidation of glyceraldehyde produces glyceric acid, tartaric acid, and glycolic acid (GA) along with LA, which dramatically decreases the selectivity of the

desired LA product. Anaerobic transformation of GLY offers an advantage by circumventing overoxidation reactions and concurrently generating hydrogen gas (H_2), a clean energy carrier and LA. Scheme 1.11 shows the possible products formed by the catalytic transformation of GLY.



Scheme 1.11. Plausible pathways for the catalytic conversion of GLY to H_2 gas and valuable co-products.

In recent years, we have witnessed the emergence of a combined dehydrogenation and transfer hydrogenation approach in the catalytic transformation of glycerol over heterogeneous-based catalytic systems.^[115-116] Tang et al. reported the catalytic conversion of GLY to LA, coupled with the transfer hydrogenation of cyclohexene to cyclohexane over the Pt/ZrO₂ catalyst.^[115] They achieved a remarkable 96% GLY conversion with a high yield of LA (95%) and a selectivity of 36% towards cyclohexane at 160 °C in 4.5 h under N₂ pressure (20 bar). Oberhauser et al. successfully developed a Pt-based catalyst supported over Ketjenblack (C^k) for the transformation of glycerol to LA and achieved complete conversion of GLY with 95% yield of LA in 6 h at 140 °C using ethylene gas as an H₂ acceptor to prevent undesired hydrogenation reactions.^[116]

Hence, the above-mentioned reports clearly showed that glycerol could be explored as a viable liquid hydrogen storage material (LHSM), but it has gained limited attention for hydrogen production over heterogeneous catalysts.

1.6. Research gaps for hydrogen production from polyols

- Extensive research has been focused on hydrogen production from polyols like ethylene glycol and glycerol through APR and SR processes, albeit at elevated reaction temperatures (>250 °C).
- Notably, Pt-based catalytic systems have been employed in these processes, but the high cost associated with these necessitates the development of cost-effective catalytic systems capable of operating at lower temperatures.
- APR and SR processes suffer from several drawbacks, such as the purity of hydrogen gas being compromised due to the co-production of other gases (CO_x and alkanes), and the overall hydrogen yield remains suboptimal. Consequently, the hydrogen gas produced cannot be directly utilized in fuel cells.
- Catalytic transformations of these polyols to yield hydrogen gas have been investigated in detail, but the co-production of valuable platform chemicals has received limited attention to date.

1.7. Objectives of the thesis

- To develop ruthenium-based heterogeneous catalysts that can efficiently facilitate H₂ gas production from C-2 and C-3 based polyols i.e., ethylene glycol and glycerol, under ambient reaction conditions.
- To employ various spectroscopic techniques to characterize the synthesized catalysts comprehensively.
- To produce high-purity hydrogen gas without any contaminants of other gases such as CO, CO₂, and alkanes under mild reaction conditions so that it can be directly utilized in fuel cell applications.
- Thoroughly investigate the reaction pathways in the dehydrogenation of polyols by performing time-dependent and controlled experiments.
- To scale up the developed catalytic system to enable its recyclability and bulk-scale experiments.

1.8. Organization of the thesis

This thesis consists of six chapters.

Chapter 1 introduces hydrogen production from various resources, storage, and its applications. This chapter also includes the relevant literature survey for the hydrogen gas production from C-2 and C-3 based polyols i.e., ethylene glycol and glycerol over various heterogeneous catalysts.

Chapter 2 presents the selective H₂ gas generation from aqueous glycerol over the ruthenium catalyst. Further, the effect of base concentration, temperature, and different types of bases in tuning the catalytic activity for the catalytic reaction is also investigated in detail.

Chapter 3 describes the investigation of the role of support in the catalytic conversion of glycerol into H₂ gas and lactic acid in water over the supported Ru catalyst. Moreover, various supported catalysts have been explored to achieve a high yield of H₂ gas and lactic acid.

Chapter 4 involves the selective catalytic conversion of ethylene glycol to H₂ gas. The effect of different reaction parameters (base concentration, type of bases, temperature effect) was investigated to optimize the best catalytic reaction condition to produce hydrogen gas efficiently. Moreover, time-dependent and controlled experiments have been performed to explain the plausible reaction pathway for H₂ gas production from ethylene glycol.

Chapter 5 demonstrates the selective production of H₂ gas from ethylene glycol through the upcycling of PET-based plastic waste over Ru catalyst at low temperatures in water with a high yield of formic acid and terephthalic acid.

Chapter 6 summarizes the work presented in this thesis, including the findings and future scope of the work.

1.9. References

1. Bockris J. O. M., (2013), The Hydrogen Economy: Its History, *Int. J. Hydrog. Energy*, 38, 2579-2588 (DOI: 10.1016/j.ijhydene.2012.12.026)
2. IEA (2023), *World Energy Outlook 2023*, 1-355
3. Uddin K., (2019), Nuclear Energy, Environment and Public Safety: North-South Politics. *Strateg. Plan. Energy Environ.*, 38, 31-41 (DOI:

10.1080/10485236.2019.12054410)

4. Kleijne K., Hanssen S. V., Dinteren L. M., Huijbregts A.J., Zelm R., Coninck H., (2022), Limits to Paris Compatibility of CO₂ Capture and Utilization, *One Earth*, 5, 168-185 (DOI: 10.1016/j.oneear.2022.01.006)
5. Singh S., Jain S., Ps V., Tiwari A. K., Nouni M. R., Pandey J. K., Goel S., (2015), Hydrogen: A Sustainable Fuel for Future of the Transport Sector, *Renew. Sustain. Energy Rev.*, 51, 623-633 (DOI: 10.1016/j.rser.2015.06.040)
6. Dunn S., (2022), Hydrogen Futures: Toward a Sustainable Energy System, *Int. J. Hydrog. Energy*, 27, 235-264 (DOI: 10.1016/S0360-3199(01)00131-8)
7. Midilli A., Ay M., Dincer I., Rosen M. A., (2005), On Hydrogen and Hydrog. Energy Strategies I : Current Status and Needs, *Renew. Sustain. Energy Rev.*, 9, 255–271 (DOI: 10.1016/j.rser.2004.05.003)
8. El-Shafie M., Kambara S., Hayakawa Y., (2019), Hydrogen Production Technologies Overview. *J. Power Energy Eng.*, 7, 107-154 (DOI: 10.4236/jpee.2019.71007)
9. Hwang H. T., Varma A., (2014), Hydrogen Storage for Fuel Cell Vehicles, *Curr. Opin. Chem. Eng.*, 5, 42-48 (DOI: 10.1016/j.coche.2014.04.004)
10. Handwerker M., Wellnitz J., Marzbani H., (2021), Comparison of Hydrogen Power trains with the Battery Powered Electric Vehicle and Investigation of Small-Scale Local Hydrogen Production Using Renewable Energy, *Hydrogen*, 2, 76-100 (DOI: 10.3390/hydrogen2010005)
11. Paul A., Shukla N., Paul S. K., Trianni A., (2021), Sustainable Supply Chain Management and Multi-Criteria Decision-Making Methods: A Systematic Review. *Sustain.*, 13, 7104 (DOI: 10.3390/su13137104)
12. Uddin M. N., Nageshkar V. V., Asmatulu R., (2020), Improving Water-Splitting Efficiency of Water Electrolysis Process via Highly Conductive Nanomaterials at Lower Voltages, *Energy, Ecol. Environ.*, 5, 108-117 (DOI: 10.1007/s40974-020-00147-5)
13. Nikolaidis P., Poullikkas A., (2017), A Comparative Overview of Hydrogen Production Processes, *Renew. Sustain. Energy Rev.*, 67, 597-

611 (DOI: 10.1016/j.rser.2016.09.044)

14. Amin M., Shah H. H., Fareed A. G., Khan W. U., Chung E., Zia A., Rahman Farooqi Z. U., Lee C., (2022), Hydrogen Production through Renewable and Non-Renewable Energy Processes and Their Impact on Climate Change, *Int. J. Hydrog. Energy*, 47, 33112-33134 (DOI: 1016/j.ijhydene.2022.07.172)
15. Lipman T. E., (2019), Hydrogen Production Science and Technology. *Fuel Cells, Hydrog. Prod.*, 274, 783-798 (DOI: 10.1007/978-1-4939-7789-5-755)
16. Hariharan D., Yang R., Zhou Y., Gainey B., Mamalis S., Smith R. E., Lugo-Pimentel M. A., Castaldi M. J., Gill R., Davis A., Modroukas D., Lawler B., (2019), Catalytic Partial Oxidation Reforming of Diesel, Gasoline, and Natural Gas for Use in Low Temperature Combustion Engines, *Fuel*, 246, 295-307 (DOI: 10.1016/j.fuel.2019.02.003)
17. Kim J., Park J., Qi M., Lee I., Moon I., (2021), Process Integration of an Autothermal Reforming Hydrogen Production System with Cryogenic Air Separation and Carbon Dioxide Capture Using Liquefied Natural Gas Cold Energy, *Ind. Eng. Chem. Res.*, 60, 7257-7274 (DOI: 10.1021/acs.iecr.0c06265)
18. Baruah R., Dixit M., Basarkar P., Parikh D., Bhargav A., (2015), Advances in Ethanol Autothermal Reforming, *Renew. Sustain. Energy Rev.*, 51, 1345–1353 (DOI: 10.1016/j.rser.2015.07.060)
19. Wang S., Dai G., Yang H., Luo Z., (2017), Lignocellulosic Biomass Pyrolysis Mechanism: A State-of-the-Art Review, *Prog. Energy Combust. Sci.*, 62, 33-86 (DOI: 10.1016/j.pecs.2017.05.004)
20. Schneider S., Bajohr S., Graf F., Kolb T., (2020), State of the Art of Hydrogen Production via Pyrolysis of Natural Gas, *Chemie-Ingenieur-Technik*, 92, 1023-1032 (DOI:10.1002/cite.202000021)
21. Mularski J., Pawlak-Kruczek H., Modlinski N., (2020), A Review of Recent Studies of the CFD Modelling of Coal Gasification in Entrained Flow Gasifiers, Covering Devolatilization, Gas-Phase Reactions, Surface Reactions, Models and Kinetics, *Fuel*, 271, 117620 (DOI: 10.1016/j.fuel.2020.117620)
22. Hosseini S. E., Wahid M. A., (2016), Hydrogen Production from

- Renewable and Sustainable Energy Resources: Promising Green Energy Carrier for Clean Development, *Renew. Sustain. Energy Rev.*, 57, 850-866 (DOI: 10.1016/j.rser.2015.12.112)
23. Safari F., Dincer I., (2020), A Review and Comparative Evaluation of Thermochemical Water Splitting Cycles for Hydrogen Production, *Energy Convers. Manag.*, 205, 112182 (DOI: 10.1016/j.enconman.2019.112182)
 24. Dincer I., Zamfirescu C., (2012), Sustainable Hydrogen Production Options and the Role of IAHE, *Int. J. Hydrog. Energy*, 37, 16266-16286 (DOI: 10.1016/j.ijhydene.2012.02.133)
 25. Terlouw T., Bauer C., McKenna R., Mazzotti M., (2022) Large-Scale Hydrogen Production via Water Electrolysis: A Techno-Economic and Environmental Assessment, *Energy Environ. Sci.*, 15, 3583-3602 (DOI: 10.1039/d2ee01023b)
 26. Hu K., Fang J., Ai X., Huang D., Zhong Z., Yang X., Wang L., (2022) Comparative study of alkaline water electrolysis, proton exchange membrane water electrolysis and solid oxide electrolysis through multiphysics modeling, *Appl. Energy*, 312, 118788 (DOI: 10.1016/j.apenergy.2022.118788)
 27. Emam A. S., Hamdan M. O., Abu-Nabah B. A., Elnajjar E., (2024) A review on recent trends, challenges, and innovations in alkaline water electrolysis, *Int. J. Hydrog. Energy*, 64, 599-625 (DOI: 10.1016/j.ijhydene.2024.03.238)
 28. Abanades S., (2019), Metal Oxides Applied to Thermochemical Water-Splitting for Hydrogen Production Using Concentrated Solar Energy, *Chem Engineering*, 3, 1-28 (DOI: 10.3390/chemengineering3030063)
 29. Ikuero T., Bade S. B., Akinmoladun A., Oni B. A., (2024) The integration of wind and solar power to water electrolyzer for green hydrogen production, *Int. J. Hydrog. Energy*, (DOI: 10.1016/j.ijhydene.2024.02.139)
 30. Saraswat S. K., Rodene D. D., Gupta R. B., (2018) Recent advancements in semiconductor materials for photoelectrochemical water splitting for hydrogen production using visible light, 89, 228-248 (DOI: 10.1016/j.rser.2018.03.063)

31. Ong H. C., Chen W. H., Farooq A., Gan Y. Y., Lee K. T., Ashokkumar V., (2019), Catalytic Thermochemical Conversion of Biomass for Biofuel Production: A Comprehensive Review, *Renew. Sustain. Energy Rev.*, 113, 109266 (DOI: 10.1016/j.rser.2019.109266)
32. Uddin M. N., Techato K., Taweekun J., Rahman M. M., Rasul M. G., Mahlia T. M. I., Ashrafur S. M., (2018), An Overview of Recent Developments in Biomass Pyrolysis Technologies, *Energies*, 11, 3115 (DOI: 10.3390/en11113115)
33. Hossain M. A., Jewaratnam J., Ganesan P., (2016), Prospect of Hydrogen Production from Oil Palm Biomass by Thermochemical Process – A Review, *Int. J. Hydrog. Energy*, 41, 16637–16655 (DOI: 10.1016/j.ijhydene.2016.07.104)
34. Patel M., Zhang X., Kumar A., (2016), Techno-Economic and Life Cycle Assessment on Lignocellulosic Biomass Thermochemical Conversion Technologies: A Review, *Renew. Sustain. Energy Rev.*, 53, 1486-1499 (DOI: 10.1016/j.rser.2015.09.070)
35. Gollakota A. R. K., Kishore N., Gu, S., (2017), A Review on Hydrothermal Liquefaction of Biomass, *Renew. Sustain. Energy Rev.*, 81, 1378-1392 (DOI: 10.1016/j.rser.2017.05.178)
36. Argun H., Kargi, F., (2011), Bio-Hydrogen Production by Different Operational Modes of Dark and Photo-Fermentation: An Overview, *Int. J. Hydrog. Energy*, 36, 7443-7459 (DOI: 10.1016/j.ijhydene.2011.03.116)
37. Ahluwalia R. K., Roh H. S., Peng J. K., Papadias D., Baird A. R., Hecht E. S., Ehrhart B. D., Muna A., Ronevich J. A., Houchins C., Killingsworth N. J., Aceves, S. M., (2023), Liquid Hydrogen Storage System for Heavy Duty Trucks: Configuration, Performance, Cost, and Safety, *Int. J. Hydrog. Energy*, 48, 13308-13323 (DOI: 10.1016/j.ijhydene.2022.12.152)
38. Wan Z., Tao Y., Shao J., Zhang Y., You H., (2021), Ammonia as an Effective Hydrogen Carrier and a Clean Fuel for Solid Oxide Fuel Cells, *Energy Convers. Manag.*, 228, 113729 (DOI: 10.1016/j.enconman.2020.113729)

39. Zheng J., Zhou H., Wang C. G., Ye E., Xu J. W., Loh X. J., Li Z., (2021), Current Research Progress and Perspectives on Liquid Hydrogen Rich Molecules in Sustainable Hydrogen Storage, *Energy Storage Mater.*, 35, 695-722 (DOI: 10.1016/j.ensm.2020.12.007)
40. Griffiths S., Sovacool B. K., Kim J., Bazilian M., Uratani J. M., (2021), Industrial Decarbonization via Hydrogen: A Critical and Systematic Review of Developments, Socio-Technical Systems and Policy Options, *Energy Res. Soc. Sci.*, 80, 102208 (DOI: 10.1016/j.erss.2021.102208)
41. Muthukumar P., Kumar A., Afzal M., Bhogilla S., Sharma P., Parida A., Jana S., Kumar E. A., Pai R. K., Jain I. P., (2023), Review on Large-Scale Hydrogen Storage Systems for Better Sustainability, *Int. J. Hydrog. Energy*, 48, 33223 (DOI: 10.1016/j.ijhydene.2023.04.304)
42. Eberle U., Felderhoff M., Schüth F., (2009), Chemical and Physical Solutions for Hydrogen Storage, *Angew. Chem. Int. Ed.*, 48, 6608-6630 (DOI: 10.1002/anie.200806293)
43. Züttel A., (2003), Materials for Hydrogen Storage, *Mater. Today*, 6, 24-33 (DOI:10.1016/S1369-7021(03)00922-2)
44. Bogdanović B., Schwickardi M., (1997), Ti-Doped Alkali Metal Aluminium Hydrides as Potential Novel Reversible Hydrogen Storage Materials, *J. Alloys Compd.*, 254, 1-9 (DOI: 10.1016/S0925-8388(96)03049-6)
45. Jain I. P., Jain P., Jain A., (2010), Novel Hydrogen Storage Materials: A Review of Lightweight Complex Hydrides, *J. Alloys Compd.* 503, 303-339 (DOI: 1016/j.jallcom.2010.04.250)
46. Song Y., Guo Z. X., (2006), Electronic Structure, Stability and Bonding of the Li-N-H Hydrogen Storage System, *Phys. Rev. B.*, 74, 1-7 (DOI: 10.1103/PhysRevB.74.195120)
47. Principi G., Agresti F., Maddalena A., Lo Russo S., (2009), The Problem of Solid-State Hydrogen Storage, *Energy*, 34, 2087-2091 (DOI: 10.1016/j.energy.2008.08.027)
48. Qu D., (2008), Investigation of Hydrogen Physisorption Active Sites on the Surface of Porous Carbonaceous Materials, *Chem. A Eur. J.*, 14, 1040-1046 (DOI: 10.1002/chem.200701042)
49. Chen Z., Kirlikovali K. O., Idrees K. B., Wasson M. C., Farha O. K.,

- (2022), Porous Materials for Hydrogen Storage, *Chem*, 8, 693-716 (DOI: 10.1016/j.chempr.2022.01.012)
50. Yadav M., Xu Q., (2012), Liquid-Phase Chemical Hydrogen Storage Materials, *Energy Environ. Sci.*, 5, 9698-9725 (DOI: 10.1039/c2ee22937d)
51. Lu Z. H., Yao Q., Zhang Z., Yang Y., Chen X., (2014), Nanocatalysts for Hydrogen Generation from Ammonia Borane and Hydrazine Borane, *J. Nanomater.*, 2014, 1-12 (DOI: 10.1155/2014/729029)
52. Awasthi M. K., Rai R. K., Behrens S., Singh S. K., (2021), Low-Temperature Hydrogen Production from Methanol over a Ruthenium Catalyst in Water, *Catal. Sci. Technol.*, 11, 136-142 (DOI: 10.1039/d0cy01470b)
53. Patra S., Singh S. K., (2020), Hydrogen Production from Formic Acid and Formaldehyde over Ruthenium Catalysts in Water, *Inorg. Chem.*, 59, 4234-4243 (DOI: 10.1021/acs.inorgchem.9b02882)
54. Singh S. K., Xu Q., (2013), Nanocatalysts for Hydrogen Generation from Hydrazine, *Catal. Sci. Technol.*, 3, 1889-1900 (DOI: 10.1039/c3cy00101f)
55. Huang C., Yu Y., Yang J., Yan Y., Wang D., Hu F., Wang X., Zhang R., Feng G., (2019), Ru/La₂O₃ Catalyst for Ammonia Decomposition to Hydrogen, *Appl. Surf. Sci.*, 476, 928-936 (DOI: 10.1016/j.apsusc.2019.01.112)
56. Zou Y. Q., von Wolff N., Anaby A., Xie Y., Milstein D., (2019), Ethylene Glycol as an Efficient and Reversible Liquid-Organic Hydrogen Carrier, *Nat. Catal.*, 2, 415-422 (DOI: 10.1038/s41929-019-0265-z)
57. Werpy T., Petersen G., (2004), Top Value-Added Chemicals from Biomass, 76 (DOI: 10.2172/15008859)
58. Li S., Zhang C., Zhang P., Wu G., Ma X., Gong J., (2012), On the Origin of Reactivity of Steam Reforming of Ethylene Glycol on Supported Ni Catalysts, *Phys. Chem. Chem. Phys.*, 14, 4066-4069 (DOI: 10.1039/c2cp24089k)
59. Nguyen L. Q., Abella L. C., Gallardo S. M., Hinode H., (2008), Effect of Nickel Loading on the Activity of Ni/ZrO₂ for Methane Steam

- Reforming at Low Temperature, *React. Kinet. Catal. Lett.*, 93, 227-232 (DOI: 10.1007/s11144-008-5253-2)
60. Barbelli M. L., Pompeo F., Santori G. F., Nichio N. N., (2013), Pt Catalyst Supported on α -Al₂O₃ Modified with CeO₂ and ZrO₂ for Aqueous-Phase-Reforming of Glycerol, *Catal. Today*, 213, 58-64 (DOI: 10.1016/j.cattod.2013.02.023)
 61. Simpson A. P., Lutz A. E., (2007), Exergy Analysis of Hydrogen Production via Steam Methane Reforming, *Int. J. Hydrog. Energy*, 32, 4811-4820 (DOI: 10.1016/j.ijhydene.2007.08.025)
 62. Boskovic G., Baerns M., (2004), Catalyst Deactivation, *Springer Ser. Chem. Phys.*, 75, 477-503 (DOI: 10.1007/978-3-662-05981-4-14)
 63. Cortright R. D., Davda R. R., Dumesic J. A., (2002), Hydrogen from Catalytic Reforming of Biomass-Derived Hydrocarbons in Liquid Water, *Nature*, 418, 964-967 (DOI: 10.1038/nature01009)
 64. Davda R. R., Shabaker J. W., Huber G. W., Cortright R. D., Dumesic J. A., (2003), Aqueous-Phase Reforming of Ethylene Glycol on Silica-Supported Metal Catalysts, *Appl. Catal. B Environ.*, 43, 13-26 (DOI: 10.1016/S0926-3373(02)00277-1)
 65. Yue H., Zhao Y., Ma X., Gong J., (2012), Ethylene Glycol: Properties, Synthesis, and Applications, *Chem. Soc. Rev.*, 41, 4218-4244 (DOI: 10.1039/c2cs15359a)
 66. Genta M., Iwaya T., Sasaki M., Goto M., Hirose T., (2005), Depolymerization Mechanism of Poly(Ethylene Terephthalate) in Supercritical Methanol, *Ind. Eng. Chem. Res.*, 44, 3894-3900 (DOI: 10.1021/ie0488187)
 67. Zhao X. L., Lü Y. A., Liao W. P., Jin M. S., Suo Z. H., (2015), Hydrogen Production from Steam Reforming of Ethylene Glycol over Supported Nickel Catalysts, *J. Fuel Chem. Technol.*, 43, 581-588 (DOI: 10.1016/s1872-5813(15)30017-7)
 68. Eleat D., Taghizadeh M., (2022), Catalytic Performance and Kinetic Modeling of Ethylene Glycol Steam Reforming over Surfactant-Modified Pd–Ni/KIT-6, *Int. J. Hydrog. Energy*, 47, 11456-11471 (DOI: 10.1016/j.ijhydene.2022.01.196)
 69. Wang Y., Chen M., Li X., Yang Z., Liang T., Zhou Z., Cao Y., (2018),

- Hydrogen Production via Steam Reforming of Ethylene Glycol over Attapulgite Supported Nickel Catalysts, *Int. J. Hydrog. Energy*, 43, 20438-20450 (DOI: 10.1016/j.ijhydene.2018.09.109)
70. Kiadehi A. D., Taghizadeh M., (2018), Evaluation of a Micro-Channel Reactor for Steam Reforming of Ethylene Glycol: A Comparative Study of Catalytic Activity of Pt or/and Ni Supported γ -Alumina Catalysts, *Int. J. Hydrog. Energy*, 43, 4826-4838 (DOI: 10.1016/j.ijhydene.2018.01.103)
71. Cesar D. V., Santori G. F., Pompeo F., Baldanza M. A., Henriques C. A., Lombardo E., Schmal M., Cornaglia L., Nichio N. N., (2016), Hydrogen Production from Ethylene Glycol Reforming Catalyzed by Ni and Ni–Pt Hydrotalcite-Derived Catalysts, *Int. J. Hydrog. Energy*, 41, 22000-22008 (DOI: 10.1016/j.ijhydene.2016.07.168)
72. Sundari R., Vaidya P. D., (2015), On the Efficacy of Ru/Al₂O₃ Catalyst for Steam Reforming of Ethylene Glycol, *Chem. Eng. Commun.*, 202, 1446-1454 (DOI: 10.1080/00986445.2014.934446)
73. Shejale A. D., Yadav G. D., (2021), Sustainable and Selective Hydrogen Production by Steam Reforming of Bio-Based Ethylene Glycol: Design and Development of Ni–Cu/Mixed Metal Oxides Using M (CeO₂, La₂O₃, ZrO₂)–MgO Mixed Oxides, *Int. J. Hydrog. Energy*, 46, 4808-4826 (DOI: 10.1016/j.ijhydene.2019.11.031)
74. Mei D., Lebarbier Dagle V., Xing R., Albrecht K. O., Dagle R. A., (2016), Steam Reforming of Ethylene Glycol over MgAl₂O₄ Supported Rh, Ni, and Co Catalysts, *ACS Catal.*, 6, 315-325 (DOI: 10.1021/acscatal.5b01666)
75. Chen G., Xu N., Li X., Liu Q., Yang H., Li W., (2015) Hydrogen Production by Aqueous-Phase Reforming of Ethylene Glycol over a Ni/Zn/Al Derived Hydrotalcite Catalyst, *RSC Adv.*, 5, 60128-60134 (DOI: 10.1039/c5ra07184d)
76. Joshi A. N., Vaidya P. D., (2023) Recent Studies on Aqueous-Phase Reforming: Catalysts, Reactors, Hybrid Processes and Techno-Economic Analysis, *Int. J. Hydrog. Energy*, 49, 117-137 (DOI: 10.1016/j.ijhydene.2023.06.314)
77. Shabaker J. W., Dumesic J. A., (2004) Kinetics of Aqueous-Phase

- Reforming of Oxygenated Hydrocarbons: Pt/Al₂O₃ and Sn-Modified Ni Catalysts, *Ind. Eng. Chem. Res.*, 43, 3105-3112 (DOI: 10.1021/ie049852o)
78. Huber G. W., Shabaker J. W., Dumesic J. A., (2003) Raney Ni-Sn Catalyst for H₂ Production from Biomass-Derived Hydrocarbons, *Science*, 300, 2075-2077 (DOI: 10.1126/science.1085597)
79. Chu X., Liu J., Sun B., Dai R., Pei Y., Qiao M., Fan K., (2011) Aqueous-Phase Reforming of Ethylene Glycol on Co/ZnO Catalysts Prepared by the Coprecipitation Method, *J. Mol. Catal. A Chem.*, 335, 129-135 (DOI: 10.1016/j.molcata.2010.11.024)
80. Tao J., Hou L., Yan B., Chen G., Li W., Chen H., Cheng Z., Lin F., (2019) Hydrogen Production via Aqueous-Phase Reforming of Ethylene Glycol over a Nickel-Iron Alloy Catalyst: Effect of Cobalt Addition, *Energy Fuels*, 34, 1153-1161 (DOI: 10.1021/acs.energyfuels.9b02149)
81. Kim H. D., Park H. J., Kim T. W., Jeong K. E., Chae H. J., Jeong S. Y., Lee C. H., Kim C. U., (2012) Hydrogen Production through the Aqueous Phase Reforming of Ethylene Glycol over Supported Pt-Based Bimetallic Catalysts, *Int. J. Hydrog. Energy*, 37, 8310-8317 (DOI: 10.1016/j.ijhydene.2012.02.160)
82. Haasterecht T. Van, Ludding C. C. I., De Jong K. P., Bitter J. H., (2013) Stability and Activity of Carbon Nanofiber-Supported Catalysts in the Aqueous Phase Reforming of Ethylene Glycol, *J. Energy Chem.*, 22, 257-269 (DOI: 10.1016/S2095-4956(13)60032-7)
83. Farias da Costas A. A., de Oliveira A. de N., Esposito R., Auvigne A., Len C., Luque R., Noronha R. C. R., Nascimento L. A. S. do., (2023) Glycerol and Microwave-Assisted Catalysis: Recent Progresses in Batch and Flow Devices, *Sustain. Energy Fuels*, 7, 1768-1792 (DOI: 10.1039/d2se01647h)
84. Kaur J., Sarma A. K., Jha M. K., Gera P., (2020) Valorisation of Crude Glycerol to Value-Added Products: Perspectives of Process Technology, Economics and Environmental Issues, *Biotechnol. Reports*, 27, e00487 (DOI: 10.1016/j.btre.2020.e00487)
85. Cui Y., Galvita V., Rihko-Struckmann L., Lorenz H., Sundmacher K., (2009) Steam Reforming of Glycerol: The Experimental Activity of La₁-

- XCexNiO₃ Catalyst in Comparison to the Thermodynamic Reaction, Equilibrium. *Appl. Catal. B Environ.*, 90, 29-37 (DOI: 10.1016/j.apcatb.2009.02.006)
86. Papageridis K. N., Siakavelas G., Charisiou N. D., Avraam D. G., Tzounis L., Kousi K., Goula M. A., (2016) Comparative Study of Ni, Co, Cu Supported on γ -Alumina Catalysts for Hydrogen Production via the Glycerol Steam Reforming Reaction, *Fuel Process. Technol.*, 152, 156-175 (DOI: 10.1016/j.fuproc.2016.06.024)
 87. Saidi M., Moradi P., (2020) Conversion of Biodiesel Synthesis Waste to Hydrogen in Membrane Reactor: Theoretical Study of Glycerol Steam Reforming, *Int. J. Hydrog. Energy*, 45, 8715-8726 (DOI: 10.1016/j.ijhydene.2020.01.064)
 88. Hirai T., Ikenaga N. O., Miyake T., Suzuki T., (2005) Production of Hydrogen by Steam Reforming of Glycerin on Ruthenium Catalyst, *Energy Fuels*, 19, 1761-1762 (DOI: 10.1021/ef050121q)
 89. Adhikari S., Fernando S., Haryanto A., (2007) Production of Hydrogen by Steam Reforming of Glycerin over Alumina-Supported Metal Catalysts, *Catal. Today*, 129, 355-364 (DOI: 10.1016/j.cattod.2006.09.038)
 90. Sundari R., Vaidya P. D., (2012) Reaction Kinetics of Glycerol Steam Reforming Using a Ru/Al₂O₃ Catalyst, *Energy Fuels*, 26, 4195-4204 (DOI: 10.1021/ef300658n)
 91. Kousi K., Kondarides D. I., Verykios X. E., Papadopoulou C., (2017) Glycerol Steam Reforming over Modified Ru/Al₂O₃ Catalysts, *Appl. Catal. A Gen.*, 542, 201-211 (DOI: 10.1016/j.apcata.2017.05.027)
 92. Bossola F., Pereira-Hernández X. I., Evangelisti C., Wang Y., Dal Santo V., (2017) Investigation of the Promoting Effect of Mn on a Pt/C Catalyst for the Steam and Aqueous Phase Reforming of Glycerol. *J. Catal.*, 349, 75-83 (DOI: 10.1016/j.jcat.2017.03.002)
 93. Buffoni I. N., Gatti M. N., Santori G. F., Pompeo F., Nichio N. N., (2017) Hydrogen from Glycerol Steam Reforming with a Platinum Catalyst Supported on a SiO₂-C Composite, *Int. J. Hydrog. Energy*, 42, 12967-12977 (DOI: 10.1016/j.ijhydene.2017.04.047)
 94. Rezende S. M. de, Franchini C. A., Dieuzeide M. L., Duarte de Farias A.

- M., Amadeo N., Fraga M. A., (2015) Glycerol Steam Reforming over Layered Double Hydroxide-Supported Pt Catalysts, *Chem. Eng. J.*, 272, 108-118 (DOI: 10.1016/j.cej.2015.03.033)
95. Zhang B., Tang X., Li Y., Xu Y., Shen W., (2007) Hydrogen Production from Steam Reforming of Ethanol and Glycerol over Ceria-Supported Metal Catalysts, *Int. J. Hydrog. Energy*, 32, 2367-2373 (DOI: 10.1016/j.ijhydene.2006.11.003)
 96. Ebshish A., Yaakob Z., Taufiq-Yap Y. H., Bshish A. Shaibani A., (2013) Catalytic Steam Reforming of Glycerol over Cerium and Palladium-Based Catalysts for Hydrogen Production, *J. Fuel Cell Sci. Technol.*, 10, 1-6 (DOI: 10.1115/1.4023687)
 97. Kamonsuangkasem K., Therdthianwong S., Therdthianwong A., Thammajak N., (2017) Remarkable Activity and Stability of Ni Catalyst Supported on CeO₂-Al₂O₃ via CeAlO₃ Perovskite towards Glycerol Steam Reforming for Hydrogen Production, *Appl. Catal. B Environ.*, 218, 650-663 (DOI: 10.1016/j.apcatb.2017.06.073)
 98. Profeti L. P. R., Ticianelli E. A., Assaf E. M., (2009) Production of Hydrogen via Steam Reforming of Biofuels on Ni/CeO₂-Al₂O₃ Catalysts Promoted by Noble Metals, *Int. J. Hydrog. Energy*, 34, 5049-5060 (DOI: 10.1016/j.ijhydene.2009.03.050)
 99. Demsash H. D., Mohan R., (2016) Steam Reforming of Glycerol to Hydrogen over Ceria Promoted Nickel–Alumina Catalysts, *Int. J. Hydrog. Energy*, 41, 22732-22742 (DOI: 10.1016/j.ijhydene.2016.10.082)
 100. Iriondo A., Barrio V. L., Cambra J. F., Arias P. L., Guemez M. B., Sanchez-Sanchez M. C., Navarro R. M., Fierro J. L. G., (2010) Glycerol Steam Reforming over Ni Catalysts Supported on Ceria and Ceria-Promoted Alumina, *Int. J. Hydrog. Energy*, 35, 11622-11633 (DOI: 10.1016/j.ijhydene.2010.05.105)
 101. Wei Z., Karim A. M., Li Y., King D. L., Wang Y., (2015) Elucidation of the Roles of Re in Steam Reforming of Glycerol over Pt-Re/C Catalysts, *J. Catal.*, 322, 49-59 (DOI: 10.1016/j.jcat.2014.11.006)
 102. Wen G., Xu Y., Ma H., Xu Z., Tian Z., (2008) Production of Hydrogen by Aqueous-Phase Reforming of Glycerol, *Int. J. Hydrog. Energy*, 33,

- 6657-6666 (DOI: 10.1016/j.ijhydene.2008.07.072)
103. Dietrich P. J., Lobo-Lapidus R. J., Wu T., Sumer A., Akatay M. C., Fingland B. R., Guo N., Dumesic J. A., Marshall C. L., Stach E., Jellinek J., Delgass W. N., Ribeiro F. H., Miller J. T., (2012) Aqueous Phase Glycerol Reforming by PtMo Bimetallic Nano-Particle Catalyst: Product Selectivity and Structural Characterization, *Top. Catal.*, 55, 53-69 (DOI: 10.1007/s11244-012-9775-5)
 104. Boga D. A., Oord R., Beale A. M., Chung Y. M., Bruijninx P. C. A., Weckhuysen B. M., (2013) Highly Selective Bimetallic Pt-Cu/Mg(Al)O Catalysts for the Aqueous-Phase Reforming of Glycerol, *ChemCatChem*, 5, 529-537 (DOI: 10.1002/cctc.201200112)
 105. Pendem C., Sarkar B., Siddiqui N., Konathala L. N. S., Baskar C., Bal R., (2018) K-Promoted Pt-Hydrotalcite Catalyst for Production of H₂ by Aqueous Phase Reforming of Glycerol, *ACS Sustain. Chem. Eng.*, 6, 2122-2131 (DOI: 10.1021/acssuschemeng.7b03512)
 106. Rahman M. M., (2020) Aqueous-Phase Reforming of Glycerol over Carbon-Nanotube-Supported Catalysts, *Catal. Letters*, 150, 2674-2687 (DOI: 10.1007/s10562-020-03167-2)
 107. Guo Y., Liu X., Wang Y., (2019), Catalytic and DRIFTS Studies of Pt-Based Bimetallic Alloy Catalysts in Aqueous-Phase Reforming of Glycerol, *Ind. Eng. Chem. Res.*, 58, 2749-2758 (DOI: 10.1021/acs.iecr.8b05774)
 108. Nozawa T., Mizukoshi Y., Yoshida A., Naito S., (2014) Aqueous Phase Reforming of Ethanol and Acetic Acid over TiO₂ Supported Ru Catalysts, *Appl. Catal. B Environ.*, 146, 221-226 (DOI: 10.1016/j.apcatb.2013.06.017)
 109. Gogoi P., Kanna N., Begum P., Deka R. C., Satyanarayana C. V. V., Raja T., (2020) Controlling and Stabilization of Ru Nanoparticles by Tuning the Nitrogen Content of the Support for Enhanced H₂ Production through Aqueous-Phase Reforming of Glycerol, *ACS Catal.*, 10, 2489-2507 (DOI: 10.1021/acscatal.9b04063)
 110. Gogoi P., Nagpure A. S., Kandasamy P., Satyanarayana C. V. V., Raja T., (2020) Insights into the Catalytic Activity of Ru/NaY Catalysts for Efficient H₂ Production through Aqueous Phase Reforming, *Sustain.*

Energy Fuels, 4, 678-690 (DOI: 10.1039/c9se00797k)

111. Luo F., Fortenberry A., Ren J., Qiang Z., (2020) Recent Progress in Enhancing Poly(Lactic Acid) Stereocomplex Formation for Material Property Improvement, *Front. Chem.*, 8, 1-8 (DOI: 10.3389/fchem.2020.00688)
112. Yankov D., (2022) Fermentative Lactic Acid Production from Lignocellulosic Feedstocks: From Source to Purified Product, *Front. Chem.*, 10, 1-34 (DOI: 10.3389/fchem.2022.823005)
113. Zhang G., Zhao J., Jin X., Qian Y., Zhou M., Jia X., Sun F., Jiang J., Xu W., Sun B., (2022) Combined Dehydrogenation of Glycerol with Catalytic Transfer Hydrogenation of H₂ Acceptors to Chemicals: Opportunities and Challenges, *Front. Chem.*, 10, 1-15 (DOI: 10.3389/fchem.2022.962579)
114. Akbulut D., Özkur S., (2022) A Review of the Catalytic Conversion of Glycerol to Lactic Acid in the Presence of Aqueous Base, *RSC Adv.*, 12, 18864-18883 (DOI: 10.1039/d2ra03085c)
115. Tang Z., Liu P., Cao H., Bals S., Heeres H. J., Pescarmona P. P., (2019) Pt/ZrO₂ Prepared by Atomic Trapping: An Efficient Catalyst for the Conversion of Glycerol to Lactic Acid with Concomitant Transfer Hydrogenation of Cyclohexene, *ACS Catal.*, 9, 9953-9963 (DOI: 10.1021/acscatal.9b02139)
116. Oberhauser W., Evangelisti C., Tiozzo C., Vizza F., Psaro R., (2016) Lactic Acid from Glycerol by Ethylene-Stabilized Platinum-Nanoparticles, *ACS Catal.*, 6, 1671-1674 (DOI: 10.1021/acscatal.5b02914)

Chapter 2

Catalytic Transformation of Glycerol to Hydrogen Gas and Lactic Acid over Ruthenium Catalyst in Water

2.1. Introduction

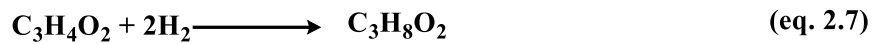
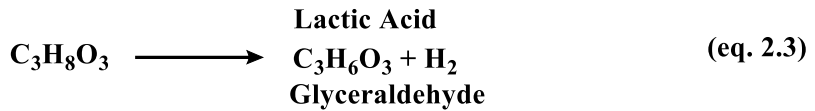
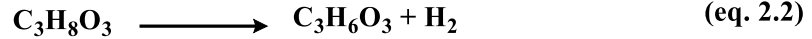
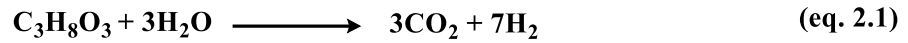
The ever-increasing energy demand, depletion of fossil fuel resources, and the consequences of using fossil fuels in terms of the upsurge in atmospheric CO₂ (global warming) have driven the attention of the scientific community to explore sustainable alternatives to fossil fuels. In this regard, utilizing biomass waste, one of the most abundant renewable resources, for the production of fuels is considered as a promising route to reduce the global dependency on fossil fuel resources.^[1,2] Further, the utilization of biomass-derived substrates for the production of hydrogen gas, which is identified as a clean fuel of the future, will not only have a crucial role in diminishing CO₂ emissions but also provide a sustainable route to utilize biomass waste.^[3-5] Hydrogen is being produced at an industrial scale by electrolysis of water,^[6] methane reforming,^[7] enzymatic pathway,^[8-9] gasification of biomass waste,^[10] steam reforming,^[11] aqueous phase reforming,^[12] and catalytic dehydrogenation of liquid hydrogen carriers.^[13-19] However, global efforts are also being made to explore alternate and effective ways to produce hydrogen gas, and therefore, the selection of sustainable resources and mild reaction conditions for hydrogen production are a few of the crucial factors that need specific attention.

In this regard, glycerol (GLY), a crude byproduct of biodiesel and an important product of biomass can be explored as a potential source for hydrogen production. Since GLY constitutes 10 wt% of biodiesel, a gradual increase in biodiesel production also resulted in a huge glycerol production.^[20] According to the International Energy Agency (IEA), global biodiesel production was 41 billion litres in 2019 and is estimated to increase to 46 billion litres by 2025, which will also increase glycerol production.^[21] Advantageously, glycerol is a high boiling liquid, non-flammable and non-toxic in comparison to other alcohols such as methanol.^[22] Moreover, glycerol can also be used as an

important precursor for the production of various fine chemicals such as lactic acid, glyceric acid, glycolic acid, propanediol, ethylene glycol, and so on.^[23-25] Among these, lactic acid is one of the most important intermediates having wide applications in pharmaceuticals, cosmetics, textiles, food industries, leather industries, and for the production of polylactic acid-based biodegradable plastic.^[26-28] Industrially, lactic acid (LA) is produced either by anaerobic fermentation of carbohydrates or chemically. In the fermentation process, there are several drawbacks, such as longer reaction time, complicated separation, purification, and non-ecological processes.^[29-30] Chemically, it can be produced using HCN and CH₃CHO, but due to environmental problems, it is of less interest.^[31]

The literature revealed the production of H₂ from GLY via steam and aqueous-phase reforming (APR) at higher temperatures (> 200 °C). However, APR requires lower temperatures in the conversion of bio-based oxygenated hydrocarbons to hydrogen gas than steam reforming.^[32] Nevertheless, GLY to H₂ gas production involves several key reaction steps (Scheme 1), leading to the generation of several intermediate products (such as glyceraldehyde and lactic acid), which may further decompose to H₂ gas during the process. The APR process involves C-C cleavage followed by a water gas shift reaction, which favors at low temperatures. Many metal-based catalysts such as Pt, Pd, Ru, Fe, Ni and Co have been explored in APR.^[33-37] Dumesic et al. made a breakthrough in hydrogen production from APR of biomass-derived oxygenated hydrocarbons. Several Pt-based catalysts such as Pt/Al₂O₃,^[38] Pt-Re/C,^[39] Pt-Cu/Mg(Al)O,^[40] Pt-KIT/28,^[41] Pt-Ni/MWCNT,^[42] PtFe/ γ -Al₂O₃^[43] have been explored in APR of glycerol by various research groups in the temperature range of 200-250 °C. Notably, Pt-based catalysts displayed high activity with appreciably good resistance towards carbon formation during APR.^[38] Alloying of Pt with Cu, Ni and Fe further enhanced the GLY conversion and selectivity towards hydrogen gas as compared to the monometallic Pt catalyst.^[40,42-43] Recent investigations demonstrated that basic supports enhance the activity in the H₂ production through APR of GLY. On the other hand, Ni supported on Al₂O₃-MgO was also explored to achieve appreciably good conversion of GLY (78-69%) with H₂ selectivity of 55-72% at 250 °C.^[44] Notably, Ni is highly active in C-C bond cleavage, but carbon

deposition decreases the activity of Ni in APR. Further, the addition of MgO enhances the stability of Ni from sintering, and the addition of Al₂O₃ improves the catalyst stability.^[44]



Scheme 2.1. Key reactions involved in the transformation of GLY to H₂ gas.

Goula et al. reported Ce-Sm-XCu (X = 5, 7, and 10 wt%) catalysts for steam reforming of GLY to H₂ in the temperature range of 400-700 °C.^[45] Prasad et al. utilized a MgO-La₂O₃ supported Co catalyst for the complete conversion of GLY at 700 °C.^[46] Although the glycerol reforming process led to the production of H₂ gas, it suffers from the cumbersome post-production purification of H₂ gas due to CO, CO₂, and CH₄ contamination. Alternatively, H₂ gas can be produced from oxidant-free^[47-48] or O₂-free^[49] dehydrogenation of GLY to LA. Despite the fact that the dehydrogenative pathway for the transformation of GLY is an attractive route to obtain both H₂ gas, a clean fuel, and LA, a large section of research is focused mostly towards the oxidative transformation of GLY to LA using Cu, Pd or Au based catalysts.^[50-51] Notably, selective oxidation of GLY resulted in lower selectivity of LA due to the formation of several undesired byproducts such as glyceric acid, tartaric acid and glycolic acid.^[52] Shimizu et al. reported the oxidant-free dehydrogenation of neat GLY to LA (75%) over Pt/C catalyst using KOH under a nitrogen atmosphere (1 MPa) at 160 °C.^[47-48] Performing reaction under neat conditions advantageously enhanced the LA yield and diminished the production of undesired hydrogenated products (1,2-PD and other C1-C3 alcohols). It has been observed that the particle size of Pt, metal-to-support interaction, and interface play a crucial role in tuning the catalyst performance for the dehydrogenation of GLY.^[47-48] Yang et al. explored monometallic Pt or Co and

bimetallic Pt-Co supported on CeO_x for the dehydrogenation of GLY to LA at 200 °C.^[53] Psaro et al. explored the dehydrogenative transformation of GLY to LA at 140 °C over Pt nanoparticles (1.5 nm) supported on a high surface area carbon material, wherein ethylene was used as a hydrogen acceptor to achieve high selectivity of LA by eliminating undesired side reactions.^[51] The catalytic conversion of GLY to LA with moderate conversion was also reported over CuPd/reduced graphene oxide (56% conv.) at 140 °C.^[54] Although there are several reports for the catalytic conversion of GLY to LA, most of these catalytic reactions were carried out at a higher temperature (>140 °C) and/or in the presence of gases (N₂ and ethylene) or vacuum.^[47-48, 55] A few molecular catalysts based on Ir,^[56-59] Ru,^[60-61] and Fe^[62] have also been explored for the transformation of GLY to LA with the production of H₂ gas at 115-180 °C.

Therefore, it is evident that despite glycerol having a high potential to be explored as an efficient liquid hydrogen storage material (LHSM), hydrogen production from GLY over heterogeneous catalysts has not yet been explored extensively. Herein, we report the efficient and selective production of H₂ gas from GLY over the ruthenium catalyst (unsupported catalyst) in water under mild reaction conditions (110 °C). Reaction parameters were optimized to achieve a high yield of H₂ gas by eliminating the undesired side reactions. Moreover, the studied ruthenium catalyst displayed appreciably high long-term stability for the transformation of bulk-scale GLY to H₂ gas in water.

2.2. Experimental section

2.2.1. Materials and instrumentation

High-purity chemicals and metal salts were purchased from Sigma-Aldrich, Alfa-Aesar and used without further purification. All the catalytic reactions were performed under inert conditions using high-purity argon gas purchased from Inox Air Product Ltd., India. NMR spectra were recorded in deuterated solvent (D₂O) using Bruker Avance 400 and AVANCE NEO Ascend 500 Bruker spectrometer. Transmission electron microscopic (FEI-TEM) images were obtained using a Tecnai G² 20 (FEI) S-Twin at operating voltages of 200 kV. The samples for TEM analysis were prepared by the drop-costing method. Briefly, ruthenium nanoparticles were dispersed in ethanol under ultrasonication for 1 hour, and then highly dispersed particles were spread onto a

carbon-coated Cu grid and dried at room temperature. Particle size was calculated using ImageJ software for at least 50-100 particles, and the average particle size distribution curve was plotted using Origin software. Scanning electron microscopic (SEM) images and elemental mapping data were collected using a Nova nano FE-SEM 450 (FEI) equipped with an EDS detector. Powder X-ray diffraction (P-XRD) measurements were performed using a Rigaku SmartLab Automated Multipurpose X-ray diffractometer with a scintillation detector. The measurements were conducted using Cu K α radiation ($\lambda = 1.5418$ Å) with a step size of 0.02° in the 2θ range of $20-80^\circ$. The exposure time for each P-XRD measurement was 20 minutes. XPS data was recorded using Al K α (1486.61 eV) X-rays using SPECS Surface Nano Analysis GmbH instrument, Germany. Samples were excited by using monochromatic Al K-alpha (1486.61 eV) with the X-ray source operating at 100 W. Scans were collected at a pass energy of 30 eV over the binding energy range 1200-0 eV. Charge correction was made relative to the position of C 1s (284.6 eV) as reference. The nitrogen physisorption isotherms were measured at 77 K using Quantachrome Autosorb iQ₂ TPX automated gas sorption system, and the specific surface area was calculated using the Brunauer-Emmett-Teller (BET) equation in the relative pressure (P/P₀) range of 0.05-0.3. The sample was degassed at 200 °C for 4 h under a high vacuum before analysis. The binding energy values were charge-corrected to the C 1s signal (284.6 eV). The gas chromatography (GC) analyses were performed on a Shimadzu GC-2014 system using a shin carbon-ST packed column with a thermal conductivity detector (TCD) using argon as a carrier gas. Parameters were set for the program to detect H₂, CO₂, CO, and CH₄ gas (detector temperature: 200 °C, and oven temperature program: 90 °C (hold time: 1 min), 90-200 °C (rate: 15 °C per minute). Inductively coupled plasma atomic emission spectroscopy (ICP-AES) was performed with ARCOS, a simultaneous spectrometer of SPECTRO analytical instruments. The sample was digested using aquaregia in the thermal autoclave at 170 °C for 12 h, diluted with water and then carried out for analysis.

2.2.2. Procedure for the synthesis of ruthenium catalyst

Ruthenium catalyst was synthesized following our previously reported procedure using sodium borohydride (NaBH₄) as a reducing agent and polyvinylpyrrolidone (PVP) as a surface stabilizing agent.^[63] Typically, an aqueous solution of sodium borohydride (0.025 g in 5 mL water) was added dropwise to a solution of ruthenium(III) chloride (0.1 mmol) and polyvinylpyrrolidone (0.050 g) in water (5 mL) at room temperature. The contents of the flask were sonicated for 10 min. at room temperature to obtain a black suspension of ruthenium nanoparticles. Further, ruthenium nanoparticles were collected by centrifugation and washed several times with deionized water and finally with ethanol, then dried overnight under vacuum and further used for characterization.

2.2.3. Procedure for catalytic conversion of GLY to H₂ gas

In a two-necked test tube fitted with a condenser and a gas burette, an aqueous suspension of ruthenium catalyst (0.1 mmol in 0.370 mL), GLY (6.84 mmol, 0.5 mL), and NaOH (7.52 mmol, 0.301 g) were added. The reaction vessel was then de-aerated by a repeated process of vacuuming and flushing with argon gas three times. Further, the reaction mixture was stirred at 110 °C in an oil bath. The amount of H₂ gas produced was measured by the water displacement method using a burette, and the presence of H₂ gas in the evolved gaseous product was confirmed by a gas chromatography-thermal conductivity detector (GC-TCD) analysis. After completion of the reaction, 4 mL of deionized water was added to the reaction vessel, and the reaction mixture was sonicated for 10 minutes. Further, the catalyst was recovered from the reaction mixture by centrifugation at 6500 rpm for 5 minutes. GLY conversion and the formation of sodium lactate (SL) and other products were estimated by analyzing the crude reaction mixture by ¹H NMR. The yield of SL and other byproducts i.e., sodium formate (SF), 1,2-propanediol (PD) and sodium glycolate (SG), was determined by ¹H NMR using sodium acetate as an internal standard by using the following equation.

$$\text{Yield} = C_f(\text{P})/C_i(\text{GLY}) \times 100 (\%)$$

where,

$$C_f(\text{GLY}) = \text{millimoles of carbon in the final glycerol}$$

$C_f(P)$ = millimoles of carbons in the final product

2.2.4. Heterogeneity test of ruthenium catalyst

Typically, an aqueous suspension (0.370 mL) of ruthenium catalyst (0.1 mmol) was stirred with a large excess of elemental mercury (Hg) at room temperature for 3 h prior to the catalytic reaction. Further, glycerol (6.84 mmol, 0.5 mL), and NaOH (7.52 mmol, 0.301 g) were added in the reaction vessel fitted with a condenser and gas burette. The reaction vessel was then de-aerated by a repeated process of vacuuming and flushing with argon gas three times. Further, the reaction mixture was stirred at 110 °C in an oil bath, and the progress of the reaction was monitored for the specified duration.

2.2.5. Recyclability experiment for the catalytic conversion of GLY to H₂ gas over ruthenium catalyst

Initially, an aqueous suspension of ruthenium catalyst (0.1 mmol in 0.370 mL), GLY (6.84 mmol, 0.5 mL), and NaOH (13.68 mmol, 0.547 g) were added in a two-necked test tube fitted with a condenser and a gas burette. The reaction vessel was then de-aerated by a repeated process of vacuuming and flushing with argon gas three times. Further, the reaction mixture was stirred at 110 °C in an oil bath. For the subsequent catalytic runs, the ruthenium catalyst was separated by centrifugation from the reaction mixture, and the catalyst was re-used for the next catalytic run by adding a fresh content of GLY (6.84 mmol, 0.5 mL), water (0.370 mL), and NaOH (13.68 mmol, 0.547 g) in the reaction vessel, and the reaction mixture was stirred at 110 °C in an oil bath. The progress of the reaction was monitored by measuring the evolved H₂ gas by the water displacement method.

2.2.6. Bulk-scale hydrogen production from GLY over ruthenium catalyst

For bulk-scale conversion of GLY to H₂ gas, an aqueous suspension of ruthenium catalyst (0.1 mmol in 1.48 mL), GLY (27.36 mmol, 2.0 mL), and NaOH (1.1 equiv. or 2.0 equiv.) were added in a two necked reaction vessel equipped with a condenser and a gas burette. The reaction vessel was then de-aerated under a vacuum and flushed with argon gas by repeating this process three times. Further, the reaction mixture was stirred at 110 °C in an oil bath.

2.2.7. Gas composition analysis

The identification of gaseous products during the dehydrogenation of GLY was confirmed as H₂ and with no detectable level of CO, CO₂ and CH₄ using a Shimadzu GC-2014 system. The chromatograph was equipped with a shin carbon-ST packed column with a thermal conductivity detector (TCD) using argon as a carrier gas. Parameters were set for the program to detect H₂, CO₂, CO, and CH₄ (detector temperature, 200 °C; oven temperature program, 90 °C (hold time: 1 min), 90-200 °C (rate: 15 °C per minute)).

2.3. Results and discussion

2.3.1. Synthesis and characterization of ruthenium catalyst

Ruthenium catalyst was prepared by aqueous phase reduction of an aqueous solution of ruthenium(III) chloride using sodium borohydride (NaBH₄) in the presence of polyvinylpyrrolidone (PVP) as a stabilizer.^[63] Energy-dispersive X-ray spectroscopy (EDX) and elemental mapping evidenced the presence of ruthenium nanoparticles (Figures 2.1 and 2.2). Transmission electron microscopy (TEM) images revealed the presence of well dispersed ruthenium nanoparticles with an average particle size of 2.7 nm (Figures 2.3a-b). The P-XRD pattern exhibited the presence of a major diffraction peak at 2θ of 44° corresponding to the (101) plane of the hexagonal-close packed (hcp) ruthenium nanoparticles (Figure 2.3c).^[64] Further, X-ray photoelectron spectroscopy (XPS) measurements for the ruthenium catalyst were performed. In the XPS spectra, the binding energies of 461.6 eV and 483.6 eV in the Ru 3p region can be assigned to Ru 3p_{3/2} and Ru 3p_{1/2}, respectively corresponding to the metallic ruthenium, Ru(0) (Figure 2.3d).^[65] Further, the BET surface area of the synthesized ruthenium nanoparticles was found to be 19 m²/g (Figure 2.4).

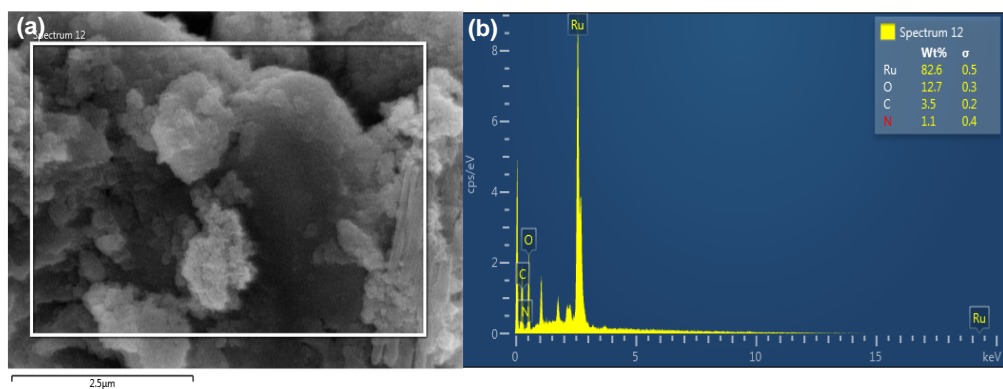


Figure 2.1. (a) SEM image and corresponding (b) EDX spectra of fresh ruthenium catalyst.

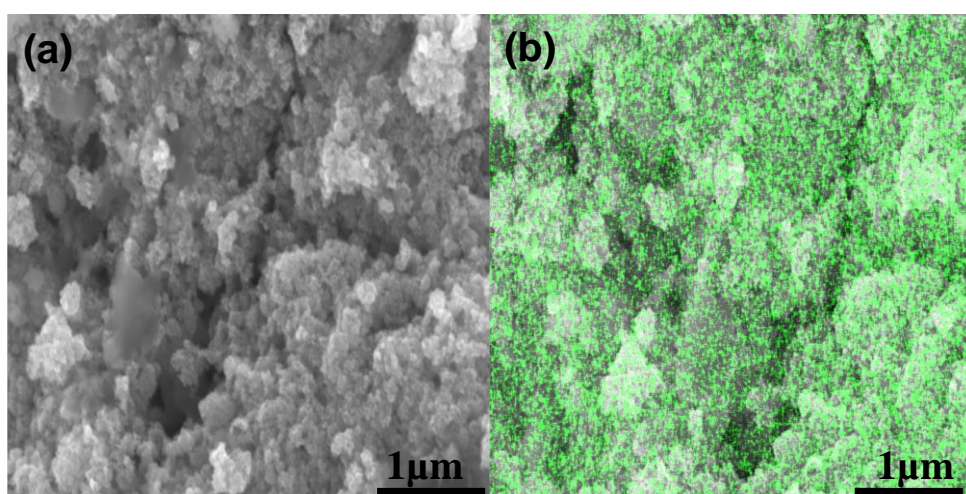


Figure 2.2. (a) SEM image and corresponding (b) elemental mapping of fresh ruthenium catalyst.

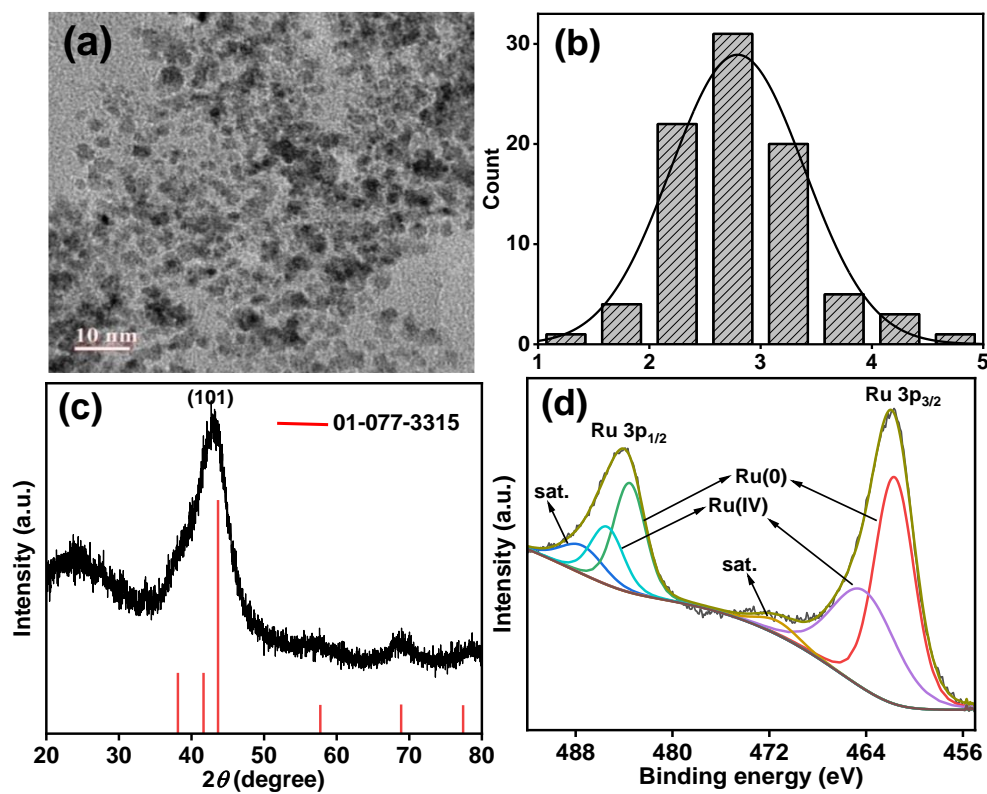


Figure 2.3. (a) TEM image and corresponding (b) particle size distribution, (c) P-XRD pattern, and (d) XPS profile of Ru 3p region of fresh ruthenium catalyst.

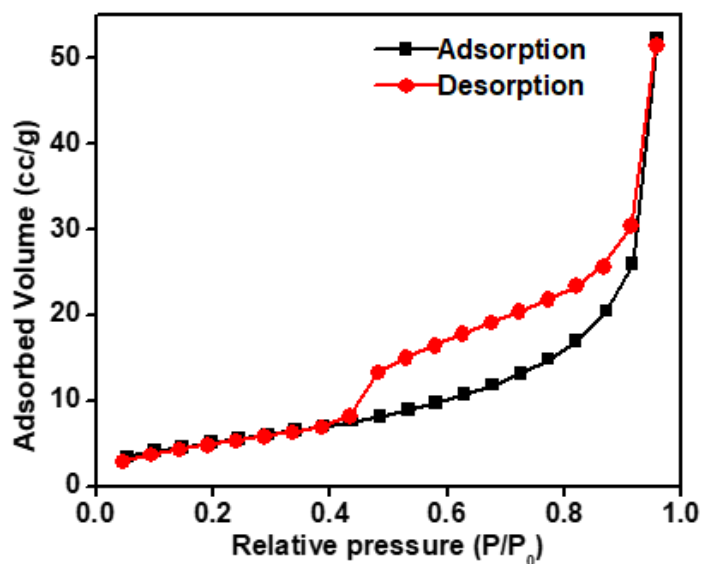


Figure 2.4. N₂ adsorption-desorption isotherm of fresh ruthenium catalyst.

2.3.2. Catalytic reaction for hydrogen production from glycerol

At the outset, a catalytic reaction for hydrogen production from GLY was performed over the ruthenium catalyst in water in the presence of NaOH at 110 °C under an argon atmosphere. In this process, the amount of H₂ gas produced was measured by the water displacement method and the composition of the generated gas was confirmed by GC-TCD analysis, wherein selective evolution of H₂ gas with no traces of CO₂ and CO was observed (Figures 2.5 and 2.6). Notably, the reaction could not proceed in the absence of a catalyst (Table 2.1, entry 1). No conversion of GLY was observed for the catalytic reaction performed in the absence of a base (Table 2.1, entry 2), suggesting the crucial role of the base for hydrogen production from GLY. As shown in Table 2.1, the reaction performed with NaOH/GLY molar ratio of 0.5 produced only 44 mL (1.8 mmol) of H₂ gas with 39% conversion of GLY in 4 h (Table 2.1, entry 3). Further, upon increasing the NaOH/GLY molar ratio to 1.1 (Table 2.1, entry 4), the amount of gas released was also significantly enhanced by several folds to 162 mL (6.6 mmol) with 86% conversion of GLY and a remarkable increase in the selectivity for SL (81%) in 7 h (Figure 2.5). However, other by-products such as SF, PD and SG were observed only in lesser content as compared to SL.

Further, performing the reaction with neat GLY (in the absence of water) exhibited poor H₂ gas production (1.96 mmol) with a lower conversion of glycerol (35%) (Table 2.1, entry 5), suggesting the important role of water in GLY dehydrogenation reaction. The observed trend can be attributed to the fact that water improves the viscosity of GLY and the mass transfer of the base.^[62]

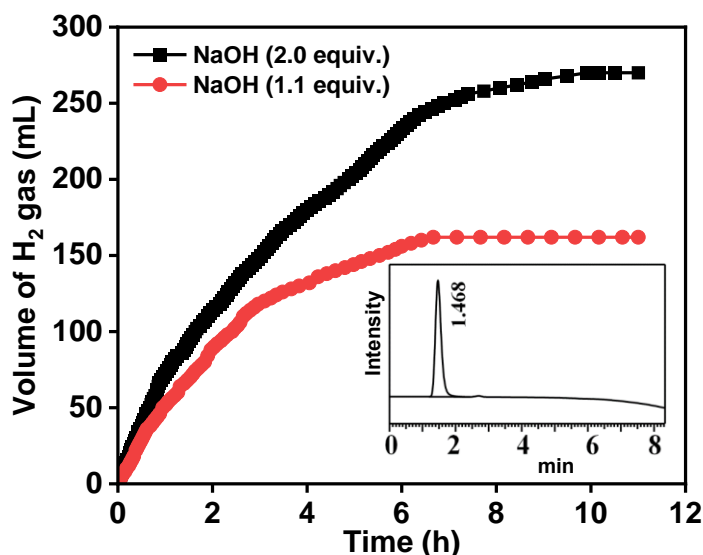


Figure 2.5. Time course plot for the production of hydrogen gas from GLY over the ruthenium catalyst (inset: GC-TCD analysis of gas evolved during the catalytic reaction). Reaction conditions: Ruthenium catalyst (0.1 mmol), GLY (6.84 mmol), NaOH (7.52 mmol and 13.68 mmol), water (20.52 mmol), and 110 °C.

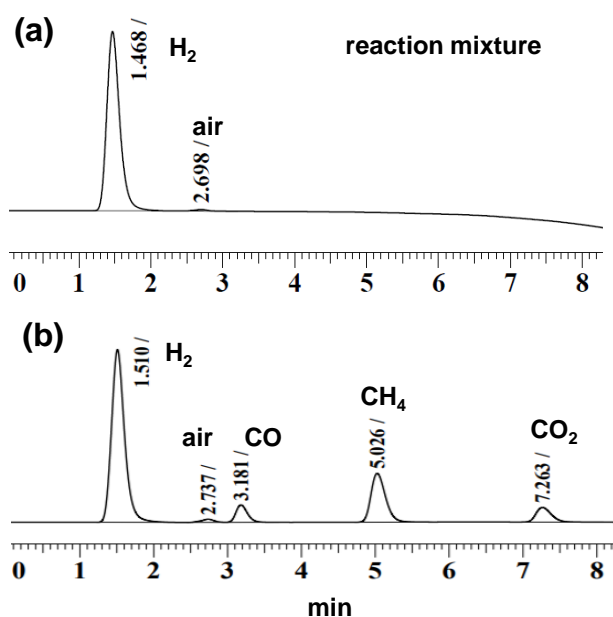


Figure 2.6. GC-TCD analysis of the (a) gas produced from GLY over the ruthenium catalyst and (b) standard mixture of gases with the composition of CO (24.965%), CO₂ (24.962%), CH₄ (25.012%) and H₂ (25.061%). Reaction conditions: Ruthenium catalyst (0.1 mmol), GLY (6.84 mmol), NaOH (7.52 mmol), water (20.52 mmol), and 110 °C.

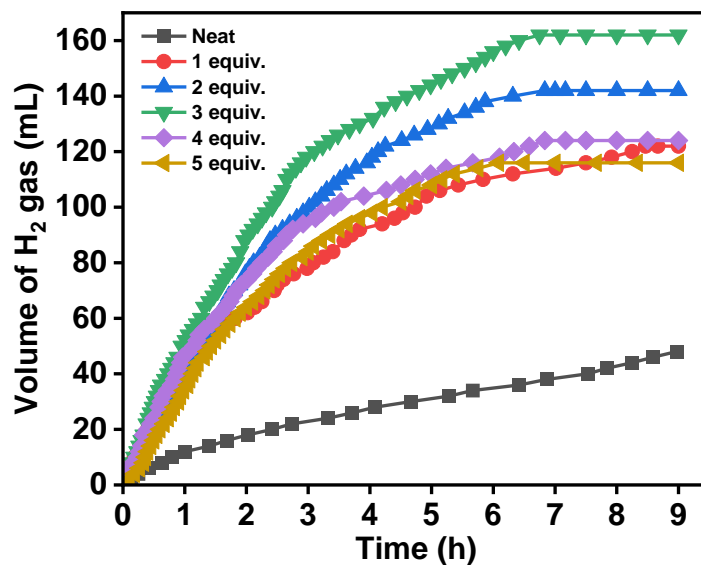
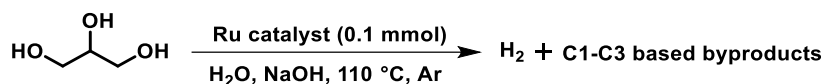


Figure 2.7. Effect of water concentration on hydrogen production from GLY over the ruthenium catalyst. Reaction conditions: Ruthenium catalyst (0.1 mmol), GLY (6.84 mmol), NaOH (7.52 mmol), water (0-5 equiv.), and 110 °C.

To further investigate the role of water, dehydrogenation of GLY was performed with varying GLY/water molar ratio (1:1 to 1:5). Results inferred that with the increase in water content from 1:1 to 1:3, the amount of H₂ gas evolved also increased from 4.98 mmol (1:1) to 6.6 mmol (1:3) (Table 2.1, entries 4, 6 and 7). However, with a further increase in water content for the GLY/water ratio of 1:4 and 1:5, the amount of released H₂ gas decreased to 5.06 mmol and 4.73 mmol, respectively (Table 2.1, entries 8 and 9) (Figure 2.7). These results demonstrated that higher reaction efficiency for the dehydrogenation of GLY can be achieved by optimizing the GLY/water molar ratio.

Table 2.1. Reaction optimization for hydrogen production from glycerol over the ruthenium catalyst.^a



Entry	H ₂ O (equiv.)	Base (equiv.)	t (h)	Conv. (%)	H ₂ gas (mL) ^b	n(H ₂)/ n(GLY)	Selectivity of byproducts (%) ^c				CB (%) ^d
							SL (Yield) ^[e]	PD	SG	SF	
1 ^e	3	1.1	6	-	-	-	-	-	-	-	-
2	3	0	6	-	-	-	-	-	-	-	-
3	3	0.5	4	39	44	0.26	71 (27)	13	9	3	98
4	3	1.1	7	86	162	0.96	81 (69)	3	2	11	97
5	0	1.1	9	35	48	0.28	70 (24)	2	5	23	99
6	1	1.1	8.5	65	122	0.72	80 (52)	1	2	15	99
7	2	1.1	7	72	142	0.84	82 (59)	2	2	13	99
8	4	1.1	7	66	124	0.74	79 (52)	3	4	13	99
9	5	1.1	6.5	64	116	0.69	80 (51)	3	3	13	99

^aReaction conditions: Ruthenium catalyst (0.1 mmol), GLY (6.84 mmol), NaOH, water, 110 °C. ^bVolume of gas was measured by the water displacement method. ^cConversion and selectivity were calculated by ¹H NMR using sodium acetate as an internal standard. ^dCB is carbon balance. ^eReaction in the absence of the catalyst. GLY (glycerol), SL (sodium lactate), PD (1,2-propanediol), SG (sodium glycolate), SF (sodium formate).

Further, the effect of the base was also investigated by performing the catalytic dehydrogenation of GLY in the presence of different bases such as NaOH, KOH, Na₂CO₃, K₂CO₃, and KO^tBu at 110 °C, where NaOH outperformed others (Table 2.2). According to the previous literature reports, KOH also exhibited a good conversion of GLY.^[47,56-61] Under optimized reaction conditions, high efficiency was observed with NaOH for the release of hydrogen gas from GLY (0.96 equiv. of H₂ gas with 86% conversion of GLY) as compared to KOH (0.4 equiv. of H₂ gas with 43% conversion of GLY) at 110 °C (Table 2.2, entries 7 and 1). Notably, no activity was observed in the presence of weak bases (Na₂CO₃ and K₂CO₃), while the reaction was very sluggish with KO^tBu (Table 2.2, entries 2-4). Ruthenium catalyst was also

active at a temperature as low as 90 °C to release 3.10 mmol of H₂ gas (0.45 equiv. H₂ gas) in 9 h (Table 2.2, entry 5). Performing the catalytic reaction at a higher temperature resulted in an increase in reaction efficiency, where 5.31 mmol of H₂ gas (0.77 equiv. of H₂ gas) was released in 8.5 h at 100 °C (Table 2.2, entry 6). High efficiency for the release of H₂ gas (6.6 mmol of H₂ gas) from GLY (86% conv.) was observed at 110 °C in 7 h, while the analogous amount of H₂ gas was released in lesser time (5 h) at 120 °C (Table 2.2, entries 7-8). The apparent activation energy for H₂ generation from GLY over the ruthenium catalyst was estimated as 77 kJ mol⁻¹ (Figure 2.8).

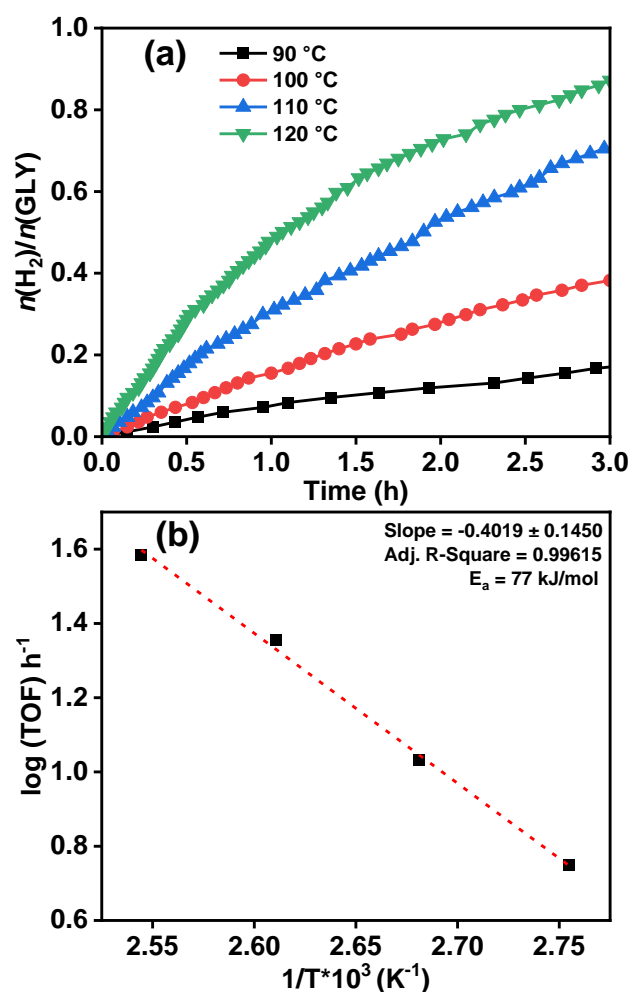
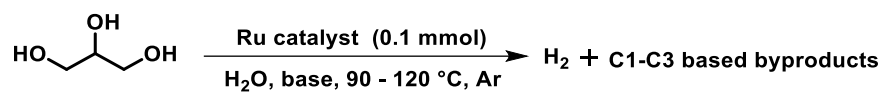


Figure 2.8. (a) Temperature-dependent study for hydrogen production from GLY over the ruthenium catalyst at 90-120 °C. (b) Arrhenius plot of initial TOF values to calculate activation energy. Reaction conditions: Ruthenium catalyst (0.1 mmol), GLY (6.84 mmol), NaOH (7.52 mmol), water (20.52 mmol), and 110 °C.

Table 2.2. Effect of the base and temperature on hydrogen production from GLY over the ruthenium catalyst.^a



Entry	Base (equiv.)	T(°C) /t(h)	Conv. (%)	H ₂ gas (mL) ^b	n(H ₂)/n(GLY)	Selectivity of byproducts (%) ^c				CB (%) ^d
						SL (yield) ^c	PD	SG	SF	
1	KOH (1.1)	110/6	43	68	0.40	78 (32)	2	6	13	98
2	Na ₂ CO ₃ (1.1)	110/6	-	-	-	-	-	-	-	-
3	KO ^t Bu (1.1)	110/7	26	48	0.28	85 (18)	0	4	8	99
4	K ₂ CO ₃ (1.1)	110/6	-	-	-	-	-	-	-	-
5	NaOH (1.1)	90/9	50	76	0.45	84 (42)	1	4	4	96
6	NaOH (1.1)	100/8.5	72	130	0.77	81 (58)	5	2	11	98
7	NaOH (1.1)	110/7	86	162	0.96	81 (69)	3	2	11	97
8	NaOH (1.1)	120/5	88	192	1.14	75 (66)	1	2	17	96
9	NaOH (1.5)	110/8	93	212	1.26	73 (68)	1	2	18	94
10	NaOH (2.0)	110/10	>99	270	1.61	70 (70)	<1	1	24	96

^aReaction conditions: Ruthenium catalyst (0.1 mmol), GLY (6.84 mmol), base, water (20.52 mmol), 90-120 °C. ^bVolume of gas was measured by the water displacement method. ^cConversion and selectivity were calculated by ¹H NMR using sodium acetate as an internal standard. ^dCB is carbon balance. GLY (glycerol), SL (sodium lactate), PD (1,2-propanediol), SG (sodium glycolate), SF (sodium formate).

Table 2.3. Hydrogen Production from glycerol using varying loading of ruthenium catalyst.^a

Entry	Catalyst mol (%)	t (h)	Conv. (%)	H ₂ gas (mL) ^b	n(H ₂)/n(GLY)	Sel. of byproducts (%) ^c				CB (%) ^d
						SL (yield) ^c	PD	SG	SF	
1	0	6	-	-	-	-	-	-	-	-
2	0.25	5	32	24	0.14	80 (25)	2	2	14	99
3	0.5	6.5	56	70	0.41	81 (45)	3	2	12	98
4	1.0	7	72	130	0.77	82 (59)	2	3	10	97
5	1.5	7	86	162	0.96	81 (69)	3	2	11	97
6	2.0	6	74	134	0.80	80 (59)	2	4	12	98

^aReaction conditions: Ruthenium catalyst, GLY (6.84 mmol), NaOH, water, 110 °C. ^bVolume of gas was measured by the water displacement method. ^cConversion and selectivity were calculated by ¹H NMR using sodium acetate as an internal standard. ^dCB is carbon balance. GLY (glycerol), SL (sodium lactate), PD (1,2-propanediol), SG (sodium glycolate), SF (sodium formate).

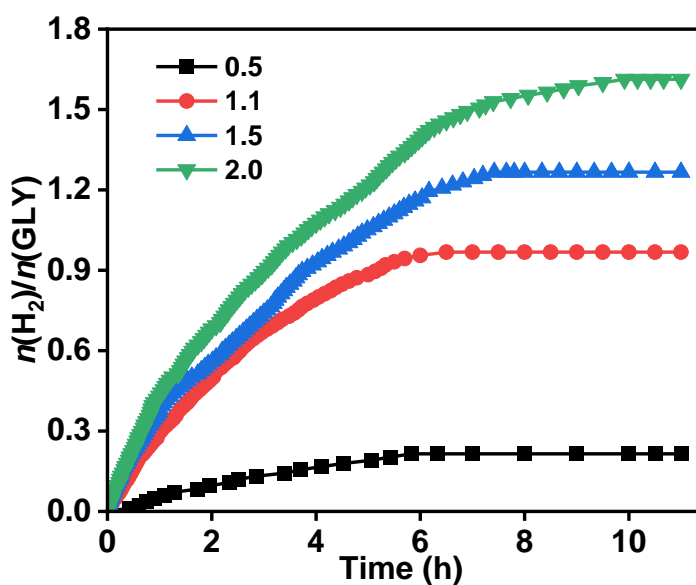


Figure 2.9. Effect of base concentration on hydrogen production from GLY over the ruthenium catalyst. Reaction conditions: Ruthenium catalyst (0.1 mmol), GLY (6.84 mmol), NaOH (0.5- 2.0 equiv.), water (20.52 mmol), and 110 °C.

Hence, our findings inferred that high efficiency for the generation of H₂ gas from GLY with an appreciably high yield of SL can be achieved at the optimized reaction condition performed over the ruthenium catalyst (1.5 mol %) with (NaOH)/*n*(glycerol) of ≥ 1.1 and *n*(GLY)/*n*(water) of 1:3 at 110 °C. Notably, H₂ gas generation from glycerol can also be achieved using ruthenium catalysts as low as 0.25 mol% (Table 2.3). The above findings inferred the crucial role of water, base, and reaction temperature in tuning the efficiency of reaction to produce H₂ gas from GLY and the selectivity towards SL. However, the base content greatly influenced the reaction efficiency for H₂ gas production as well as SL selectivity (Table 2.2).

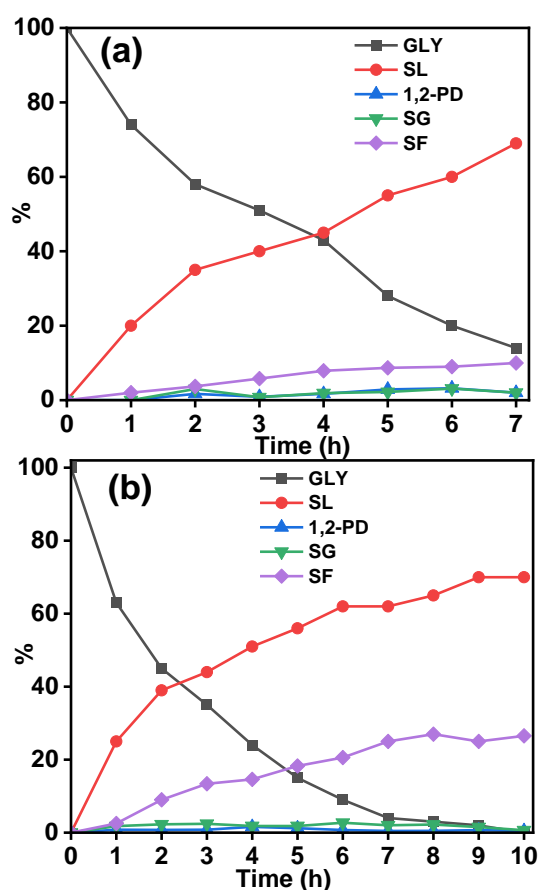


Figure 2.10. Time course plot for the distribution of GLY and various products in the presence of (a) 1.1 equiv. and (b) 2.0 equiv. of NaOH during the hydrogen production from GLY over the ruthenium catalyst. Reaction conditions: Ruthenium catalyst (0.1 mmol), GLY (6.84 mmol), NaOH (7.52 mmol and 13.68 mmol), water (20.52 mmol), 110 °C. GLY (glycerol), SL (sodium lactate), PD (1,2-propanediol), SG (sodium glycolate), and SF (sodium formate).

Upon increasing the $n(\text{NaOH})/n(\text{GLY})$ from 1.1 to 2.0, a significant enhancement in the amount of H_2 gas released per mol of GLY was also observed (Figure 2.5 and Figure 2.9). Compared to 0.96 equiv. of H_2 per mol of GLY (86% conv.) released in the presence of 1.1 equiv. of NaOH, the release of 1.26 equiv. of H_2 per mol of GLY (conv. 93%) was achieved with 1.5 equiv. of NaOH at 110 °C (Table 2.2, entries 7, 9). Notably, there was no significant change in the selectivity of SL and SF with 1.1-1.5 equiv. of NaOH. However, for the reaction with a higher $n(\text{NaOH})/n(\text{GLY})$ ratio of 2.0, complete conversion of GLY (>99%) with the release of a significantly high 1.6 equiv. of H_2 gas (11.02 mmol) per mol of glycerol was achieved (Table 2.2, entry 10). Notably, the observed high amount of H_2 gas released was compensated by a decrease in the SL selectivity to 70% and an increase in SF selectivity to 24% (Figure 2.10, and Table 2.2, entry 10). Notably, the dehydrogenation of GLY with a lower concentration of base $n(\text{NaOH})/n(\text{GLY})$ ratio of 0.5 inferred the formation of PD (sel. 13%) with <5% sel. for SF (Table 2.1, entry 3). On the other hand, only traces (~1%) of PD formation were observed for the catalytic dehydrogenation of GLY performed with a higher base $n(\text{NaOH})/n(\text{GLY})$ ratio of 1.5-2.0 (Table 2.2, entries 9, 10) (Figures 2.11 and 2.12) and only a very poor selectivity (~2%) of SG was observed for the catalytic reactions performed for dehydrogenation of GLY. Further, ^{13}C NMR analysis of the reaction aliquot obtained under the optimized reaction condition suggested only a negligible trace of carbonate, which is in line with the observed high selectivity for hydrogen gas (Figure 2.13).

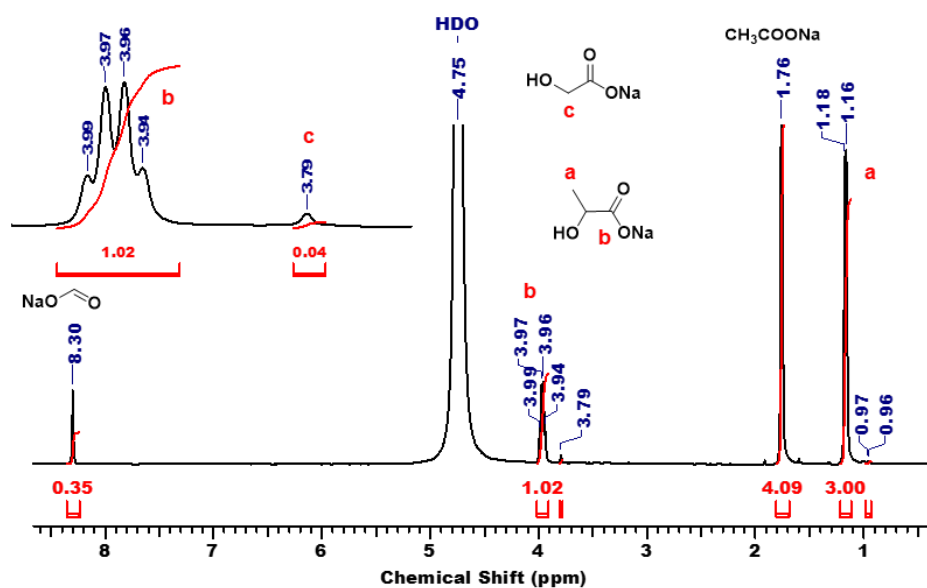


Figure 2.11. ^1H NMR spectra of the crude reaction mixture of the catalytic reaction in $\text{D}_2\text{O}:\text{H}_2\text{O}$ (1:9) for hydrogen production from GLY over the ruthenium catalyst. Reaction conditions: Ruthenium catalyst (0.1 mmol), GLY (6.84 mmol), NaOH (10.26 mmol), water (20.52 mmol), and 110 °C.

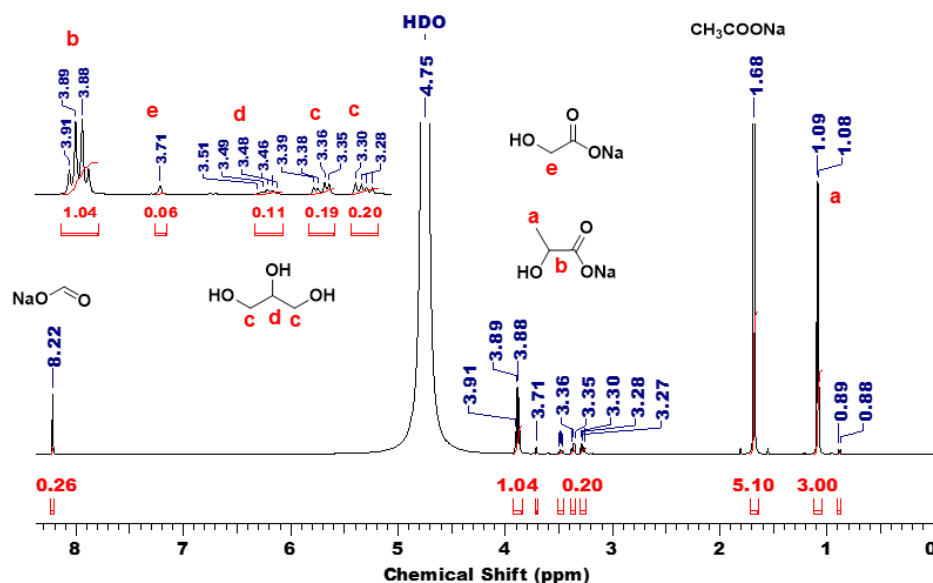


Figure 2.12. ^1H NMR spectra of the crude reaction mixture of the catalytic reaction in $\text{D}_2\text{O}:\text{H}_2\text{O}$ (1:9) for hydrogen production from GLY over the ruthenium catalyst. Reaction conditions: Ruthenium catalyst (0.1 mmol), GLY (6.84 mmol), NaOH (13.68 mmol), water (20.52 mmol), and 110 °C.

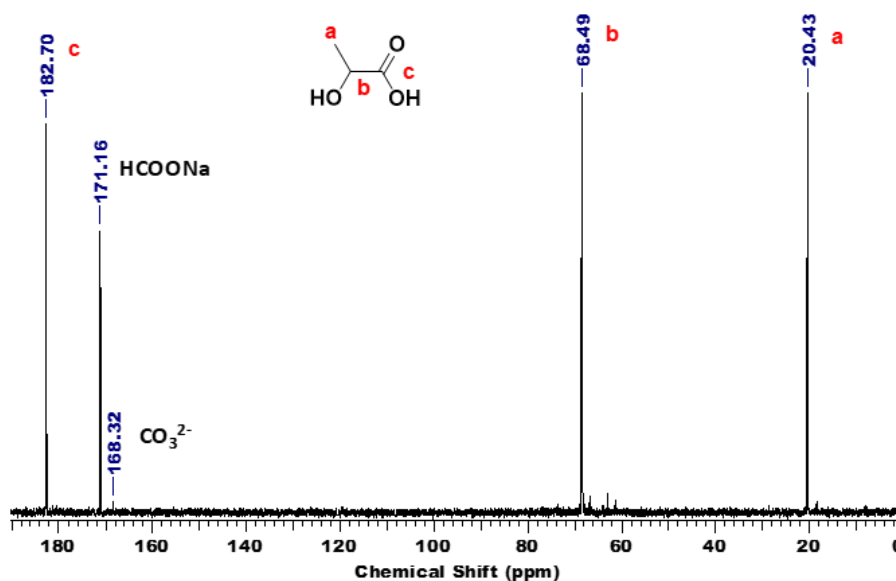
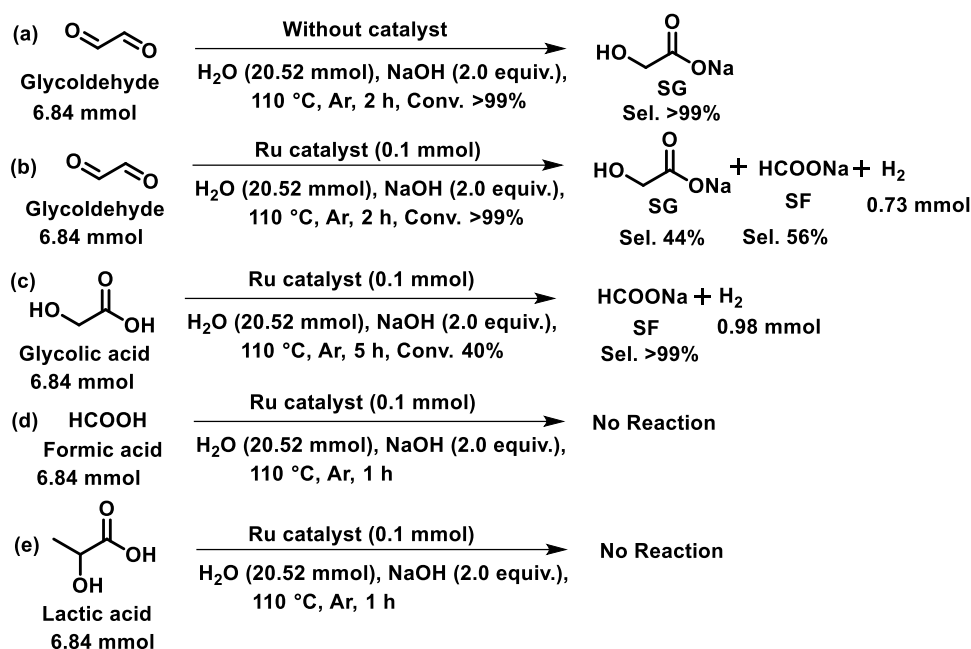


Figure 2.13. ¹³C NMR spectra of the crude reaction mixture of the catalytic reaction in D₂O:H₂O (1:9) for hydrogen production from GLY over the ruthenium catalyst. Reaction conditions: Ruthenium catalyst (0.1 mmol), GLY (6.84 mmol), NaOH (13.68 mmol), water (20.52 mmol), and 110 °C.

Further, based on the conversion of GLY to SL (Scheme 2.1, reaction 2) and the conversion of GLY to SF (Scheme 2.1, reaction 6), the amount of H₂ gas that will be released during the dehydrogenation of GLY over ruthenium catalyst at 110 °C was estimated. In good correlation with the carbon balance, 97% accuracy matching for the obtained and the estimated (based on the stoichiometry) amount of H₂ gas for the dehydrogenation of GLY in the presence of 2.0 equiv. base (Table 2.2, entry 10). Analogously, for the reaction performed with 1.1 and 1.5 equiv. base, an accuracy of 90% and 96%, respectively, was observed for hydrogen gas amount (Table 2.2, entries 7 and 9). The observed deviation in the observed and the estimated amount of hydrogen gas can be attributed to the formation of PD via hydrogenation during the catalytic reaction (Scheme 2.1, reaction 7). Further, to investigate the involvement of these intermediates in the conversion of GLY to H₂ gas, we performed several control experiments using various substrates in the presence of 2.0 equiv. of NaOH (Scheme 2.2). It is postulated that the sodium glycolate (SG) observed in the catalytic reaction can be produced from glycolaldehyde, where glycolaldehyde produces hydrogen gas in the presence of a base to yield glyoxal, which further undergoes rearrangement to SG (Scheme 2.3).



Scheme 2.2. Controlled reactions to investigate the pathway of hydrogen production from glycerol over the ruthenium catalyst.

In agreement with the above, we observed the transformation of glyoxal to SG in the presence of a base under the catalyst-free condition (Scheme 2.2 and Figure 2.14), while treating glyoxal with the ruthenium catalyst at 110 °C resulted in the formation of SG (sel. 44%), H₂ gas and SF (sel. 56%) (Scheme 2.2 and Figure 2.15). Further, treating glycolic acid (GA) with ruthenium catalyst in the presence of 2.0 equiv. of NaOH resulted in the generation of H₂ gas along with SF, suggesting that GA dehydrogenation also occurred under the catalytic reaction (Scheme 2.2 and Figure 2.16). These findings are consistent with the observed lower selectivity of SG during the catalytic dehydrogenation of GLY (Tables 2.2 and 2.3). Notably, further transformation of formic acid (FA) was not observed even in the presence of the ruthenium catalyst (Scheme 2.2, Figures 2.17.) However, in the case of dehydrogenation of lactic acid (LA), no conversion was observed (Scheme 2.2, Figure 2.18).

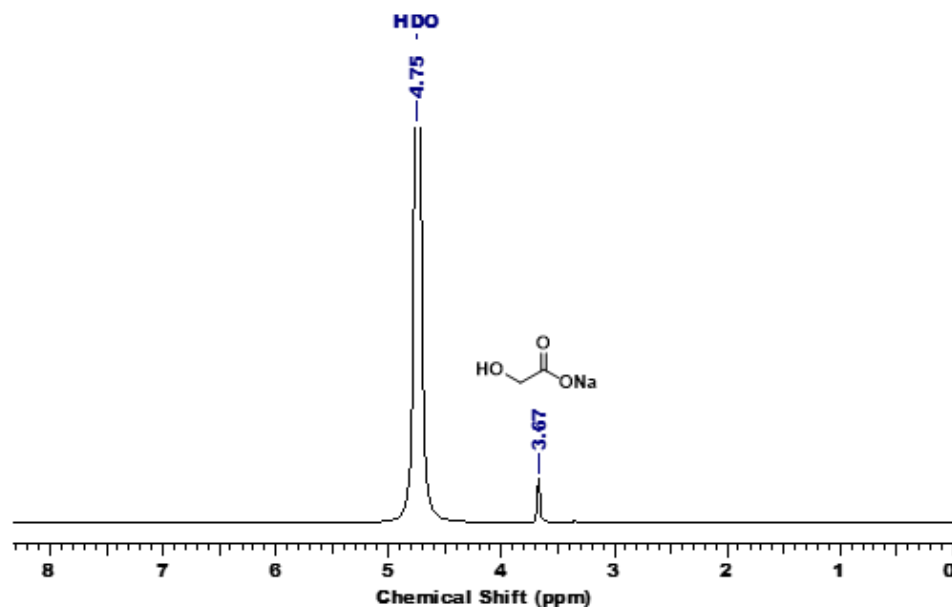


Figure 2.14. ¹H NMR spectra of the crude reaction mixture of glyoxal treated with the base under catalyst-free conditions. Reaction conditions: Glyoxal (6.84 mmol), NaOH (13.68 mmol), water (20.52 mmol), and 110 °C.

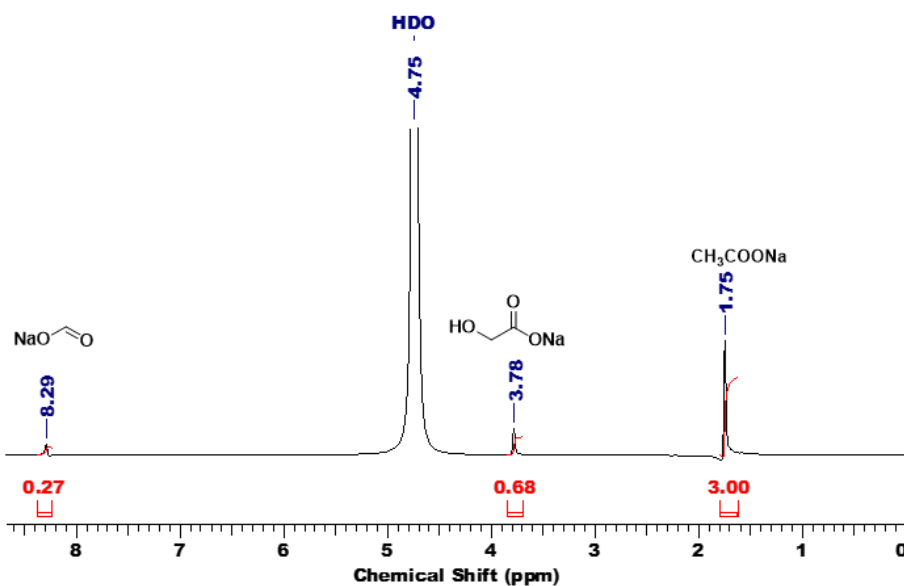


Figure 2.15. ¹H NMR spectra of the crude reaction mixture of glyoxal treated with the base in the presence of ruthenium catalyst. Reaction conditions: Ruthenium catalyst (0.1 mmol), glyoxal (6.84 mmol), NaOH (13.68 mmol), water (20.52 mmol), and 110 °C.

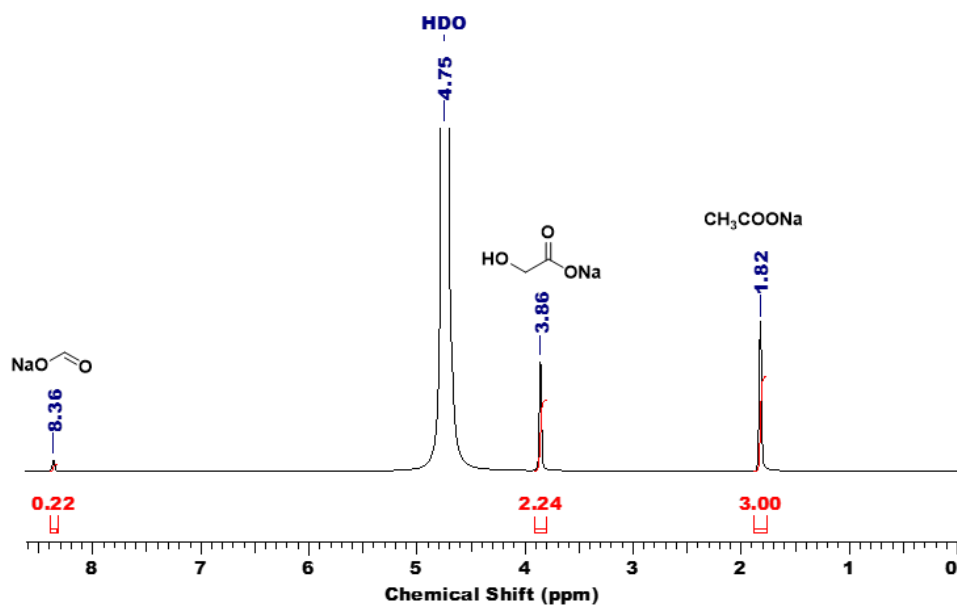


Figure 2.16. ¹H NMR spectra of the crude reaction mixture of glycolic acid treated with the base in the presence of ruthenium catalyst. Reaction conditions: Ruthenium catalyst (0.1 mmol), glycolic acid (6.84 mmol), NaOH (13.68 mmol), water (20.52 mmol), and 110 °C.

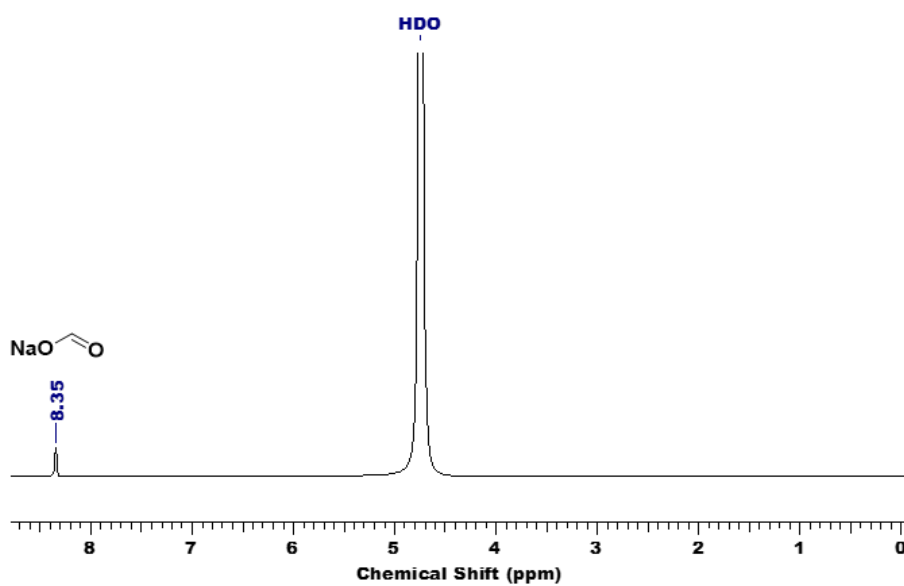


Figure 2.17. ¹H NMR spectra of the crude reaction mixture of formic acid treated with the base in the presence of ruthenium catalyst. Reaction conditions: Ruthenium catalyst (0.1 mmol), formic acid (6.84 mmol), NaOH (13.68 mmol), water (20.52 mmol), and 110 °C.

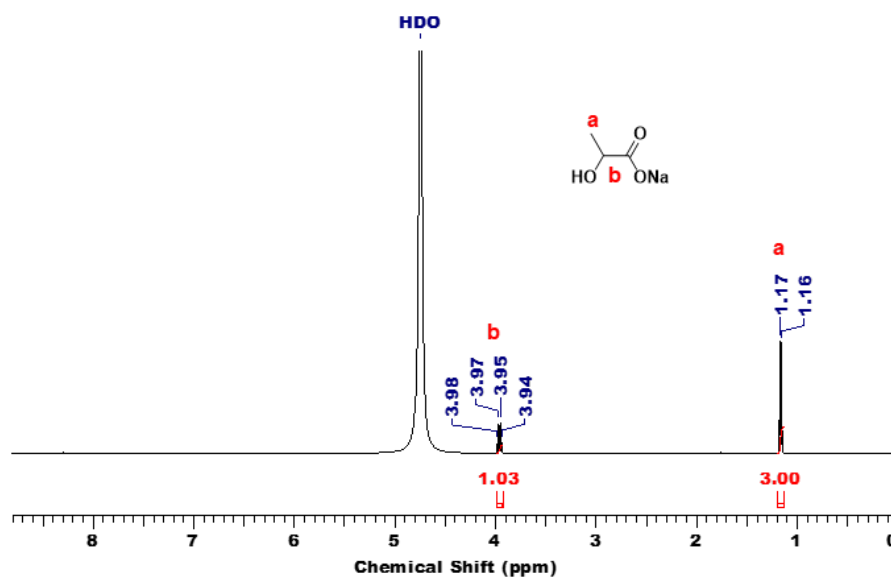
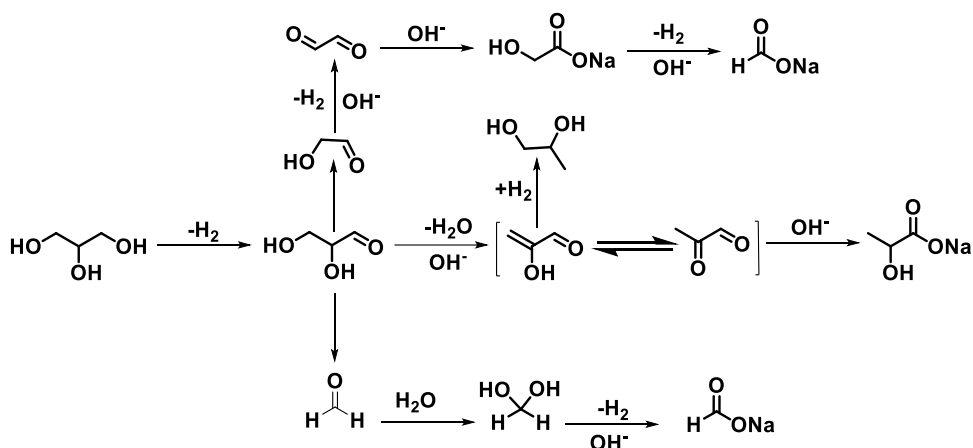


Figure 2.18. ¹H NMR spectra of the crude reaction mixture of lactic acid treated with the base in the presence of ruthenium catalyst. Reaction conditions: Ruthenium catalyst (0.1 mmol), lactic acid (6.84 mmol), NaOH (13.68 mmol), water (20.52 mmol), and 110 °C.

Therefore, this experimental evidence clearly suggests that for the conversion of GLY to H₂ gas and SL, in the initial step, the dehydrogenation of GLY resulted in the formation of glyceraldehyde, which further got involved in two competitive pathways. Firstly, glyceraldehyde undergoes base-catalyzed dehydration to pyruvaldehyde, which can further be transformed to sodium lactate *via* the Cannizzaro reaction in the presence of a base. Notably, PD can also be formed by the hydrogenation of pyruvaldehyde in the presence of in situ-generated H₂ gas.^[47] Secondly, glyceraldehyde can undergo a base-catalyzed retro-aldol reaction *via* C-C bond cleavage to formaldehyde and glycolaldehyde, which can further be dehydrogenated to SG *via* glyoxal, followed by the dehydrogenation of SG to SF (Scheme 2.3).



Scheme 2.3. Plausible reaction pathway for hydrogen production from glycerol over the ruthenium catalyst.

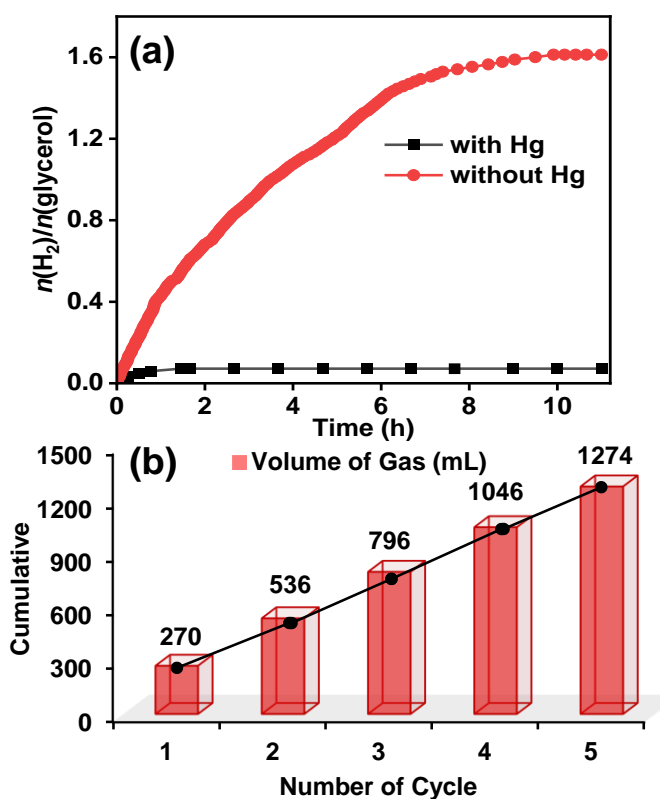


Figure 2.19. (a) Mercury poisoning test for the hydrogen production from GLY over the ruthenium catalyst. Reaction conditions: Ruthenium catalyst (0.1 mmol), Hg, GLY (6.84 mmol), NaOH (13.68 mmol), water (20.52 mmol), and 110 °C, and (b) Recyclability experiments for hydrogen production from GLY over the ruthenium catalyst. Reaction conditions: Ruthenium catalyst (0.1 mmol), GLY (6.84 mmol), NaOH (13.68 mmol), water (20.52 mmol), and 110 °C.

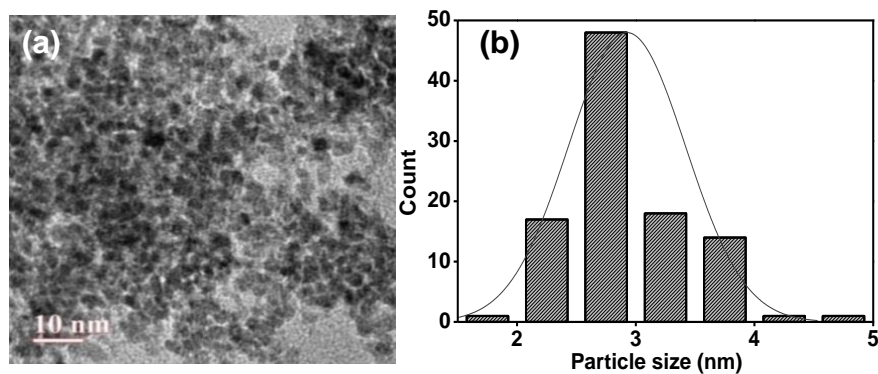


Figure 2.20. (a) TEM image, and corresponding (b) particle size distribution curve for the spent ruthenium catalyst.

Further, to validate the heterogeneity of the ruthenium catalyst, a catalyst poisoning experiment was also carried out by treating the ruthenium catalyst with an excess of elemental Hg prior to the catalytic reaction. Results inferred that the release of H₂ gas was drastically diminished in the presence of elemental Hg, suggesting that the active form of the catalyst is heterogeneous (Figure 2.19 a). Moreover, the studied ruthenium catalyst exhibited appreciably good recyclability for hydrogen generation from GLY under the optimized reaction conditions. After each catalytic run, the ruthenium catalyst was recovered by centrifugation and was recycled for five consecutive catalytic runs (over 52 h) for the generation of over 1.2 L of hydrogen gas from ~2.5 mL of glycerol (Figure 2.19 b). The observed slightly less amount of hydrogen gas released in the fifth cycle could be attributed to the agglomeration of nanoparticles and loss of catalyst during the recovery process. The TEM (average particle size of ~2.75 nm), XPS, and P-XRD analysis of the recovered catalyst inferred no significant change in the catalyst, suggesting the high stability of the ruthenium catalyst under the catalytic reaction conditions (Figure 2.20 and Figures 2.21-2.22). ICP-AES analysis of the reaction aliquot suggested no significant leaching of ruthenium (0.20 wt%). Further, the studied ruthenium catalyst was found to be stable, with no decomposition of the PVP stabilizer observed during the reaction condition, as evidenced by the absence of any peak corresponding to PVP in the ¹H NMR of the reaction aliquot (Figure 2.23).

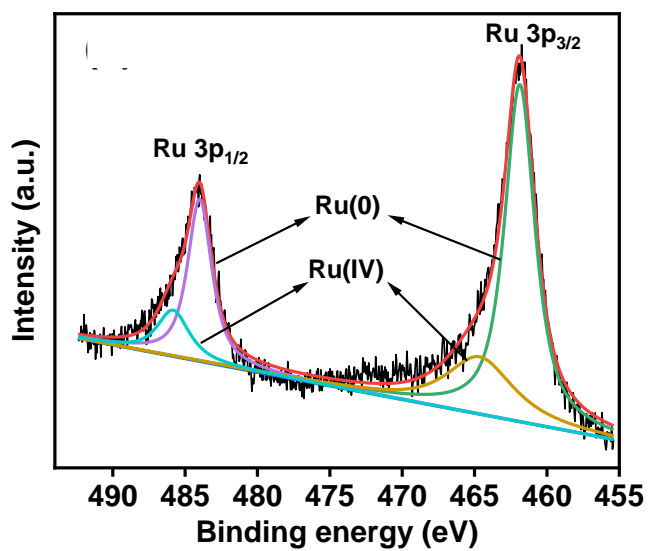


Figure 2.21. XPS profile of Ru 3p region of the spent ruthenium catalyst.

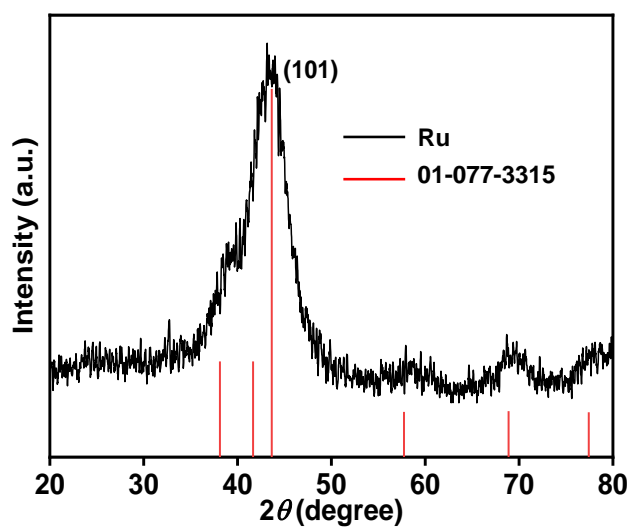


Figure 2.22. P-XRD pattern of the spent ruthenium catalyst.

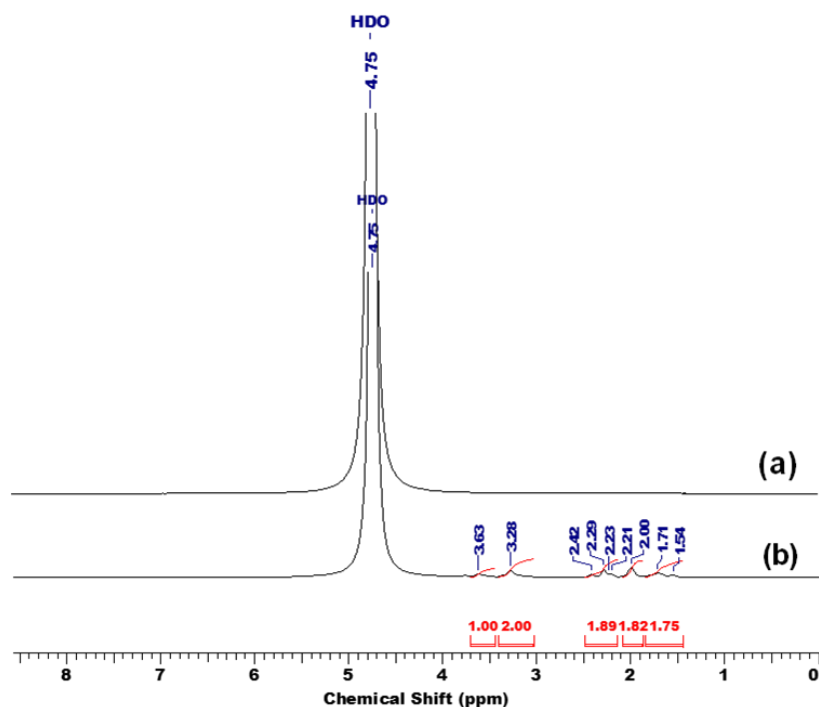


Figure 2.23. ^1H NMR spectra of (a) PVP (polyvinyl pyrrolidone) under optimized reaction conditions and (b) pure PVP in $\text{D}_2\text{O}:\text{H}_2\text{O}$ (1:9).

Further, the studied catalytic system was also employed for the bulk-scale production of hydrogen gas from glycerol (Figure 2.24). As shown in Figure 2.24, over 700 mL (28.6 mmol) of H_2 gas was produced from 2 mL of glycerol in the presence of 2.0 equiv. of NaOH over the ruthenium catalyst (0.1 mmol) at 110 °C in 36 h. During the evolution of hydrogen gas, 64% yield of lactic acid was also achieved. These results clearly evidenced the robustness and long-term stability of the ruthenium catalyst for the selective hydrogen gas production (68 L H_2 per gram of Ru with H_2 yield of 350 L per L of glycerol) from glycerol in water at 110 °C. The product lactic acid was purified by extracting the crude reaction mixture using 2-methyl butanol to remove 1,2-PD. Further, the aqueous portion was acidified (pH ~1.5) with 1M HCl, then again extracted with diethyl ether (5×10 mL). Then, the combined organic portion was dried over Na_2SO_4 . The purified lactic acid was obtained by removing the organic solvent under reduced pressure and was analyzed by ^1H NMR and ^{13}C NMR in D_2O (Figures 2.25 and 2.26).

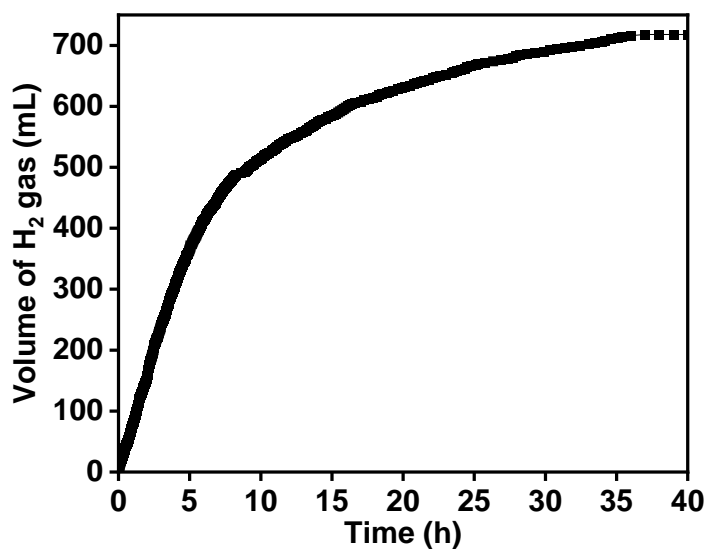


Figure 2.24. Time course plot for the bulk-scale production of hydrogen gas from GLY over the ruthenium catalyst. Reaction conditions: Ruthenium catalyst (0.1 mmol), GLY (2 mL), NaOH (54.72 mmol), water (1.48 mL), and 110 °C.

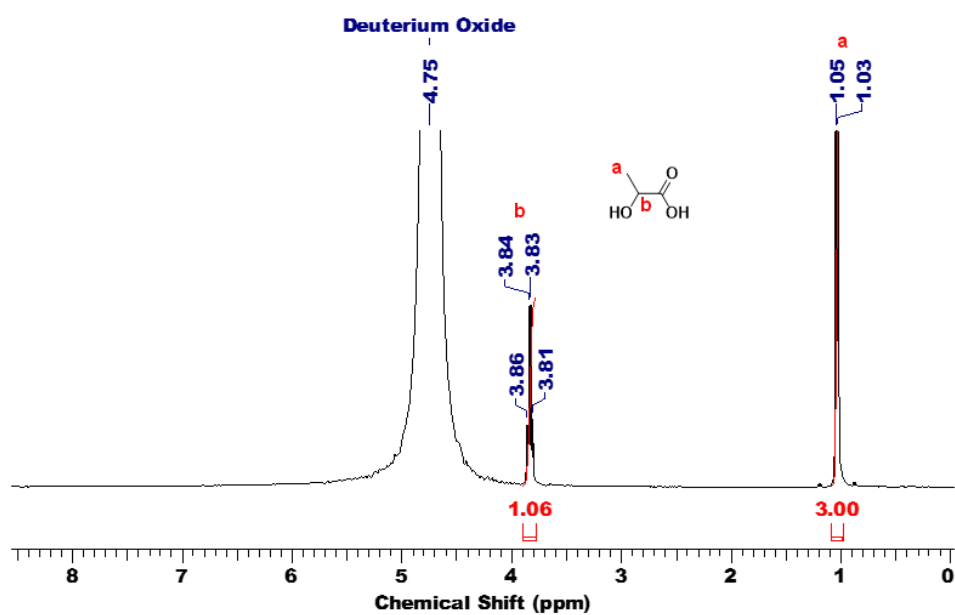


Figure 2.25. ¹H NMR spectra of purified lactic acid in D₂O.

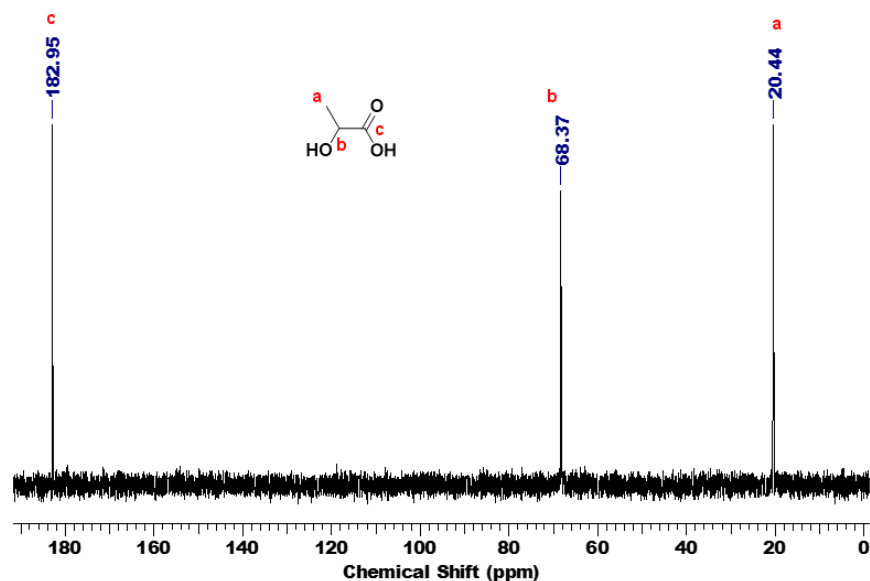


Figure 2.26. ^{13}C NMR spectra of purified lactic acid in D_2O .

Notably, recently reported Ru-NMC-3 and RuPt-NMC-3 catalysts explored for the aqueous phase reforming of GLY and exhibited 92% conversion at 250 °C with only 88.5% H_2 selectivity.^[66] Noticeably, the Ru/NaY catalyst explored for the aqueous phase reforming of GLY (conv. up to 88%) at 250 °C with 600 psi (N_2) resulted in only 74% H_2 selectivity with contamination of CO_2 as high as 24%.^[67] Moreover, for the long-term stability investigation, the H_2 selectivity of only 65% was reported for Ru/NaY. Han *et al.* explored Ru-Zn-Cu(I)/HAP catalyst for GLY to LA conversion, where complete conversion of glycerol was only achieved at 140 °C in 21 h, while at lower temperature 100 °C and 120 °C conversion of GLY dropped significantly to only 26.7% and 42.2%, respectively in 12 h.^[55] Therefore, in view of the literature reports on the catalytic conversion of GLY to H_2 gas and/or lactic acid, our experimental findings inferred that the studied ruthenium catalyst displayed high performance for the conversion of GLY to the purified hydrogen gas and LA in water at 110 °C. The observed high yield ($n(\text{H}_2)/n(\text{GLY})$; 0.96~1.61) and selectivity (>99.9%) for H_2 gas over the ruthenium catalyst is noteworthy. Moreover, an appreciably high yield (70%) for LA is also achieved during the production of H_2 gas from GLY. Advantageously, the ruthenium catalyst exhibited high long-term stability for hydrogen production (productivity of 7.9×10^{-2} mol $\text{H}_2/\text{g Ru/h}$ from glycerol over 36 h in water at 110 °C).

2.4. Conclusions

Herein, we demonstrated a highly efficient catalytic process for the selective production of hydrogen gas from GLY over the ruthenium catalyst in the presence of NaOH in water at 90-120 °C. Our findings evidenced the crucial role of the base and water in achieving higher selectivity for H₂ gas production. Hydrogen gas content as high as 11 mmol (1.6 equiv. H₂ per mol of GLY) with >99% conversion of GLY was achieved over the ruthenium catalyst. Moreover, high yield of LA (70%) was also achieved over the studied ruthenium catalyst. Several controlled and catalytic reactions were also performed to investigate the dehydrogenation pathway of GLY, which corroborates well with our experimental findings. Our results also worked well for the bulk production of H₂ gas from glycerol with appreciably high long-term stability of the ruthenium catalyst for over 36 h and produced 70 L H₂ per gram of Ru with the H₂ yield of 350 L H₂ per L of GLY. Therefore, our present study provides new developments in exploring GLY as an efficient liquid hydrogen storage material (LHSM), where a selectively higher content of H₂ gas can be produced from GLY in water at a relatively lower temperature range.

Note: The content of this chapter is published as Kumar et al., ChemCatChem, 14, e202101951 (DOI: 10.1002/cctc.202101951) and reproduced with permission from Wiley VCH with license number 5671331334907.

2.5. References

1. Gumisiriza R., Hawumba J. F., Okure M., Hensel O. (2017), Biomass Waste to-Energy Valorisation Technologies: A Review Case for Banana Processing in Uganda, Biotechnol. Biofuels, 10, 1-29 (DOI: 10.1186/s13068-016-0689-5)
2. Clauser N. M., González G., Mendieta C. M., Kruyeniski J., Area, M. C. Vallejos M. E. (2021), Biomass Waste as Sustainable Raw Material for Energy and Fuels, Sustain., 13, 1-21 (DOI: 10.3390/su13020794)
3. Sanchez N., Ruiz R. Y., Cifuentes B., Cobo M. (2019), Controlling Sugarcane Press-mud Fermentation to Increase Bioethanol Steam Reforming for Hydrogen Production, Waste Manag., 98, 1-13 (DOI: 10.1016/j.wasman.2019.08.006)
4. Xu C., Paone E., Rodríguez-Padrón D., Luque R., Mauriello F. (2020),

- Reductive Catalytic Routes Towards Sustainable Production of Hydrogen, Fuels and Chemicals from Biomass Derived Polyols, *Renew. Sustain. Energy Rev.*, 127, 1-11 (DOI: 10.1016/j.rser.2020.109852)
5. Davda R. R., Shabaker J. W., Huber G. W., Cortright R. D., Dumesic J. A. (2005), A Review of Catalytic Issues and Process Conditions for Renewable Hydrogen and Alkanes by Aqueous-Phase Reforming of Oxygenated Hydrocarbons over Supported Metal Catalysts, *Appl. Catal. B Environ.*, 56, 171-186 (DOI: 10.1016/j.apcatb.2004.04.027)
 6. Merki D., Fierro S., Vrabel H., Hu X. (2011), Amorphous Molybdenum Sulfide Films as Catalysts for Electrochemical Hydrogen Production in Water, *Chem. Sci.*, 1262-1267 (DOI: 10.1039/c1s00117e)
 7. Chen L., Qi Z., Zhang S., Su J., Somorjai G. A. (2020), Catalytic Hydrogen Production from Methane: A Review on Recent Progress and Prospect, *Catalysts*, 10, 858-875 (DOI: 10.3390/catal10080858)
 8. Han W., Yan Y., Shi Y., Gu J., Tang J., Zhao H. (2016), COD Capture: A Feasible Option Towards Energy Self-Sufficient Domestic Wastewater Treatment, *Sci. Rep.*, 6, 1-9 (DOI: 10.1038/srep25054)
 9. Woodward J., Orr M., Cordray K., Greenbaum E. (2000), Enzymatic Production of Biohydrogen, *Nature*, 405, 1014–1015 (DOI: 10.1038/35016633)
 10. Azadi P., Farnood R. (2011), Review of Heterogeneous Catalysts for Sub and supercritical Water Gasification of Biomass and Wastes, *Int. J. Hydrog. Energy*, 36, 9529-9541 (DOI: 10.1016/j.ijhydene.2011.05.081)
 11. Saeidabad N. G., Noh Y. S., Eslami A. A., Song H. T., Kim H. D., Fazeli A., Moon D. J. (2020), A Review on Catalysts Development for Steam Reforming of Biodiesel Derived Glycerol; Promoters and Supports, *Catalysts*, 10, 910-932 (DOI: 10.3390/catal10080910)
 12. Fasolini A., Cucciniello R., Paone E., Mauriello F., Tabanelli T. (2019), A Short Overview on the Hydrogen Production Via Aqueous Phase Reforming (APR) of Cellulose, C6-C5 Sugars and Polyols, *Catalysts*, 9, 910-934 (DOI: 10.3390/catal9110917)
 13. Awasthi M. K., Rai R. K., Behrens S., Singh S. K. (2021), Low-Temperature Hydrogen Production From Methanol over a Ruthenium Catalyst in Water, *Catal. Sci. Technol.*, 11, 136-142 (DOI: 10.1039/D0CY01234A)

10.1039/d0cy01470b)

14. Awasthi M. K., Singh, S. K. (2021), Ruthenium Catalyzed Hydrogen Production from Formaldehyde–Water Solution, *Sustain. Energy Fuels*, 5, 549-555 (DOI: 10.1039/d0se01330g)
15. Patra S., Singh S. K. (2020), Hydrogen Production from Formic Acid and Formaldehyde over Ruthenium Catalysts in Water, *Inorg. Chem.*, 59, 4234-4243 (DOI: 10.1021/acs.inorgchem.9b02882)
16. Patra S., Awasthi M. K., Rai R. K., Deka H., Mobin S. M., Singh S. K. (2019), Dehydrogenation of Formic Acid Catalyzed by Water-Soluble Ruthenium Complexes: X-ray Crystal Structure of a Diruthenium Complex, *Eur. J. Inorg. Chem.*, 2019, 1046-1053 (DOI: 10.1002/ejic.201801501)
17. Sordakis K., Tang C., Vogt L. K., Junge H., Dyson P. J., Beller M., Laurenczy G. (2018), Homogeneous Catalysis for Sustainable Hydrogen Storage in Formic Acid and Alcohols, *Chem. Rev.*, 118, 372-433 (DOI: 10.1021/acs.chemrev.7b00182)
18. Mellmann D., Sponholz P., Junge H., Beller M. (2016), Formic acid as a Hydrogen Storage Material-development of Homogeneous Catalysts for Selective Hydrogen Release, *Chem. Soc. Rev.*, 45, 3954-3988 (DOI: 10.1039/c5cs00618j)
19. Singh A. K., Singh S., Kumar A. (2016), Hydrogen Energy Future with Formic Acid: A Renewable Chemical Hydrogen Storage System, *Catal. Sci. Technol.*, 6, 12-40 (DOI: 10.1039/c5cy01276g)
20. Yang F., Hanna M. A., Sun R. (2012), Value-Added Uses for Crude Glycerol–A Byproduct of Biodiesel Production, *Biotechnol. Biofuels*, 5, 1-10 (DOI: 10.1186/1754-6834-5-13)
21. Kent R. (2018), *Renewables, Plast. Eng.*, 74, 56-57 (DOI: 10.1002/peng.20026)
22. Vaidya P. D., Rodrigues A. E. (2009), Glycerol Reforming for Hydrogen Production: A Review, *Chem. Eng. Technol.*, 32, 1463-1469 (DOI: 10.1002/ceat.200900120)
23. D'Hondt E., Van De Vyver S., Sels B. F., Jacobs P. A. (2008), Catalytic Glycerol Conversion into 1,2-propanediol in Absence of Added Hydrogen, *Chem. Commun.*, 6011-6012 (DOI: 10.1039/b812886c)

24. Jin X., Roy D., Thapa P. S., Subramaniam B., Chaudhari R. V. (2013), Atom Economical Aqueous-Phase Conversion (APC) of Biopolyols to Lactic Acid, Glycols, and Linear Alcohols Using Supported Metal Catalysts, *ACS Sustain. Chem. Eng.*, 1, 1453-1462 (DOI: 10.1021/sc400189d)
25. Jin X., Shen J., Yan W., Zhao M., Thapa P. S., Subramaniam B., Chaudhari R. V. (2015), Sorbitol Hydrogenolysis over Hybrid Cu/CaO-Al₂O₃ Catalysts: Tunable Activity and Selectivity with Solid Base Incorporation, *ACS Catal.*, 5, 6545-6558 (DOI: 10.1021/acscatal.5b01324)
26. Yin H., Zhang C., Yin H., Gao D., Shen L., Wang A. (2016), Hydrothermal Conversion of Glycerol to Lactic Acid Catalyzed by Cu/hydroxyapatite, Cu/MgO, and Cu/ZrO₂ and Reaction Kinetics, *Chem. Eng. J.*, 288, 332-343 (DOI: 10.1016/j.cej.2015.12.010)
27. Arvela P. M., Simakova I. L., Salmi T., Murzin D. Y. (2014), Production of Lactic Acid/Lactates from Biomass and Their Catalytic Transformations to Commodities, *Chem. Rev.*, 114, 1909-1971 (DOI: 10.1021/cr400203v)
28. Shen L., Zhou X., Wang A., Yin H., Yin H., Cui W. (2017), Hydrothermal Conversion of High-concentrated Glycerol to Lactic Acid Catalyzed by Bimetallic CuAu_x (X = 0.01–0.04) Nanoparticles and Their Reaction Kinetics, *RSC Adv.*, 7, 30725-30739 (DOI: 10.1039/c7ra04415a)
29. Li C., Gao M., Zhu W., Wang N., Ma X., Wu C., Wang Q. (2021), Recent Advances in the Separation and Purification of Lactic Acid from Fermentation Broth, *Process Biochem.*, 104, 142-151 (DOI: 10.1016/j.procbio.2021.03.011)
30. Komesu A., Maciel M. R. W., de Oliveira J. R. A., Martins L. H. D. S., Filho R. M. (2017), Purification of Lactic Acid Produced by Fermentation: Focus on Non-traditional Distillation Processes, *Sep. Purif. Rev.*, 46, 241-254 (DOI: 10.1080/15422119.2016.1260034)
31. Chen G., Xu N., Li X., Liu Q., Yang H., Li W. (2015), Hydrogen Production by Aqueous-Phase Reforming of Ethylene Glycol over a Ni/Zn/Al Derived Hydrotalcite Catalyst, *RSC Adv.*, 5, 60128-60134

(DOI: 10.1039/c5ra07184d)

32. Coronado I., Stekrova M., Reinikainen M., Simell P., Lefferts L., Lehtonen J. (2016), A Review of Catalytic Aqueous-Phase Reforming of Oxygenated Hydrocarbons Derived from Biorefinery Water Fractions, *Int. J. Hydrog. Energy*, 41, 11003-11032 (DOI: 10.1016/j.ijhydene.2016.05.032)
33. Lin L. L., Zhou W., Gao R., Yao S. Y., Zhang X., Xu W. Q., Zheng S. J., Jiang Z., Yu Q. L., Li Y. W., Shi C., Wen X. D., Ma D. (2017), Low-temperature Hydrogen Production from Water and Methanol using Pt/ α -MoC Catalysts, *Nature*, 544, 80-83 (DOI: doi.org/10.1038/nature21672)
34. Hollak S. A. W., Ariens M. A., de Jong K. P., van Es D. S. (2014), Hydrothermal Deoxygenation of Triglycerides over Pd/C aided by In Situ Hydrogen Production from Glycerol Reforming, *ChemSusChem*, 7, 1057-1062 (DOI: 10.1002/cssc.201301145)
35. Nielsen M., Alberico E., Baumann W., Drexler H. J., Junge H., Gladiali S., Beller M. (2013), Low-temperature Aqueous-Phase Methanol Dehydrogenation to Hydrogen and Carbon dioxide, *Nature*, 495, 85-89 (DOI: 10.1038/nature11891)
36. Chu X. W., Liu J., Sun B., Dai R., Pei Y., Qiao M. H., Fan K. N. (2011), Aqueous-Phase Reforming of Ethylene Glycol on Co/ZnO Catalysts Prepared by the Coprecipitation Method, *J. Mol. Catal. A: Chem.*, 335, 129-135 (DOI: 10.1016/j.molcata.2010.11.024)
37. Guo Y., Liu X. H., Azmat M. U., Xu W. J., Ren J. W., Wang Y. Q., Lu G. Z. (2012), Hydrogen Production by Aqueous-Phase Reforming of Glycerol over Ni-B Catalysts, *Int. J. Hydrog. Energy*, 37, 227-234 (DOI: 10.1016/j.ijhydene.2011.09.111)
38. Cortright D. R., Davda R. R., Dumesic J. A. (2002), Hydrogen from Catalytic Reforming of Biomass-derived Hydrocarbons in Liquid Water, *Nature*, 418, 964-967 (DOI: 10.1038/nature01009)
39. King D. L., Zhang L., Xia G., Karim A. M., Heldebrant D. J., Wang X., Peterson T., Wang Y. (2010), Aqueous Phase Reforming of Glycerol for Hydrogen Production over Pt-Re Supported on Carbon, *Appl. Catal. B: Environ.*, 99, 206-213 (DOI: 10.1016/j.apcatb.2010.06.021)
40. Boga D. A., Oord R., Beale A. M., Chung Y. M., Bruijninx P. C. A.,

- Weckhuysen B. M. (2013), Highly Selective Bimetallic Pt-Cu/Mg(Al)O Catalysts for the Aqueous-Phase Reforming of Glycerol, *ChemCatChem*, 5, 529-537 (DOI: 10.1002/cctc.201200112)
41. Pendem C., Sarakar B., Siddiqui N., Konathala L. N. S., Baskar C., Bal R. (2018), K-Promoted Pt-Hydrotalcite Catalyst for Production of H₂ by Aqueous Phase Reforming of Glycerol, *ACS Sustain. Chem. Eng.*, 6, 2122-2131 (DOI: 10.1021/acssuschemeng.7b03512)
 42. Rahman M. M. (2020), Aqueous-Phase Reforming of Glycerol over Carbon-Nanotube-Supported Catalysts, *Catal. Lett.*, 150, 2674-2687 (DOI: 10.1007/s10562-020-03167-2)
 43. Guo Y., Lui X., Wang Y. (2019), Catalytic and DRIFTS Studies of Pt-Based Bimetallic Alloy Catalysts in Aqueous-Phase Reforming of Glycerol, *Ind. Eng. Chem. Res.*, 58, 2749-2758 (DOI: 10.1021/acs.iecr.8b05774)
 44. Baston F., Kazemeini M. (2020), Renewable Hydrogen Production by Aqueous-Phase Reforming of Glycerol using Ni/Al₂O₃-MgO Nanocatalyst: Effect of the Ni Loading, *Biomass Conv. Biorefin.*, 13, 237-246 (DOI: 10.1007/s13399-020-01150-w)
 45. Polychronopoulou K., Charisiou N. D., Siakavelas G. I., Alkhoori A. A., Sebastian V., Hinder S. J., Baker M. A., Goula M. A. (2019), Ce-Sm-xCu Cost-Efficient Catalysts for H₂ Production through the Glycerol Steam Reforming Reaction, *Sustain. Energy Fuels*, 3, 673-691 (DOI: 10.1039/c8se00388b)
 46. Surendar M., Padmakar D., Lingaiah N., Rao K. S. R., Prasad P. S. S. (2017), Influence of La₂O₃ Composition in MgO-La₂O₃ Mixed Oxide-Supported Co Catalysts on the Hydrogen Yield in Glycerol Steam Reforming, *Sustain. Energy Fuels*, 1, 354-361 (DOI: 10.1039/c6se00023a)
 47. Siddiki S. M. A. H., Touchy A. S., Kon K., Toyao T., Shimizu K. I. (2017), Oxidant-free Dehydrogenation of Glycerol to Lactic Acid by Heterogeneous Platinum Catalysts, *ChemCatChem*, 9, 2816-2821 (DOI: 10.1002/cctc.201700099)
 48. Kon K., Siddiki S. M. A. H., Shimizu K. I. (2013), Size and Support-Dependent Pt Nanocluster Catalysis for Oxidant-free Dehydrogenation

- of Alcohols, *J. Catal.*, 304, 63-71 (DOI: 10.1016/j.jcat.2013.04.003)
49. Oberhauser W., Evangelisti C., Tiozzo C., Vizza, F., Psaro R. (2016), Lactic Acid from Glycerol by Ethylene-Stabilized Platinum-Nanoparticles, *ACS Catal.*, 6, 1671-1674 (DOI: 10.1021/acscatal.5b02914)
 50. Zavrazhnov S. A., Esipovich A. L., Danov S. M., Zlobin S. Y., Belousov A. S. (2018), Catalytic Conversion of Glycerol to Lactic Acid: State of the Art and Prospects, *Kinet. Catal.*, 59, 459-471 (DOI: 10.1134/S0023158418040171)
 51. Razali N., Abdullah A. Z. (2017), Production of Lactic Acid from Glycerol via Chemical Conversion using Solid Catalyst: A review, *Appl. Catal. A Gen.*, 543, 234-246 (DOI: 10.1016/j.apcata.2017.07.002)
 52. Komanoya T., Suzuki A., Nakajima K., Kitano M., Kamata K., Hara M. (2016), A Combined Catalyst of Pt Nanoparticles and TiO₂ with Water-Tolerant Lewis Acid Sites for One-Pot Conversion of Glycerol to Lactic Acid, *ChemCatChem*, 8, 1094-1099 (DOI: 10.1002/cctc.201501197)
 53. Zhang G., Jin X., Guan Y., Yin B., Chen X., Liu Y., Feng X., Shan H., Yang C. (2019), Toward Selective Dehydrogenation of Glycerol to Lactic Acid over Bimetallic Pt–Co/CeO_x Catalysts, *Ind. Eng. Chem. Res.*, 2019, 58, 14548-14558 (DOI: 10.1021/acs.iecr.9b01918)
 54. Jin X., Dang L., Lohrman J., Subramaniam B., Ren S., Chaudhari R. V. (2013), Lattice-Matched Bimetallic CuPd-Graphene Nanocatalysts for Facile Conversion of Biomass-Derived Polyols to Chemicals, *ACS Nano*, 7, 1309-1316 (DOI: 10.1021/nn304820v)
 55. Jiang Z., Zhang Z., Wu T., Zhang P., Song J., Xie C., Han B. (2017), Efficient Generation of Lactic Acid from Glycerol over a Ru-Zn-Cu(I)/Hydroxyapatite Catalyst, *Chem. Asian J.*, 12, 1598-1604 (DOI: 10.1002/asia.201700412)
 56. Sharninghausen L. S., Campos J., Manas M. G., Crabtree R. H. (2014), Efficient Selective and Atom Economic Catalytic Conversion of Glycerol to Lactic Acid, *Nat. Commun.*, 5, 1-9 (DOI: 10.1038/ncomms6084)
 57. Lu Z., Demianets I., Hamze R., Terrile N. J., Williams T. J. (2016), A Prolific Catalyst for Selective Conversion of Neat Glycerol to Lactic

- Acid, *ACS Catal.*, 6, 2014-2017 (DOI: 10.1021/acscatal.5b02732)
58. Sun Z., Liu Y., Chen J., Huang C., Tu T. (2015), Robust Iridium Coordination Polymers: Highly Selective, Efficient, and Recyclable Catalysts for Oxidative Conversion of Glycerol to Potassium Lactate with Dihydrogen Liberation, *ACS Catal.*, 5, 6573-6578 (DOI: 10.1021/acscatal.5b01782)
59. Cheong Y. J., Sung K., Kim J. A., Kim Y. K., Jang H. Y. (2020), Highly Efficient Iridium-Catalyzed Production of Hydrogen and Lactate from Glycerol: Rapid Hydrogen Evolution by Bimetallic Iridium Catalysts, *Eur. J. Inorg. Chem.*, 2020, 4064-4068 (DOI: 10.1002/ejic.202000670)
60. Li Y., Nielsen M., Li B., Dixneuf P. H., Junge H., Beller M. (2015), Ruthenium-Catalyzed Hydrogen Generation from Glycerol and Selective Synthesis of Lactic Acid, *Green Chem.*, 17, 193-198 (DOI: 10.1039/c4gc01707b)
61. Dutta M., Das K., Prathapa S. J., Srivastava H. K., Kumar A. (2020), Selective and High Yield Transformation of Glycerol to Lactic Acid using NNN Pincer Ruthenium Catalysts, *Chem. Commun.*, 56, 9886-9889 (DOI: 10.1039/d0cc02884c)
62. Sharninghausen L. S., Mercado B. Q., Crabtree R. H., Hazari N. (2015), Selective Conversion of Glycerol to Lactic Acid with Iron Pincer Precatalysts, *Chem. Commun.*, 51, 16201-16204 (DOI: 10.1039/c5cc06857f)
63. Rai R. K., Gupta K., Behrens S., Li J., Xu Q., Singh S. K. (2015), Highly Active Bimetallic Nickel–Palladium Alloy Nanoparticle Catalyzed Suzuki–Miyaura Reactions, *ChemCatChem*, 7, 1806-1812 (DOI: 10.1002/cctc.201500145)
64. Dwivedi A. D., Rai R. K., Gupta K., Singh S. K. (2017), Catalytic Hydrogenation of Arenes in Water Over In Situ Generated Ruthenium Nanoparticles Immobilized on Carbon, *ChemCatChem*, 9, 1930-1938 (DOI: 10.1002/cctc.201700056)
65. Morgan D. J. (2015), Resolving Ruthenium: XPS Studies of Common Ruthenium Materials, *Surf. Interface Anal.*, 47, 1072–1079 (DOI: 10.1002/sia.5852)
66. Gogoi P., Kanna N., Begum P., Deka R. C., Satyanarayana C. V. V.,

Raja T. (2020), Controlling and Stabilization of Ru Nanoparticles by Tuning the Nitrogen Content of the Support for Enhanced H₂ Production through Aqueous-Phase Reforming of Glycerol, *ACS Catal.*, 10, 2489-2507 (DOI: 10.1021/acscatal.9b04063)

67. Gogoi P., Nagpure A. S., Kandasamy P., Satyanarayana C. V. V., Raj T. (2020), Insights Into the Catalytic Activity of Ru/NaY Catalysts for Efficient H₂ Production through Aqueous Phase Reforming, *Sustain. Energy Fuels*, 4, 678-690 (DOI: 10.1039/c9se00797k)

Chapter 3

Investigating the Role of Support in the Catalytic Transformation of Glycerol to Hydrogen Gas and Lactic Acid over the Ru/support Catalyst

3.1. Introduction

In the recent past, there has been considerable effort in exploring sustainable and environmentally benign energy resources to meet the ever-increasing global energy demand driven by population growth and industrialization.^[1,2] In this regard, hydrogen (H₂), a sustainable energy carrier with high energy density (120 MJ/kg), has garnered significant attention and is widely regarded as the most promising solution to address these energy crisis and climate change issues.^[3-6] The low volumetric energy density, high diffusivity, and flammability of hydrogen gas make it challenging to store or transport, one of the biggest hurdles to its extensive applications. Despite these hurdles, hydrogen gas is being produced at the industrial scale through processes such as the reforming of methane,^[7] aqueous phase reforming (APR),^[8] and steam reforming (SR) of non-renewable resources.^[9] Notably, these processes are very energy-intensive and emit greenhouse gases along with H₂ gas. On the other hand, there are several liquid organic molecules, such as methanol,^[10-13] formic acid,^[14-17] formaldehyde,^[17-19] and other polyols^[20-23] showing high potential to store appreciably high volumetric and gravimetric content of H₂, which can be released in the presence of a suitable catalyst. Advantageously, being liquid, these enable the easy storage and transportation of H₂ gas.

According to the Organization for Economic Co-operation and Development (OECD) and the Food and Agricultural Organization (FAO), global biodiesel production is projected to increase to 9.5 billion litres by 2030.^[24] The major by-product of the transesterification of triglycerides is glycerol (GLY), formed in abundance (10 wt% of biodiesel) during biodiesel production.^[25] Due to its non-toxicity and ability to be transformed into several valuable platform chemicals, including lactic acid (LA), propanediol (PD),

ethylene glycol (EG), glycolic acid (GA) and so on, glycerol (GLY) has emerged as a versatile bio-platform substrate.^[25] Further, LA is one of the important products of GLY transformation, which has vast applications in many industries. Notably, LA can be produced from GLY by catalytic oxidation or acceptor-less dehydrogenation processes. Dehydrogenation of GLY to LA is considered an attractive route for simultaneous production of H₂ gas along with LA. Hence, GLY, a waste in biodiesel industries, can be explored as a promising resource for hydrogen production.

Catalytic reforming of glycerol via steam reforming (SR) or aqueous-phase reforming (APR) has been extensively explored for H₂ production. Several catalysts, such as Pt/SiO₂,^[26] Ni/M (M = CeO₂, MgO, TiO₂),^[27] Ce-Sm-5Cu,^[28] Ni/La/Co/Al₂O₃,^[29] Co/MgO-La₂O₃,^[30] and others have been explored for the production of H₂ gas via the SR process, albeit at high temperatures (>200 °C). On the other hand, the APR process works at relatively lower temperatures than the SR process. For the APR of GLY to H₂ gas, a plethora of catalysts, including Ru/NaY,^[22] Ru-NMC-3,^[31] RuPt-NMC-3,^[31] PtMo/C,^[32] PtRe/C,^[33] Pt/Al₂O₃,^[34] Pt-KHT/28,^[35] Pt-Cu/Mg(Al)O,^[36] PtFe/γ-Al₂O₃,^[37] Ni/Al₂O₃-La₂O₃^[38] and others have been investigated at 200-250 °C. Dumesic and co-workers achieved the breakthrough for the generation of H₂ gas from biomass-derived compounds through APR.^[34] Although the reforming of GLY has resulted in the generation of H₂ gas, the purity of H₂ gas is compromised due to the co-production of other gases (CO, CO₂, and CH₄) following a series of uncontrolled pathways i.e., C₃H₈O₃ → 4H₂ + 3CO; CO + H₂O → CO₂ + H₂; CO + 3H₂ → CH₄ + H₂O; CO₂ + 4H₂ → CH₄ + 2H₂O.

Even though the dehydrogenative method for converting GLY to LA is an appealing choice to generate both H₂ gas and LA, most of the research focuses on the oxidative conversion of GLY to LA employing Cu, Ni, Au, or Pd-based catalysts.^[39-49] During the former process, excessive oxidation of glyceraldehyde produces glyceric acid, tartaric acid, and glycolic acid (GA) along with LA, which dramatically decreases the selectivity of the desired LA product.

In literature, some non-noble metal-based catalysts such as Cu,^[39] Cu₂O,^[40] CuO/ZrO₂,^[41] CuO/CeO₂,^[42] CuO/Al₂O₃,^[43] Cu-Cu₂O@NC,^[44]

$\text{Co}_3\text{O}_4/\text{CeO}_2$,^[45] Ni/HAP ,^[46] were also explored for the conversion of GLY to LA. Moreover, noble metal based supported catalysts such as, AuCu/CeO_2 ,^[47] M/CeO_2 ($\text{M} = \text{Au}, \text{Pt}$),^[48] Pd/HAP ,^[49] M/ZnO ^[50] ($\text{M} = \text{Pt}, \text{Pd}, \text{Rh}, \text{and Au}$), Pt/C ,^[51] $\text{Pt}/\text{carbon material}$,^[52] $\text{Pt}/\text{L-Nb}_2\text{O}_5$,^[53] $\text{Pt}/\text{support}$ ($\text{ZrO}_2, \text{TiO}_2, \text{C}$),^[54] Pt/ZrO_2 ,^[55] $\text{Ru-Zn-Cu(I)}/\text{HAP}$,^[56] $\text{Au}/\text{HAP}/\text{BN}$,^[57] were primarily developed for the transformation of GLY to LA at higher temperature (>160 °C) under gaseous atmosphere (He, N_2 or ethylene). Wang et al. reported the hydrothermal conversion of GLY to LA over the Pd/HAP catalyst at 230 °C using NaOH (1.1 equiv.) and exhibited complete conversion of GLY with 95% selectivity of LA in 90 1.5 h. The interaction between Pd and HAP (synergistic effect) was vital for the efficient conversion of GLY to LA. The catalytic process was found to be strongly influenced by temperature, NaOH concentration, and Pd loading.^[49] Urbano et al. studied different noble metals ($\text{Pt}, \text{Pd}, \text{Rh Au}$) supported over ZnO under H_2 or He pressure (20 bar) at 180 °C in alkaline medium and achieved complete conversion of glycerol with 68% selectivity for lactic acid (LA) over the Rh/ZnO catalyst due to strong metal-support interaction (SMSI).^[50] Shimizu et al. explored the influence of reaction atmosphere (N_2, H_2 , or O_2) for the oxidant-free and solvent-free dehydrogenative transformation of glycerol at 160 °C Pt/C catalyst and achieved 95% conversion of GLY with a 93% yield of LA in the presence of N_2 gas (1 bar).^[51] Psaro et al. performed catalytic transformation of GLY to SL over the Pt-based catalysts with different Pt particle size ($\text{Pt}^1@C^k$, 1.4 nm and $\text{Pt}^2@C^k$, 2.4 nm) at 140 °C using ethylene gas (~ 60 bar), where C^k represents ketjenblack having high surface area carbon material.^[52] They observed high selectivity of LA (95%) in the case of $\text{Pt}^1@C^k$ catalyst while less selectivity of LA (89%) in the case of $\text{Pt}^2@C^k$ catalyst. Shishido et al. explored a bifunctional catalyst ($\text{Pt}/\text{L-Nb}_2\text{O}_5$) for the base-free catalytic transformation of GLY for continuous production of LA. They achieved $>70\%$ selectivity of LA with 24% GLY conversion after 80 h under an oxygen atmosphere at 140 °C.^[53] Ftouni et al. investigated the Pt-based catalyst stabilized over different supports ($\text{ZrO}_2, \text{TiO}_2, \text{C}$) under H_2 or He atmosphere at 180 °C and observed that Pt/ZrO_2 performed well over others, and 80% yield of LA was found in 8 h. The reaction atmosphere (He or H_2) played a major role in the selectivity of LA (<10 h), while no major difference was observed in the selectivity of LA after 24 h.^[54] Pescarmona et al.

investigated a Pt/ZrO₂ catalyst to facilitate a one-pot transfer hydrogenation reaction between glycerol and cyclohexene to produce LA (95%) and cyclohexane without additional H₂ gas at 160 °C in 4.5 h under N₂ atmosphere (20 bar), which clearly indicates that GLY has a potential to be explored as hydrogen storage material.^[55] These reports highlight how the size of metal nanoparticles, strong-metal support interaction (SMSI), reaction atmosphere, and temperature influence the transformation of GLY to LA and other products. These findings also imply that noble metal-based catalysts work effectively for the conversion of GLY to LA, but the generation of H₂ gas from GLY has received limited attention to date.

Recently, we also reported selective hydrogen production from aqueous glycerol using NaOH over ruthenium nanoparticles, where we achieved complete conversion of GLY for the production of selective H₂ gas (1.6 equiv.) with co-production of LA (70% yield) at 110 °C.^[21] It is evident from the literature reports that most of the catalytic systems are active at high temperature and pressure conditions. Moreover, the purity of hydrogen gas is also one of the major issues as contaminants such as CO, CO₂, and CH₄ were also produced along with H₂ gas. In this regard, herein, we explored ruthenium nanoparticles stabilized over various supports (La(OH)₃, Mg(OH)₂, ZnO, ZrO₂, TiO₂) for the selective production of H₂ gas along with LA from aqueous glycerol (GLY) at lower temperature (90-130 °C). Controlled experiments were performed to elucidate the plausible dehydrogenation pathway of GLY to H₂ and SL. The developed supported ruthenium catalysts showed high activity for bulk-scale generation of H₂ gas from GLY, where support played a crucial role in tuning the catalytic activity. Additionally, H₂ gas was produced from various other terminal diols such as ethylene glycol (EG), 1,3-propanediol (PDO), 1,4-butanediol (BDO), 1,5-pentanediol (PO) and 1,6-hexanediol (HDO).

3.2. Experimental section

3.2.1. Materials and instrumentation

RuCl₃.xH₂O (>99%), NaBH₄ (98%), cetyltrimethylammonium bromide (CTAB) (98%), TiO₂ (99.5%), ZrO₂ (99%), glycerol (99.5%), ethylene glycol (>99%), glyoxal solution (40 wt% in water), lactic acid (>90%), formic acid

(>96%), and 1,6-hexanediol (HDO) (99%) were purchased from Sigma Aldrich, India. Glycolic acid (>98%) 1,2-propanediol (PD) (>98%), 1,3-propanediol (PO) (98%), 1,4-butanediol (BDO) (>99%), and 1,5-pentanediol (PDO) (>97%) were purchased from TCI analytics, India. MgO (99%), and ZnO (98%) were procured from S. D. Fine Chemical Limited, India. High-purity argon gas was procured from Sigma Gases, India. Distilled water was used for performing all the experiments. All other chemical reagents and metal salts were available commercially and were used as received without any further purification. NMR spectra were recorded in deuterated solvents using Bruker Ascend 500 and Bruker Avance 400 spectrometer (500 MHz and 400 MHz). Transmission electron microscopy (TEM) images of the sample were obtained on Titan ST at the accelerating voltage of 300 kV. The samples for TEM analysis were prepared by the drop-casting method. Briefly, ruthenium nanoparticles were dispersed in ethanol under ultra-sonication for 1 hour, and then highly dispersed particles were spread onto a carbon-coated Cu grid and dried at room temperature. Particle size was calculated using ImageJ software for at least 50-100 particles, and the average particle size distribution curve was plotted using Origin software. Scanning electron microscopic images and elemental mapping data were collected using a JOEL-7610F plus equipped with an EDS detector. Powder X-ray diffraction (P-XRD) measurements were performed using a Rigaku SmartLab Automated Multipurpose X-ray diffractometer with a scintillation detector. The measurements were conducted using Cu K α radiation ($\lambda = 1.5418 \text{ \AA}$) with a step size of 0.02° in the 2θ range of $20-80^\circ$. The exposure time for each P-XRD measurement was 20 minutes. The nitrogen physisorption isotherms were measured at 77 K using Quantachrome Autosorb iQ₂ TPX automated gas sorption system, and the specific surface area was calculated using the Brunauer-Emmett-Teller (BET) equation in the relative pressure (P/P₀) range of 0.05-0.3. Samples were degassed at 200 °C for 8 h under high vacuum before analysis. XPS data was recorded using Al K-alpha (1486.61 eV) X-rays using SPECS Surface Nano Analysis GmbH instrument, Germany. Samples were excited by using monochromatic Al K-alpha (1486.61 eV) with the X-ray source operating at 100 W. Scans were collected at a pass energy of 30 eV over the binding energy range 1200-0 eV. Charge correction was made relative to the position of C 1s (284.6 eV) as reference. The gas chromatography

(GC) analyses were performed on a Shimadzu GC-2014 system using a shin carbon-ST packed column with a thermal conductivity detector (TCD) using argon as a carrier gas. Parameters were set for the program to detect H₂, CO₂, CO, and CH₄ gas (detector temperature: 200 °C, and oven temperature program: 90 °C (hold time: 1 min), 90-200 °C (rate: 15 °C per minute). Inductively coupled plasma atomic emission spectroscopy (ICP-AES) was performed with ARCOS, a simultaneous spectrometer of SPECTRO analytical instruments. The sample was digested using aquaregia in the thermal autoclave at 170 °C for 12 h, diluted with water and then carried out for analysis.

3.2.2. Catalyst synthesis

The wet impregnation method was used for the synthesis of supported Ru catalysts using the support La(OH)₃, ZnO, Mg(OH)₂, ZrO₂, and TiO₂. Typically, 90 mg of support was dispersed in 5 mL of distilled water in a 25 mL round bottom flask under sonication for 20 min. To this, ruthenium (III) chloride (0.1 mmol) and CTAB (0.050 g) were added, and the resulting mixture was heated at 60 °C for 2 h. The mixture was cooled to room temperature and then aqueous solution of NaBH₄ (0.050 g in 5 mL water) was added dropwise under sonication to reduce Ru³⁺ to Ru⁰. The obtained mixture was sonicated for 30 minutes, and then the precipitates were collected by centrifugation, washed several times with distilled water and ethanol, and dried under vacuum before using for the catalytic reactions.

3.2.3. Catalytic test

In a 25 mL round bottom flask fitted with a condenser and a water displacement set-up, a specified amount of the catalyst, glycerol (GLY), water and base were added. The reaction set-up was de-aerated by a repeated process of vacuuming and flushing with argon gas at least three times. The reaction mixture was stirred (600 rpm) in a pre-heated oil bath at 90-130 °C under an argon atmosphere. The amount of H₂ gas evolved was quantified using a water displacement set-up, which was calibrated (thrice using water) as 4.0 ± 0.1 mL/cm. The composition of the evolved gas was analyzed by GC-TCD. After the reaction, the catalyst was recovered from the reaction mixture by centrifugation. The conversion of GLY and the yields of other co-products were determined by ¹H NMR of the

reaction mixture using sodium acetate as an internal standard using the following equation.

$$\text{Yield} = C_f(\text{P})/C_i(\text{GLY}) \times 100 (\%)$$

where,

$C_f(\text{GLY})$ = millimoles of carbon in the final glycerol

$C_f(\text{P})$ = millimoles of carbons in the final product

3.2.4. Heterogeneity test

Typically, an aqueous suspension of Ru/La(OH)₃ catalyst (100 mg catalyst in 0.740 mL water) was stirred with a large excess of elemental mercury Hg(0) at room temperature for 3 h prior to the catalytic reaction. Then GLY (13.68 mmol, 1 mL) and NaOH (27.36 mmol, 1.095 g) were added to the above reaction vessel (25 mL round bottom flask) fitted with a condenser and gas burette. The water displacement set-up was then de-aerated by a repeated process of vacuum and flushing with argon gas at least three times. The reaction mixture was stirred at 130 °C in a pre-heated oil bath at a rpm of 600, and the progress of the reaction was monitored for the specified duration.

3.2.5. Recyclability experiment

Catalytic reaction was performed as specified in section 3.4. After the completion of the reaction, the catalyst was recovered from the reaction mixture by centrifugation, washed several times with distilled water and ethanol, dried overnight under vacuum and then reused for the next catalytic run.

3.2.6. Bulk-scale reaction

Typically, the bulk-scale reaction was performed using GLY (68.5 mmol) and water (205.5 mmol) in the presence of Ru/La(OH)₃ catalyst (100 mg) and NaOH (2.0 equiv.) under the optimized reaction conditions at 130 °C. Similarly, bulk-scale reaction for ethylene glycol (68.5 mmol) was also performed using water (205.5 mmol) and NaOH (2.0 and 3.0 equiv.) over Ru/La(OH)₃ catalyst (100 mg) at 130 °C. A bulk scale reaction was performed in a 50 mL round bottom flask using a reaction set-up, as mentioned in section 3.2.3.

3.3. Results and discussion

3.3.1. Synthesis, characterization, and screening of catalysts for the transformation of GLY to H₂ gas and SL

Supported metal catalysts have more advantages in terms of high dispersion, catalytic activity, stability, and reusability than unsupported metal catalysts.⁵⁸ Metal hydroxide and metal oxides are an important class of support materials having unique properties such as high surface area and high thermal stability.⁵⁹ Various Ru/support catalysts with different metal oxides, such as ZrO₂, Nb₂O₅, CeO₂, Al₂O₃, ZnO, etc., were explored extensively for the transformation of GLY to lactic acid (LA).^[41–43,50,53] Therefore, at the outset, we synthesized various Ru catalysts supported over different basic (La(OH)₃, Ru/Mg(OH)₂), amphoteric (ZnO, ZrO₂), and acidic (TiO₂) using wet-impregnation methods followed by NaBH₄ induced reduction. P-XRD patterns of the synthesized supported ruthenium catalysts showed dominant peaks corresponding to the support material only, while no peaks for Ru were observed, suggesting that Ru is well dispersed over supports (Figure 3.1).

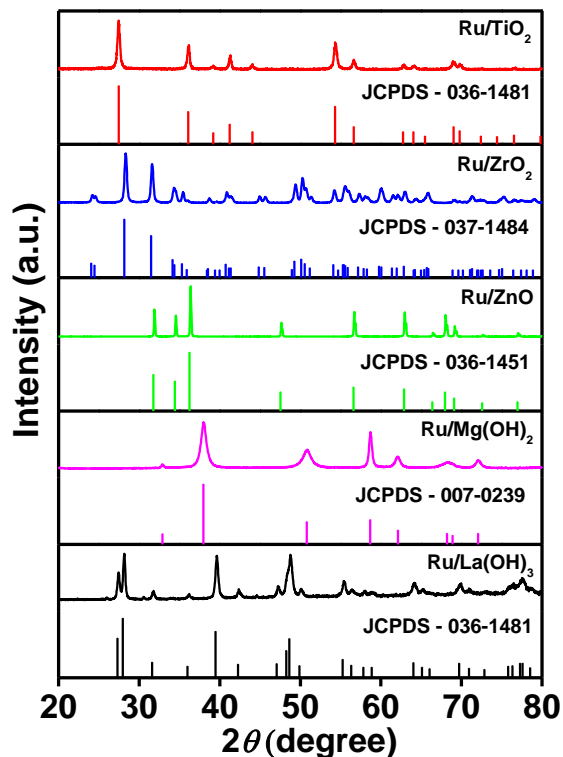
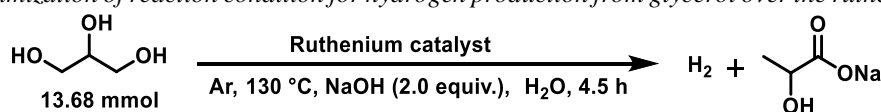


Figure 3.1. P-XRD pattern of the ruthenium-based supported catalysts.

We further screened these catalysts for the dehydrogenation of GLY in water ($n(\text{GLY})/n(\text{H}_2\text{O})$ of 1:3) using NaOH (2.0 equiv.) at 130 °C (Table 3.1 and Figure 3.2). Over the Ru/La(OH)₃ catalyst, high catalytic activity was achieved with the complete conversion of GLY and evolution of 470 mL H₂ gas (TOF 105 h⁻¹) with 86% yield of sodium lactate (SL) in 4.5 h (Table 3.2, entry 1). Ru/Mg(OH)₂ also showed appreciably good catalytic activity with the release of 402 mL of H₂ gas (TOF 60 h⁻¹) along with GLY conversion of 80% and yield of SL (59%) in 4.5 h (Table 3.2, entry 2). Ru/ZnO showed 70% conversion of GLY with 290 mL of H₂ (TOF 40 h⁻¹) and 61% yield of SL in 4.5 h (Table 3.2, entry 3). On the other hand, Ru/ZrO₂ and Ru/TiO₂ showed 67% (TOF 59 h⁻¹) and 62% (TOF 62 h⁻¹) conversion with SL yield of 52% and 51%, respectively in 4.5 h (Table 3.2, entries 4-5). Notably, the reaction could not proceed if only La(OH)₃ is used (Table 3.2, entry 6), while with Ru nanoparticles alone, 85% GLY conversion with the evolution of 478 mL H₂ gas (TOF 82 h⁻¹) along with SL (63% yield) and sodium formate (SF, 20% yield) in 4.5 h was observed (Table 3.2, entry 7).

Table 3.1. Optimization of reaction condition for hydrogen production from glycerol over the ruthenium catalyst.^a



Entry	Catalyst	H ₂ gas (mL) ^b	$n(\text{H}_2)/$ $n(\text{GLY})$	Conv. (%)	Yield of products (%) ^c				CB (%) ^d	Initial TOF (h ⁻¹) ^e
					SL	SG	PD	SF		
1	Ru/La(OH) ₃	470	1.4	>99	86	-	-	12	98	105
2	Ru/Mg(OH) ₂	402 (522) ^[f]	1.2	80 (>99) ^[f]	59	1	-	16	96	60
3	Ru/ZnO	290 (450) ^[g]	0.9	70 (>99) ^[g]	61	1	-	6	98	40
4	Ru/ZrO ₂	290 (490) ^[h]	0.9	67 (>99) ^[h]	52	2	-	9	96	59
5	Ru/TiO ₂	254 (340) ^[i]	0.8	62 (88) ^[i]	51	2	-	6	97	62
6	La(OH) ₃	-	-	n. r.	-	-	-	-	-	-
7	Ru	478 (534) ^[j]	1.4	85 (>99) ^[j]	63	-	-	20	98	82

^aReaction conditions: Ru/support (100 mg), GLY (13.68 mmol), NaOH (2.0 equiv.), water (41.04 mmol), 130 °C and 600 rpm. ^bVolume of gas was measured by the water displacement method. ^cYield (at 4.5 h) was calculated by ¹H NMR using sodium acetate as an internal standard. ^dCB is carbon balance based on the yield and conversion at 4.5 h. ^eInitial turnover frequency at 1 h. SL (sodium lactate), SG (sodium glycolate), PD (1,2-propanediol), and SF (sodium formate). In parenthesis, gas evolved and conv.% in ^f7 h, ^g8 h, ^h8 h, ⁱ7 h, ^j6.5 h. n. r. (no reaction)

The observed enhanced yield for SL (86%) over Ru/La(OH)₃ catalyst as compared to Ru alone (63%), inferred the prominent effect of the support in tuning the catalytic activity. We could observe the good selectivity (87%) towards SL in the case of Ru/ZnO, presumably due to the presence of Zn²⁺, which favoured the 1,2-hydride shift of pyruvaldehyde to SL compared to the *in-situ* hydrogenation of pyruvaldehyde to 1,2-PDO.^[56] Moreover, the complete conversion of GLY to H₂ gas and SL over Ru/Mg(OH)₂, Ru/ZnO and Ru/ZrO₂ catalysts took a longer time (7-8 h) at 130 °C (Table 3.1), as compared to the Ru/La(OH)₃. The observed trend in catalytic activity over supported ruthenium catalysts depends significantly on the basic nature of the supports with the order of Ru/La(OH)₃ > Ru/Mg(OH)₂ > Ru/ZnO > Ru/ZrO₂ > Ru/TiO₂. Moreover, there was no significant change in the particle size (~1.5-1.8 nm) as well as metal dispersion (72-87%) of ruthenium nanoparticles over the supports (Table 3.2), which indicates that supports play an important role in tuning the catalytic activity through strong-metal support interaction (SMSI) in hydrogen production from GLY. Results inferred that Ru/La(OH)₃ performed well over other supported catalysts in terms of the high yield of H₂ and SL. Therefore, the optimization of reaction conditions and the effect of different reaction parameters were studied with Ru/La(OH)₃. We further characterized the Ru/La(OH)₃ catalyst in detail to investigate its chemical composition, electronic state and textural properties using XPS, BET and TEM analysis. BET surface area for the Ru/La(OH)₃ catalyst was found to be 81 m²/g (Figure 3.3 and Table 3.2). The wide scan XPS of Ru/La(OH)₃ catalyst also confirmed the presence of all elements i.e., Ru, La and O (Figure 3.4 a). XPS peaks centered at the binding energy of 463.3 eV and 485.7 eV were assigned to the Ru 3p_{3/2} and Ru 3p_{1/2}, respectively (Figure 3.4 b). The binding energies of metallic Ru in Ru/La(OH)₃ were found to be higher than that of the bare Ru nanoparticles.^[21] The increase in binding energies of the Ru 3p region is presumably due to the support-metal interactions in the Ru/La(OH)₃ catalyst. For La 3d, deconvolution of peaks resulted in doublets at 834.5 eV and 851.2 eV corresponding to the La(III) 3d_{5/2} and La(III) 3d_{3/2} respectively.

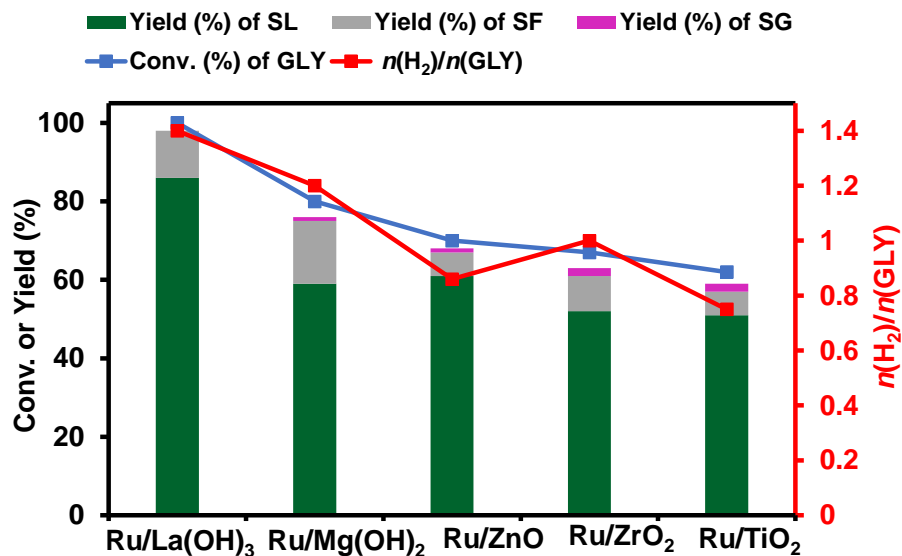


Figure 3.2. Effect of different supports on the dehydrogenation of GLY to H₂ gas and SL. Reaction Conditions: Ru/support (100 mg), GLY (13.68 mmol), NaOH (27.36 mmol), water (41.04 mmol), 130 °C, 4.5 h, and 600 rpm.

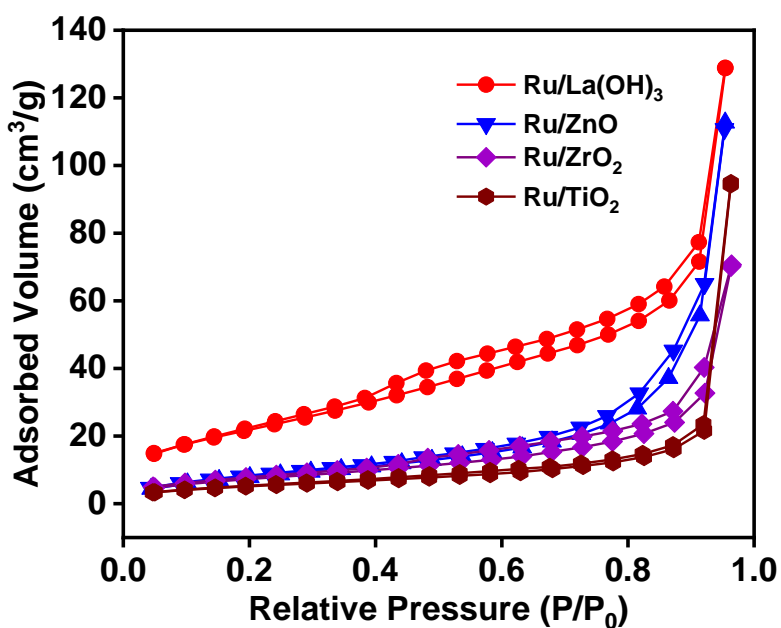


Figure 3.3. N₂ adsorption-desorption isotherm of supported ruthenium catalysts.

Table 3.2. Textural properties of Ru-based supported catalysts.

Entry	Catalyst	Specific Surface area (m ² /g) ^a	Metal loading (wt. %) ^b	Particle size (nm) ^c	Dispersion (wt. %) ^d
1	Ru/La(OH) ₃	81	9.0	1.5	87
2	Ru/ZnO	30	8.2	1.5	87
3	Ru/Mg(OH) ₂	172	7.5	1.7	76
4	Ru/ZrO ₂	30	8.3	1.8	72
5	Ru/TiO ₂	27	8.6	1.5	87

^acalculated using N₂ adsorption-desorption isotherms. ^bCalculated using ICP-AES.

^cParticle size was calculated by TEM analysis. ^ddispersion was calculated by the equation described in reference 31.

Additionally, the peaks at 837.9 eV and 854.6 eV are satellite peaks due to the shake-up processes (Figure 3.4 c). Spin-orbit coupling of 16.7 eV was observed confirming the +3 oxidation state of La.^[61-62] In the O 1s spectra, two peaks centered at 530.6 eV and 531.90 eV were observed for oxygen bonded to La i.e. La-O, and adsorbed water molecules/hydroxyl groups present on the catalyst surface respectively (Figure 3.4 d). TEM image of Ru/La(OH)₃ catalyst illustrated the presence of well-dispersed Ru nanoparticles (average particle size of ~1.5 nm) over La(OH)₃ support (Figures 3.4 e-f). Similarly, TEM analysis of other supported Ru catalysts also showed the presence of spherical Ru nanoparticles having an average particle size in the range of 1.5-1.8 nm (Figure 3.5). The actual loading of Ru in Ru/La(OH)₃ catalyst as calculated by ICP-AES measurement was found to be 9.0 wt%. The metal loading of other supported Ru catalysts is mentioned in Table 3.3. The FE-SEM images of Ru/La(OH)₃ showed no visible Ru nanoparticles due to their small particle size. However, EDX and elemental mapping evidenced the presence of Ru in Ru/La(OH)₃ catalysts (Figures 3.6 and 3.7).

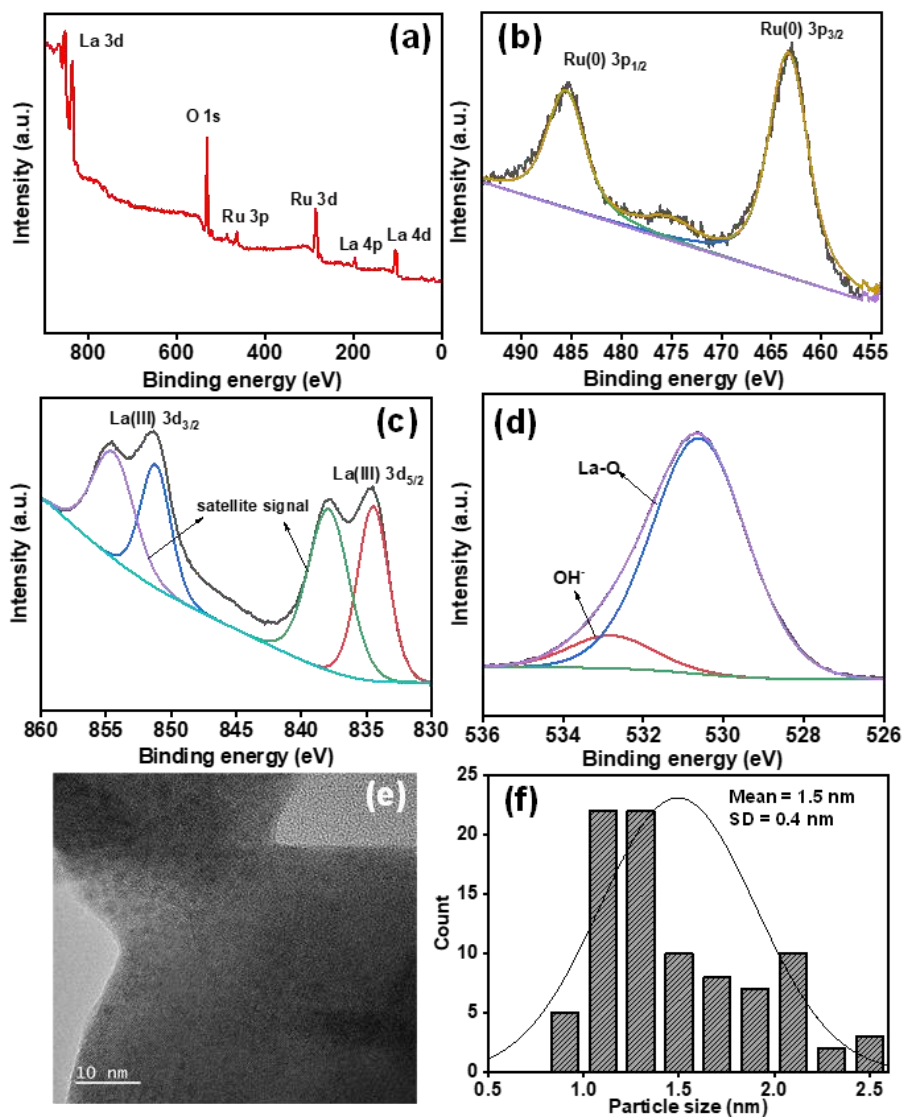


Figure 3.4. XPS spectra (a) wide scan, (b) Ru 3p region, (c) La 3d region, (d) O 1s region, (e) TEM image, and corresponding (f) particle size distribution curve for Ru/La(OH)₃ catalyst.

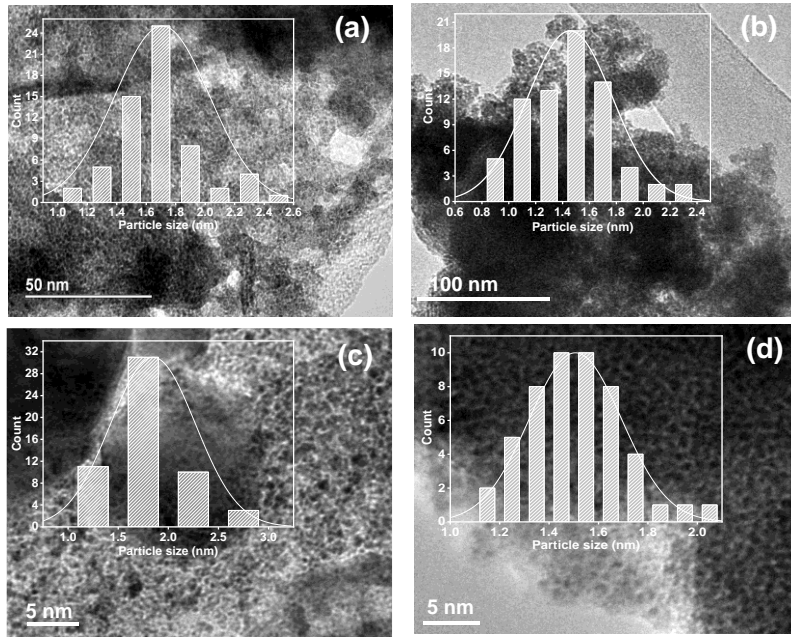


Figure 3.5. TEM image and corresponding particle size distribution (inset) for (a) Ru/Mg(OH)_2 , (b) Ru/ZnO , (c) Ru/ZrO_2 and (d) Ru/TiO_2 catalysts.

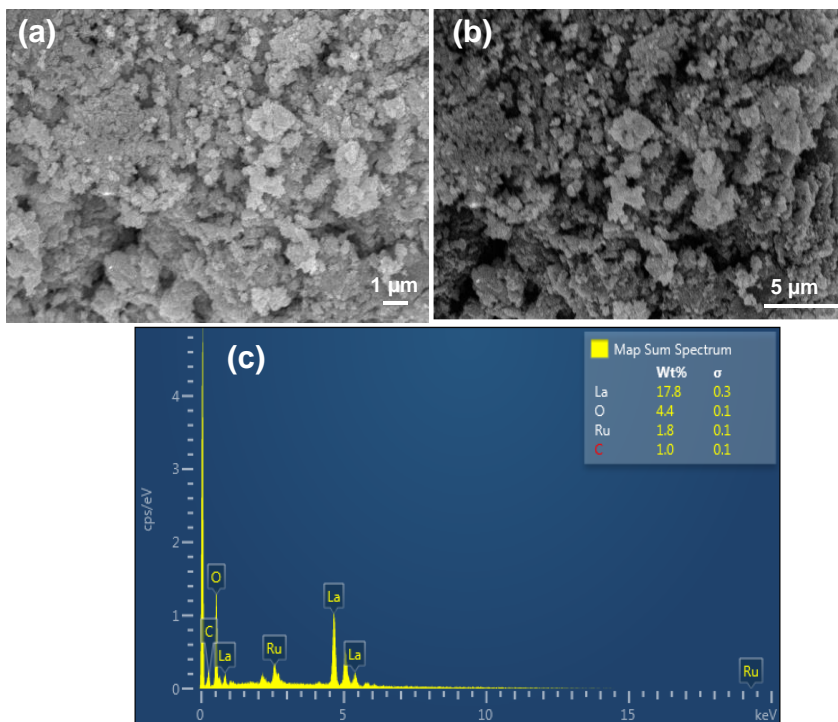


Figure 3.6. (a-b) SEM images and corresponding (c) EDX spectra for the Ru/La(OH)_3 catalyst.

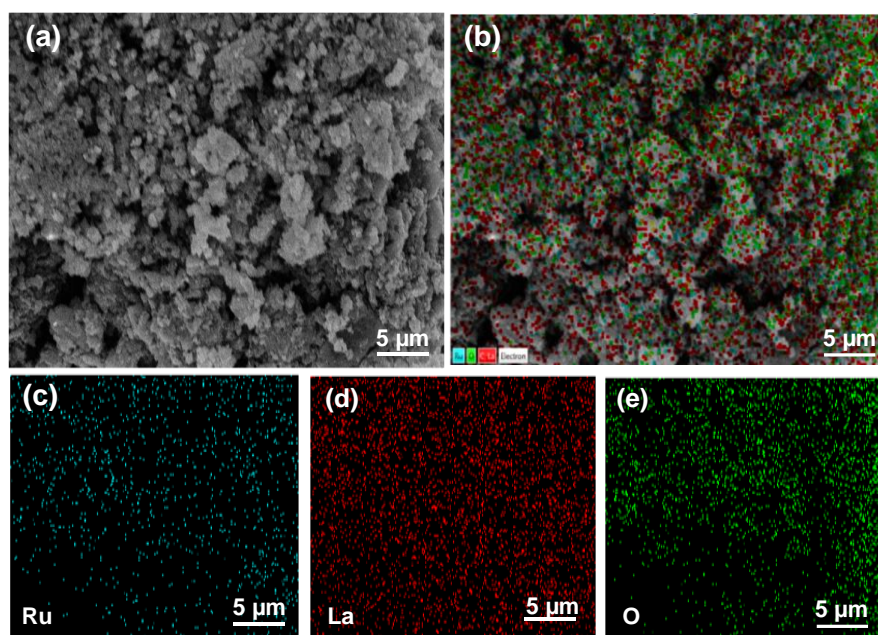


Figure 3.7. (a) SEM image and corresponding (b) elemental mapping showing the presence of (c) Ru (cyan), (d) La (red), and (e) O (green) in the Ru/La(OH)₃ catalyst.

3.3.2. Catalytic transformation of GLY to H₂ and SL over the Ru/La(OH)₃

Notably, the dehydrogenation of glycerol (GLY) was conducted without base and without catalyst at 130 °C, where no conversion of GLY, in either case, was observed (Table 3.3, entries 1 and 2), suggesting the crucial role of base and the catalyst for the dehydrogenation of GLY. Notably, the reaction could not proceed if only La(OH)₃ was used (Table 3.3, entry 3), while with bare Ru nanoparticles, 85% GLY conversion with the evolution of 478 mL H₂ gas (TOF 82 h⁻¹) along with SL (63% yield) and sodium formate (SF, 20% yield) in 4.5 h was observed (Table 3.3, entry 4). Reaction with neat GLY over the Ru/La(OH)₃ inferred, 70% conversion of GLY with the release of 260 mL [$n(\text{H}_2)/n(\text{GLY}) \sim 0.8$] of H₂ in 8 h (Table 3.3, entry 5). GC-TCD of the released gas confirmed the presence of only H₂ gas without any other gaseous contamination (CO, CO₂, CH₄ or alkanes), confirming the selective production of H₂ from GLY (Figure 3.8).

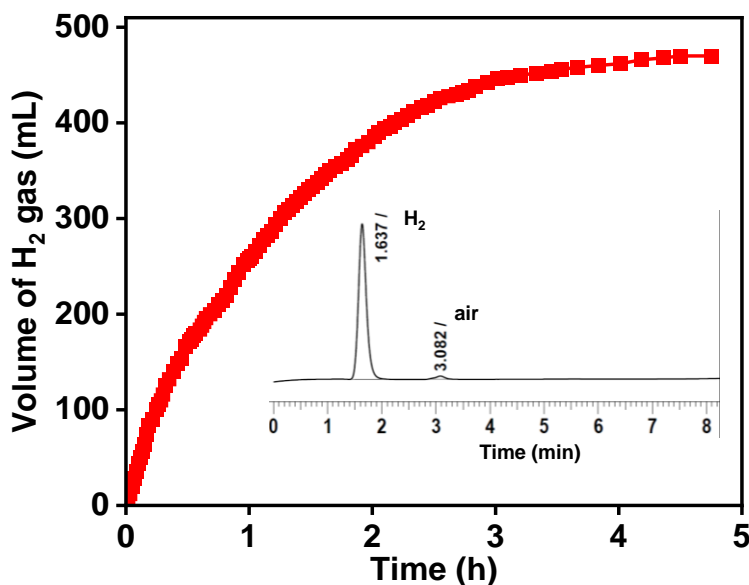
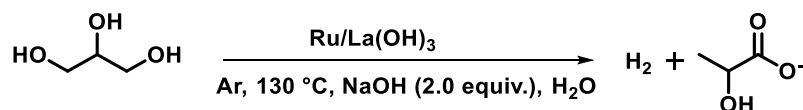


Figure 3.8. Time course plot for hydrogen gas production from GLY over the $Ru/La(OH)_3$ catalyst. Reaction conditions: $Ru/La(OH)_3$ (100 mg), GLY (13.68 mmol), NaOH (27.36 mmol), water (41.04 mmol), 130 °C, and 600 rpm.

The conversion of GLY was enhanced to 95% when one equivalent of water was added to the reaction, releasing 446 mL [$(n(H_2)/n(GLY)) \sim 1.3$] of gas in 6 h (Table 3.3, entry 6), inferring the crucial role of water in the H_2 production from GLY. On further increase in the water content (GLY/ H_2O molar ratio of 1:3), enhanced conversion of GLY (>99%) was achieved with the release of 470 mL [$(n(H_2)/n(GLY)) \sim 1.4$] of gas in 4.5 h with appreciably good yields of SL (86%) (Table 3.3, entry 7). The observed enhanced yield for SL (86%) over $Ru/La(OH)_3$ catalyst as compared to bare Ru nanoparticles (63% yield of SL) inferred the prominent effect of the support in tuning the catalytic activity. Since water reduces the mass transfer of NaOH and the viscosity of GLY, an enhanced catalytic transformation of GLY to H_2 and SL was achieved in the presence of water.^[33]

Table 3.3. Optimization of reaction conditions for hydrogen production from glycerol over Ru/La(OH)₃ catalyst.^a



Entry	$n(\text{GLY})/$ $n(\text{H}_2\text{O})$	t (h)	H ₂ gas (mL) ^b	$n(\text{H}_2)/$ $n(\text{GLY})$	Conv. (%)	Yield of products (%) ^c				CB (%) ^d	Initial TOF (h ⁻¹) ^e
						SL	SG	PD	SF		
1 ^f	1:3	4.5	-	-	n. r.	-	-	-	-	-	-
2 ^g	1:3	4.5	-	-	n. r.	-	-	-	-	-	-
3 ^h	1:3	4.5	-	-	n. r.	-	-	-	-	-	-
4	1:3	4.5	478	1.2	85	63	-	-	20	98	82
5	1:0	8	260	0.8	70	51	3	3	9	96	33
6	1:1	6	446	1.3	95	77	<1	<1	14	97	82
7	1:3	4.5	470	1.4	>99	86	-	-	12	98	105
8	1:6	5.5	456	1.3	93	76	3	1	10	97	97
9	1:10	6.5	386	1.1	81	66	3	1	7	96	67
10	1:20	6.5	156	0.5	69	47	9	1	3	91	38
11 ⁱ	1:3	3.5	138	0.4	52	37	1	10	1	97	36
12 ^j	1:3	4	270	0.8	85	70	2	4	5	96	68
13 ^k	1:3	5	356	1.0	93	79	1	1	8	96	85

^aReaction conditions: Ru/La(OH)₃ (100 mg), GLY (13.68 mmol), NaOH (27.36 mmol), water (0-20 equiv.), 130 °C and 600 rpm. ^bVolume of gas was measured by water displacement method. ^cYield was calculated by ¹H NMR using sodium acetate as an internal standard. ^dCB is carbon balance. ^eInitial turnover frequency at 1 h. ^fReaction in the absence of NaOH. ^gReaction in the absence of catalyst. ^hLa(OH)₃, ⁱNaOH (0.5 equiv.), ^jNaOH (1.0 equiv.), ^kNaOH (2.0 equiv.). The results reported are the average of at least two repeated reactions. SL (sodium lactate), SG (sodium glycolate), PD (1,2-propanediol), and SF (sodium formate).

However, upon the further increase in the water content, the amount of H₂ gas release was decreased to 456 mL (93% GLY conversion) and 386 mL (81% GLY conversion) for $n(\text{GLY})/n(\text{H}_2\text{O})$ ratio of 1:6 and 1:10, respectively (Table 3.3, entries 8 and 9). For the more diluted aqueous solution of GLY ($n(\text{GLY})/n(\text{H}_2\text{O})$ ratio of 1:20), lesser GLY conversion (69%) with the release of only 156 mL of H₂ gas was observed (Table 3.3, entry 10). These results inferred the crucial role of the $n(\text{GLY})/n(\text{H}_2\text{O})$ ratio in achieving a high yield of H₂ gas and SL for the catalytic transformation of GLY over the Ru/La(OH)₃ catalyst (Figure 3.9 a and Figure 3.10).

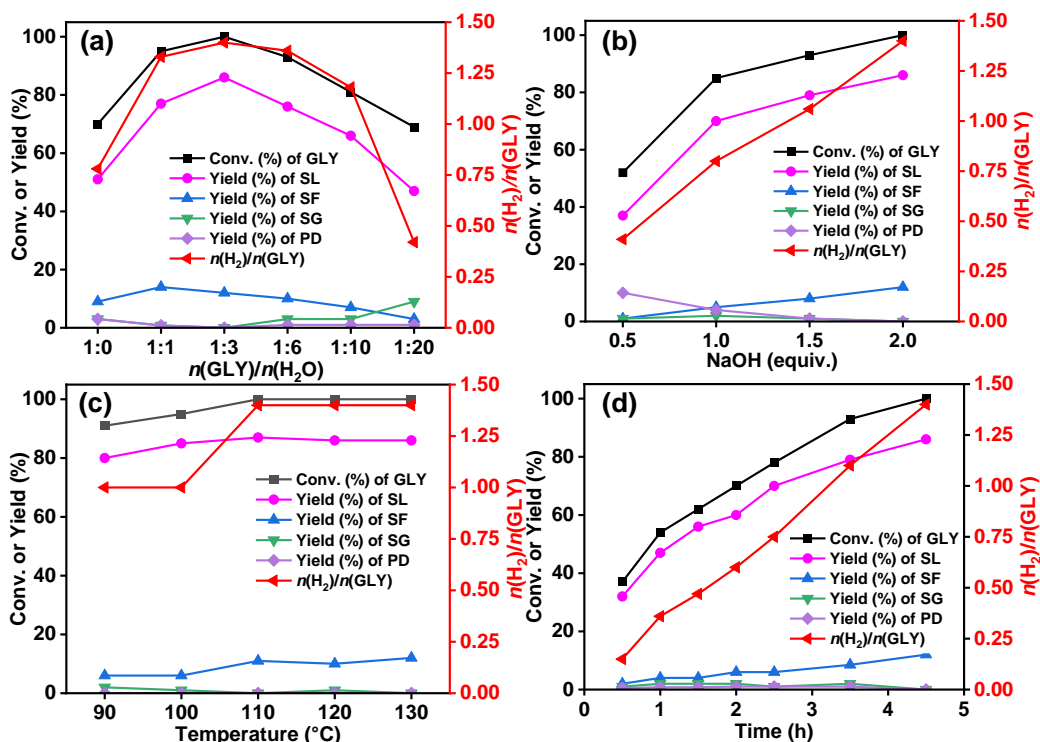


Figure 3.9. Effect of (a) $n(\text{GLY})/n(\text{H}_2\text{O})$ ratio, (b) NaOH concentration, and (c) temperature on the catalytic dehydrogenation of GLY over $\text{Ru}/\text{La}(\text{OH})_3$ catalyst. Reaction condition: $\text{Ru}/\text{La}(\text{OH})_3$ (100 mg), GLY (13.68 mmol), NaOH (0.5-2.0 equiv.), water (0-20 equiv.), 90-130 °C, and 600 rpm. (d) Time-dependent catalytic dehydrogenation of GLY over the $\text{Ru}/\text{La}(\text{OH})_3$ catalyst. Reaction condition: $\text{Ru}/\text{La}(\text{OH})_3$ (100 mg), GLY (13.68 mmol), NaOH (27.36 mmol), water (41.04 mmol), 130 °C, and 600 rpm.

Moreover, efficiency for producing the selective H_2 gas and SL was found to be significantly influenced by the concentration of NaOH (Table 3.3, entries 9-11, Figure 3.4 b and Figure 3.11). Upon varying the NaOH concentration from 0.5 equiv. to 1.5 equiv., a significant enhancement in the volume of H_2 gas as well as the conversion of GLY was observed at 130 °C. Results inferred that when the reaction was carried out with 0.5 equiv. of NaOH, only 138 mL (0.4 equiv.) of H_2 gas with GLY conversion of 52% in 3.5 h was observed (Table 3.3, entry 9). Further, on increasing the NaOH concentration to 1.0 equiv., the volume of the gas increased to 270 mL (0.8 equiv.) with 85% conversion of GLY and 70% yield of SL in 4 h (Table 3.3, entry 10). The reaction conducted using 1.5 equiv. NaOH, resulted in 356 mL (1.0 equiv.) of H_2 gas with 93% GLY conversion (Table 3.3, entry 11). Moreover, other by-

products such as SG and PD were formed in less amount as compared to SL and SF. These results clearly inferred that NaOH plays an important role in promoting the deprotonation of hydroxyl groups of GLY, thus enhancing the dehydrogenation of GLY to SL over the Ru/La(OH)₃.

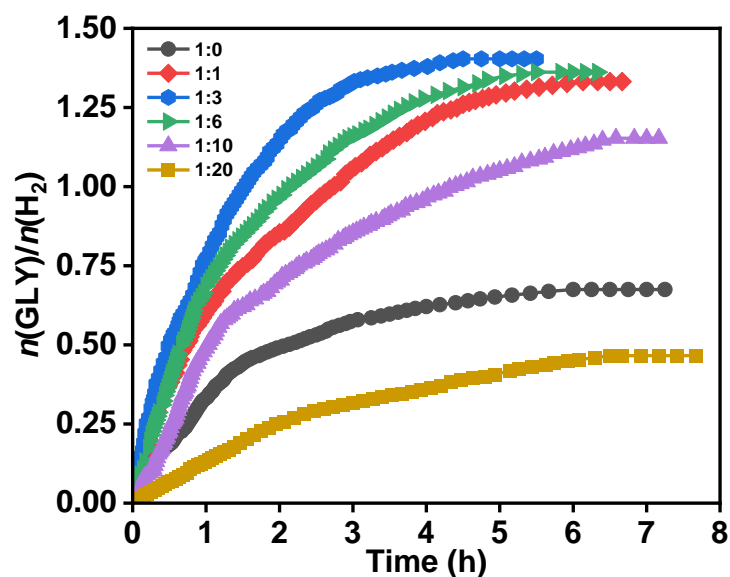


Figure 3.10. Effect of water content on hydrogen production from GLY over the Ru/La(OH)₃ catalyst. Reaction conditions: Ru/La(OH)₃ (100 mg), GLY (13.68 mmol), NaOH (27.36 mmol), water (0-20 equiv.), 130 °C, and 600 rpm.

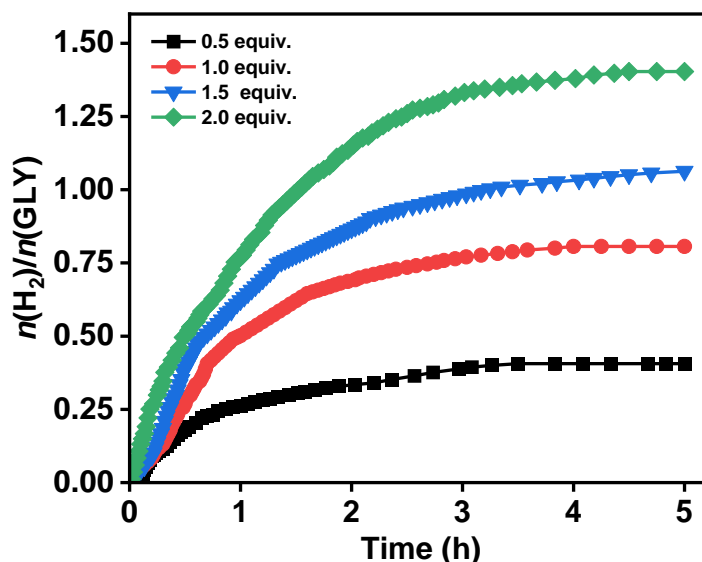


Figure 3.11. Effect of base concentration on hydrogen production from GLY over the Ru/La(OH)₃ catalyst. Reaction conditions: Ru/La(OH)₃ (100 mg), GLY (13.68 mmol), NaOH (0.5-2.0 equiv.), water (41.04 mmol), 130 °C, and 600 rpm.

Notably, high yield of PD (10%) was observed while using 0.5 equiv. of NaOH, while with the high base amount (1.0-2.0 equiv.), less PD yield was observed, inferred that further dehydrogenation of produced PD occurred in the presence of base to produce H₂ gas and SL. It has been observed that the GLY conversion and the selectivity for H₂ and SL increased linearly with the increase in stirring speed up to 600 rpm but did not change significantly for stirring speed \geq 600 rpm, suggesting that external mass transfer limitations are not applicable for the stirring speed of \geq 600 rpm (Table 3.4).^[62,63]

Table 3.4. Effect of stirring speed on the dehydrogenation of GLY over the Ru/La(OH)₃ catalyst.^a

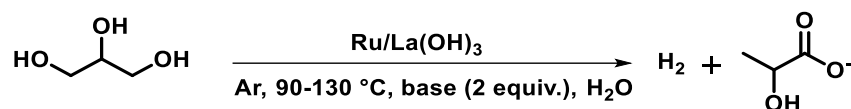
Entry	rpm	Conv. (%)	t (h)	$n(\text{H}_2)$ $/n(\text{GLY})^b$	Yield of byproducts (%) ^c				CB (%) ^d	Average reaction rate (mol/g _{Ru} / h $\times 10^{-2}$)
					SL	SG	PD	SF		
1	-	91	6	1.1	75	3	2	7	96	2.07
2	200	93	6	1.2	78	4	1	7	97	2.12
3	400	>99	5	1.4	82	2	-	11	96	2.28
4	600	>99	4.5	1.4	86	-	-	12	98	3.04
5	800	>99	4.5	1.4	84	-	-	12	96	3.04

^aReaction conditions: Ru/La(OH)₃ (100 mg), GLY (13.68 mmol), NaOH (27.36 mmol), water (41.04 mmol), 130 °C. ^bVolume of gas was measured by water displacement method. ^cYield was calculated by ¹H NMR using sodium acetate as an internal standard. ^eYield was calculated by ¹H NMR using sodium acetate as an internal standard. ^dCB is carbon balance. SL (sodium lactate), SG (sodium glycolate), PD (1,2-propanediol), and SF (sodium formate).

Moreover, the promotional effect of different types of bases such as NaOH, KOH, KO^tBu, Na₂CO₃ and K₂CO₃ in the dehydrogenation of GLY was also investigated (Table 3.5). We observed high catalytic activity for GLY dehydrogenation ($n(\text{H}_2)/n(\text{GLY}) \sim 1.4$), using NaOH with complete conversion of GLY as compared to KOH [$n(\text{H}_2)/n(\text{GLY}) \sim 0.9$] with 88% conversion of GLY under the optimum reaction conditions (Table 3.5, entry 1 and 2). Moreover, the rate of generation of H₂ gas was sluggish with KOH (initial TOF 56 h⁻¹) compared to that observed using NaOH (initial TOF 105 h⁻¹). This is possible because of the larger ionic radius of the K⁺ ion than that of the Na⁺ ion,

causing steric hindrance in the dehydrogenation of GLY.^[64] Notably, no conversion of GLY was observed for the reactions performed with Na₂CO₃ and K₂CO₃, while with KO^tBu, only 72% conversion of GLY was achieved (Table 3.5, entries 3-5). At 90 °C, 13.3 mmol of H₂ gas (~1.0 equiv.) was observed in 14 h (Table 3.6, entry 1), while, at elevated temperatures (100-130 °C) higher yield of H₂ gas was observed over the Ru/La(OH)₃ catalyst with no significant change in the selectivity of SL (Table 3.6, entries 2-4). Notably, GLY was completely dehydrogenated for the reactions performed at ≥110 °C, where increase in the initial TOF was also observed upon increase in the reaction temperature (Table 3.6 and Figure 3.10 c). The Activation energy for the selective H₂ generation from GLY over the Ru/La(OH)₃ catalyst was estimated as 37.5 kJ/mol using the Arrhenius equation (Figure 3.12).

Table 3.5. Effect of different types of bases in hydrogen production from glycerol over the Ru/La(OH)₃ catalyst.^a



Entry	Base	T (°C) /t (h)	H ₂ gas (mL) ^b	n(H ₂)/ n(GLY)	Conv. (%)	Yield of products (%) ^c				CB (%) ^d	Initial TOF (h ⁻¹) ^e
						SL	SG	PD	SF		
1	NaOH	130/4.5	470	1.4	>99	86	-	-	12	98	105
2	KOH	130/8	308	0.9	88	72	2	2	7	95	56
3	KO ^t Bu	130/8	208	0.6	72	62	2	1	5	98	38
4	Na ₂ CO ₃	130/4.5	-	-	n. r.	-	-	-	-	-	-
5	K ₂ CO ₃	130/4.5	-	-	n. r.	-	-	-	-	-	-

^aReaction conditions: Ru/La(OH)₃ (100 mg), GLY (13.68 mmol), base (27.36 mmol), water (41.04 mmol), 90-130 °C and 600 rpm. ^bVolume of gas was measured by the water displacement method. ^cYield was calculated by ¹H NMR using sodium acetate as an internal standard. ^dCB is carbon balance. ^eInitial turnover frequency at 1 h. SL (sodium lactate), SG (sodium glycolate), PD (1,2-propanediol), and SF (sodium formate).

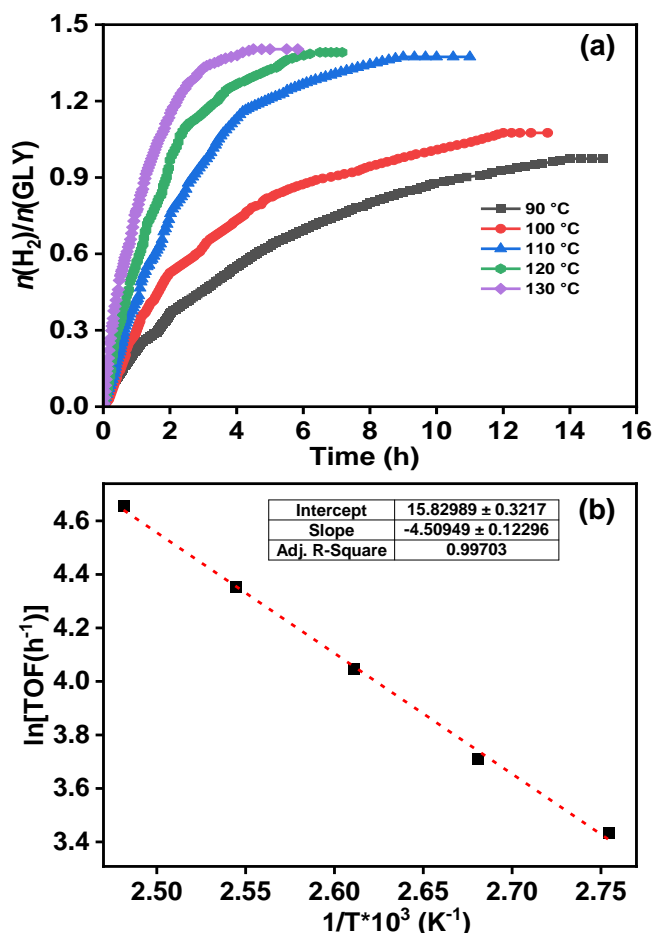
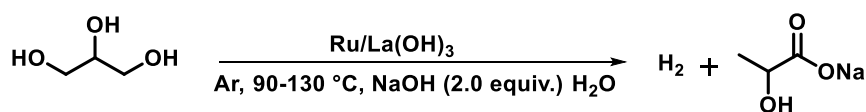


Figure 3.12. (a) Temperature-dependent study for hydrogen production from GLY over the Ru/La(OH)₃ catalyst (b) Arrhenius plot of initial TOF values to calculate activation energy.

Moreover, enhancement in hydrogen gas production from GLY was observed for the reactions performed with higher catalyst loading (Table 3.6, entries 5-6). The aforementioned findings demonstrated the vital role of base concentration, $n(\text{GLY})/n(\text{H}_2\text{O})$ ratio, and the reaction temperature for achieving high catalytic activity for producing H₂ gas from GLY. Hence, high catalytic activity for GLY dehydrogenation with a good yield of SL over Ru/La(OH)₃ catalyst was achieved using $n(\text{NaOH})/n(\text{GLY})$ of 2.0 equiv. and $n(\text{GLY})/n(\text{H}_2\text{O})$ of 1:3 at 130 °C (Table 3.3, and entry 5). LA was purified by acidifying (pH ~1.5) the crude reaction mixture containing SL with 1 M HCl, and then the organic product (LA) was extracted using diethyl ether (5×10 mL). The organic fraction was dried over Na₂SO₄. The purified LA was obtained by removing the organic solvent under reduced pressure and was analyzed by NMR (¹H and ¹³C) in D₂O (Figures 3.13 and 3.14).

Table 3.6. Optimization of reaction condition for hydrogen production from glycerol over the Ru/La(OH)₃ catalyst.^a



Entry	T (°C) /t (h)	H ₂ gas (mL) ^b	n(H ₂)/ n(GLY)	Conv. (%)	Yield of products (%) ^c				CB (%) ^d	Initial TOF (h ⁻¹) ^e
					SL	SG	PD	SF		
1	90/14	326	1.0	91	80	2	-	6	97	31
2	100/12	360	1.1	95	85	1	-	6	97	41
3	110/9	460	1.4	>99	87	-	-	11	98	57
4	120/6.5	466	1.4	>99	86	1	-	10	97	77
5 ^f	130/8.5	88	0.3	52	41	2	-	5	96	10
6 ^g	130/10	144	0.4	70	56	3	-	6	95	21
7 ^h	130/6.5	354	1.1	95	79	2	-	11	97	52

^aReaction conditions: Ru/La(OH)₃ (100 mg), GLY (13.68 mmol), NaOH (27.36 mmol), water (41.04 mmol), 130 °C and 600 rpm. ^bVolume of gas was measured by water displacement method. ^cYield was calculated by ¹H NMR using sodium acetate as an internal standard. ^dCB is carbon balance. ^eInitial turnover frequency at 1 h. ^fRu catalyst (1 wt%), ^gRu catalyst (2.5 wt%), ^hRu catalyst (5 wt%).

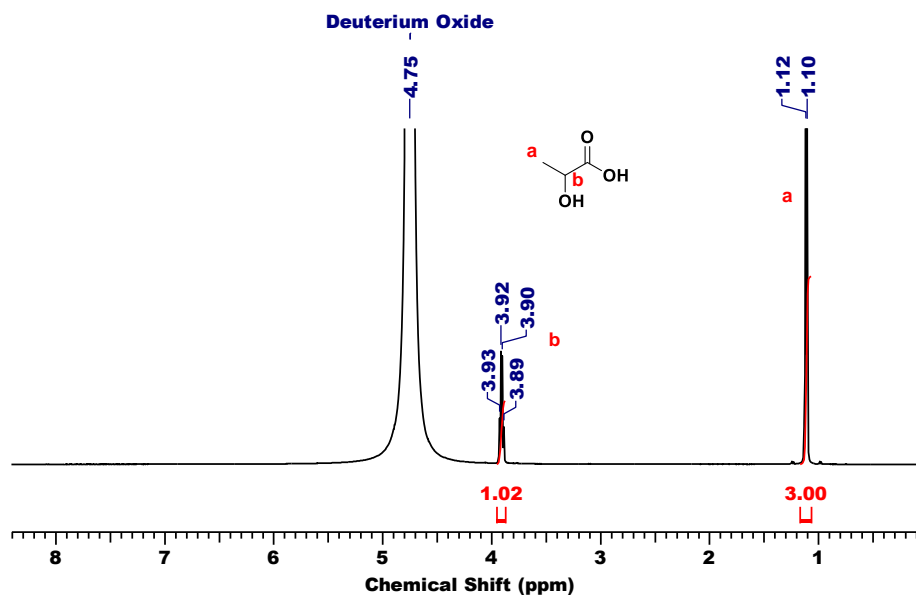


Figure 3.13. ¹H NMR spectra of purified lactic acid in D₂O.

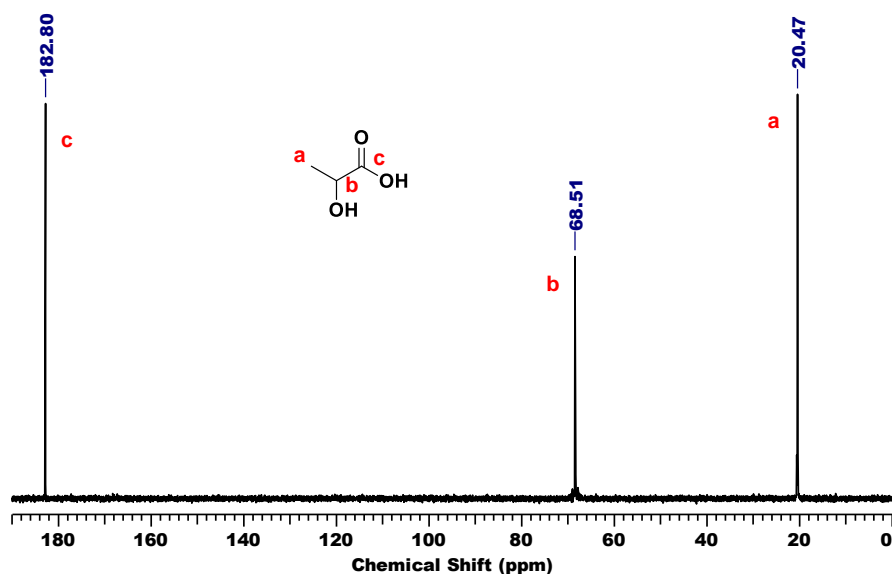
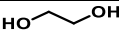
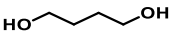
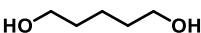
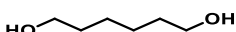


Figure 3.14. ^{13}C NMR spectra of purified lactic acid in D_2O .

3.3.3. Scope of $\text{Ru/La}(\text{OH})_3$ catalyst for H_2 production from various terminal diols

Encouraged by the high catalytic activity observed for the dehydrogenation of GLY, $\text{Ru/La}(\text{OH})_3$ catalyst was also employed for the dehydrogenation of ethylene glycol (EG) and other terminal diols such as 1,3-propanediol (PDO), 1,4-butanediol (BDO), 1,5-pentanediol (PO) and 1,6-hexanediol (HDO), which were converted to sodium formate (SF) and other by-products due to C-C bond cleavage and/or aldol condensation. EG dehydrogenated completely over the $\text{Ru/La}(\text{OH})_3$ in 8 h and produced 870 mL (35 mmol) of H_2 gas (Table 3.7, entry 1), whereas PO produced 532 mL (22 mmol) of H_2 gas with 99% conversion (Table 3.7, entry 2) in 4 h. Further, in the case of BDO, 67% conversion was achieved in 9 h with 390 mL (16 mmol) of H_2 gas (Table 3.7, entry 3). However, for PDO, only 96 mL (4 mmol) of H_2 gas was evolved with 22% conversion of PDO in 7.5 h (Table 3.7, entry 4), whereas no evolution of H_2 gas was observed for HDO (Table 3.7, entry 5). These results inferred that the catalytic efficacy of $\text{Ru/La}(\text{OH})_3$ for the dehydrogenation reactions decreases with the increase in carbon chain length in terminal diols.

Table 3.7. Hydrogen production from other terminal diols over the Ru/La(OH)₃ catalyst.^a

Entry	Substrate	t (h)	H ₂ gas (mL) ^b	n(H ₂)/n(diols)	Conv. (%)	Yield of SF (%) ^c
1		8	870	2.6	>99	52
2		4	532	1.6	99	50
3		9	390	1.2	67	19
4		7.5	96	0.3	22	5
5		4.5	-	-	n. r.	-

^aReaction conditions: Ru/La(OH)₃ (100 mg), substrate (13.68 mmol), NaOH (27.36 mmol), water (41.04 mmol), 130 °C, and 600 rpm. ^bVolume of gas was measured by water displacement method. ^cYield was calculated by ¹H NMR using sodium acetate as an internal standard. The results reported are the average of at least two repeated reactions. EG (ethylene glycol), PDO (1,3-propanediol), BDO (1,4-butanediol), PO (1,5-pentanediol), HDO (1,6-hexanediol), and SF (sodium formate).

Furthermore, the time-dependent ¹H NMR analysis of the catalytic reaction mixture at different time intervals during the dehydrogenation of GLY inferred the continuous consumption of GLY with increase in the yield of SL and SF. On the other hand, the yield of SG (<2%) and PD (<1%) was found to be constant throughout the reaction (Figure 3.10 d). Further to investigate the participation of these intermediates in the catalytic hydrogen production from GLY, several control experiments were performed using various substrates in the presence of NaOH (2.0 equiv.) (Scheme 3.1). In agreement with the plausible reaction pathway, we observed the complete conversion of glyoxal to SG (yield 94%) using NaOH without catalyst (Reaction (a), Scheme 3.1, and Figure 3.15). On the other hand, treating glyoxal with Ru/La(OH)₃ catalyst under optimized reaction conditions resulted in the formation of H₂ gas (4.3 mmol), SG (yield 64%) and SF (yield 32%) suggesting that presumably sodium glycolate (SG) transformed to SF with the release of H₂ over Ru/La(OH)₃ catalyst (Reaction (b), Scheme 3.1, and Figure 3.16). To investigate it further, performing reaction with GA over Ru/La(OH)₃ catalyst in the presence NaOH (2.0 equiv.) indeed resulted in the production of H₂ gas (8.5 mmol) along with SF (yield 62%) (Reaction (c), Scheme 3.1, and Figure 3.17). Notably, further

conversion of LA and formic acid (FA) over Ru/La(OH)₃ was not observed during our investigation under optimized reaction conditions (Reaction (d-e), Scheme 3.1, and Figures 3.18 and 3.19). Therefore, this experimental evidence clearly inferred that for the selective catalytic dehydrogenation of GLY to H₂ gas and SL, followed the reaction pathway where initially, GLY dehydrogenated to glyceraldehyde with the release of one equivalent of H₂ gas. Glyceraldehyde can further be transformed by two competing pathways. In the first pathway, glyceraldehyde is transformed to pyruvaldehyde through base-catalyzed dehydration, which can subsequently be converted into SL through the Cannizzaro reaction. Notably, pyruvaldehyde could also be hydrogenated (using in-situ generated H₂) to generate PD, which can be further dehydrogenated to corresponding products.^[51] In another pathway, glyceraldehyde can be converted into formaldehyde and glycolaldehyde through a base-catalyzed retro-aldol reaction via C-C bond cleavage, where glycolaldehyde can further be dehydrogenated to SG via glyoxal, followed by the dehydrogenation of SG to SF (Scheme 3.2).

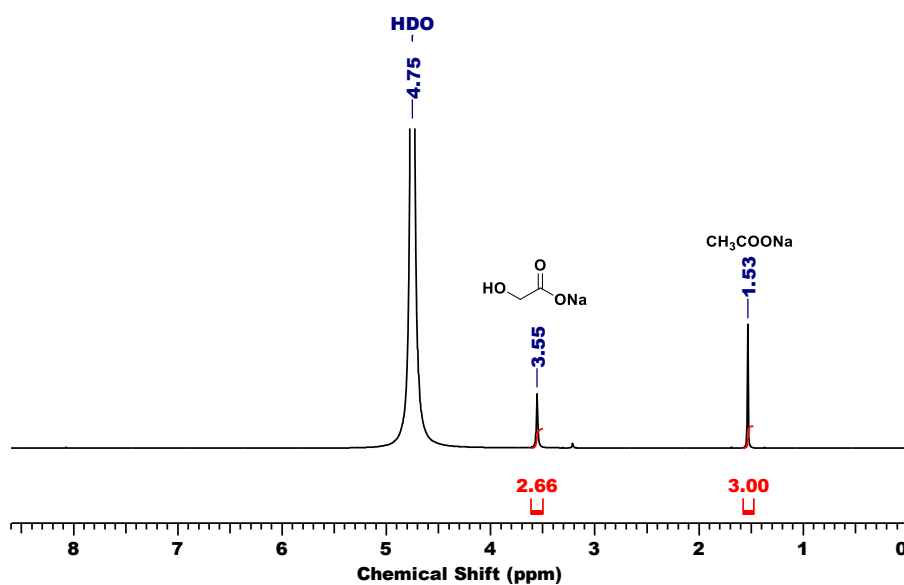


Figure 3.15. ¹H NMR spectra of the crude reaction mixture of the catalytic reaction for hydrogen production from glyoxal without catalyst. Reaction conditions: glyoxal (13.68 mmol), NaOH (27.36 mmol), water (41.04 mmol), 130 °C, and 600 rpm.

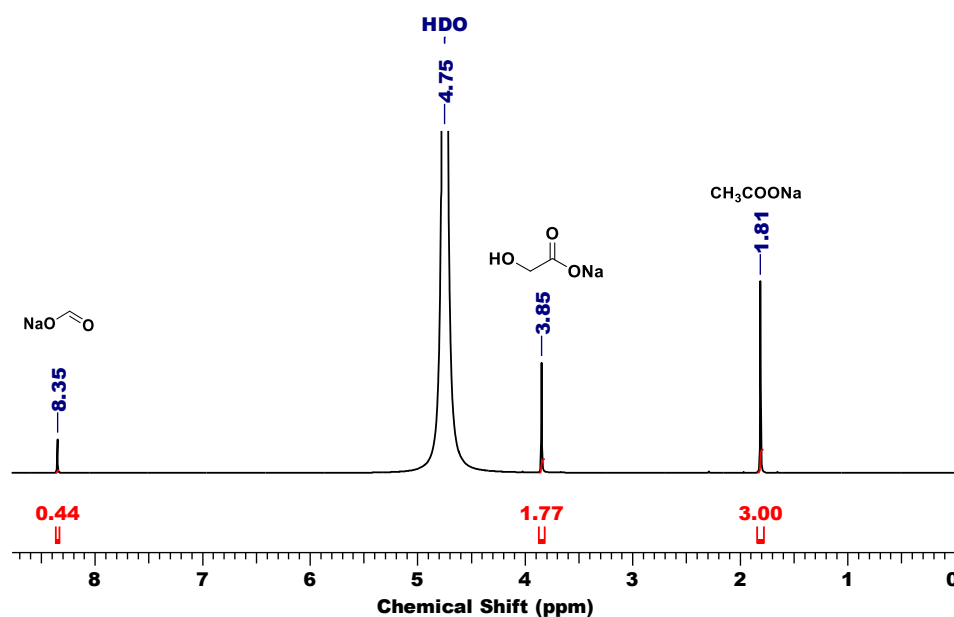


Figure 3.16. ^1H NMR spectra of the crude reaction mixture of the catalytic reaction for hydrogen production from glyoxal over the $\text{Ru/La}(\text{OH})_3$ catalyst. Reaction conditions: $\text{Ru/La}(\text{OH})_3$ (100 mg), glyoxal (13.68 mmol), NaOH (27.36 mmol), water (41.04 mmol), 130 °C, and 600 rpm.

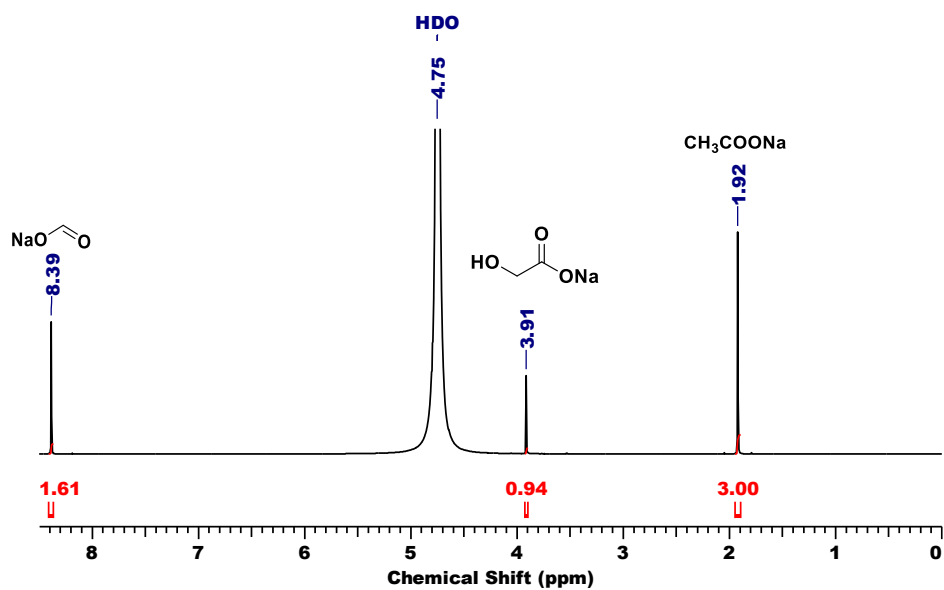


Figure 3.17. ^1H NMR spectra of the crude reaction mixture of the catalytic reaction for hydrogen production from glycolic acid over the $\text{Ru/La}(\text{OH})_3$ catalyst. Reaction conditions: $\text{Ru/La}(\text{OH})_3$ (100 mg), glycolic acid (13.68 mmol), NaOH (27.36 mmol), water (41.04 mmol), 130 °C, and 600 rpm.

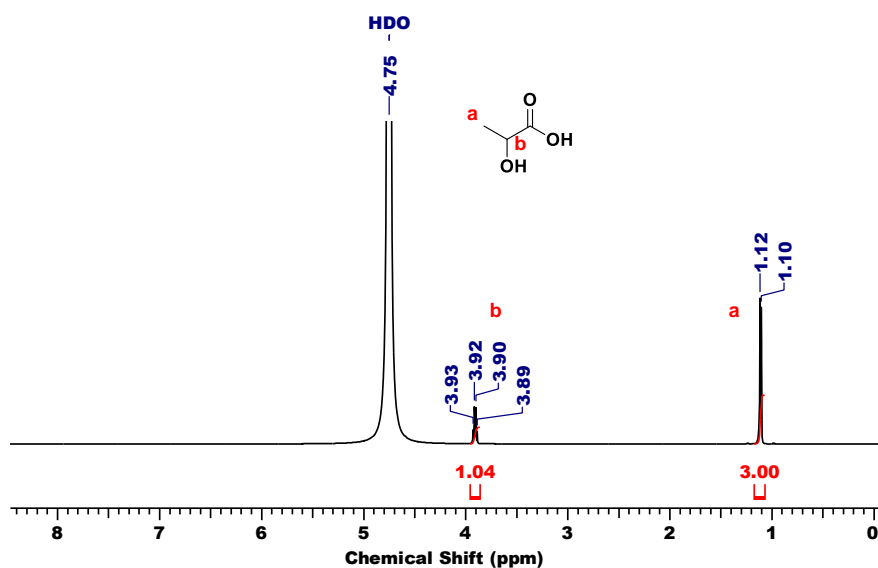


Figure 3.18. ^1H NMR spectra of the crude reaction mixture of the catalytic reaction for hydrogen production from lactic acid over the $\text{Ru/La}(\text{OH})_3$ catalyst. Reaction conditions: $\text{Ru/La}(\text{OH})_3$ (100 mg), lactic acid (13.68 mmol), NaOH (27.36 mmol), water (41.04 mmol), 130 °C, and 600 rpm.

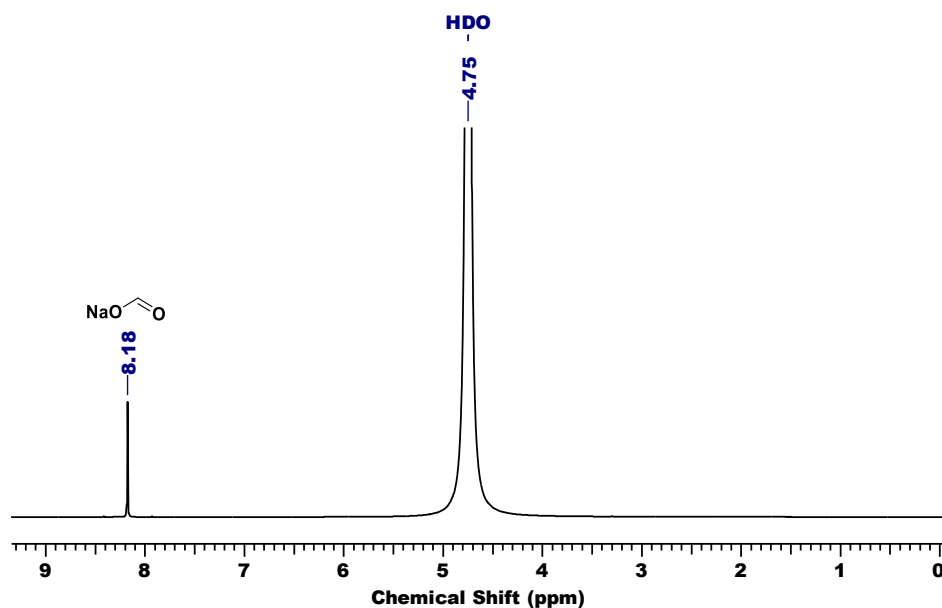
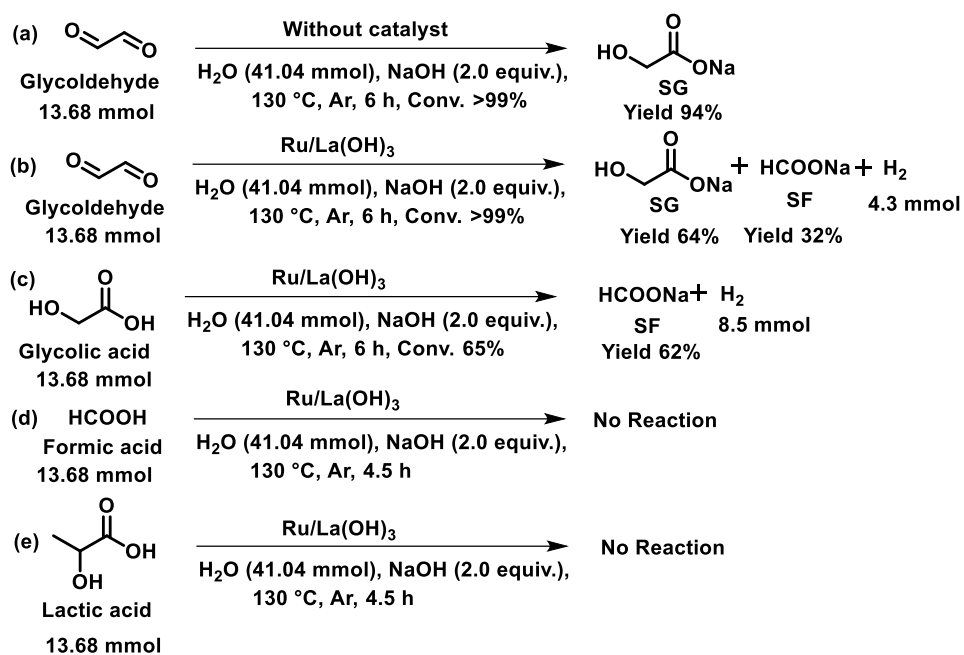
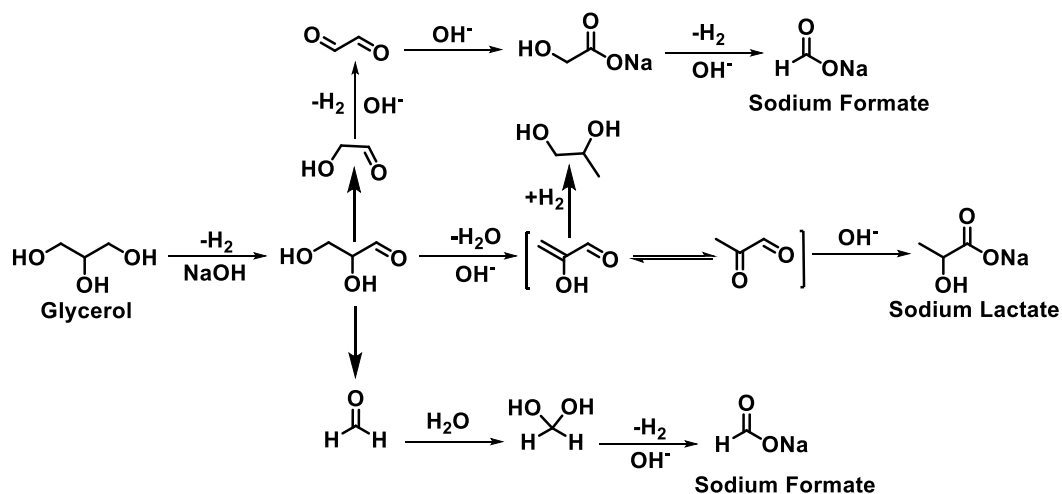


Figure 3.19. ^1H NMR spectra of the crude reaction mixture of the catalytic reaction for hydrogen production from formic acid over the $\text{Ru/La}(\text{OH})_3$ catalyst. Reaction conditions: $\text{Ru/La}(\text{OH})_3$ (100 mg), formic acid (13.68 mmol), NaOH (27.36 mmol), water (41.04 mmol), 130 °C, and 600 rpm.



Scheme 3.1. Control experiments to elucidate the reaction intermediates in the catalytic transformation of GLY to H₂ and SL.



Scheme 3.2. Plausible reaction pathways for hydrogen production from GLY over the Ru/La(OH)₃ catalyst.

3.3.4. Catalyst stability and recyclability

The mercury poisoning experiment was conducted to investigate the heterogeneity of the Ru/La(OH)₃ catalyst, where the Ru/La(OH)₃ catalyst was treated with an excess of elemental Hg(0) before proceeding to the catalytic reaction. A significant quenching of the reaction was observed, inferring the

heterogeneous nature of the catalyst (Figure 3.20). Moreover, the bulk-scale H₂ gas generation from GLY was conducted, where ~2.2 L (90 mmol) of H₂ gas was produced in 18 h from 5 mL (68.5 mmol) of GLY with a productivity of 12 L H₂/gRu/h and the yield of SL (82%) in the presence of NaOH (2.0 equiv.) at 130 °C (Figure 3.21). A catalyst recyclability experiment was also performed, where the Ru/La(OH)₃ catalyst was recycled and reused for six consecutive runs without any significant loss in the catalytic activity with cumulative H₂ yield ~2.8 L H₂ from 82.08 mmol of GLY (Figure 3.22). The slight loss in the catalytic efficacy in the dehydrogenation of GLY may be ascribed to the agglomeration of ruthenium nanoparticles and loss of catalyst during the recovery process. Moreover, bulk-scale dehydrogenation of EG was also performed, and we observed the release of ~ 4.3 L H₂ gas from 3.8 mL of EG in 42 h using NaOH (3.0 equiv.) and ~3.7 L of H₂ gas from 3.8 mL of EG in 37 h in the presence of 2.0 equiv. NaOH (Figure 3.23).

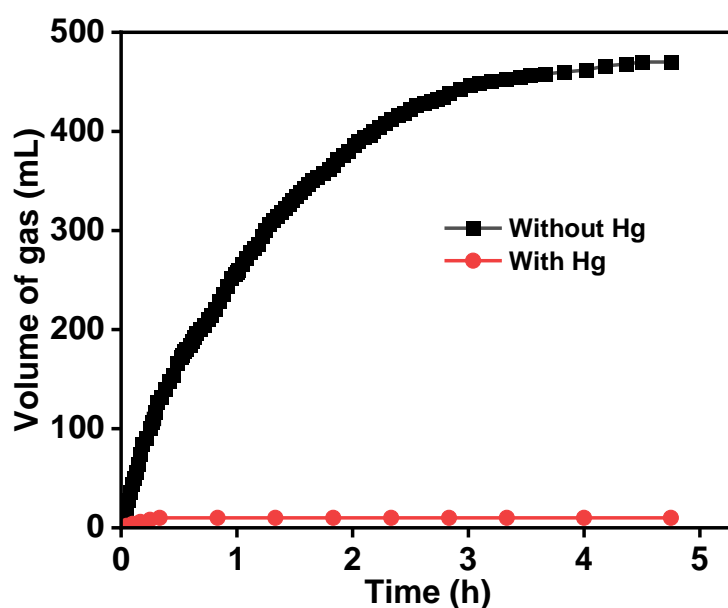


Figure 3.20. Hg poisoning experiment to validate the heterogeneous nature of the Ru/La(OH)₃ catalyst.

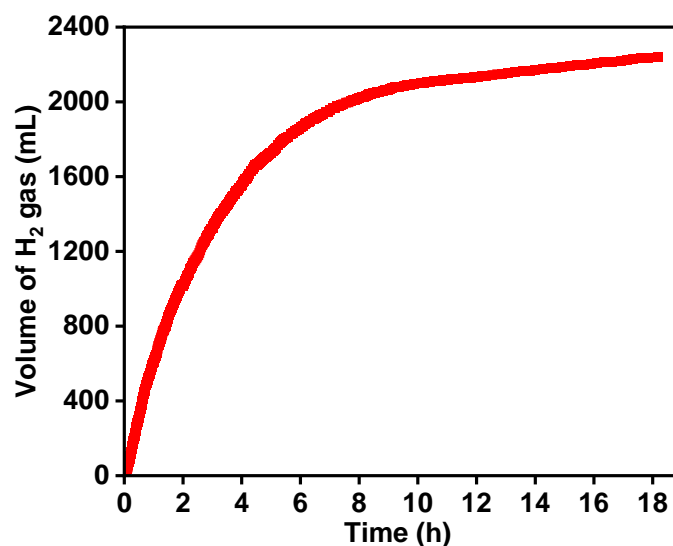


Figure 3.21. Time course plot for the bulk-scale production of hydrogen gas from GLY over the Ru/La(OH)₃ catalyst. Reaction conditions: Ru/La(OH)₃ (100 mg), GLY (68.4 mmol), NaOH (136.8 mmol), water (205.2 mmol), 130 °C, and 600 rpm.

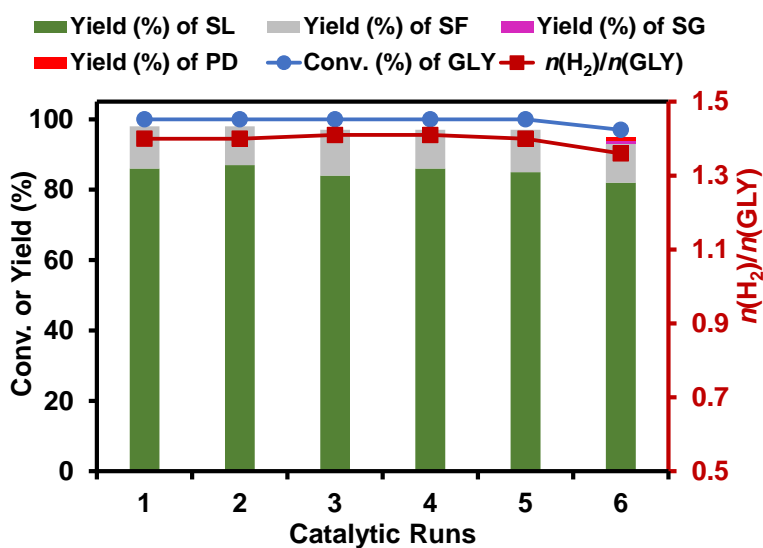


Figure 3.22. Recyclability experiment for hydrogen production from GLY over the Ru/La(OH)₃ catalyst. Reaction conditions: Ru/La(OH)₃ (100 mg), GLY (13.68 mmol), NaOH (27.36 mmol), water (41.04 mmol), 130 °C, and 600 rpm.

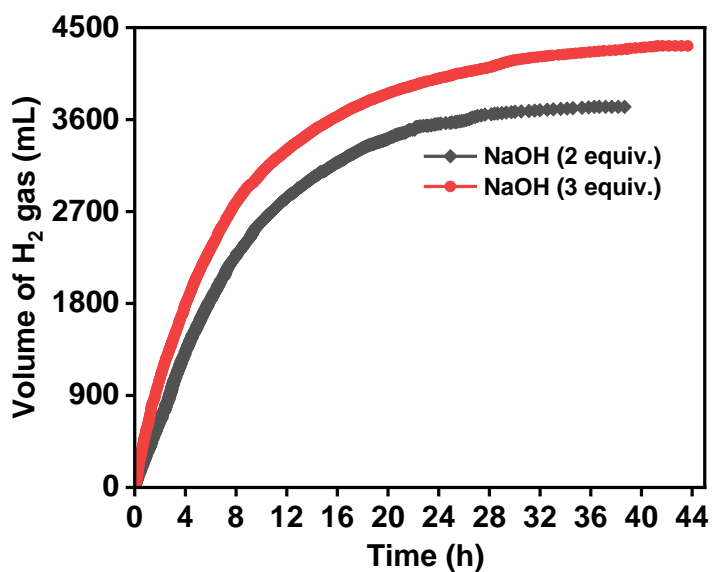


Figure 3.23. Time course plot for the bulk-scale production of hydrogen gas from EG over the Ru/La(OH)_3 catalyst. Reaction conditions: Ru/La(OH)_3 (100 mg), EG (68.4 mmol), NaOH, water (205.2 mmol), 130 °C, and 600 rpm.

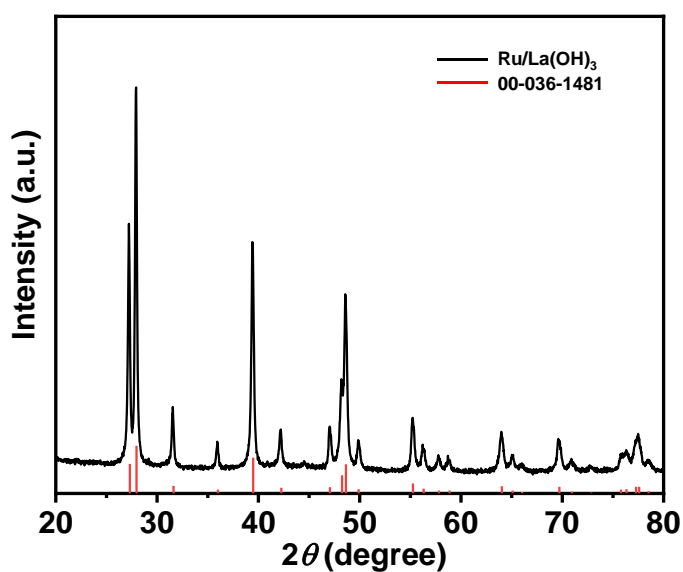


Figure 3.24. P-XRD pattern of the spent Ru/La(OH)_3 catalyst.

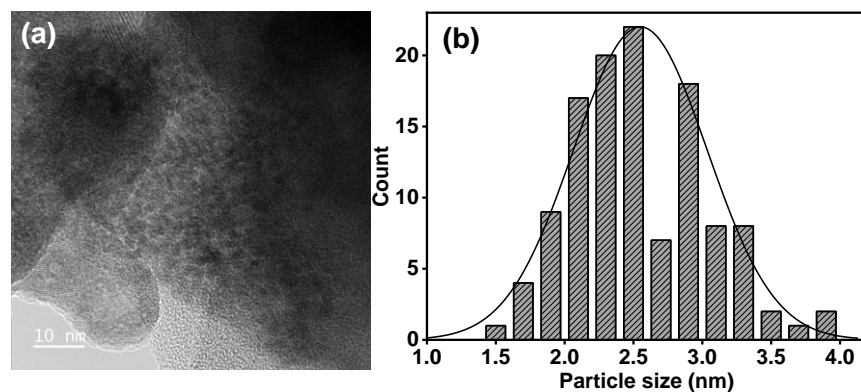


Figure 3.25. (a) TEM image, and corresponding (b) particle size distribution graph of the spent Ru/La(OH)₃ catalyst.

Noticeably, the P-XRD pattern of the spent Ru/La(OH)₃ catalyst was found to be analogous to the fresh Ru/La(OH)₃ catalyst (Figure 3.24). TEM analysis of the spent catalyst showed a slight increase in the particle size (~2.5 nm) as compared to the fresh Ru/La(OH)₃ catalyst (particle size ~1.5 nm), probably due to agglomeration of ruthenium nanoparticles (Figure 3.25). ICP analysis of the reaction solution showed no significant leaching of Ru (~0.06 wt%). These findings confirm the robustness and the long-term stability of the Ru/La(OH)₃ catalyst, which is reflected in the observed enhanced catalytic activity of Ru/La(OH)₃ for the dehydrogenation of GLY to H₂ and SL.

Notably, literature revealed that most of the catalytic transformation of aqueous GLY to H₂ gas has been performed at high temperatures (200-750 °C), while LA production from GLY was obtained at lower temperatures (<200 °C) (Table S5). For instance, Raja et al. explored different metal loading of Ru nanoparticles over NaY support (2-5 wt% Ru-NaY) for the APR of GLY and achieved (conv. up to 88%) at 250 °C and under a continuous flow of N₂ gas (40 bar), resulted in 74% selectivity of H₂ gas with the contamination of other gases (24%) over the 3wt% Ru-NaY catalyst. They noted that the catalytic activity in APR of GLY was significantly improved by examining the structure-activity relationship between of Ru and NaY support, metal loading and dispersion of Ru metal.^[22] In the similar way, they also developed Ru based catalysts (Ru-NMC-3 and RuPt-NMC-3) for APR of GLY and afforded 92% conversion with 88.5% H₂ selectivity at 250 °C.^[31] Han et al. developed Ru-Zn-Cu(I) catalyst supported over hydroxyapatite (HAP) for the transformation of

GLY to LA at 140 °C and achieved >99% GLY conversion with the yield of 70.9% in 24 h. However, when catalytic reaction was performed over Ru/HAP catalyst, they achieved 63.7% yield of LA and 28.5% FA with complete conversion of GLY and 13.7% selectivity for methane gas at 140 °C in 12 h.^[56] It indicates that Zn⁺² and Cu(I) played an important role in achieving the good selectivity of LA. Zn⁺² ions help in the 1,2-hydride shift of reaction intermediate (pyruvaldehyde) to LA and Cu(I) restrained in the C-C bond cleavage of glyceraldehyde to improve the yield of LA. Banat et al. developed Au and 1D HAP nanohybrid supported on boron nitride (Au/BN/HAP) for the catalytic conversion of GLY to LA (Sel. 99.5%) at 100 °C in 2 h.^[57] It was found that BN had a high affinity to adsorb GLY, which enhanced the catalytic activity to convert GLY to LA over the supported catalyst. In comparison to earlier reported catalytic systems, our Ru/La(OH)₃ based catalytic system, having highly dispersed ruthenium metal nanoparticles (87%) and strong metal-support interaction (SMSI) between Ru and La(OH)₃, showed high catalytic activity for the selective dehydrogenation of GLY with high yield of H₂ ($n(\text{H}_2)/n(\text{GLY}) \sim 1.4$) and SL (86%) yield in water at 130 °C.

3.4. Conclusions

Herein, we demonstrated an efficient catalytic process for the selective dehydrogenation of aqueous glycerol (GLY) to H₂ gas and sodium lactate (SL) over Ru/La(OH)₃ catalyst in aq. NaOH solution at 90-130 °C. Our findings inferred the crucial role of base concentration, $n(\text{GLY})/n(\text{H}_2\text{O})$ ratio, reaction temperature, and different supported catalysts in achieving complete conversion of GLY selectively to H₂ and SL. We observed that Ru/La(OH)₃ outperformed other supported ruthenium catalysts to achieve a high H₂ yield (1.4 equiv. per mmol of GLY) along with a high yield of LA (86%) at 130 °C in the presence of NaOH (2.0 equiv.). To validate the catalytic dehydrogenation pathway of GLY, several controlled experiments were carried out under optimized reaction conditions, which corroborated well with experimental results. Advantageously, we could generate H₂ gas on a large scale from GLY over the Ru/La(OH)₃ catalyst, displaying the remarkably high long-term stability of the Ru/La(OH)₃ catalyst with an efficiency of producing 220 L H₂/gRu with a productivity of 12 L H₂/gRu/h. Moreover, the developed catalytic methodology

was also equally effective for the bulk-scale dehydrogenation of EG to yield ~ 4.3 L H₂ gas from 3.8 mL of EG in 42 h using NaOH (3.0 equiv.) at 130 °C. Therefore, the developed catalytic system provides new insights into exploring GLY, EG and other terminal diols as important substrates for selectively producing purified hydrogen gas in aqueous conditions.

3.5. References

1. Midilli A., Ay M., Dincer I., Rosen M. A., (2005), On Hydrogen and Hydrogen Energy Strategies I: Current Status and Needs, *Renew. Sustain. Energy Rev.*, 9, 255-271 (DOI: 10.1016/j.rser.2004.05.003)
2. Balat M., (2008), Potential Importance of Hydrogen as a Future Solution to Environmental and Transportation Problems, *Int. J. Hydrog. Energy*, 33, 4013-4029 (DOI: 10.1016/j.ijhydene.2008.05.047)
3. Bockris J. O. M., (2013), The hydrogen Economy: Its History, *Int. J. Hydrog. Energy*, 38, 2579-2588, (DOI: 10.1016/j.ijhydene.2012.12.026)
4. Singh S., Jain S., Ps V., Tiwari A. K., Nouni M. R., Pandey J. K., Goel S., (2015), Hydrogen: A Sustainable Fuel for Future of the Transport Sector, *Renew. Sustain. Energy Rev.*, 51, 623-633 (DOI: 10.1016/j.rser.2015.06.040)
5. Barreto L., Makihira A., Riahi K., (2003), The Hydrogen Economy in the 21st Century: A Sustainable Development Scenario, *Int. J. Hydrog. Energy*, 28, 267-284 (DOI: 10.1016/s0360-3199(02)00074-5)
6. Mueller-Langer F., Tzimas E., Kaltschmitt M., Peteves S., (2007), Techno-economic Assessment of Hydrogen Production Processes for the Hydrogen Economy for the Short and Medium Term, *Int. J. Hydrog. Energy*, 32, 3797-3810 (DOI: 10.1016/j.ijhydene.2007.05.027)
7. Chen L., Qi Z., Zhang S., Su J., Somorjai G. A., (2020), Catalytic Hydrogen Production from Methane: A Review on Recent Progress and Prospect, *Catalysts*, 10, 858-875 (DOI: 10.3390/catal10080858)
8. Fasolini A., Cucciniello R., Paone E., Mauriello F., Tabanelli T., (2019), A Short Overview on the Hydrogen Production Via Aqueous Phase Reforming (APR) of Cellulose, C6-C5 Sugars and Polyols, *Catalysts*, 9, 1-17 (DOI: 10.3390/catal9110917)

9. Mei D., Dagle V. L., Xing R., Albrecht K. O., Dagle R. A., (2016), Steam Reforming of Ethylene Glycol over MgAl₂O₄ Supported Rh, Ni, and Co Catalysts, *ACS Catal.*, 6, 315-325 (DOI: 10.1021/acscatal.5b01666)
10. Palo D. R., Dagle R. A., Holladay J. D., (2007), Methanol Steam Reforming for Hydrogen Production Daniel, *Chem. Rev.*, 107, 3992-4021 (DOI: 10.1021/cr050198b)
11. Nielsen M., Alberico E., Baumann W., Drexler H. J., Junge H., Gladiali S., Beller M., (2013), Low-temperature Aqueous-phase Methanol Dehydrogenation to Hydrogen and Carbon dioxide, *Nature*, 495, 85-89 (DOI: 10.1038/nature11891)
12. Lin L., Zhou W., Gao R., Yao S., Zhang X., Xu W., Zheng S., Jiang Z., Yu Q., Li Y. W., Shi C., Wen X. D., Ma D., (2017), Low-temperature Hydrogen Production from Water and Methanol using Pt/ α -MoC Catalysts, *Nature*, 544, 80-83 (DOI: 10.1038/nature21672)
13. Awasthi M. K., Rai R. K., Behrens S., Singh S. K., (2021), Low-temperature Hydrogen Production from Methanol over a Ruthenium Catalyst in Water, *Catal. Sci. Technol.*, 11, 136-142 (DOI: 10.1039/d0cy01470b)
14. Mellmann D., Sponholz P., Junge H., Beller M., (2016), Formic Acid as a Hydrogen Storage Material – Development of Homogeneous Catalysts for Selective Hydrogen Release, *Chem. Soc. Rev.*, 45, 3954-3988 (DOI: 10.1039/c5cs00618j)
15. Boddien A., Mellmann D., Gärtner F., Jackstell R., Junge H., Dyson P. J., Laurency G., Ludwig R., Beller M., (2011) Efficient Dehydrogenation of Formic Acid Using an Iron Catalyst, *Science*, 333, 1733-1736 (DOI: 10.1126/science.1206613)
16. Hull J. F., Himeda Y., Wang W. H., Hashiguchi B., Periana R., Szalda D. J., Muckerman J. T., Fujita E., (2012), Reversible Hydrogen Storage using CO₂ and a Proton-switchable Iridium Catalyst in Aqueous Media under Mild Temperatures and Pressures, *Nat. Chem.*, 4, 383-388 (DOI: 10.1038/nchem.1295)
17. Patra S., Singh S. K., (2020), Hydrogen production from Formic Acid and Formaldehyde over Ruthenium Catalysts in Water, *Inorg. Chem.*,

- 59, 4234-4243 (DOI: 10.1021/acs.inorgchem.9b02882)
18. Heim L. E., Schlörer N. E., Choi J. H., Pechtl M. H. G., (2014), Selective and Mild Hydrogen Production using Water and Formaldehyde, *Nat. Commun.*, 5, 1-8 (DOI: 10.1038/ncomms4621)
 19. Trincado M. Sinha V., Rodriguez-Lugo R. E., Pribanic B., De Bruin B., Grützmacher H., (2017), Homogeneously Catalysed Conversion of Aqueous Formaldehyde to H₂ and Carbonate, *Nat. Commun.*, 8, 1-11 (DOI: 10.1038/ncomms14990)
 20. Van Haasterecht T., Van Deelen T. W., De Jong K. P., Bitter J. H., (2014), Transformations of Polyols to Organic Acids and Hydrogen, *Catal. Sci. Technol.*, 4, 2353-2366 (DOI: 10.1039/c4cy00249k)
 21. Kumar A., Awasthi M. K., Priya B., Singh S. K., (2022), Selective Hydrogen Production from Glycerol over Ruthenium Catalyst, *ChemCatChem*, e202101951 (DOI: 10.1002/cctc.202101951)
 22. Gogoi P., Nagpure A. S., Kandasamy P., Satyanarayana C. V. V., Raja T., (2020), Insights into the Catalytic Activity of Ru/NaY Catalysts for Efficient H₂ Production through Aqueous Phase Reforming, *Sustain. Energy Fuels*, 4, 678-690 (DOI: 10.1039/c9se00797k)
 23. Kumar A., Priya B., Singh S. K., (2023), Ruthenium-Catalyzed Transformation of Ethylene Glycol for Selective Hydrogen Gas Production in Water, *ACS Sustain. Chem. Eng.*, 11, 3999-4008 (DOI: 10.1021/acssuschemeng.2c04521)
 24. *Agricultural Outlook 2021-2030*, OECD-FAO, 2021 (accessed on Oct. 8th, 2023).
 25. Farias da Costas A. A., de Oliveira A. D. N., Esposito R., Auvigne A., Len C., Luque R., Noronha R. C. R., do Nascimento L. A. S., (2023), Glycerol and Microwave-assisted Catalysis: recent progress in batch and flow devices, *Sustain. Energy Fuels*, 7, 1768-1792 (DOI: 10.1039/d2se01647h)
 26. Pompeo F., Santori G. F., Nichio N. N., (2011), Hydrogen Production by Glycerol Steam Reforming with Pt/SiO₂ and Ni/SiO₂ catalysts, *Catal. Today*, 172, 183-188 (DOI: 10.1016/j.cattod.2011.05.001)
 27. Adhikari S., Fernando S. D., To S. D. F., Bricka R. M., Steele P. H., Haryanto A., (2008), Conversion of Glycerol to Hydrogen via a Steam

- Reforming Process over Nickel Catalysts, *Energy Fuels*, 22, 1220-1226 (DOI: 10.1021/ef700520f)
28. Polychronopoulou K., Charisiou N. D., Siakavelas G. I., Alkhour A. A., Sebastian V., Hinder S. J., Baker M. A., Goula M. A., (2019), Ce-Sm-xCu Cost-efficient Catalysts for H₂ Production through the Glycerol Steam Reforming Reaction, *Sustain. Energy Fuels*, 3, 673-691 (DOI: 10.1039/c8se00388b)
 29. Ming F., Qingli X., Wei Q., Zhikai Z., Suping Z., Yongjie Y., (2016), Hydrogen Production from Glycerol Steam Reforming over Ni/La/Co/Al₂O₃ Catalyst, *Energy Sources, Part A: Recover. Util. Environ. Eff.*, 38, 2128-2134 (DOI: 10.1080/15567036.2015.1052596)
 30. Surendar M., Padmakar D., Lingaiah N., Rama Rao K. S., Sai Prasad P. S., (2017), Influence of La₂O₃ Composition in MgO-La₂O₃ Mixed Oxide-supported Co catalysts on the Hydrogen Yield in Glycerol Steam Reforming, *Sustain. Energy Fuels*, 1, 354-361 (DOI: 10.1039/c6se00023a)
 31. Gogoi P., Kanna N., Begum P., Deka R. C., Satyanarayana C. V. V., Raja T., (2020), Controlling and Stabilization of Ru Nanoparticles by Tuning the Nitrogen Content of the Support for Enhanced H₂ Production through Aqueous-Phase Reforming of Glycerol, *ACS Catal.*, 10, 2489-2507 (DOI: 10.1021/acscatal.9b04063)
 32. Dietrich P. J., Lobo-Lapidus R. J., Wu T., Sumer A., Akatay M. C., Fingland B. R., Guo N., Dumesic J. A., Marshall C. L., Stach E., Jellinek J., Delgass W. N., Ribeiro F. H., Miller J. T., (2012), Aqueous Phase Glycerol Reforming by PtMo Bimetallic Nano-Particle Catalyst: Product Selectivity and Structural Characterization, *Top. Catal.*, 55, 53-69 (DOI: 10.1007/s11244-012-9775-5)
 33. King D. L., Zhang L., Xia G., Karim A. M., Heldebrant D. J., Wang X., Peterson T., Wang Y., (2010), Aqueous Phase Reforming of Glycerol for Hydrogen Production over Pt-Re Supported on Carbon, *Appl. Catal. B Environ.*, 99, 206-213 (DOI: 10.1016/j.apcatb.2010.06.021)
 34. Cortright R. D., Davda R. R., Dumesic J. A., (2002), Hydrogen from Catalytic Reforming of Biomass-derived Hydrocarbons in Liquid Water, *Nature*, 418, 964-967 (DOI: 10.1038/nature01009)

35. Pendem C., Sarkar B., Siddiqui N., Konathala L. N. S., Baskar C., Bal R., (2018), K-Promoted Pt-Hydrotalcite Catalyst for Production of H₂ by Aqueous Phase Reforming of Glycerol, *ACS Sustain. Chem. Eng.*, 6, 2122-2131 (DOI: 10.1021/acssuschemeng.7b03512)
36. Boga D. A., Oord R., Beale A. M., Chung Y. M., Bruijninx P. C. A., Weckhuysen B. M., (2013), Highly Selective Bimetallic Pt-Cu/Mg(Al)O Catalysts for the Aqueous-Phase Reforming of Glycerol, *ChemCatChem*, 5, 529-537 (DOI: 10.1002/cctc.201200112)
37. Guo Y., Liu X., Wang Y., (2019), Catalytic and DRIFTS Studies of Pt-Based Bimetallic Alloy Catalysts in Aqueous-Phase Reforming of Glycerol, *Ind. Eng. Chem. Res.*, 58, 2749-2758 (DOI: 10.1021/acs.iecr.8b05774)
38. Iriondo A., Barrio V. L., Cambra J. F., Arias P. L., Güemez M. B., Navarro, Sánchez-Sánchez M. C., Fierro J. L. G., (2008), Hydrogen Production from Glycerol Over Nickel Catalysts Supported on Al₂O₃ Modified by Mg, Zr, Ce or La, *Top. Catal.*, 49, 46-58 (DOI: 10.1007/s11244-008-9060-9)
39. Yin H., Yin H., Wang A., Shen L., Liu Y., Zheng Y., (2017), Catalytic Conversion of Glycerol to Lactic Acid Over Metallic Copper Nanoparticles and Reaction Kinetics, *J. Nanosci. Nanotechnol.*, 17, 1255-1266 (DOI: 10.1166/jnn.2017.12573)
40. Shen L., Yin H., Yin H., Liu S., Wang A., (2017), Conversion of Glycerol to Lactic Acid Catalyzed by Different-Sized Cu₂O Nanoparticles in NaOH Aqueous Solution, *J. Nanosci. Nanotechnol.*, 17, 780-787 (DOI: 10.1166/jnn.2017.12395)
41. Shen L., Yu Z., Zhang D., Yin H., Wang C., Wang A., (2019), Glycerol Valorization to Lactic Acid Catalyzed by Hydroxyapatite-supported Palladium Particles, *J. Chem. Technol. Biotechnol.*, 94, 204-215 (DOI: 10.1002/jctb.5765)
42. Yang G. Y., Ke Y. H., Ren H. F., Liu C. L., Yang R. Z., Dong W. S., (2016), The Conversion of Glycerol to Lactic Acid Catalyzed by ZrO₂-supported CuO Catalysts, *Chem. Eng. J.*, 283, 759-767 (DOI: 10.1016/j.cej.2015.08.027)
43. Palacio R., Torres S., Royer S., Mamede A. S., López D., Hernández D.,

- (2018), CuO/CeO₂ Catalysts for Glycerol Selective Conversion to Lactic Acid, *Dalton Trans.*, 47, 4572-4582 (DOI: 10.1039/c7dt04340f)
44. Roy D., Subramaniam B., Chaudhari R. V., (2011), Cu-based Catalysts Low Temperature Activity for Glycerol Conversion to Lactic Acid, *ACS Catal.*, 1, 548-551 (DOI: 10.1021/cs200080j)
45. Zhang J., Wu X., Chen J., Wang X., Mai Y., (2023), Efficient and Stable Cu-Cu₂O@NC Catalysts for Selective Catalytic Conversion of Glycerol to Lactic Acid, *ChemCatChem*, 15, e202201139 (DOI: 10.1002/cctc.202201139)
46. Palacio R., Torres S., Lopez D., Hernandez D., (2018), Selective Glycerol Conversion to Lactic Acid on Co₃O₄/CeO₂ Catalysts, *Catal. Today*, 302, 196-202 (DOI: 10.1016/j.cattod.2017.05.053)
47. Qiu L., Yin H., Yin H., Wang A., (2017), Catalytic Conversion of Glycerol to Lactic Acid Over Hydroxyapatite-Supported Metallic Ni(0) Nanoparticles, *J. Nanosci. Nanotechnol.*, 18, 4734-4745 (DOI: 10.1166/jnn.2018.15327)
48. Palacio R., López D., Hernández D., (2019), Bimetallic AuCu Nanoparticles Supported on CeO₂ as Selective Catalysts for Glycerol Conversion to Lactic Acid in Aqueous Basic Medium, *J. Nanoparticle Res.*, 21, 148 (DOI: 10.1007/s11051-019-4594-2)
49. Purushothaman R. K. P., van Haveren J., van Es D. S., Melián-Cabrera I., Meeldijk J. D., Heeres H. J., (2014), An Efficient One-Pot Conversion of Glycerol to Lactic Acid using Bimetallic Gold-Platinum Catalysts on a nanocrystalline CeO₂ support, *Appl. Catal. B Environ.*, 147, 92-100 (DOI: 10.1016/j.apcatb.2013.07.068)
50. Checa M., Auneau F., Hidalgo-Carrillo J., Marinas A., Marinas J. M., Pinel C., Urbano F. J., (2012), Catalytic Transformation of Glycerol on Several Metal Systems Supported on ZnO, *Catal. Today*, 196, 91-100 (DOI: 10.1016/j.cattod.2012.02.036)
51. Siddiki S. M. A. H., Touchy A. S., Kon K., Toyao T., Shimizu K. I., (2017), Oxidant-free Dehydrogenation of Glycerol to Lactic Acid by Heterogeneous Platinum Catalysts, *ChemCatChem*, 9, 2816-2821 (DOI: 10.1002/cctc.201700099)
52. Oberhauser W., Evangelisti C., Tiozzo C., Vizza F., Psaro R., (2016),

- Lactic Acid from Glycerol by Ethylene-stabilized Platinum-Nanoparticles, *ACS Catal.*, 6, 1671-1674 (DOI: 10.1021/acscatal.5b02914)
53. Feng S., Takahashi K., Miura H., Shishido T., (2020), One-pot Synthesis of Lactic Acid from Glycerol over a Pt/L-Nb₂O₅ Catalyst under Base-free Conditions, *Fuel Process. Technol.*, 197, 106202 (DOI: 10.1016/j.fuproc.2019.106202)
54. Ftouni J., Villandier N., Auneau F., Besson M., Djakovitch L., Pinel C., (2015), From Glycerol to Lactic Acid under Inert Conditions in the Presence of Platinum-based Catalysts: The influence of Support, *Catal. Today*, 257, 267-273 (DOI: 10.1016/j.cattod.2014.09.034 0920-5861)
55. Tang Z., Liu P., Cao H., Bals S., Heeres H. J., Pescarmona P. P., (2019), Pt/ZrO₂ Prepared by Atomic Trapping: An Efficient Catalyst for the Conversion of Glycerol to Lactic Acid with Concomitant Transfer Hydrogenation of Cyclohexene, *ACS Catal.*, 9, 9953-9963 (DOI: 10.1021/acscatal.9b02139)
56. Jiang Z., Zhang Z., Wu T., Zhang P., Song J., Xie C., Han B., (2017), Efficient Generation of Lactic Acid from Glycerol over a Ru-Zn-Cu(I), Hydroxyapatite Catalyst, *Chem. An Asian J.*, 12, 1598-1604 (DOI: 10.1002/asia.201700412)
57. Bharath G., Rambabu K., Hai A., Taher H., Banat F., (2020), Development of Au and 1D Hydroxyapatite Nanohybrids Supported on 2D Boron Nitride Sheets as Highly Efficient Catalysts for Dehydrogenating Glycerol to Lactic Acid, *ACS Sustain. Chem. Eng.*, 8, 7278-7289 (DOI: 10.1021/acssuschemeng.9b06997)
58. Ndolomingo M. J., Bingwa N., Meijboom R., (2020), Review of Supported Metal Nanoparticles: Synthesis Methodologies, Advantages and Application as Catalysts, *J. Mater. Sci.*, 55, 6195-6241 (DOI: 10.1007/s10853-020-04415-x)
59. Yuan Z., Gao Z., Xu B. Q., (2015), Acid-base Property of the Supporting Material Controls the Selectivity of Au Catalyst for Glycerol Oxidation in Base-free Water, *Chinese J. Catal.*, 36, 1543-1551 (DOI: 10.1016/S1872-2067(15)60936-6)
60. Fu C., Wang J., Yang M., Su X., Xu J., Jiang B., (2011), Effect of La

Doping on Microstructure of SnO₂ Nanopowders Prepared by co-precipitation method, *J. Non. Cryst. Solids*, 357, 1172-1176 (DOI: 10.1016/j.jnoncrysol.2010.10.019)

61. Wang X., Maeda N., Meier D. M., (2021), Synergistic Effects of Bimetallic AuPd and La₂O₃ in the Catalytic Reduction of NO with CO Catalysts, 11, 1–11 (DOI: 10.3390/catal11080916)
62. Lahr D. G., Shanks B. H., (2003), Kinetic Analysis of the Hydrogenolysis of Lower Polyhydric Alcohols: Glycerol to Glycols, *Ind. Eng. Chem. Res.*, 42, 5467-5472 (DOI: 10.1021/ie030468l)
63. Mondal S., Malviya H., Biswas P., (2019), Kinetic Modelling for the Hydrogenolysis of Bio- glycerol in the Presence of a Highly Selective Cu-Ni-Al₂O₃ Catalyst in a Slurry Reactor, *React. Chem. Eng.*, 4, 595-609 (DOI: 10.1039/c8re00138c)
64. Zhang G., Jin X., Guan Y., Yin B., Chen X., Liu Y., Feng X., Shan H., Yan C., (2019), Toward Selective Dehydrogenation of Glycerol to Lactic Acid over Bimetallic Pt-Co/CeO_x Catalysts, *Ind. Eng. Chem. Res.*, 58, 14548-14558 (DOI: 10.1021/acs.iecr.9b01918)

Chapter 4

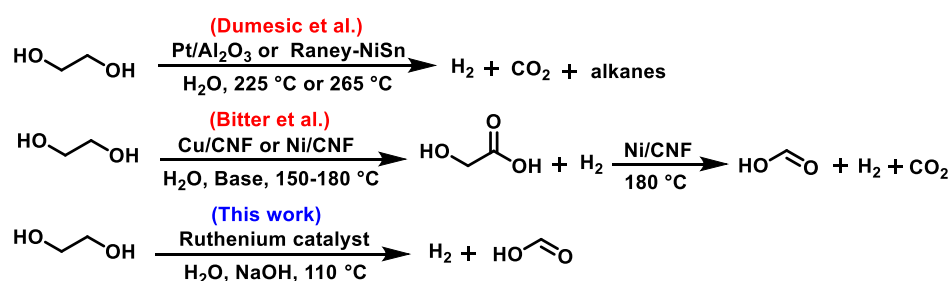
Selective Hydrogen Gas Production from Ethylene Glycol over Ruthenium Catalyst in Water

4.1. Introduction

The rising demand for energy, the depletion of non-renewable resources, and abrupt climate changes have compelled the scientific community to explore environmentally sustainable alternatives to meet the global energy demand.^[1,2] In this context, molecular hydrogen is a promising, clean, renewable fuel and alternative energy carrier, owing to its high gravimetric energy density and the release of only water/water vapour as a byproduct when used in a fuel cell or combustion engine.^[3-9] However, the efficient storage of hydrogen gas is challenging due to its low volumetric energy density. Worldwide, hydrogen gas is stored and transported under high pressure or as a liquid under cryogenic temperature. On the other hand, hydrogen is one of the most abundant elements in nature. Still, it is chemically bonded in organic compounds, and its availability as molecular H₂ gas in the earth's atmosphere is negligible. On an industrial scale, hydrogen is produced by methane reforming,^[10] aqueous phase reforming,^[11] and steam reforming of fossil fuels,^[12] which are highly energy-intensive processes with the emissions of greenhouse gases. On the other hand, with the intervention of a suitable catalyst, hydrogen can be produced from several promising and potential small organic molecules such as, methanol,^[13-16] formic acid,^[17-22] formaldehyde,^[20, 23-25] and other polyols.^[26-28]

However, attempts are also being made around the world to find alternative, effective, and sustainable resources for the production of hydrogen gas. In this regard, ethylene glycol (EG), a vicinal diol, is an inexpensive and renewable source which can store 6.5 wt% of hydrogen. Notably, EG can be produced by hydrogenolysis of biomass-derived polyols,^[29] and alternatively by hydration of petrochemically derived ethylene oxide,^[30] depolymerization of polyethylene terephthalate (PET) and so on.^[31] Hydrogen production from EG via steam reforming has been explored over Ru/Al₂O₃,^[32] Ni/CeO₂-Al₂O₃,^[33] Rh or Ni/MgAl₂O₄,^[12] Pt or Ni/γ-Al₂O₃,^[34] Ni-Pt/Al₂O₃,^[35] Ni-

Cu/La₂O₃-MgO,^[36] Ni/Attapulgite^[37] and others. Compared to the steam reforming process, which works at a high temperature (>200 °C), aqueous phase reforming is getting a lot of recognition for hydrogen production from biomass-derived oxygenated compounds at a relatively lower temperature (<200 °C).³⁸ A variety of catalysts such as Ni-Zn-Al/HT,^[38] Ni/Mg/Al,^[39] Co/ZnO,^[40] Ni-Pt/HT,^[41] NiFeCo,^[42] Pt-Co/CeO₂-ZrO₂,^[43] Pt/CNF,^[44] Pt/Al₂O₃,^[45] Pt-Mn/CMK-3,^[46] M/SiO₂ (where M = Ni, Pt, Pd, Ru, Rh),^[47] and Raney-NiSn^[48] have been explored for aqueous phase reforming of EG to produce hydrogen gas. For instance, Pt/Al₂O₃ catalyst was reported by Dumesic et al. for EG reforming to achieve 90% conversion with 96% H₂ selectivity at 225 °C (Scheme 4.1).^[45] However, selective hydrogen production is a major challenge in the aqueous phase reforming of EG due to the involvement of side reactions to form CO₂, CO, and other short alkanes. Bitter et al. developed a catalytic system for the EG to glycolic acid (GA) conversion at 150 °C using Cu supported on carbon nanofiber (CNF), and for converting GA to formic acid (FA), H₂, and CO₂ at 180 °C over the Ni supported on carbon nanofiber (CNF), where the selectivity of hydrogen gas was found to be 99% in alkaline medium (Scheme 4.1).^[26]



Scheme 4.1. Catalytic hydrogen production from ethylene glycol over various catalysts.

A few molecular catalysts, mainly based on Rh, Ir, Ru, and Mn have also been explored for EG reforming.^[49-53] For instance, Beller et al. employed Ru-PNP catalyst for EG reforming at 125 °C in diglyme.^[50] Tang et al. reported Rh Cp* bipyrimidine (Cp*Ru-bpym) from EG to GA at 100 °C in water.^[51] Milstein et al. achieved reforming of EG to GA and H₂ at 115 °C in THF-water, where the reactivity of Ru-PNP-based catalyst drastically decreased at a reaction temperature of 100 °C.^[52] Moreover, the reaction was sluggish when

water was used as the only solvent at 115 °C. Recently, Maji et al. employed Mn-PNP complex for EG reforming to GA and H₂ as a byproduct at 140 °C in tAmOH in 12 h.^[53] Therefore, it is evident from these reports that most heterogeneous catalyst works well at high temperature, while homogeneous catalysts are primarily explored in non-aqueous solvents. Recently, we also developed and explored several efficient catalysts for low-temperature hydrogen production from methanol,^[16] formic acid,^[20-21] formaldehyde,^[25] glycerol,^[26] and others in water-based conditions. We envisioned that the dehydrogenation of EG may lead to the selective production of hydrogen gas along with the generation of formic acid as a valuable byproduct. Such processes led to the selective production of 3.0 equivalents of hydrogen gas from EG, which is free from CO or CO₂ contaminations, and thus, purification costs can be significantly reduced.

Herein, we developed an efficient process to produce hydrogen gas from ethylene glycol (EG) over the ruthenium catalyst (unsupported catalyst) in water at a low temperature (110 °C). Reaction parameters are optimized and standardized to achieve high productivity and selectivity of hydrogen gas with complete conversion of EG. Attempts are made to understand the reaction pathway for EG dehydrogenation by identifying reaction intermediates and utilizing them under controlled reaction conditions. Moreover, attempts are also made to evaluate the potential of the developed catalytic system for the large-scale production of purified hydrogen gas from EG.

4.2. Experimental section

4.2.1. Materials and instrumentation

High-purity chemicals and metal salts were purchased from Sigma-Aldrich, Alfa-Aesar and used without further purification. All the catalytic reactions were performed under inert conditions using high-purity Argon gas purchased from Inox Air Products Ltd., India. ¹H NMR (500 MHz) was recorded in deuterated solvent (D₂O) using Bruker Ascend 500 spectrometer. Chemical shifts were referenced to the internal solvent resonances and were reported relative to tetramethylsilane. Transmission Electron Microscopic (FEI-TEM) images were obtained using the FEI TALOS 200S instrument at a working

voltage of 200 kV. The samples for TEM analysis were prepared by the drop-casting method. Briefly, ruthenium nanoparticles were dispersed in ethanol under ultra-sonication for 1 hour, and then highly dispersed particles were spread onto a carbon-coated Cu grid and dried at room temperature. Particle size was calculated using ImageJ software for at least 50-100 particles, and the average particle size distribution curve was plotted using Origin software. Scanning Electron Microscopic images and elemental mapping data were collected using a JOEL-7610F plus equipped with an EDS detector. Powder X-ray diffraction (P-XRD) measurements were performed using a Rigaku SmartLab Automated Multipurpose X-ray diffractometer with a scintillation detector. The measurements were conducted using Cu K α radiation ($\lambda = 1.5418 \text{ \AA}$) with a step size of 0.02° in the 2θ range of $20\text{-}80^\circ$. The exposure time for each P-XRD measurement was 20 minutes. The nitrogen physisorption isotherms were measured at 77 K using Quantachrome Autosorb iQ₂ TPX automated gas sorption system, and the specific surface area was calculated using the Brunauer-Emmett-Teller (BET) equation in the relative pressure (P/P₀) range of 0.05-0.3. The sample was degassed at 200 °C for 4 h under high vacuum before analysis. X-ray photoelectron Spectroscopy (XPS) was performed using Omnicron ESCA (Electron Spectroscopy for Chemical Analysis), Oxford Instrument, Germany. Aluminum (Al) anode was used as a monochromatic X-ray source (1486.7 eV) for XPS measurements. The binding energy values were charge-corrected to the C 1s signal (284.6 eV). The gas chromatography (GC) analyses were performed on a Shimadzu GC-2014 system using a shin carbon-ST packed column with a thermal conductivity detector (TCD) using argon as a carrier gas. Parameters were set for the program to detect H₂, CO₂, CO, and CH₄ gas (detector temperature: 200 °C, and oven temperature program: 90 °C (hold time: 1 min), 90-200 °C (rate: 15 °C per minute)). Inductively coupled plasma atomic emission spectroscopy (ICP-AES) was performed with ARCOS, a simultaneous spectrometer of SPECTRO analytical instruments. The sample was digested using aquaregia in the thermal autoclave at 170 °C for 12 h, diluted with water and then carried out for analysis.

4.2.2. Synthesis of the ruthenium catalyst

Typically, ruthenium (III) chloride (0.1 mmol) and polyvinylpyrrolidone (50 mg) dissolved in water (5 mL) was added dropwise to an aqueous solution of sodium borohydride (25 mg in 5 mL water) to obtain a black suspension of ruthenium nanoparticles.^[54] The content of the flask was sonicated for 10 minutes at room temperature to obtain ruthenium catalyst as black suspension. Ruthenium catalyst was collected as a black solid by centrifugation, washed several times with deionized water, and then dried under vacuum.

4.2.3. Catalytic hydrogen production from EG over the ruthenium catalyst

In a two-necked reaction vessel fitted with a condenser and water displacement set-up, a specified amount of ruthenium catalyst was suspended in ethylene glycol (EG) in the presence of a specified amount of water and base. The reaction mixture was stirred in an oil bath at 110 °C under the argon atmosphere. The amount of H₂ gas evolved was measured using a burette through the water displacement process, and the evolved gas was analyzed using a gas chromatography-thermal conductivity detector (GC-TCD). After the reaction, the catalyst was recovered from the reaction mixture by centrifugation at 6500 rpm for 5 minutes. EG conversion and the formation of other organic products were estimated by ¹H NMR of the crude reaction mixture. The yields of the products (sodium formate (SF) and sodium glycolate (SG)) were determined using sodium acetate as an internal standard using the following equation.

$$\text{Yield} = C_f(\text{P})/C_i(\text{EG}) \times 100 (\%)$$

where,

$C_f(\text{GLY})$ = millimoles of carbon in the final ethylene glycol

$C_f(\text{P})$ = millimoles of carbons in the final product

4.2.4. Recyclability experiment

Typically, the reaction performed using EG (5 mmol), NaOH (10.5 mmol) and ruthenium catalyst (0.1 mmol) was performed in water at 110 °C under the optimized reaction condition. For the subsequent catalytic runs, the ruthenium catalyst was separated from the reaction mixture by centrifugation, and the catalyst was re-used for subsequent catalytic runs. The progress of the reaction was monitored by measuring the evolved H₂ gas by the water displacement method and analyzed the released gaseous products by GC-TCD analysis.

4.2.5. Bulk scale hydrogen production from EG over the ruthenium catalyst

Typically, the reaction was performed using bulk scale aqueous solution of EG (50 mmol) in the presence of the ruthenium catalyst and NaOH (2.1 and 3.5 equiv.) under the optimized reaction condition at 110 °C.

4.2.6. Heterogeneity test for the ruthenium catalyst

Ruthenium catalyst (0.1 mmol), suspended in water (0.360 mL) was stirred with a large excess of elemental mercury (Hg) at room temperature for three hours before the catalytic reaction. Further, ethylene glycol (5 mmol, 0.280 mL) and NaOH (10.5 mmol, 420 mg) were added to the reaction vessel, fitted with a condenser and water displacement set-up. Further, the reaction mixture was stirred at 110 °C in an oil bath under an argon atmosphere to investigate the reaction quenching in the presence of elemental mercury.

4.2.7. Gas composition analysis

The identification of gaseous products during the dehydrogenation of EG was confirmed as H₂ and with no detectable level of CO, CO₂ and CH₄ using a Shimadzu GC-2014 system. The chromatograph was equipped with a shin carbon-ST packed column with a thermal conductivity detector (TCD) using argon as a carrier gas. Parameters were set for the program to detect H₂, CO₂, CO, and CH₄ (detector temperature, 200 °C; oven temperature program, 90 °C (hold time: 1 min), 90-200 °C (rate: 15 °C per minute)).

4.3. Results and discussion

4.3.1. Catalyst characterization

Transmission electron microscopy (TEM) images of the ruthenium catalyst revealed the presence of ruthenium nanoparticles of ~2.6 nm particle size (Figure 4.1a-c). Notably, the presence of a major peak of 44° in the P-XRD is consistent with the (101) plane of the hexagonal-close packed (hcp) ruthenium (Figure 4.1d).^[55] Energy-dispersive X-ray spectroscopy (EDX) and elemental mapping also evidenced the presence of ruthenium element (Figure 4.2). Further, the surface area of the ruthenium catalyst was calculated using the

Brunauer-Emmett-Teller (BET) equation applied to adsorption data in the relative pressure (P/P_0) range of 0.05-0.30 and found to be $19 \text{ m}^2/\text{g}$ (Figure 4.3).

The dominant peaks corresponding to the binding energy of Ru $3p_{3/2}$ and Ru $3p_{1/2}$ of Ru catalyst in X-ray photoelectron spectroscopy (XPS) measurements are observed at 461.5 eV and 483.6 eV, respectively, which is consistent with the formation of metallic ruthenium (74%) (Figure 4.4). Though Ru $3d_{3/2}$ peak shows significant overlapping with the peak of C 1s (284.6 eV), the binding energy of Ru $3d_{5/2}$ at 280.3 is corresponding to Ru(0).^[56-57] The presence of minor peaks at the binding energy of 464.7 eV and 484.2 eV corresponds to the oxidized Ru(IV) of 3p region (26%) is possibly due to the formation of an oxide layer over the ruthenium catalyst during sample preparation and handling under ambient conditions. Therefore, metallic Ru (0) is the active component of the ruthenium catalyst for the dehydrogenation of EG under the optimized reaction conditions.^[28]

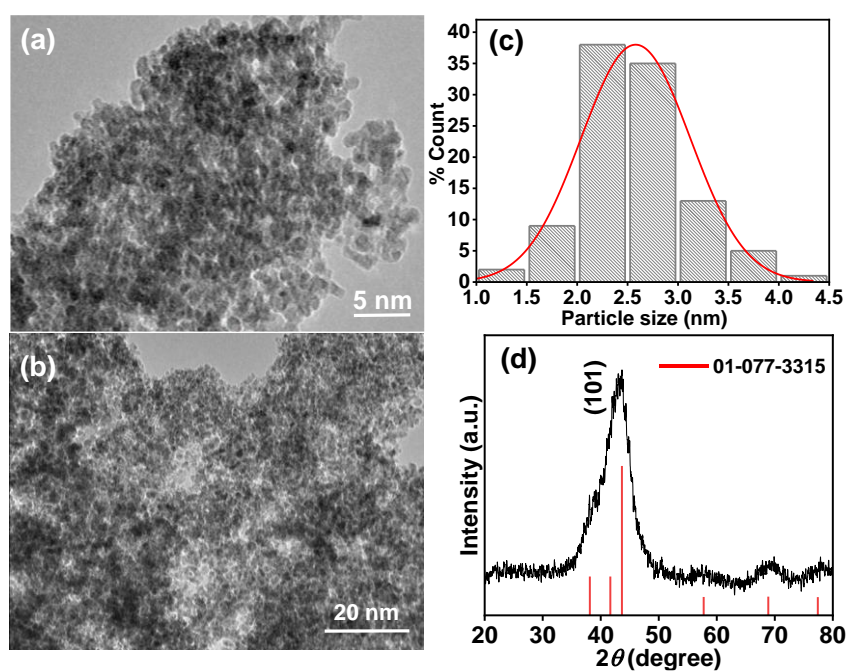


Figure 4.1. (a-b) TEM images, and corresponding (c) Particle size distribution curve, and (d) The P-XRD pattern of the fresh ruthenium catalyst.

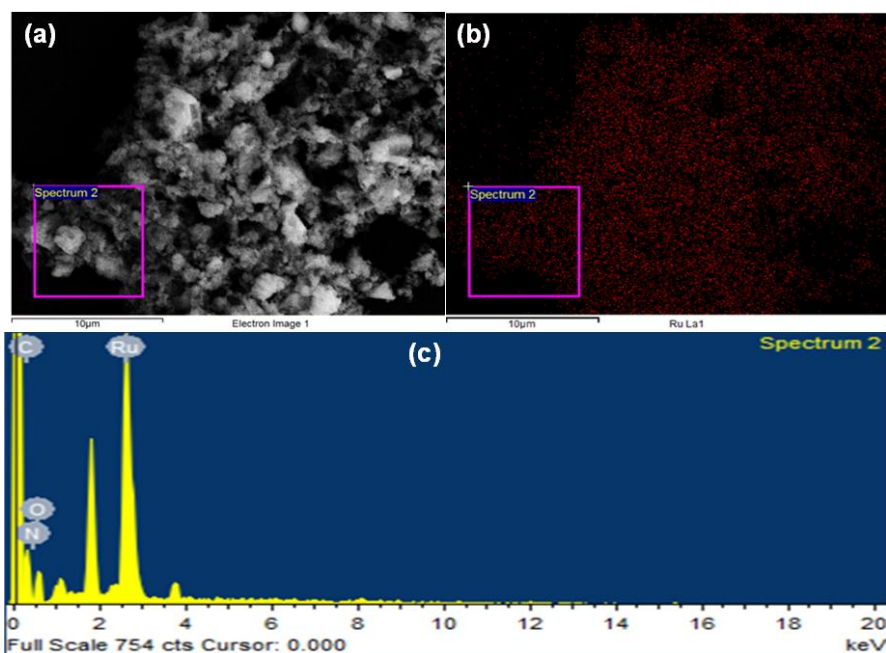


Figure 4.2. (a) SEM image corresponding to (b) elemental mapping and (c) EDX spectra of fresh ruthenium catalyst.

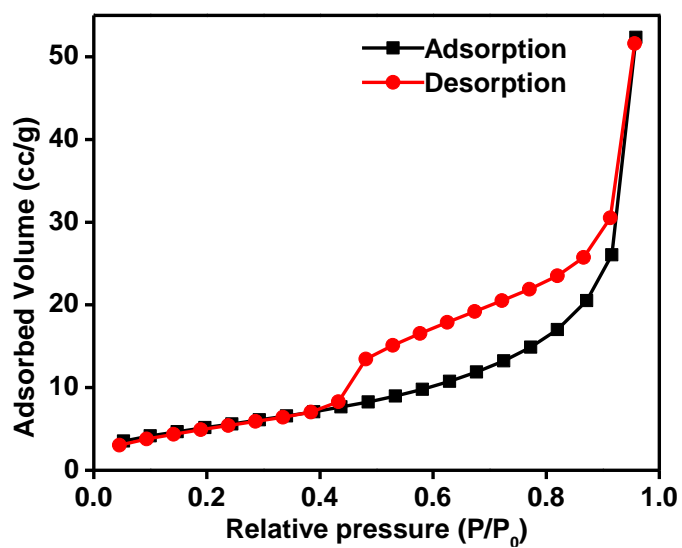


Figure 4.3. N_2 adsorption-desorption isotherm of fresh ruthenium catalyst.

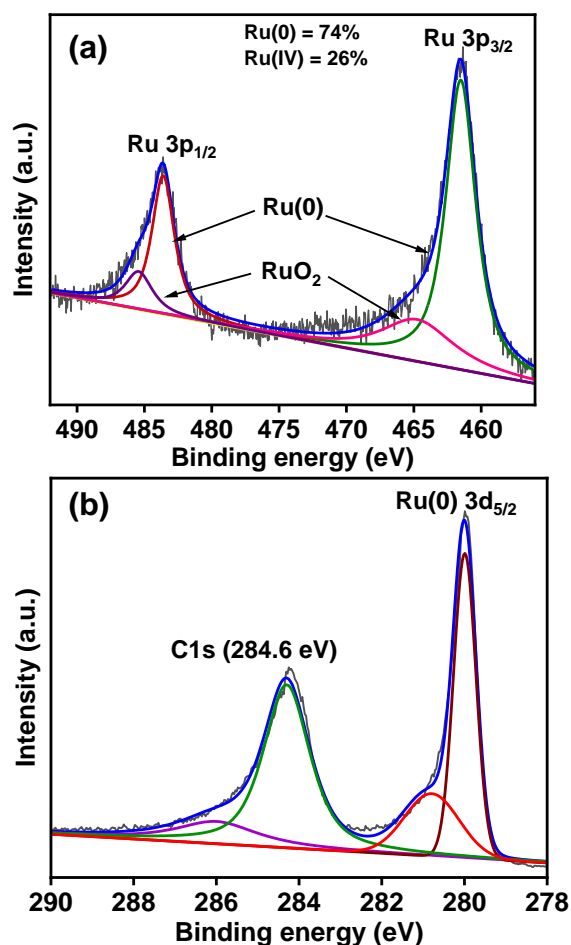


Figure 4.4. (a) XPS spectra of Ru 3p region and (b) Ru 3d region of fresh ruthenium catalyst.

4.3.2. Catalytic hydrogen production from EG

We began our investigations by evaluating the performance of the ruthenium catalyst synthesized by aqueous phase reduction of $\text{RuCl}_3 \cdot x\text{H}_2\text{O}$ using NaBH_4 in the presence of PVP to produce hydrogen gas from neat EG in the presence of NaOH at 110 °C. The reaction showed 52% conversion with 80 mL (0.6 equiv. of H_2 per EG) of hydrogen gas release in 9 h (Table 4.1, entry 1). The evolved gas was analyzed (by GC-TCD) as H_2 gas only with no traces of CO , CO_2 , or CH_4 suggesting the selective production of H_2 gas from EG (Figure 4.5 and 4.6). Based on the NMR spectroscopy of reaction mixture, sodium formate (SF) and sodium glycolate (SG) were observed as the only major products.

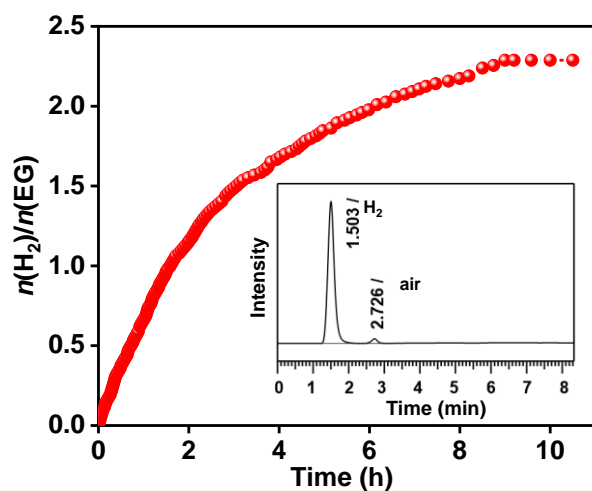


Figure 4.5. Time course plot (GC-TCD data in inset) for hydrogen gas production from EG over the ruthenium catalyst at 110 °C. Reaction conditions: Ruthenium catalyst (0.1 mmol), EG (5 mmol), NaOH (10.5 mmol), and water (20 mmol).

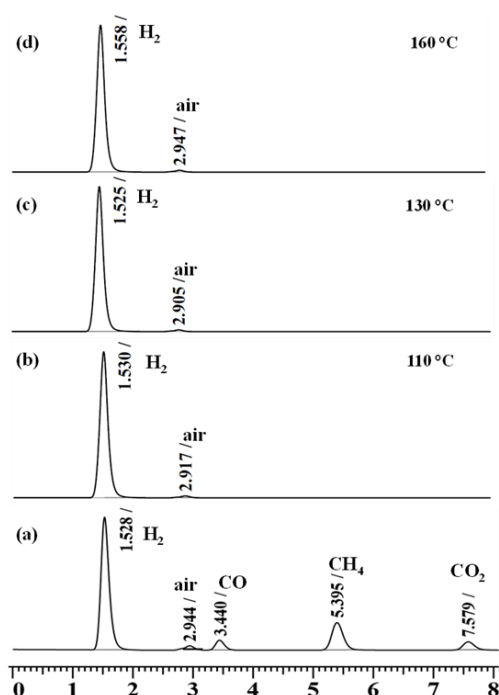


Figure 4.6. GC-TCD analysis of the (a) standard mixture of gases with the composition of CO (24.965%), CO₂ (24.962%), CH₄ (25.012%) and H₂ (25.061%), and (b-d) gas produced from EG dehydrogenation over the ruthenium catalyst at (b) 110 °C, (c) 130 °C, and (d) 160 °C. Reaction Conditions: Ruthenium catalyst (0.1 mmol), EG (5 mmol), NaOH (10.5 mmol), water (20 mmol), 110 °C, 130 °C, and 160 °C.

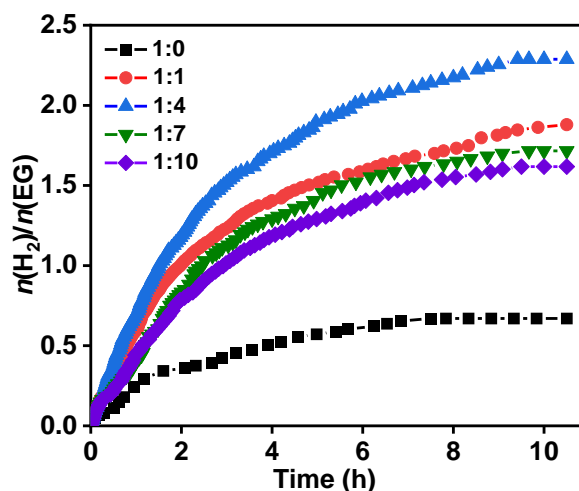
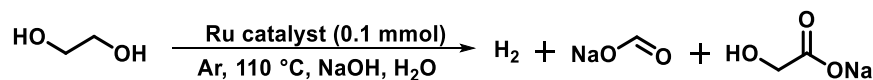


Figure 4.7. Effect of water concentration on hydrogen production from EG over the ruthenium catalyst. Reaction conditions: Ruthenium catalyst (0.1 mmol), EG (5 mmol), NaOH (10.5 mmol), water (0-10 equiv.), and 110 °C.

Indeed, the conversion of EG was increased to 83% in the presence of an equivalent amount of water to collect 230 mL (1.9 equiv. of H₂ per EG) of H₂ gas in 10 h (Table 4.1, entry 2). Using 4 equivalents of water, EG conversion was further enhanced to reach almost complete conversion (99%) with the release of 280 mL (2.3 equiv. of H₂ per EG) at 110 °C (Table 4.1, entry 3). However, with more diluted aqueous solution of EG, lower conversion with lesser volume of hydrogen gas release was observed (Table 4.1, entries 4, 5 and Figure 4.7). Notably, gas evolution was not observed for the reaction performed in the absence of catalyst (Table 4.1, entry 6). To investigate the role of PVP, the dehydrogenation of EG was performed over the Ru catalyst (synthesized without PVP) under the optimized reaction conditions, where a significantly low catalytic activity (conv. 26% in 9.5 h) was observed (Table 4.1, entry 7). The observed loss in the catalytic activity can be attributed to the agglomeration of the ruthenium nanoparticles due to the absence of PVP (average particle size of ~ 4 nm, as confirmed by TEM analysis) (Figure 4.8).

Table 4.1. Optimization of the reaction condition for hydrogen production from EG over ruthenium catalyst.^a



Entry	$n(\text{EG})/$ $n(\text{H}_2\text{O})$	NaOH (equiv.)	t (h)	Conv. (%)	H ₂ gas (mL) ^b	$n(\text{H}_2)/$ $n(\text{EG})$	Yield (%) ^c SF/SG	CB (%) ^d	Initial TOF (h ⁻¹) ^e
1	1:0	2.1	9	52	80	0.6	10/7	65	13
2	1:1	2.1	10.5	83	230	1.9	25/17	59	24
3	1:4	2.1	9.5	99	280	2.3	57/26	84	32
4	1:7	2.1	8.5	88	210	1.7	19/40	71	19
5	1:10	2.1	10	78	198	1.6	15/24	61	22
6 ^f	1:4	2.1	-	-	-	-	-	-	-
7 ^g	1:4	2.1	9.5	26	50	0.4	8/7	89	-
8	1:4	0	-	-	-	-	-	-	-
9	1:4	0.5	5	32	60	0.4	6/8	82	13
10	1:4	1.0	6	54	88	0.7	12/14	72	19
11	1:4	1.5	8	85	226	1.8	27/38	80	24
12	1:4	3	13	>99	364	3.0	74/7	81	39
13	1:4	3.5	10	>99	370	3.0	85/-	85	45

^aReaction conditions: Ruthenium catalyst (0.1 mmol), EG (5 mmol), NaOH, water, 110 °C. ^bMeasured by water displacement method. ^cCalculated by ¹H NMR using sodium acetate as an internal standard. ^dCarbon balance. ^eInitial turnover frequency at 1 h. ^fReaction in the absence of catalyst. ^gRuthenium catalyst synthesized without the use of PVP. EG (ethylene glycerol), SF (sodium formate), SG (sodium glycolate). Results reported are the average of at least two repeated reactions.

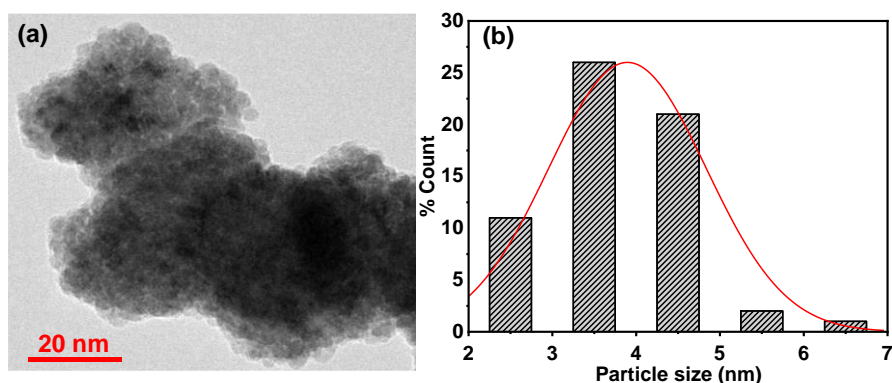


Figure 4.8. (a) TEM image and the corresponding (b) particle size distribution curve of the ruthenium catalyst synthesized without PVP.

Further, varying the NaOH concentration (0.5-3.5 equiv., 3.9-27.34 M) significantly influenced the amount of hydrogen gas released from EG (7.8 M) over the ruthenium catalyst at 110 °C (Table 4.1 and Figure 4.9). Results inferred that by varying the NaOH concentration in the range of 0-11.71 M, the conversion rate of EG increases from 0 to 0.83 M/h at 110 °C (Figure 4.9). Notably, the reaction could not proceed in the absence of NaOH (Table 4.1, entry 8), while at lower NaOH content (0.5 equiv., 3.9 M), the reaction was very sluggish with 32% conversion of EG (0.4 equiv. of H₂ per EG) (Table 4.1 and entry 9). However, the EG conversion rate was not significantly changed with the further increase in NaOH concentration from 11.71 M (2.1 equiv.) to 27.34 M (3.5 equiv.). Though an initial increase in the formation rate of SG from 0 to 0.37 M/h was observed with the increase in NaOH concentration from 0 -11.71 M, SG yield was decreased upon the increase in NaOH concentration beyond 11.71 M, where SG was not observed for the reaction performed with 27.34 M NaOH (Table 4.1, entries 12-13). Notably, the formation rate of SF displayed a linearly increasing trend with the increase in NaOH concentration (0 -27.34 M), where FA yield was significantly increased from 57% (with 2.1 equiv. of NaOH) to 85% (with 3.5 equiv. of NaOH) (Table 4.1 and Figure 4.9). These results clearly suggest the crucial role of NaOH concentrations in tuning the process of EG dehydrogenation.

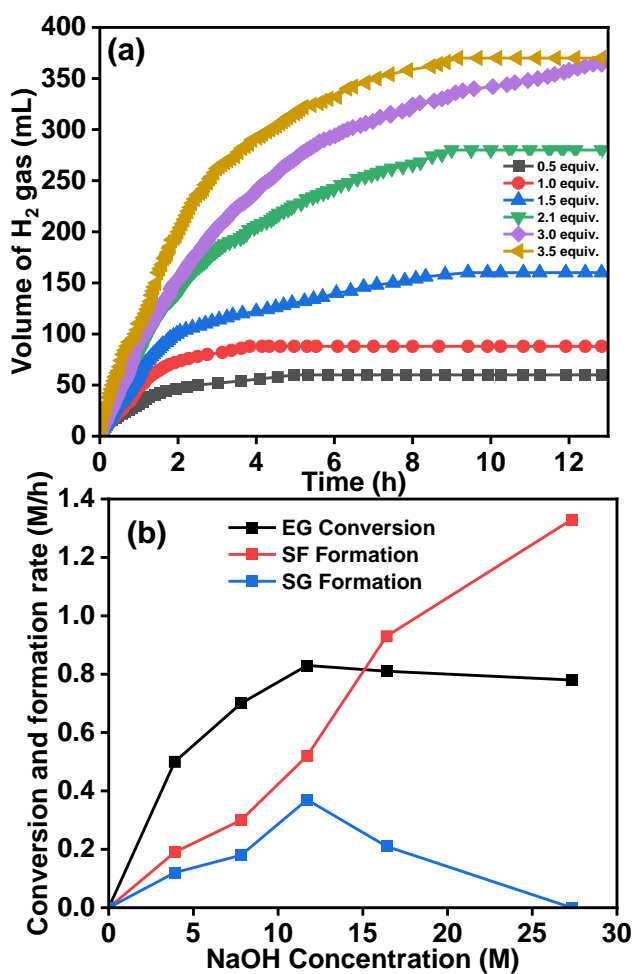


Figure 4.9. (a) Effect of base concentration on hydrogen production from EG over the ruthenium catalyst, (b) Initial reaction rate and product formation rate-NaOH concentration profile. Reaction conditions: Ruthenium catalyst (0.1 mmol), EG (5 mmol), water (20 mmol), NaOH (0.5-3.5 equiv., 3.9 M-27.34 M), 110 °C, and 600 rpm.

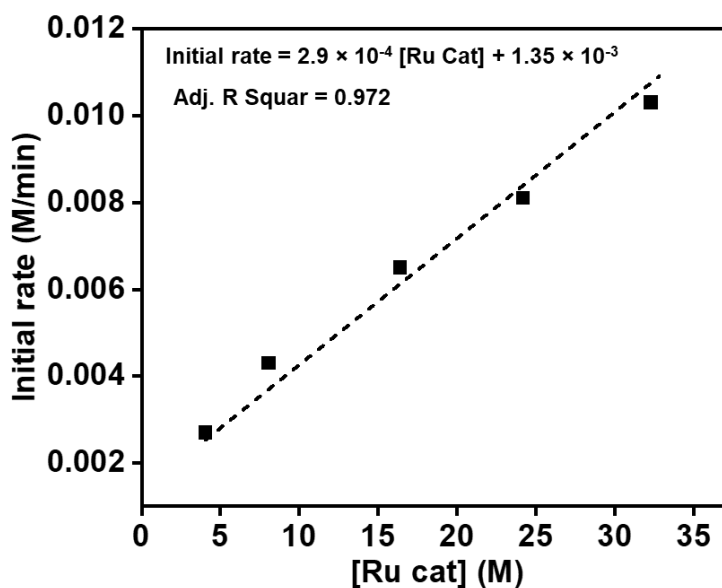
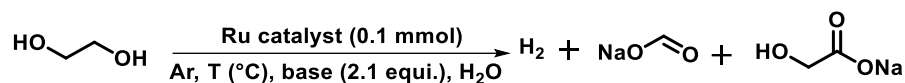


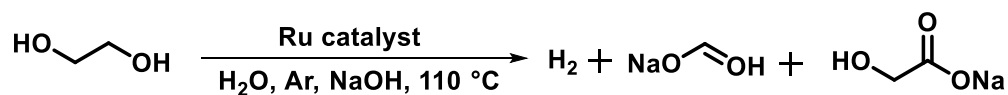
Figure 4.10. Dependence of ruthenium catalyst concentration on the reaction rate for hydrogen production from EG.

Further, the promotional effect of different bases (NaOH, KOH, K_2CO_3 , Na_2CO_3 , and KO^tBu) over the dehydrogenation of EG was also investigated (Table 4.2). Analogous to the high activity observed in the presence of NaOH (Table 4.2, entry 7), complete conversion of EG was also achieved in the presence of KOH (Table 4.2, entry 1). However, the rate of production of H_2 gas was slower with KOH compared to that observed in the presence of NaOH, which can be attributed to the larger ionic size of K^+ ion than Na^+ , which creates steric hindrance in the dehydrogenation step.^[58] Complete conversion of EG could not be achieved in the presence of KO^tBu (Table 4.2, entry 2). On the other hand, the reaction could not proceed in the presence of K_2CO_3 and Na_2CO_3 (Table 4.2, entries 3-4). Advantageously, H_2 gas generation from EG can also be achieved over varying ruthenium catalyst concentration (0.25 mol% - 2.0 mol%), where the initial rate of H_2 gas production was found to increase linearly with the increase of catalyst concentration (Table 4.3 and Figure 4.10).

Table 4.2. Optimization of the reaction conditions for hydrogen production from EG over ruthenium catalyst.^a

Entry	Base	T (°C)/ t (h)	Conv. (%)	H ₂ gas (mL) ^b	n(H ₂)/ n(EG)	Yield (%) ^c SF/SG	CB (%) ^d	Initial TOF (h ⁻¹) ^e
1	KOH	110/14.5	99	220	1.8	41/15	57	
2	KO ^t Bu	110/14	81	200	1.6	14/31	64	13
3	Na ₂ CO ₃	110/10	-	-	-	-	-	-
4	K ₂ CO ₃	110/10	-	-	-	-	-	-
5	NaOH	90/14	74	186	1.5	18/38	82	12
6	NaOH	100/11	90	234	1.9	29/42	81	19
7	NaOH	110/9.5	99	280	2.3	57/26	84	32
8	NaOH	120/8	>99	290	2.4	58/22	80	53
9	NaOH	130/6	>99	340	2.8	64/13	77	67
10	NaOH	160/3.5	>99	370	3.0	80/-	80	111

^aReaction conditions: Ru catalyst (0.1 mmol), EG (5 mmol), NaOH (10.5 mmol), water (20 mmol), 90 °C - 160 °C. ^bMeasured by water displacement method. ^cCalculated by ¹H NMR using sodium acetate as an internal standard. ^dCarbon balance. ^eInitial turnover frequency at 1 h. EG (ethylene glycerol), SF (sodium formate), SG (sodium glycolate). The results reported are the average of at least two repeated reactions.

Table 4.3. Hydrogen production from EG using varying loading of ruthenium catalyst.^a

Entry	Catalyst mol (%)	t (h)	Conv. (%)	H ₂ gas (mL) ^b	n(H ₂)/ n(EG)	Yield (%) ^c SF/SG	Initial TOF (h ⁻¹) ^d
1	0	-	-	-	-	-	-
2	0.25	14	50	122	0.98	9/15	4
3	0.5	14	84	186	1.51	26/36	13
4	1.0	13.5	96	224	1.83	41/32	17
5	1.5	12	97	234	1.91	42/41	26
6	2.0	9.5	99	280	2.3	57/26	32

^aReaction conditions: Ru catalyst (0.1mmol), EG (5 mmol), NaOH (10.5 mmol), water, 110 °C. ^bVolume of gas was measured by water displacement method. ^cYield of organic products was calculated by ¹H NMR using sodium acetate as an internal standard. ^dInitial turnover number at 1 h. SF (sodium formate), SG (sodium glycolate). The results reported are the average of at least two repeated reactions.

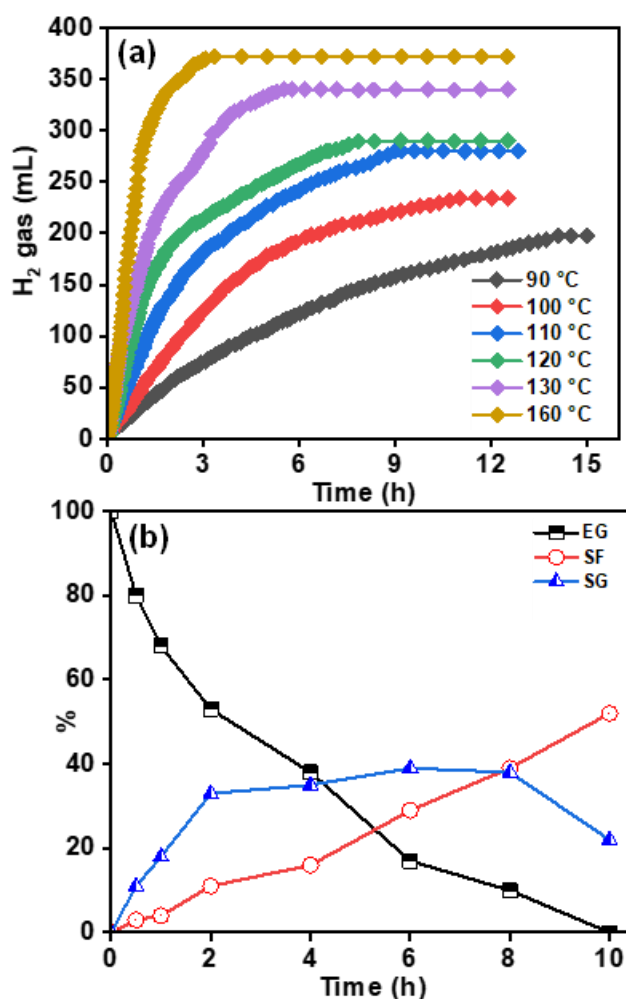


Figure 4.11. Time course plot for (a) temperature-dependent hydrogen production from EG over the ruthenium catalyst at 90-160 °C. (b) the distribution of EG, SF and SG during the catalytic dehydrogenation of EG over the ruthenium catalyst at 110 °C. Reaction conditions: Ruthenium catalyst (0.1 mmol), EG (5 mmol), NaOH (10.5 mmol), and water (20 mmol).

Notably, hydrogen gas production from EG was also observed at 90 °C to achieve 1.6 equiv. of H₂ per mol of EG in 14 h over Ru catalyst. Higher yield of hydrogen gas was obtained with further increase in the reaction temperature to 100 -160 °C (Table 4.2, entries, 6-10 and Figure 4.11). Complete conversion of EG was achieved for the reaction performed at $\geq 110^{\circ}\text{C}$, where with increase in the reaction temperature yield of SF was also increasing, while SG yield was in a decreasing trend. At 160 °C, 3.0 equiv. of H₂ gas was produced together with the 80% yield of SF for the catalytic reaction from EG dehydrogenation

over the ruthenium catalyst. Under the optimized reaction condition, the ruthenium catalyst also displayed an increasing trend in the initial TOF (h^{-1}) with the increase in reaction temperature, where the initial TOF was 32 h^{-1} at $110 \text{ }^\circ\text{C}$ which was increased by ~ 3.5 folds to 111 h^{-1} at $160 \text{ }^\circ\text{C}$, with complete selectivity for H_2 gas at all the reaction temperatures. The observed enhanced catalytic activity of the studied ruthenium catalyst is significant as compared to the earlier reported aqueous phase reforming of EG processes such as over Ru-NaY catalyst at $250 \text{ }^\circ\text{C}$ displaying EG conversion well below 80% with H_2 selectivity in the range of 50%-74%.^[28] The activation energy for the reaction was estimated as 57 kJ/mol (Figure 4.12). Moreover, from Eyring equation the estimated $\Delta G^\ddagger_{(298)}$ was found to be 95.6 kJ/mol with ΔH^\ddagger of $+53.9 \text{ kJ/mol}$ and ΔS^\ddagger of -139.8 J/mol/K (Figure 4.13). We performed GC-TCD analysis of gas produced during the dehydrogenation of EG at different reaction temperatures ($110 \text{ }^\circ\text{C}$, $130 \text{ }^\circ\text{C}$, and $160 \text{ }^\circ\text{C}$) and observed that there is no peak corresponding to CO_2 or CO gas even at the higher reaction temperature, suggesting the selective production of H_2 gas (Figure 4.6). Therefore, the observed loss in the carbon balance could be associated with the formation of C4/C6 aldol condensation products.^[51]

Further, ^1H NMR investigation of the catalytic reaction aliquots at different time intervals during the reaction inferred a continuous consumption of EG with an increasing selectivity for FA (Figure 4.11b). The increase in the yield of SF in the presence of higher concentration of base, suggesting that SG as one of the intermediate species, which further transformed to SF with the release of H_2 gas. Further to investigate the involvement of intermediate species in the catalytic dehydrogenation of EG, several control experiments were performed (Scheme 4.2). It is postulated that the SG observed in the catalytic reaction can be produced from glycolaldehyde, which produces hydrogen gas in the presence of base to yield glyoxal. Further, glyoxal undergoes rearrangement to SG (Scheme 4.2). Notably, EG dehydrogenation to SG and SF occurred at a conversion rate of 1.8 M/h under the optimized reaction condition (Reaction A, Scheme 4.2).

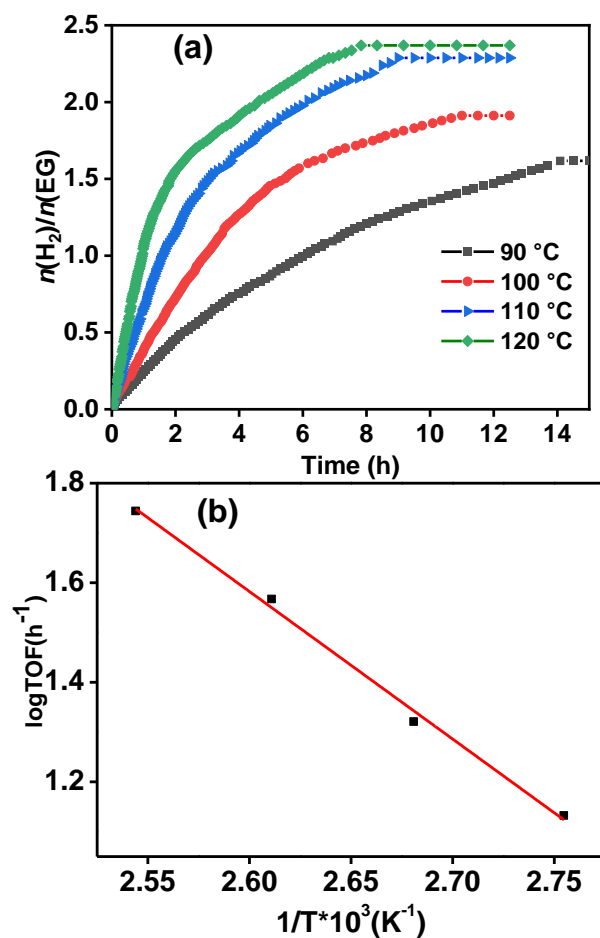


Figure 4.12. (a) Temperature-dependent study for hydrogen production from EG over the ruthenium catalyst at 90-120 °C. (b) Arrhenius plot of initial TOF values. Reaction conditions: Ruthenium catalyst (0.1 mmol), EG (5 mmol), NaOH (10.5 mmol), and water (20 mmol).

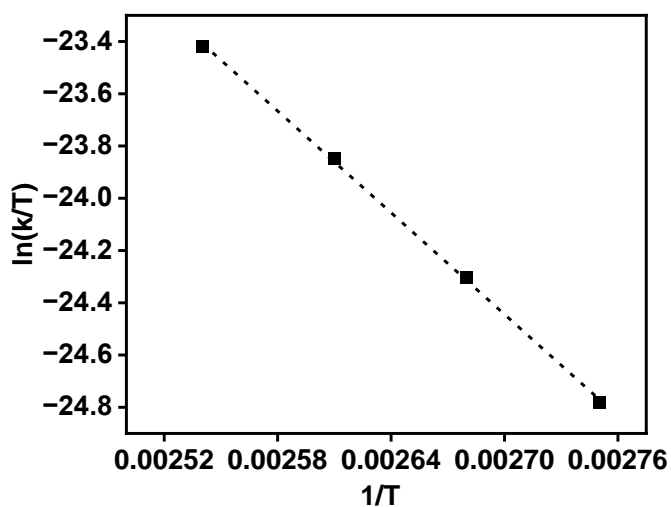


Figure 4.13. Kinetic studies for dehydrogenation of ethylene glycol over the ruthenium catalyst using Eyring analysis.

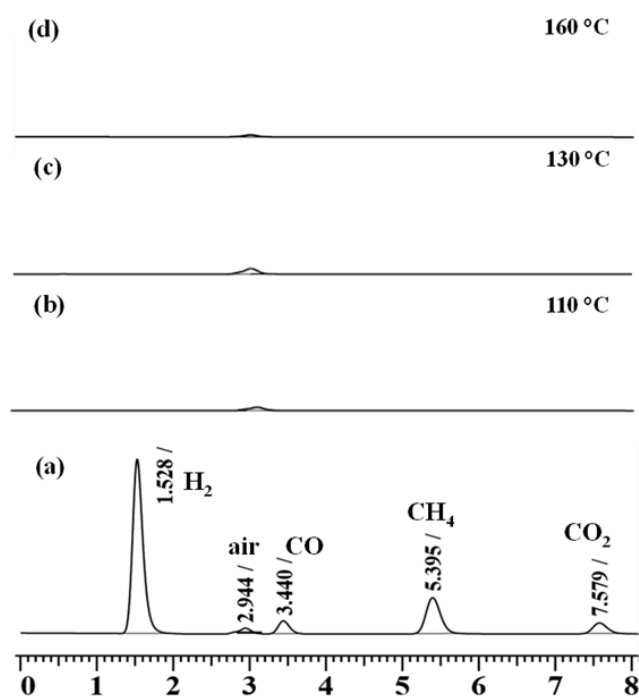
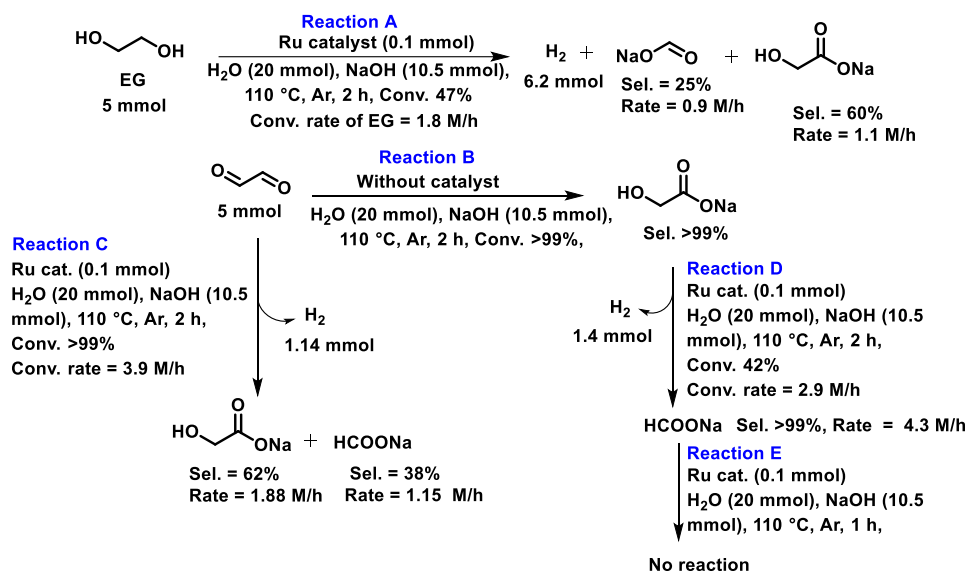


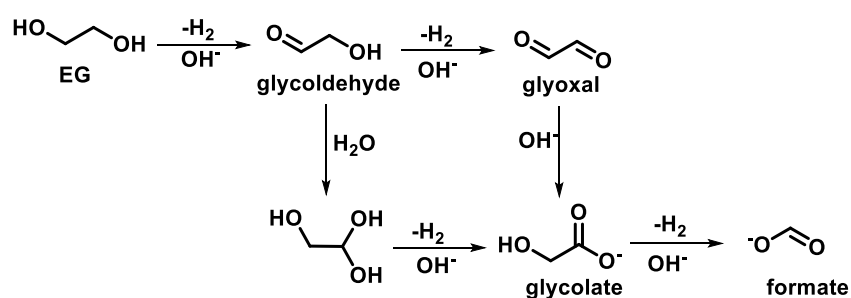
Figure 4.14. GC-TCD analysis of the (a) standard mixture of gases with the composition of CO (24.965%), CO₂ (24.962%), CH₄ (25.012%), and H₂ (25.061%), and (b-d) gas produced (if any) from formic acid dehydrogenation over ruthenium catalyst at (b) 110 °C, (c) 130 °C, and (d) 160 °C. Reaction Conditions: Ruthenium catalyst (0.1 mmol), formic acid (5 mmol), NaOH (10.5 mmol), water (20 mmol), 110 °C, 130 °C, and 160 °C.

In agreement with the possible reaction pathway, we observed the transformation of glyoxal to SG in the presence of NaOH under the catalyst-free condition (Reaction B, and Scheme 4.2) On the other hand, treating glyoxal with the ruthenium catalyst at 110 °C resulted in the formation of SG (sel. 62%) and SF (sel. 38%) with the release of H₂ gas (1.14 mmol) (Reaction C, and Scheme 4.2) Further, treating GA with ruthenium catalyst in the presence of 2.1 equiv. of NaOH resulted in the generation of H₂ gas along with SF with a conversion rate of 2.9 M/h, suggesting that dehydrogenation of SG may also occur under the catalytic dehydrogenation of EG (Reaction D, and Scheme 4.2). Notably, FA to H₂ transformation was not observed over the ruthenium catalyst (Reaction E, and Scheme 4.2). We have also performed a control experiment for the dehydrogenation of formic acid at different reaction temperatures (110 °C, 130 °C, and 160 °C), where we could not observe any gas evolution as inferred by the absence of any peak corresponding to CO₂ or H₂ in the GC-TCD

analysis (Figure 4.14). Therefore, experimental evidence clearly suggested that during the Ru-catalyzed transformation of EG, initially, EG dehydrogenate to glycolaldehyde, which further undergoes base-catalyzed dehydrogenation to glyoxal, followed by the conversion of glyoxal to SG and further dehydrogenation of SG to SF. Alternatively, glyoxal may get partially hydrated to geminal diol in an aqueous solution, which can further undergo dehydrogenation to SG (Scheme 4.3).



Scheme 4.2. Control experiments to elucidate the reaction pathway for EG transformation to H_2 gas.



Scheme 4.3. Plausible pathway for the dehydrogenation of EG into formate.

4.3.3. Catalyst stability and recyclability

A significant quenching of the reaction was observed when the ruthenium catalyst was treated with an excess of elemental mercury prior to the catalytic EG dehydrogenation, implying the heterogeneous nature of the catalyst (Figure 4.15a). In addition, the ICP-AES of the reaction aliquot revealed no significant leaching of the ruthenium catalyst (0.17 ppm). Advantageously, the ruthenium catalyst can be recovered and recycled several times to yield 1.3 L of H₂ gas from 1.4 mL of ethylene glycol in 55 h. It was also observed that the TON/cycle was not significantly changed during the recyclability experiments (Figure 4.15b). Moreover, the bulk scale hydrogen gas production from EG could also be achieved to produce over ~1.3 L (52.6 mmol) of hydrogen gas from 2.8 mL (50 mmol) of EG in the presence of 2.1 equiv. of NaOH in 52 h at 110 °C, while with 3.5 equiv. of NaOH, 2.9 L of H₂ gas was produced in ~70 h (Figure 4.16). Notably, the P-XRD pattern and XPS profile of the recovered catalyst were found to be analogous to that of the fresh catalyst (Figure 4.17). XPS spectra of the recovered catalyst also showed prominent peaks corresponding to the binding energy of Ru(0) in the Ru 3p region, with some oxide components presumably due to aerial oxidation of the catalyst (Figure 4.17b). TEM images of the recovered catalyst showed only a minor increase in the particle size (~3 nm) of the recovered catalyst as compared to the fresh catalyst (~2.6 nm) (Figure 4.18). Therefore, these findings suggest the high robustness and long-term stability of the Ru catalyst, which resulted in achieving enhanced catalytic performance during the recyclability experiments with the productivity of 290 L H₂ per gram Ru with 1035 L of H₂ gas per L of EG from EG in water at 110 °C.

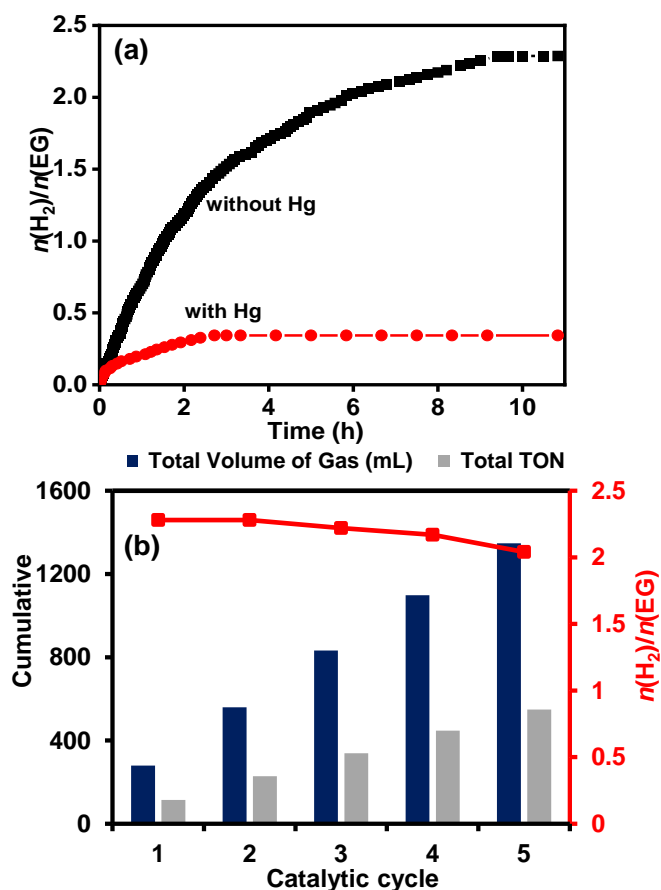


Figure 4.15. (a) Mercury poisoning test, and (b) Recyclability experiment for hydrogen production from ethylene glycol over the ruthenium catalyst. Reaction conditions: Ruthenium catalyst (0.1 mmol), EG (5 mmol), NaOH (10.5 mmol), water (20 mmol), and 110 °C.

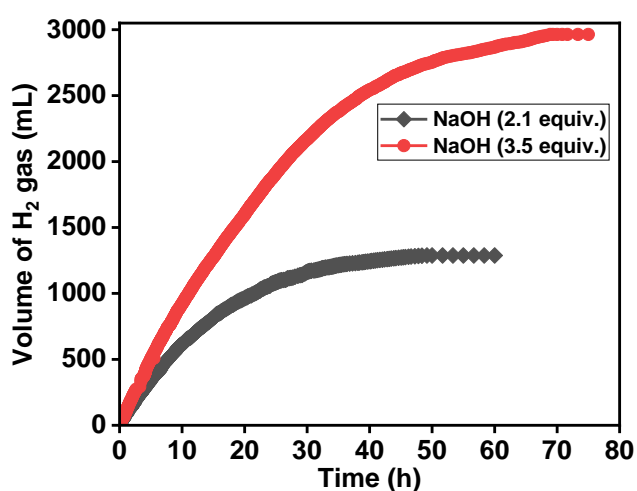


Figure 4.16. Time course plot for the bulk-scale production of hydrogen gas from EG over the ruthenium catalyst. Reaction conditions: Ruthenium catalyst (0.1 mmol), EG (50 mmol), NaOH (17.5 mmol), water (200 mmol), and 110 °C.

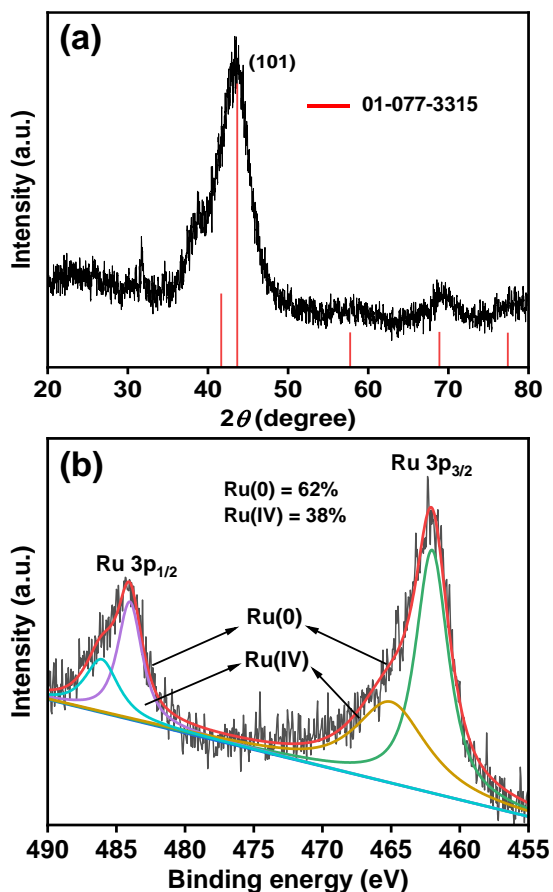


Figure 4.17. (a) P-XRD pattern, and (b) XPS spectra of the spent ruthenium catalyst.

To investigate the effect of mass transfer limitations on the dehydrogenation of EG over ruthenium catalyst, we performed reactions at different stirring rates (400, 600, and 800 rpm) and at different temperature ranges (110-160 °C) under the optimized reaction condition. As summarized in Table 4.4, results inferred that the EG conversion, product distribution, and reaction rates are not significantly changed at 600 rpm and above, suggesting that the external mass transfer limitations are not significant. These results are consistent with the previous reports.^[59-61] For instance, Lahr and Shanks reported that at the stirring speed of 500 rpm and above the catalytic activity of Ru on carbon catalysts remains unaffected for the hydrogenolysis of glycerol to glycol.^[59] Biswas et al. also showed that the catalytic activity of Cu-Ni-Al₂O₃ for the hydrogenolysis of bio-glycerol remains unaffected at 700 rpm and higher stirring speed.^[60]

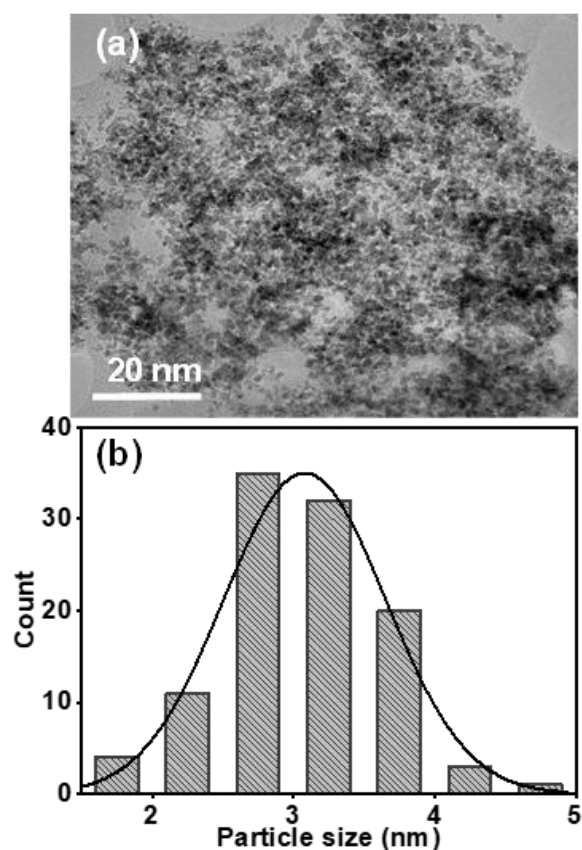


Figure 4.18. TEM image, and corresponding (b) particle size distribution curve of the spent ruthenium catalyst.

Table 4.4. Effect of stirring speed on the dehydrogenation of EG at different reaction temperatures.

Reaction Temperature	110 °C			130 °C			160 °C		
Stirring speed (rpm)	400	600	800	400	600	800	400	600	800
EG Conv. (%)	98	>99	>99	>99	>99	>99	>99	>99	>99
SF Yield (%)	47	57	58	66	64	65	67	85	87
SG Yield (%)	33	26	22	18	13	14	20	-	-
Reaction rate ($\times 10^{-2}$) (mol $g_{cat}^{-1} h^{-1}$)	5.0	5.3	5.4	7.0	8.3	8.3	15	16	16

Notably, most of the catalytic reactions for EG reforming to H₂ gas were performed at a high-temperature range (180- 400 °C) to achieve high selectivity of H₂ gas up to 99.79% (Table 4.4). Vaidya et al. explored Ru/Al₂O₃ catalyst for the steam reforming of aqueous EG to H₂ gas (conv. 13.6%, sel. of H₂ gas 36.4%) at 400°C.^[32] Noticeably, Dumesic et al. developed silica-supported metal catalysts for aqueous phase reforming of EG at 225 °C. They achieved

3.06% conversion of EG with H₂ gas sel. of 98.5% over Pd/SiO₂, while for Ru/SiO₂, they obtained 42% EG conversion with only 7% H₂ gas selectivity (7%).^[47] Bitter et al. developed Cu or Ni/CNF catalyst for the transformation of EG to GA (glycolic acid) or FA (formic acid) and H₂ at 150 °C-180 °C, where they achieved 89% conversion of EG with FA sel. of 27% and GA sel. of 31% at 150 °C in 15 h over Ni/CNF.^[26] Milstein et al. explored pincer-Ru complexes based molecular catalyst for reforming of EG in THF-water to achieve 89% conversion of EG with GA yield of 88% at 115 °C in 48 h using 5 equiv. of KOH.^[51] Mn-PNP complex was also employed for EG reforming by Maji et al. to GA and H₂ as a byproduct at 140 °C in tAmOH in 12 h, while the reaction could not occur in water.^[52] Therefore, literature reports revealed that most of the transformation of EG to H₂ gas or FA/GA were performed at high temperature (>200 °C), required organic solvents, and yield low selectivity for H₂ gas with contamination of CO₂, CO and other. In this regard, our experimental findings showed the robustness and long-term stability of the ruthenium catalyst to exhibit high catalytic activity for EG conversion to selective production of H₂ gas (better than the expensive Pd-based catalyst at a much lower reaction temperature) with the productivity of 290 L H₂ per gram of Ru with 1035 L of H₂ gas per L of EG in water at comparatively lower temperature (110-160 °C).

4.4. Conclusions

We developed a highly efficient catalytic system based on the ruthenium catalyst for selective hydrogen production from ethylene glycol (EG) in water at 90-160 °C. We could achieve hydrogen gas yield as high as 3.0 equivalent per EG and 85% yield of SF with complete conversion of EG over the ruthenium catalyst. Results inferred the crucial role of the base and the reaction temperature in achieving high activity. Advantageously, the developed ruthenium catalyzed catalytic system also performed well at bulk scale hydrogen production from EG (290 L H₂/g of Ru and 1035 L H₂/L of EG in ~70 h at 110 °C). Therefore, we believe, on further development, our developed ruthenium catalyzed hydrogen production from EG might find application for large-scale selective H₂ production using aqueous ethylene glycol at relatively low-temperature range.

Note: The content of this chapter is published as Kumar et al., ACS Sustain. Chem. Eng., 11, 3999-4008 (DOI:10.1021/acssuschemeng.2c04521) and reproduced with the permission from the American Chemical Society.

4.5. References

1. Midilli A., Ay M., Dincer I., Rosen M. A. (2005), On Hydrogen and Hydrogen Energy Strategies I: Current Status and Needs, *Renew. Sustain. Energy Rev.*, 9, 255–271 (DOI: 10.1016/j.rser.2004.05.003)
2. Balat M. (2008), Potential Importance of Hydrogen as a Future Solution to Environmental and Transportation Problems, *Int. J. Hydrog. Energy*, 33, 4013–4029 (DOI: 10.1016/j.ijhydene.2008.05.047)
3. Bockris J. O. M. (2013), The Hydrogen Economy: Its History, *Int. J. Hydrog. Energy*, 38, 2579–2588 (DOI: 10.1016/j.ijhydene.2012.12.026)
4. Singh S., Jain S., Ps V., Tiwari A. K., Nouni M. R., Pandey J. K., Goel S. (2015), Hydrogen: A Sustainable Fuel for Future of the Transport Sector, *Renew. Sustain. Energy Rev.* 51, 623–633 (DOI: 10.1016/j.rser.2015.06.040)
5. Barreto L., Makihira A., Riahi K. (2003), The Hydrogen Economy in the 21st Century: A Sustainable Development Scenario, *Int. J. Hydrog. Energy*, 28, 267–284 (DOI: 10.1016/s0360-3199(02)00074-5)
6. Mueller-Langer F., Tzimas E., Kaltschmitt M., Peteves S. (2007), Techno-Economic Assessment of Hydrogen Production Processes for the Hydrogen Economy for the Short and Medium Term, *Int. J. Hydrog. Energy*, 32, 3797–3810 (DOI: 10.1016/j.ijhydene.2007.05.027)
7. Ramachandran R., Menon R. K. (1998), An Overview of Industrial Uses of Hydrogen, *Int. J. Hydrog. Energy*, 23, 593–598 (DOI: 10.1016/s0360-3199(97)001212-2)
8. Lattin W. C., Utgikar V. P. (2007), Transition to Hydrogen Economy in the United States: A 2006 Status Report, *Int. J. Hydrog. Energy*, 32, 3230–3237 (DOI: 10.1016/j.ijhydene.2007.02.004)
9. Richards M., Shenoy A. (2007), H₂-Mhr Pre-Conceptual Design Summary for Hydrogen Production, *Nucl. Eng. Technol.*, 39, 1–8 (DOI: 10.5516/net.2009.39.1.001)

10. Chen L., Qi Z., Zhang S., Su J., Somorjai G. A. (2020), Catalytic Hydrogen Production from Methane: A Review on Recent Progress and Prospect, *Catalysts*, 10, 858–875 (DOI: 10.3390/catal10080858)
11. Fasolini A., Cucciniello R., Paone E., Mauriello F., Tabanelli T. (2019), A Short Overview on the Hydrogen Production via Aqueous Phase Reforming (APR) of Cellulose, C6-C5 Sugars and Polyols, *Catalysts*, 9, 1–17 (DOI: 10.3390/catal9110917)
12. Mei D., Lebarbier Dagle V., Xing R., Albrecht K. O., Dagle R. A. (2016), Steam Reforming of Ethylene Glycol over MgAl₂O₄ Supported Rh, Ni, and Co Catalysts, 6, 315–325 (DOI: 10.1021/acscatal.5b01666)
13. Palo D. R., Dagle R. A., Holladay J. D. (2007), Methanol Steam Reforming for Hydrogen Production, *Chem. Rev.*, 107, 3992–4021 (DOI: 10.1021/cr050198b)
14. Nielsen M., Alberico E., Baumann W., Drexler H. J., Jung, H., Gladial, S., Beller M. (2013), Low-Temperature Aqueous-Phase Methanol Dehydrogenation to Hydrogen and Carbon Dioxide, *Nature*, 495, 85–89 (DOI: 10.1038/nature11891)
15. Lin L., Zhou W., Gao R., Yao S., Zhang X., Xu W., Zheng S., Jiang Z., Yu Q., Li Y. W., Shi C., Wen X. D., Ma D. (2017), Low-Temperature Hydrogen Production from Water and Methanol Using Pt/ α -MoC Catalysts, *Nature*, 544, 80–83 (DOI: 10.1038/naturee21672)
16. Awasthi M. K., Rai R. K., Behrens S., Singh S. K. (2021), Low-Temperature Hydrogen Production from Methanol over a Ruthenium Catalyst in Water, *Catal. Sci. Technol.*, 11, 136–142 (DOI: 10.1039/d0cy01470b)
17. Mellmann D., Sponholz P., Junge H., Beller M. (2016), Formic Acid as a Hydrogen Storage Material-Development of Homogeneous Catalysts for Selective Hydrogen Release, *Chem. Soc. Rev.*, 45, 3954–3988 (DOI: 10.1039/c5cs00618)
18. Boddien A., Mellmann D., Gärtner F., Jackstell R., Junge H., Dyson P. J., Laurency G., Ludwig R., Beller M. (2011), Efficient Dehydrogenation of Formic Acid Using an Iron Catalyst, *Science*, 333, 1733–1736 (DOI: 10.1126/science.1206613)
19. Hull J. F., Himeda Y., Wang W. H., Hashiguchi B., Periana R., Szalda

- D. J., Muckerman J. T., Fujita E. (2012), Reversible Hydrogen Storage Using CO₂ and a Proton-Switchable Iridium Catalyst in Aqueous Media under Mild Temperatures and Pressures, *Nat. Chem.*, 4, 383–388 (DOI: 10.1038/nchem.1295)
20. Patra S., Singh S. K. (2020), Hydrogen Production from Formic Acid and Formaldehyde over Ruthenium Catalysts in Water, *Inorg. Chem.*, 59, 4234–4243 (DOI: 10.1021/acs.inorgchem.9b0882)
21. Patra S., Deka H., Singh S. K. (2021), Bis-Imidazole Methane Ligated Ruthenium (II) Complexes: Synthesis, Characterization, and Catalytic Activity for Hydrogen Production from Formic Acid in Water, *Inorg. Chem.*, 60, 14275–14285 (DOI: 10.1021/acs.inorgchem.1c01784)
22. Yuranov I., Autissier N., Sordakis K., Dalebrook A. F., Grasemann M., Orava V., Cendula P., Gubler L. (2018), Heterogeneous Catalytic Reactor for Hydrogen Production from Formic Acid and Its Use in Polymer Electrolyte Fuel Cells, *ACS Sustainable Chem. Eng.*, 6, 6635–6643 (DOI:10.1021/acssuschemeng.8b00423)
23. Heim L. E., Schlörer N. E., Choi J. H., Pechtl M. H. G. (2014), Selective and Mild Hydrogen Production Using Water and Formaldehyde, *Nat. Commun.*, 5, 1–8 (DOI: 10.1038/ncomms4621)
24. Trincado M., Sinha V., Rodriguez-Lugo R. E., Pribanic B., De Bruin B., Grützmacher H. (2017) Homogeneously Catalysed Conversion of Aqueous Formaldehyde to H₂ and Carbonate, *Nat. Commun.*, 8, 1–11 (DOI: 10.1038/ncomms4990)
25. Patra S., Kumar A., Singh S. K. (2022), Hydrogen Production from Formaldehyde and Paraformaldehyde in Water under Additive-Free Conditions: Catalytic Reactions and Mechanistic Insights, *Inorg. Chem.*, 61, 4618–4626 (DOI: 10.1021/acs.inorgchem.1c03529)
26. Van Haasterecht T., Van Deelen T. W., De Jong K. P., Bitter J. H. (2017), Transformations of Polyols to Organic Acids and Hydrogen in Aqueous Alkaline Media, *Catal. Sci. Technol.*, 4, 2353–2366 (DOI: 10.1039/c4cy00249k)
27. Kumar A., Awasthi M. K., Priya B., Singh S. K. (2022), Selective Hydrogen Production from Glycerol over Ruthenium Catalyst, *ChemCatChem*, 14, 1–10 (DOI: 10.1002/cctc.202101951)

28. Gogoi P., Nagpure A. S., Kandasamy P., Satyanarayana C. V. V., Raja T. (2020), Insights into the Catalytic Activity of Ru/NaY Catalysts for Efficient H₂ Production through Aqueous Phase Reforming, *Sustain. Energy Fuels*, 4, 678–690 (DOI: 10.1039/c9se00797k)
29. Pang J., Zheng M., Sun R., Wang A., Wang X., Zhang T. (2016), Synthesis of Ethylene Glycol and Terephthalic Acid from Biomass for Producing PET, *Green Chem.*, 18, 342–359 (DOI: 10.1039/c5gc01771h)
30. Yue H., Zhao Y., Ma X., Gong J. (2012), Ethylene Glycol: Properties, Synthesis, and Applications, *Chem. Soc. Rev.*, 41, 4218–4244 (DOI: 10.1039/c2cs153599)
31. Genta M., Iwaya T., Sasaki M., Goto M., Hirose T. (2005), Depolymerization Mechanism of Poly(Ethylene Terephthalate) in Supercritical Methanol, *Ind. Eng. Chem. Res.*, 44, 3894–3900 (DOI: 10.1021/ie0488187)
32. Sundari R., Vaidya P. D. (2015), On the Efficacy of Ru/Al₂O₃ Catalyst for Steam Reforming of Ethylene Glycol, *Chem. Eng. Commun.*, 202, 1446–1454 (DOI: 10.1080/00986445.2014.934446)
33. Zhao X. L., Lü Y. A., Liao W. P., Jin M. S., Suo Z. H. (2015), Hydrogen Production from Steam Reforming of Ethylene Glycol over Supported Nickel Catalysts, *J. Fuel Chem. Technol.*, 43, 581–588 (DOI: 10.1016/s1872-5813(15)30017-7)
34. Kiadehi A. D., Taghizadeh M. (2018), Evaluation of a Micro-Channel Reactor for Steam Reforming of Ethylene Glycol: A Comparative Study of Catalytic Activity of Pt or/and Ni Supported γ -Alumina Catalysts, *Int. J. Hydrog. Energy*, 43, 4826–4838 (DOI: 10.1016/j.ijhydene.2018.01.103)
35. Larimi A., Khorasheh F. (2018), Renewable Hydrogen Production by Ethylene Glycol Steam Reforming over Al₂O₃ Supported Ni-Pt Bimetallic Nano-Catalysts, *Renew. Energy*, 128, 188–199 (DOI: 10.1016/j.renene.2018.05.070)
36. Shejale A. D., Yadav G. D. (2021), Sustainable and Selective Hydrogen Production by Steam Reforming of Bio-Based Ethylene Glycol: Design and Development of Ni–Cu/Mixed Metal Oxides Using M (CeO₂,

- La₂O₃, ZrO₂)–MgO Mixed Oxides, *Int. J. Hydrog. Energy*, 46, 4808–4826 (DOI: 10.1016/j.ijhydene.2019.11.031)
37. Wang Y., Chen M., Li X., Yang Z., Liang T., Zhou Z., Cao Y. (2018), Hydrogen Production via Steam Reforming of Ethylene Glycol over Attapulgite Supported Nickel Catalysts, *Int. J. Hydrog. Energy*, 43, 20438–20450 (DOI: 10.1016/j.ijhydene.2018.09.109)
38. Chen G., Xu N., Li X., Liu Q., Yang H., Li W. (2015), Hydrogen Production by Aqueous-Phase Reforming of Ethylene Glycol over a Ni/Zn/Al Derived Hydrotalcite Catalyst, *RSC Adv.*, 5, 60128–60134 (DOI: 10.1039/c5ra07184d)
39. Zhang J. N. X. (2020), Hydrogen Production from Ethylene Glycol Aqueous, *Catalysts*, 10, 54–64 (DOI:10.3390/catal10010054)
40. Chu X., Liu J., Sun B., Dai R., Pei Y., Qiao M., Fan K. (2011), Aqueous-Phase Reforming of Ethylene Glycol on Co/ZnO Catalysts Prepared by the Coprecipitation Method, *J. Mol. Catal. A Chem.*, 335, 129–135 (DOI: 10.1016/j.molcata.2010.11.024)
41. Cesar D. V., Santori G. F., Pompeo F., Baldanza M. A., Henriques C. A., Lombardo E., Schmal M., Cornaglia L., Nichio N. N. (2016), Hydrogen Production from Ethylene Glycol Reforming Catalyzed by Ni and Ni–Pt Hydrotalcite-Derived Catalysts, *Int. J. Hydrog. Energy*, 41, 22000–22008 (DOI: 10.1016/j.ijhydene.2016.07.168)
42. Tao J., Hou L., Yan B., Chen G., Li W., Chen H., Cheng Z., Lin F. (2020), Hydrogen Production via Aqueous-Phase Reforming of Ethylene Glycol over a Nickel-Iron Alloy Catalyst: Effect of Cobalt Addition, *Energy and Fuels*, 34, 1153–1161 (DOI: 10.1021/acs.energyfuels.9b02149)
43. Jeon S., Park Y. M., Saravanan K., Han G. Y., Kim B. W., Lee J. B., Bae J. W. (Aqueous Phase Reforming of Ethylene Glycol over Bimetallic Platinum-Cobalt on Ceria–Zirconia Mixed Oxide, *Int. J. Hydrog. Energy*, 42, 9892–9902 (DOI: 10.1016/j.ijhydene.2017.01.221)
44. Van Haasterecht T., Ludding C. C. I., De Jong K. P., Bitter J. H. (2013), Stability and Activity of Carbon Nanofiber-Supported Catalysts in the Aqueous Phase Reforming of Ethylene Glycol, *J. Energy Chem.*, 22,

257–269 (DOI: 10.1016/s2095-4956(13)60032-7)

45. Cortright R. D., Davda R. R., Dumesic J. A. (2002), Hydrogen from Catalytic Reforming of Biomass-Derived Hydrocarbons in Liquid Water, *Nature*, 418, 964–967 (DOI: 10.1038/nature01009)
46. Kim H. D., Park H. J., Kim T. W., Jeong K. E., Chae H. J., Jeong S. Y., Lee C. H., Kim C. U. (2012), Hydrogen Production through the Aqueous Phase Reforming of Ethylene Glycol over Supported Pt-Based Bimetallic Catalysts, *Int. J. Hydrog. Energy*, 37, 8310–8317 (DOI: 10.1016/j.ijhydene.2012.02.160)
47. Davda R. R., Shabaker J. W., Huber G. W., Cortright R. D., Dumesic J. A. (2003), Aqueous-Phase Reforming of Ethylene Glycol on Silica-Supported Metal Catalysts, *Appl. Catal. B Environ.*, 43, 13–26 (DOI: 10.1016/s0926-3373(02)00277-1)
48. Huber G. W., Shabaker J. W., Dumesic J. A. (2003), Raney Ni-Sn Catalyst for H₂ Production from Biomass-Derived Hydrocarbons, *Science*, 300, 2075–2077 (DOI: 10.1126/science.1085597)
49. Morton D., Cole-Hamilton D. J. (1988), Molecular Hydrogen Complexes in Catalysis: Highly Efficient Hydrogen Production from Alcoholic Substrates Catalysed by Ruthenium Complexes, *J. Chem. Soc. Chem. Commun.*, 2, 1154–1156 (DOI: 10.1039/c39880001154)
50. Li Y., Nielsen M., Li B., Dixneuf P. H., Junge H., Beller M. (2015), Ruthenium-Catalyzed Hydrogen Generation from Glycerol and Selective Synthesis of Lactic Acid, *Green Chem.*, 17, 193–198 (DOI: 10.1039/c4gc01707b)
51. Zhan Y., Hou W., Li G., Shen Y., Zhang Y., Tang Y. (2019), Oxidant-Free Transformation of Ethylene Glycol toward Glycolic Acid in Water, *ACS Sustain. Chem. Eng.*, 7, 17559–17564 (DOI: 10.1021/acssuschemeng.9b04617)
52. Zou Y. Q., von Wolff N., Rauch M., Feller M., Zhou, Q. Q., Anaby, A., Diskin-Posner Y., Shimon L. J. W.; Avram L., Ben-David Y., Milstein D. (2021), Homogeneous Reforming of Aqueous Ethylene Glycol to Glycolic Acid and Pure Hydrogen Catalyzed by Pincer-Ruthenium Complexes Capable of Metal–Ligand Cooperation, *Chem. A Eur. J.*, 27, 4715–4722 (DOI: 10.1002/chem.202005450)

53. Waiba S., Maiti M., Maji B. (2022), Manganese-Catalyzed Reformation of Vicinal Glycols to α -Hydroxy Carboxylic Acids with the Liberation of Hydrogen Gas, *ACS Catal.*, 12, 3995–4001 (DOI:10.1021/acscatal.1c05844)
54. Rai R. K., Gupta K., Behrens S., Li J., Xu Q., Singh S. K. (2015), Highly active bimetallic nickel–palladium alloy nanoparticle catalyzed Suzuki–Miyaura reactions, *ChemCatChem*, 7, 1806–1812 (DOI: 10.1002/cctc.201500145)
55. Dwivedi A. D., Rai R. K., Gupta K., Singh S. K. (2017), Catalytic Hydrogenation of Arenes in Water Over in Situ Generated Ruthenium Nanoparticles Immobilized on Carbon, *ChemCatChem*, 9, 1930–1938 (DOI: 10.1002/cctc.201700056)
56. Morgan D. J. (2015), Resolving Ruthenium: XPS Studies of Common Ruthenium Materials, *Surf. Interface Anal.*, 47, 1072–1079 (DOI: 10.1002/sia.5852)
57. Ma Z., Zhao S., Pei X., Xiong X., Hu B. (2017), New insights into the support morphology-dependent ammonia synthesis activity of Ru/CeO₂ catalysts, *Catal. Sci. Technol.*, 191–199 (DOI: 10.1039/c6cy02089e)
58. Zhang G., Jin X., Guan Y., Yin B., Chen X., Liu Y., Feng X., Shan H., Yang C. (2019), Toward Selective Dehydrogenation of Glycerol to Lactic Acid over Bimetallic Pt-Co/CeO_x Catalysts, *Ind. Eng. Chem. Res.*, 58, 14548–14558 (DOI: 10.1021/acs.iecr.9b01918)
59. Lahr D. G., Shanks B. H. (2003), Kinetic Analysis of the Hydrogenolysis of Lower Polyhydric Alcohols: Glycerol to Glycols, *Ind. Eng. Chem. Res.*, 42, 5467–5472 (DOI: 10.1021/ie030468l)
60. Mondal S., Malviya H., Biswas P. (2019), Kinetic Modelling for the Hydrogenolysis of Bio-Glycerol in the Presence of a Highly Selective Cu-Ni-Al₂O₃ Catalyst in a Slurry Reactor, *React. Chem. Eng.*, 4, 595–609 (DOI: 10.1039/c8re00138c)
61. Yfanti V. L., Ipsakis D., Lemonidou A. A. (2018), Kinetic Study of Liquid Phase Glycerol Hydrodeoxygenation under Inert Conditions over a Cu-Based Catalyst, *React. Chem. Eng.*, 3, 559–571 (DOI: 10.1039/c8re00061a)

Chapter 5

Hydrogen Production from Ethylene Glycol through Upcycling of PET-based Plastics Waste over Ruthenium Catalyst in Water

5.1. Introduction

The low cost, high durability, and light weight of plastic materials, such as polyethylene terephthalate (PET), make it one of the favorite materials for wide application in almost all sectors. No wonder the worldwide consumption of PET has grown by over 24 million metric tons in 2022.^[1] Unfortunately, efficient and sustainable recycling strategies still need to be effectively placed, resulting in a huge portion of PET-based plastic waste going into landfills, negatively impacting the climate and soil health.^[2,3] Though high-temperature treatment of PET is being used as a recycling process, it leads only to low-grade PET. On the other hand, biological and chemical pathways for PET degradation/depolymerization to its primary components, terephthalic acid (TPA) and ethylene glycol (EG), enable the facile recycling and regeneration of PET.^[4,5] Notably, hydrogenolysis, hydrodeoxygenation, methanolysis, aminolysis, glycolysis and hydrolysis are a few of the popular chemical approaches for PET depolymerization.^[6-9] Hydrogenolysis and hydrodeoxygenation require higher pressure of H₂ gas for the upgradation of PET into value-added chemicals.^[6] For instance, Robertson et al. utilized a Ru-PNN-based pincer catalyst for hydrogenative depolymerization of PET at 160 °C in anisole:THF (1:1) in the presence of KOtBu under 54.4 atm of H₂ and obtained ethylene glycol (EG) and 1,4-benzene dimethanol in good yields.^[10] Klankermeyer et al. explored Ru-triphos catalyst for hydrogenolysis of PET using 1,4-dioxane as a solvent at 140 °C and 100 bar H₂ and achieved 42% conversion of PET in 16 h with a selectivity of 64% for both.^[11] Marks et al. reported a heterogeneous C/MoO₂ catalyst for solventless hydrogenolysis of PET to TPA (85% yield) and EG at 260 °C under atmospheric H₂ in 24 h.^[12] Results inferred that Mo has low activity towards the hydrogen activation, but it selectively cleaves the ester groups of PET, resulting in the formation of TPA.

By incorporating Co atoms (CoMo@NC), which aid in hydrogen activation, Cai et al. improved the performance of the Mo catalyst investigated by Marks et al. and observed an increase in the catalytic activity for hydrogenolysis of PET to TPA (91% yield) under 1 atm H₂ at 260 °C in 10 h.^[13] In a similar direction, Farha et al. also explored PET depolymerization over UiO-66 at 260 °C under 1 atm H₂ to obtain 98% yield of TPA along with monomethyl terephthalate in 24 h.^[14] Yan et al. utilized Ru/Nb₂O₅ for hydrodeoxygenation of PET to aromatics (xylene, benzene and ethyl benzene) at 280 °C and 50 bar H₂ in water.^[15] Qi et al. achieved depolymerization of PET via glycolysis to bis(hydroxyethyl)terephthalate (BHET) using EG as a solvent over ZIF-8 at 197 °C in 1.5 h.^[8] Alkaline hydrolysis can also serve as an alternative process for depolymerization of PET to TPA and EG.^[16-21] In this regard, Achilias et al. used aqueous NaOH for the upcycling of PET at 200 °C and obtained the disodium terephthalate (98% yield) and EG.^[18] Petrossian et al. explored the alkaline depolymerization of mixed PET waste and obtained TPA using NaOH (20-30%) in ethylene glycol at 110 °C in 4 h.^[19] Similarly, Meester et al. performed basic hydrolysis of PET using 5-15 wt% NaOH in an ethanol-water mixture under mild reaction conditions (<80 °C).^[20] Notably, pure TPA can be obtained after the reaction completion from the aqueous solution by adjusting the pH, whereas the separation of EG from the aqueous phase is difficult due to its high boiling point (197 °C). EG is a value-added chemical and can serve as hydrogen storage material as it contains up to 6.5 wt% of H₂.^[22] Hydrogen production from EG has been widely explored through reforming process (aqueous phase and steam reforming) over various catalysts such as Ru/Al₂O₃,^[23] Pt/ γ -Al₂O₃,^[24] Rh/MgAl₂O₄,^[25] Pt-Co/CeO₂-ZrO₂,^[26] Ni-Pt/HT^[27] and others. Aqueous phase reforming (APR) is getting a lot of attention under relatively lower temperatures (175-265 °C) as compared to the steam reforming process (>500 °C). Hydrolysis of PET requires a high temperature (180-240 °C), which is consistent with the temperature needed for the APR. Thus, efforts are being made to utilize PET in one-pot to produce high yield of H₂ and valuable chemicals at relatively lower temperatures. For instance, Uekert et al. performed hydrolysis of PET in 10 M NaOH followed by catalytic photo reforming over CdS/CdO_x with the H₂ yield of 0.238 mol/kg_{PET}.^[28] Similarly, Gong et al. explored CN-CNT-NiMo catalyst for

photocatalytic hydrogen production from PET hydrolysis at 70 °C in the presence of 5 M KOH.^[29] Mondal et al. demonstrated the electrocatalytic transformation of PET hydrolysate to formate over a Co-based coordination polymer with the coproduction of hydrogen gas.^[30] Recently, Wang et al. reported the aqueous-phase reforming (APR) of PET waste at 200-250 °C for H₂ production over Ru-ZnO catalyst supported on mesoporous carbon (Ru-ZnO/MEC).^[31] They observed the improvement in the H₂ yield on increasing the loading of ZnO (0-5 wt%) in the Ru/MEC catalysts and achieved a high H₂ yield of ~20 mmol/g_{PET} at 250 °C over Ru-5ZnO/MEC catalyst by APR of EG to H₂ along with CO and CO₂. Notably, the observed high yield of H₂ (19.97 mol/kg_{PET}) at 250 °C over Ru-5ZnO/MEC catalyst was only because of the catalytic APR of EG, while at 210 °C the H₂ yield was only ~2.5 mmol/g_{PET} with H₂ selectivity of 72% along with CO₂ (~23%) and other carbon contaminations. It is, therefore, evident that the key challenge in PET upcycling is to integrate the PET depolymerization with the efficient production of hydrogen gas in a one-pot process by (i) avoiding undesirable hydrogenation of aromatics (TPA) and (ii) achieving high selectivity for H₂ gas without any contamination of CO, CO₂, and other alkanes.

Herein, we employed an integrated approach for the complete one-pot depolymerization of PET-based plastic waste with selective production of hydrogen gas with quantitative yield over the ruthenium catalyst (unsupported catalyst) in water (in the absence of any organic solvent) with a high yield of terephthalic acid (TPA). The quantitative yield of H₂ gas from PET-based plastic waste was achieved over the ruthenium catalyst in a temperature range of 110-160 °C. Moreover, the ruthenium catalyst showed high stability with appreciably high recyclable performance for bulk-scale production of hydrogen gas from PET-based plastic waste.

5.2. Experimental section

5.2.1. Materials and instrumentation

High-purity chemicals and metal salts were purchased from Sigma-Aldrich, Alfa-Aesar and used without further purification. All the catalytic reactions were performed under inert conditions using high-purity argon gas purchased from Inox Air Products Ltd., India. NMR spectra were recorded in deuterated

solvents using AVANCE NEO Ascend 500 Bruker spectrometer (500 MHz). Chemical shifts were referenced to the internal solvent resonances and were reported relative to tetramethylsilane. Transmission electron microscopy (TEM) images of the samples were obtained on a TECNAI G2 Spirit Twin microscope by operating it at the accelerating voltage of 120 kV. The samples for TEM analysis were prepared by the drop-costing method. Briefly, ruthenium nanoparticles were dispersed in ethanol under ultra-sonication for 1 hour, and then highly dispersed particles were spread onto a carbon-coated Cu grid and dried at room temperature. Particle size was calculated using ImageJ software for at least 50-100 particles, and the average particle size distribution curve was plotted using Origin software. Scanning electron microscopic (SEM) images and elemental mapping data were collected using a JOEL-7610F plus equipped with an EDS detector. Powder X-ray diffraction (P-XRD) measurements were performed using a Rigaku SmartLab Automated Multipurpose X-ray diffractometer with a scintillation detector. The measurements were conducted using Cu K α radiation ($\lambda = 1.5418 \text{ \AA}$) with a step size of 0.02° in the 2θ range of $20\text{-}80^\circ$. The exposure time for each P-XRD measurement was 20 minutes. FT-IR (Bruker) double-beam spectrometer coupled with attenuated total reflection (ATR) facility was used to determine the chemical functional groups present in the sample in the wave number range ($4000\text{-}400 \text{ cm}^{-1}$). TGA analysis was performed by heating the sample under N₂ flow from $25\text{-}800 \text{ }^\circ\text{C}$ with a ramp rate of $20 \text{ }^\circ\text{C}$ per minute using a Mettler-Toledo TGA/DSC 1 STARe System. X-ray photoelectron spectroscopy (XPS) was performed using Omicron ESCA (Electron Spectroscopy for Chemical Analysis), Oxford Instrument, Germany. Aluminium (Al) anode was used as a monochromatic X-ray source (1486.7 eV) for XPS measurements. The binding energy values were charge-corrected to the C 1s signal (284.6 eV). The gas chromatography (GC) analyses were performed on a Shimadzu GC-2014 system using a shin carbon-ST packed column with a thermal conductivity detector (TCD) using argon as a carrier gas. Parameters were set for the program to detect H₂, CO₂, CO, and CH₄ gas (detector temperature: $200 \text{ }^\circ\text{C}$, and oven temperature program: $90 \text{ }^\circ\text{C}$ (hold time: 1 min), $90\text{-}200 \text{ }^\circ\text{C}$ (rate: $15 \text{ }^\circ\text{C}$ per minute)).

5.2.2. Synthesis of the ruthenium catalyst

Typically, ruthenium (III) chloride (0.1 mmol) and CTAB (50 mg) dissolved in water (5 mL) were added dropwise to an aqueous solution of sodium borohydride (25 mg in 5 mL water) to obtain a black suspension of ruthenium nanoparticles. The content of the flask was sonicated for 10 minutes at room temperature to obtain ruthenium catalyst as black suspension. ruthenium catalyst was collected by centrifugation, washed several times with distilled water, and then dried under vacuum and further used for catalytic reactions.

5.2.3. Catalytic reaction for one-pot depolarization and dehydrogenation of PET

In a two-necked reaction vessel (10 mL) fitted with a condenser and water displacement setup, a specified amount of the as-synthesized ruthenium catalyst was suspended in water (2 mL) in the presence of a specified amount of PET flakes and base. The reaction mixture was stirred in an oil bath at 110-160 °C under the argon atmosphere. The amount of H₂ gas evolved was measured with a water displacement set up using a burette. The burette capacity in mL/cm was calibrated (thrice using water) as 4.0 ± 0.1 mL/cm. The evolved gas was analyzed using gas chromatography-thermal conductivity detector (GC-TCD). After completion of the reaction, the catalyst was recovered from the reaction mixture by centrifugation at 6500 rpm for 5 minutes. The conversion of PET flakes and the formation of other organic products were estimated by ¹H and ¹³C NMR of the reaction mixture. To isolate pure white solid TPA (free from sodium salt), an excess of HCl was added to the reaction aliquot (obtained after one pot catalytic depolymerization and dehydrogenation) to yield a white precipitate. The obtained precipitate was collected by centrifugation, washed with distilled water to remove excess acid, and dried at 60 °C for 12 h. The yields of the products (Na₂TPA, EG, SF, and SG) were determined from ¹H NMR using sodium acetate as an internal standard.

5.2.4. Recyclability experiment

Typically, the reaction was performed using *t*-PET (0.192 g) over the as-synthesized ruthenium catalyst (0.1 mmol) in water (2 mL) at 120 °C (with 12 M NaOH) and 160 °C (with 8 M NaOH) under the optimized reaction condition.

For the subsequent catalytic runs, the ruthenium catalyst was separated from the reaction mixture by centrifugation and was re-used for subsequent catalytic runs. The progress of the reaction was monitored by measuring the evolved H₂ gas by the water displacement method and analyzing the released gaseous products by GC-TCD. Organic products formed during the reaction were analyzed by NMR.

5.2.5. Bulk scale reaction

Typically, the reaction was performed using *t*-PET (1.0 g) over the as-synthesized ruthenium catalyst (0.1 mmol) in water (10 mL) at 120 °C (with 12 M NaOH) and 160 °C (with 8 M NaOH) under the optimized reaction condition. The progress of the reaction was monitored by measuring the evolved H₂ gas by the water displacement method and analyzing the released gaseous products by GC-TCD. Organic products formed during the reaction were analyzed by NMR.

5.2.6. Mercury poisoning experiment

Typically, an aqueous suspension (2 mL) of ruthenium catalyst (0.1 mmol) was stirred with a large excess (0.3 g) of elemental mercury (Hg) at room temperature for 3 h prior to the catalytic reaction. Further, *t*-PET (0.192 g), and NaOH (24 mmol) were added to the reaction vessel fitted with a condenser and gas burette, and the reaction mixture was stirred at 120 °C in an oil bath, and the progress of the reaction was monitored.

5.2.7. Gas composition analysis

The identification of gaseous products during the dehydrogenation of PET was confirmed as H₂ and with no detectable level of CO, CO₂, and CH₄ using a Shimadzu GC-2014 system. The chromatograph was equipped with a shin carbon-ST packed column with a thermal conductivity detector (TCD) using argon as a carrier gas. Parameters were set for the program to detect H₂, CO₂, CO, and CH₄ (detector temperature, 200 °C; oven temperature program, 90 °C (hold time: 1 min), 90-200 °C (rate: 15 °C per minute)).

5.3. Results and discussion

5.3.1. Synthesis and characterization of the ruthenium catalyst

Ruthenium catalyst was prepared by aqueous phase reduction of an aqueous solution of ruthenium(III) chloride using sodium borohydride (NaBH_4) using cetyltrimethylammonium bromide (CTAB) as a stabilizer. The P-XRD pattern of the fresh ruthenium catalyst showed a prominent peak at 2θ value of 44° for Ru (101) (Figure 5.1a). Further, transmission electron microscopy (TEM) of the ruthenium catalyst inferred the presence of Ru nanoparticles with an average particle size of ~ 3 nm (Figure 5.1b-c). X-ray photoelectron spectroscopy (XPS) of the ruthenium catalyst displayed the well-resolved peaks at 462.3 eV (Ru $3p_{3/2}$) and 484.6 eV (Ru $3p_{1/2}$), corresponding to Ru(0) state of the Ru nanoparticles (Figure 5.1d). Small XPS peaks at 465.2 eV and 487.8 eV correspond to the Ru(IV), presumably for the partial oxide layer formed over the surface due to aerial oxidation. Scanning electron microscopy and EDS of the ruthenium catalyst also confirms the presence of Ru element (Figure 5.2).

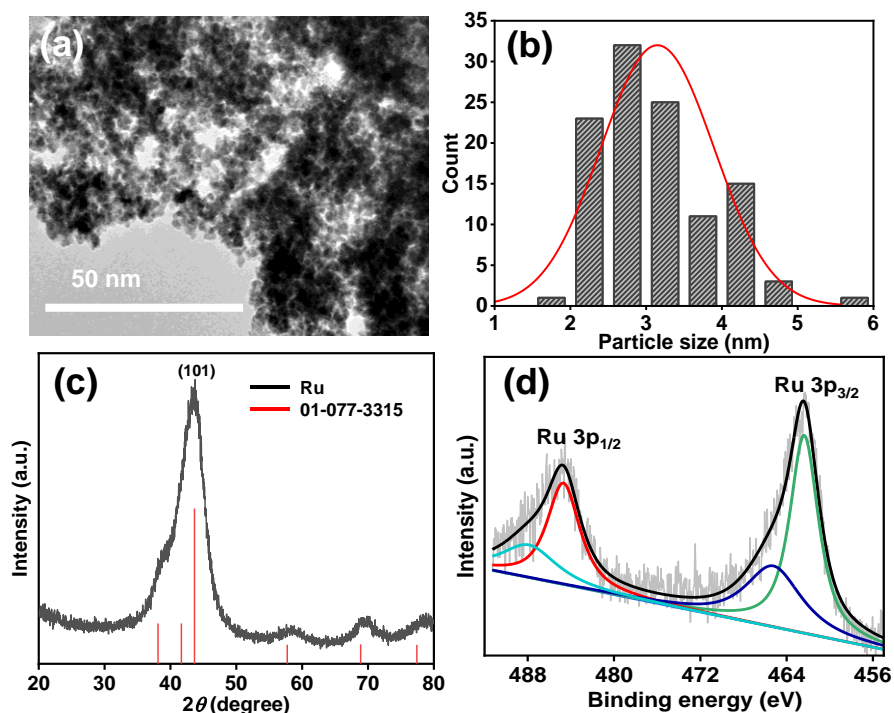


Figure 5.1. (a) TEM image, (b) the corresponding particle size distribution curve, (c) P-XRD pattern, and (d) the XPS spectra of the fresh ruthenium catalyst.

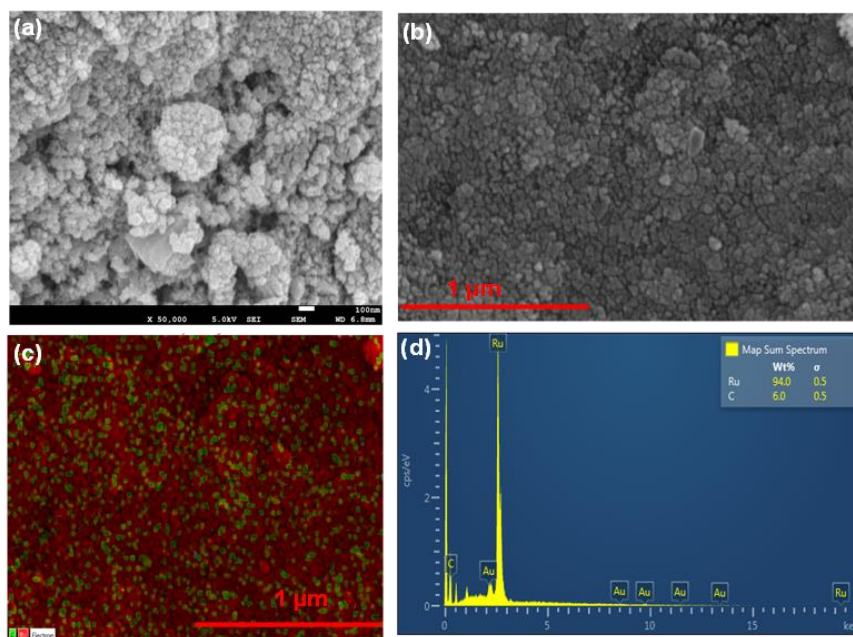


Figure 5.2. (a-b) SEM images, (c) corresponding elemental mapping, and (d) EDX spectra of fresh ruthenium catalyst.

5.3.2. Catalytic one-pot depolarization and dehydrogenation of PET-based plastic waste

Firstly, we conducted the transformation of PET flakes (obtained from waste transparent PET (*t*-PET) beverage bottles and food packets) in water over a pre-synthesized ruthenium catalyst (see experimental section) at 110 °C in the presence of NaOH (12 M), where 10.6 mmol/g_{PET} of gas was observed in 6 h (Table 5.1, entry 1). Notably, in the absence of ruthenium catalyst, the complete depolymerization of PET with a quantitative yield of Na₂TPA (5.2 mmol/g_{PET}) can also be achieved at 110 °C in 4 h in the presence of 12 M NaOH (Table 5.1, entry 2), which is milder as compared to the previous reports.^[8,10,11,14,15] The reaction duration for the complete depolymerization of PET can be significantly reduced to 1.5 h by performing the reaction at 120 °C (Table 5.1, entry 3 and Figure 5.3). ¹H NMR analysis of the reaction solution confirms the complete depolymerization of PET with the formation of Na₂TPA and EG in an equimolar ratio (Table 1, entry 2-3), where terephthalic acid (TPA) (>99% yield, 5.2 mmol/g_{PET}) was isolated as a white solid. (See experimental section).

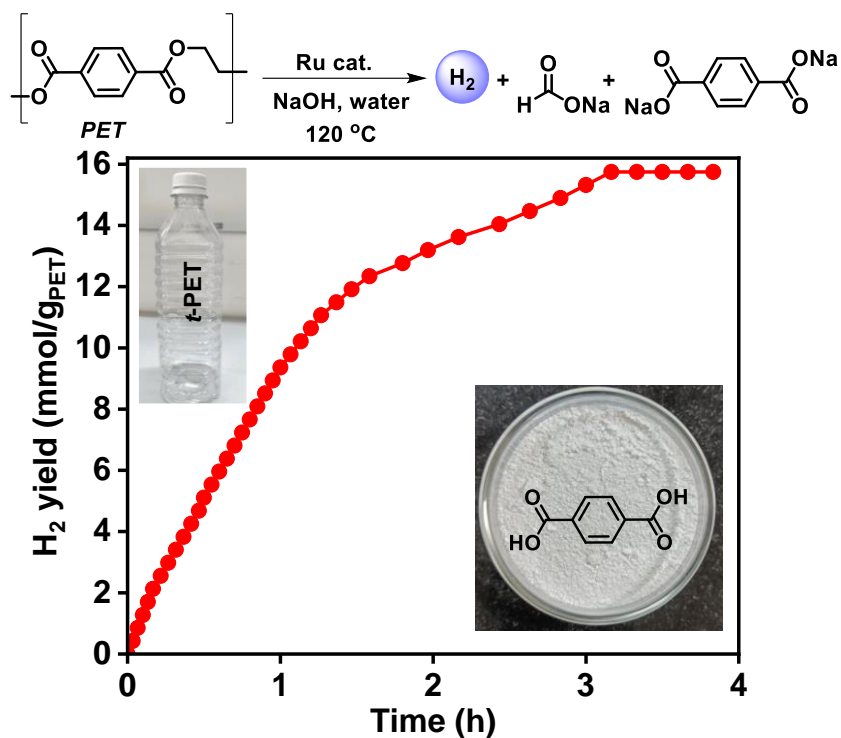


Figure 5.3. Illustrative scheme and time course plot for the one-pot depolymerization and hydrogen production from *t*-PET over the ruthenium catalyst. Reaction conditions: ruthenium catalyst (0.1 mmol), *t*-PET (0.192 g), NaOH (12 M), H₂O (2 mL), and 120 °C.

However, the reaction could not occur in the absence of NaOH (Table 5.1, entry 4). Performing the catalytic reaction of *t*-PET over ruthenium catalyst at 120 °C significantly improves the reaction performance with the release of 15.6 mmol/g_{PET} of H₂ gas (~38,000 mL/gRu) and 9.6 mmol/g_{PET} of sodium formate (SF) in only 3 h (Table 5.1, entry 4). GC-TCD analysis of the evolved gas inferred the complete selectivity for H₂ gas with no contamination of CO₂ or CO (Figure 5.4).

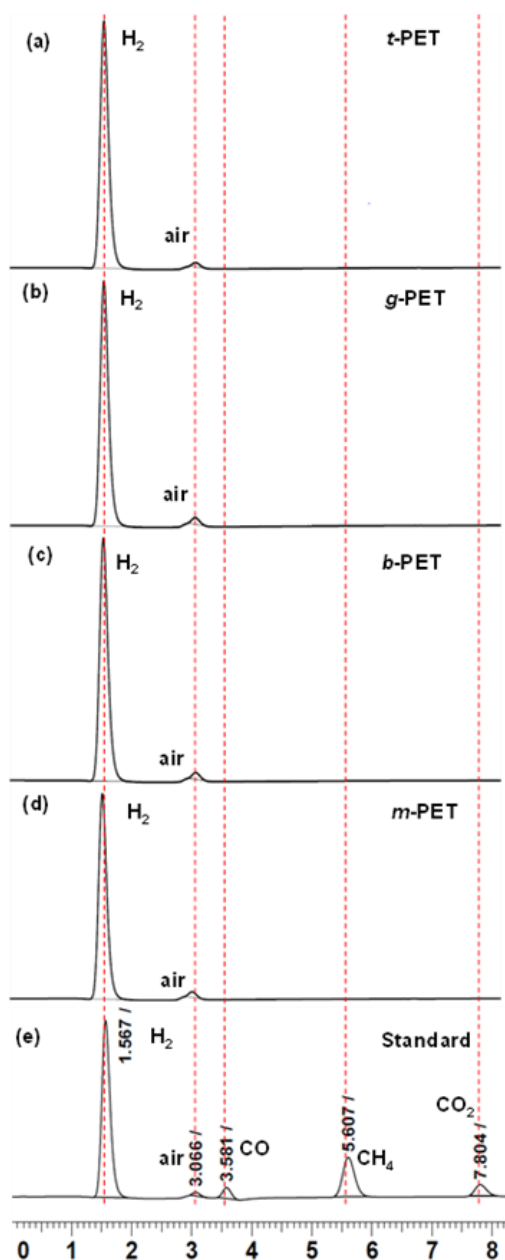


Figure 5.4. GC-TCD analysis of the gas produced from one-pot dehydrogenation of (a) *t*-PET, (b) *g*-PET, (c) *b*-PET, and (d) *m*-PET over the ruthenium catalyst along with the (e) standard mixture of gases with the composition of CO (24.965%), CO₂ (24.962%), CH₄ (25.012%) and H₂ (25.061%). Reaction conditions: Ruthenium catalyst (0.1 mmol), PET (0.192 g), NaOH (12 M), water (2 mL), and 120 °C.

¹H NMR analysis of the reaction performed at 110 °C also inferred the complete depolymerization of *t*-PET flakes with 97% carbon yield. Along with the formation of Na₂TPA (5.2 mmol), 86% of the EG generated during the depolymerization of PET was converted to SG (1.9 mmol/g_{PET}) and SF (4.6

mmol/g_{PET}) in the presence of ruthenium catalyst at 110 °C (Table 1, entry 1 and Figure 5.5). ¹H NMR of the reaction mixture obtained after the catalytic reaction confirms the complete depolymerization of PET flakes with the formation of Na₂TPA (5.2 mmol/g_{PET}) along with SF (9.6 mmol/g_{PET}) (Figure 5.6). Notably, the time-dependent PET dehydrogenation reaction at 120 °C revealed a high yield of EG, sodium glycolate (SG), and SF in the initial hours of the reactions, suggesting the depolymerization of PET with simultaneous dehydrogenation of EG. Moreover, with the progress of the reaction, EG and SG yields decreased, while SF yields almost linearly increased to 9.6 mmol/g_{PET} upon the completion of the reaction (Figure 5.7).

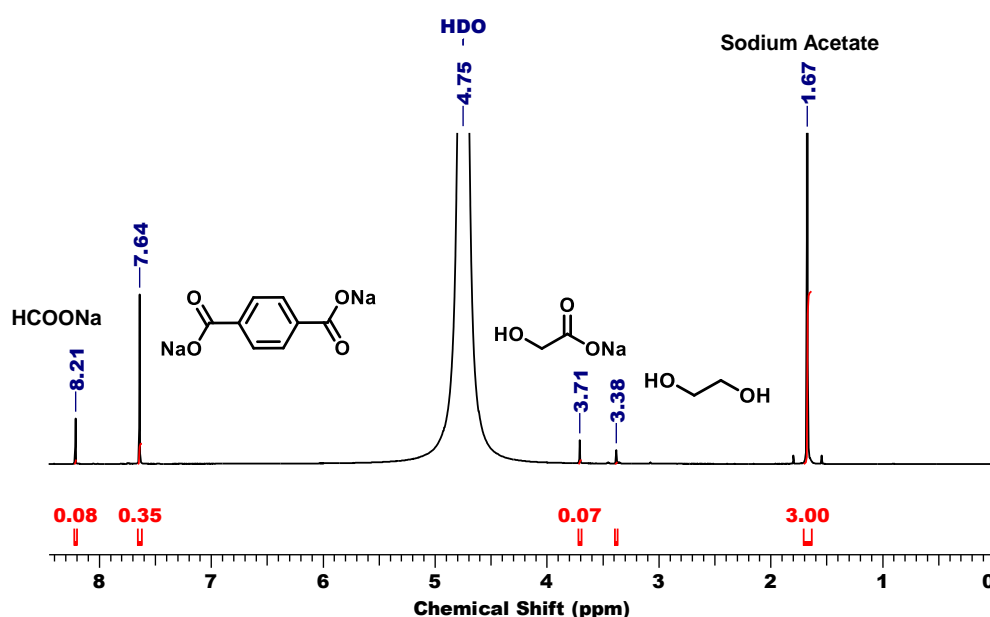


Figure 5.5. ¹H NMR spectra (in D₂O:H₂O (v/v 1:9)) of the crude reaction mixture of the catalytic depolymerization of *t*-PET. Reaction conditions: Ruthenium catalyst (0.1 mmol), *t*-PET (0.192 g), NaOH (12 M), water (2 mL), and 110 °C.

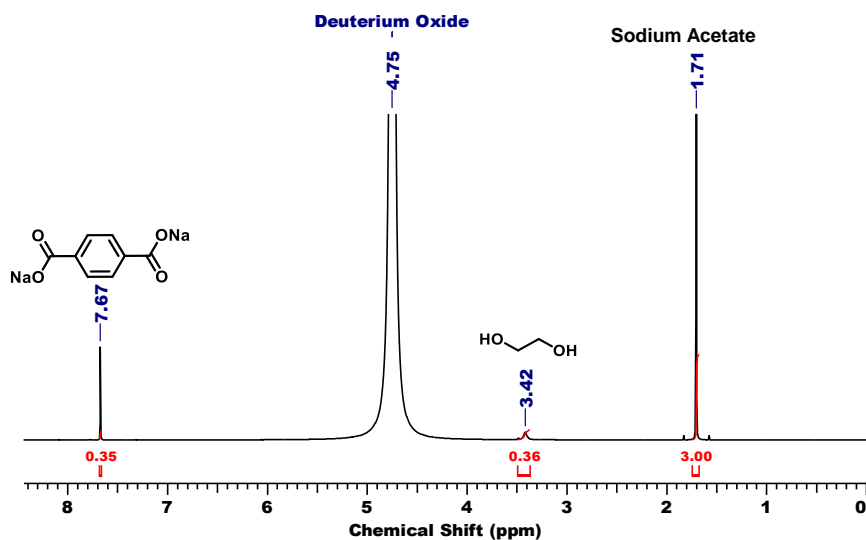


Figure 5.6. ^1H NMR spectra of the crude reaction mixture of the catalytic reaction in $\text{D}_2\text{O}:\text{H}_2\text{O}$ (1:9) depolymerization of *t*-PET. Reaction conditions: PET (0.192 g), NaOH (12 M), water (2 mL), and 120 °C.

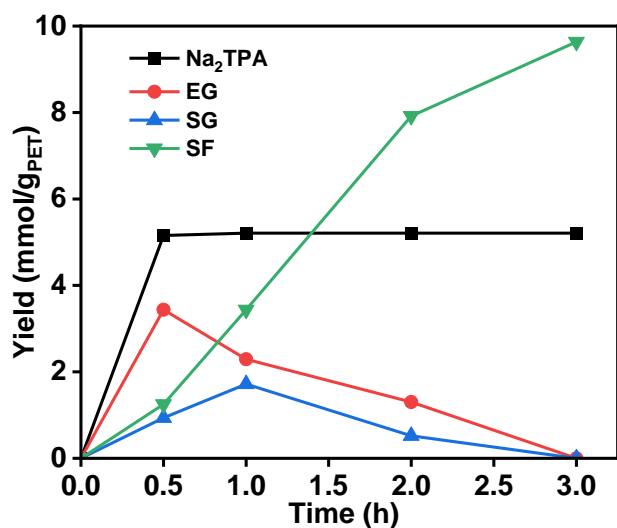


Figure 5.7. Time-dependent distribution of Na_2TPA , EG, SG, and SF for the catalytic dehydrogenation of *t*-PET over the ruthenium catalyst. Reaction conditions: Ruthenium catalyst (0.1 mmol), PET (0.192 g), NaOH (12 M), H_2O (2 mL), and 120 °C.

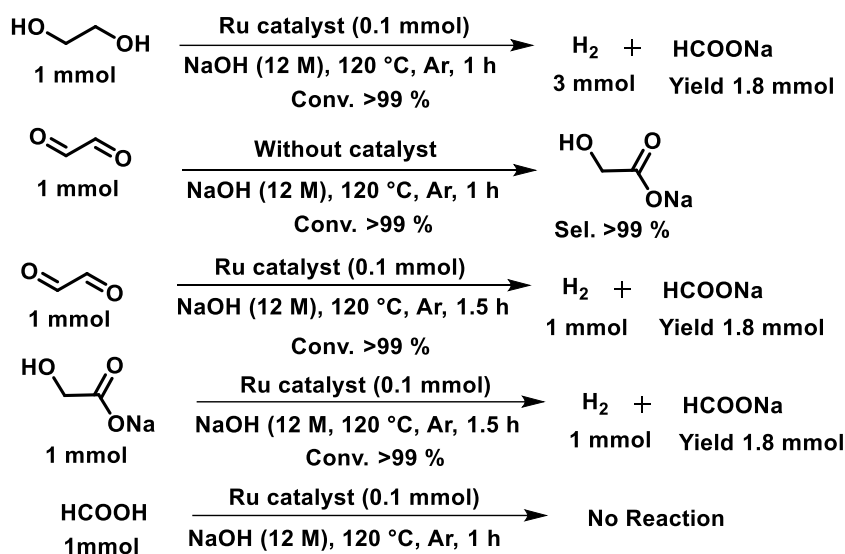
Table 5.1. Reaction optimization for the one-pot depolymerization and dehydrogenation of PET-based plastic wastes over the ruthenium catalyst.^a

Entry	PET	NaOH	T (°C)/ t (h)	Yield (mmol/g _{PET})					CB (%)
				H ₂	Na ₂ TPA	EG	SG	SF	
1	<i>t</i> -PET	12 M	110/6.0	10.6	5.2	0.7	1.9	4.6	97
2 ^b	<i>t</i> -PET	12 M	110/4.0	-	5.2	5.2	-	-	>99
3 ^b	<i>t</i> -PET	12 M	120/1.5	-	5.2	5.2	-	-	>99
4	<i>t</i> -PET	-	110/4.0	-	-	-	-	-	-
5	<i>t</i> -PET	12 M	120/3.0	15.6	5.2	-	-	9.6	96
6	<i>t</i> -PET	12 M	130/2.6	15.6	5.2	-	-	9.6	96
7	<i>t</i> -PET	12 M	140/2.0	15.6	5.2	-	-	9.8	98
8	<i>t</i> -PET	10 M	120/4.0	14.5	5.0	-	0.8	7.9	96
9	<i>t</i> -PET	8 M	120/4.5	11.5	5.2	0.57	1.6	5.8	91
10	<i>t</i> -PET	8 M	140/2.5	14.9	5.2	-	1.25	7.6	97
11	<i>t</i> -PET	8 M	160/1.0	15.6	5.2	-	-	9.5	95
12	<i>t</i> -PET	6 M	160/2.0	14.0	5.2	-	1.67	6.8	97
13	<i>t</i> -PET	4 M	160/2.0	9.4	5.0	1.3	2.3	3.0	98
14 ^c	<i>t</i> -PET	12 M	120/4.0	15.3	5.2	-	-	9.5	95
15 ^d	<i>t</i> -PET	12 M	120/4.0	-	-	-	-	-	-
16 ^e	<i>t</i> -PET	12 M	120/4.0	-	-	-	-	-	-
17 ^f	<i>t</i> -PET	12 M	120/5.0	8.5	5.0	1.9	0.9	3.2	90
18	<i>b</i> -PET	12 M	120/6.0	15.0	5.2	-	-	9.4	94
19	<i>g</i> -PET	12 M	120/6.0	15.3	5.2	-	-	9.6	96
20	<i>m</i> -PET	12 M	120/4.0	15.0	5.2	-	-	9.4	94
21 ^g	<i>t</i> -PET	12 M	120/5.5	15.3	5.2	-	-	9.5	95

^aReaction conditions: PET (0.192 g), ruthenium catalyst (0.1 mmol), NaOH (12 M), H₂O (2.0 mL), 110-140 °C. ^bReaction without ruthenium catalyst. Reaction with ^cKOH, ^dNa₂CO₃, ^eK₂CO₃, and ^fKO^tBu instead of NaOH. ^gReaction with ruthenium catalyst (0.05 mmol). CB is carbon balance.

Considering the H₂ yield and ¹H NMR findings, these results are consistent with the depolymerization of PET into Na₂TPA and EG and with subsequent *in-situ* dehydrogenation of EG over the ruthenium catalyst to yield H₂ gas with the formation of SF via SG intermediate. Several control experiments were also performed using EG, SG, and other intermediates at 120 °C to investigate it further (Scheme 5.1). Results inferred the complete conversion of EG to release 3.0 equiv. of H₂ gas with 1.8 equiv. of SF over the ruthenium catalyst at 120 °C. It is hypothesized that the SG observed in the one pot catalytic dehydrogenation of PET can be produced from glycolaldehyde, which further produces hydrogen

gas in the presence of base to yield glyoxal. Further, we observed the transformation of glyoxal to SG in the presence of NaOH under the catalyst-free condition. On the other hand, treating glyoxal with the ruthenium catalyst at 120 °C resulted in the formation of SF (1.8 mmol) with the release of H₂ gas (1.0 mmol). Moreover, catalytic reaction with SG also resulted in the release of 1.0 equiv. of H₂ gas with 1.8 equiv. of SF in 1.5 h at 120 °C over the ruthenium catalyst, suggesting that dehydrogenation of SG may also occur under the catalytic dehydrogenation of EG. Notably, SF to H₂ transformation was not observed over the ruthenium catalyst (Scheme 5.1). Therefore, experimental evidence clearly suggested that during the ruthenium-catalyzed one-pot dehydrogenation of PET-based plastics, PET initially undergoes base-assisted depolymerization to produce Na₂TPA and EG. Further, EG dehydrogenates to glycolaldehyde, followed by base-catalyzed dehydrogenation of glycolaldehyde to glyoxal, and then glyoxal to SG, and finally, dehydrogenation of SG to SF (Scheme 5.2)



Scheme 5.1. Control experiments to elucidate the plausible reaction pathway for one-pot dehydrogenation of PET.

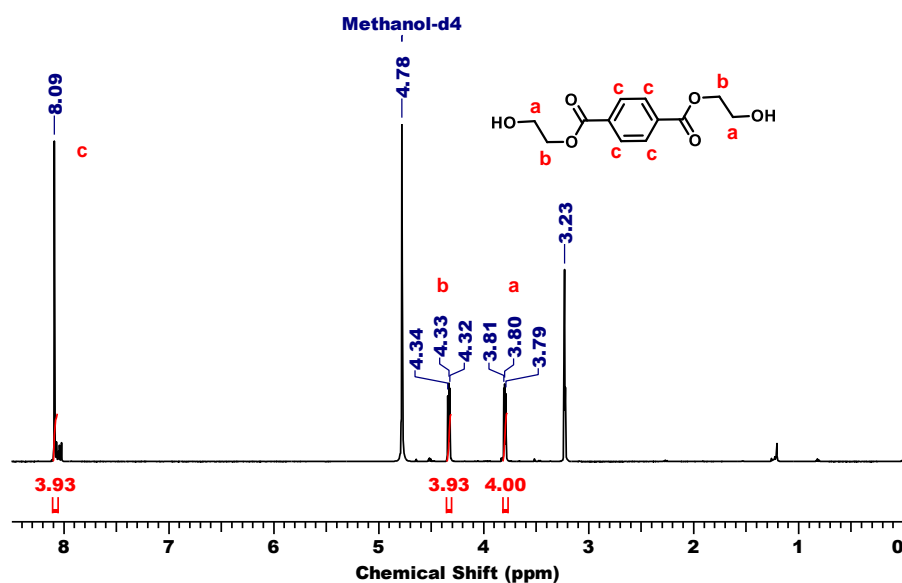
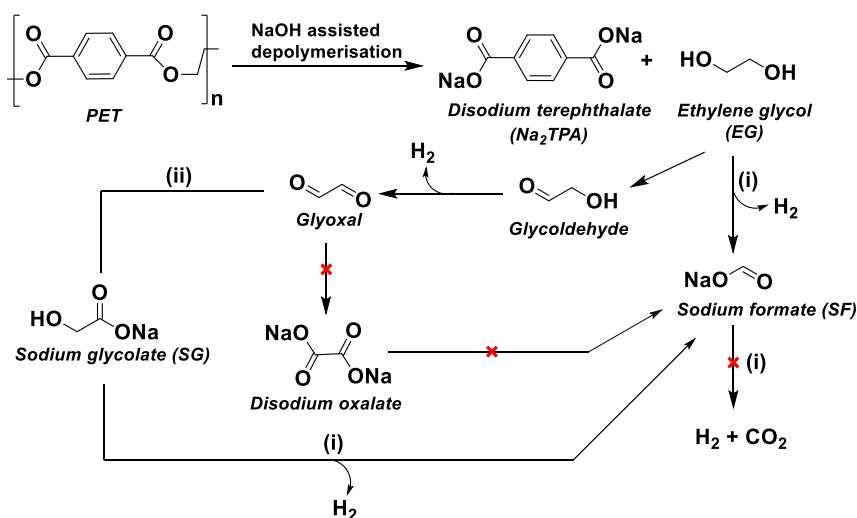


Figure 5.8. ^1H NMR spectra of bis(hydroxyethyl)terephthalate in methanol- d^4 .



Scheme 5.2. Plausible pathway for the one-pot depolymerization and catalytic dehydrogenation of PET-based plastic on the control experiments conducted (i) with and (ii) without ruthenium catalyst in the presence of NaOH (12 M), water (2.0 mL) at 120 °C.

Notably, we also synthesized bis(hydroxyethyl)terephthalate (BHET), a monomer of PET, by esterification of terephthalic acid with EG and characterized by NMR spectroscopy (Figure 5.8 and 5.9). The quantitative yield of Na_2TPA (>98%) and EG (>90%) was obtained from BHET in the absence of catalyst at 120 °C (Scheme 5.3 and Figure 5.10). On the other hand, for the reaction performed in the presence of ruthenium catalyst, we observed the

release of 2.8 equiv. of H₂ gas, along with SF (>99% yield) and Na₂TPA (99% yield) at 120 °C (Scheme 5.3 and Figure 5.11).

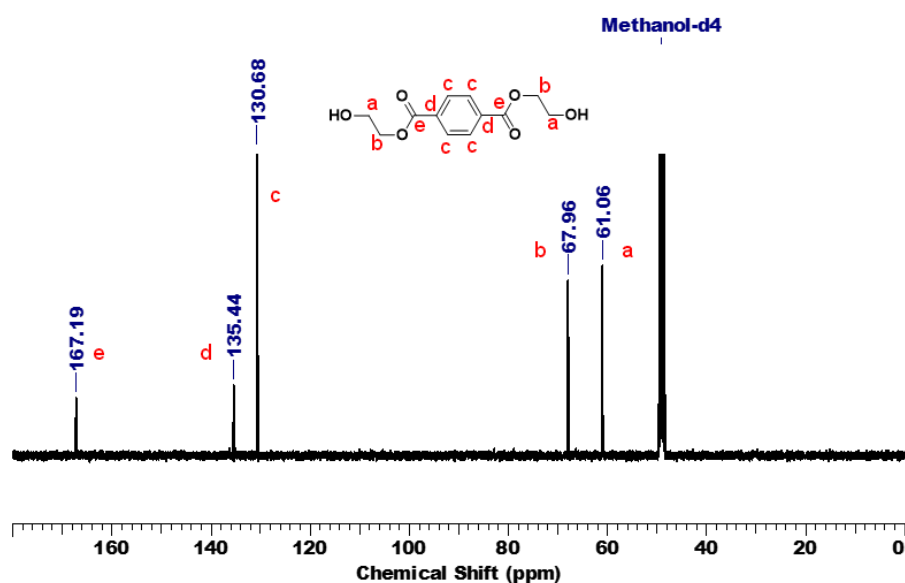


Figure 5.9. ¹³C NMR spectra of bis(hydroxyethyl)terephthalate in methanol-*d*⁴.

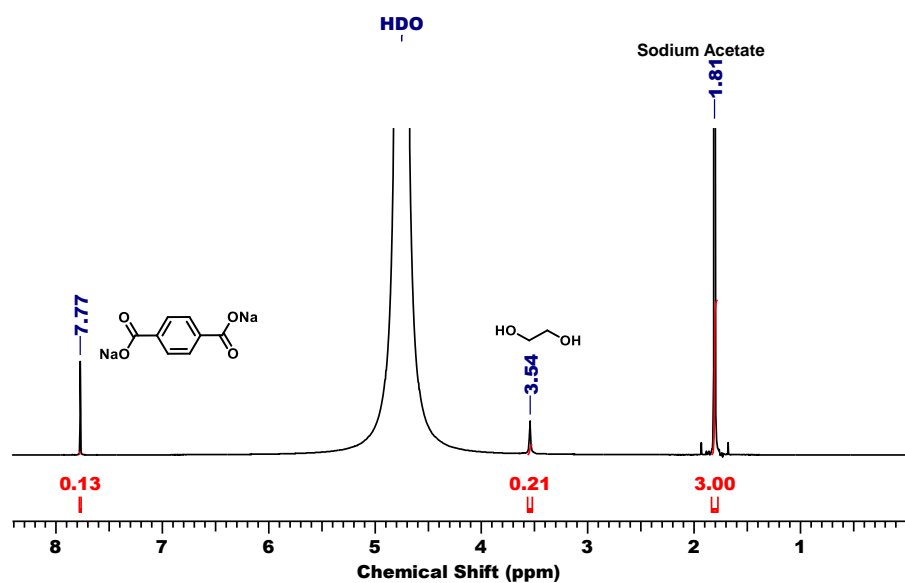
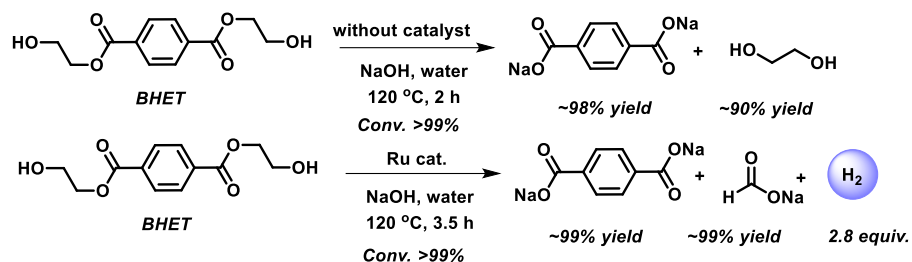


Figure 5.10. ¹H NMR spectra (in D₂O:H₂O (v/v 1:9)) of the crude reaction mixture of the depolymerization of BHET (without catalyst). Reaction conditions: BHET (1.0 mmol), NaOH (12 M), water (2 mL), 120 °C, and 2 h.



Scheme 5.3. Control experiments (a) depolymerization of BHET without ruthenium catalyst, (b) dehydrogenation of BHET over ruthenium catalyst. Reaction conditions: Ruthenium catalyst (0.1 mmol), BHET (1.0 mmol), NaOH (12 M), H₂O (2.0 mL), and 120 °C.

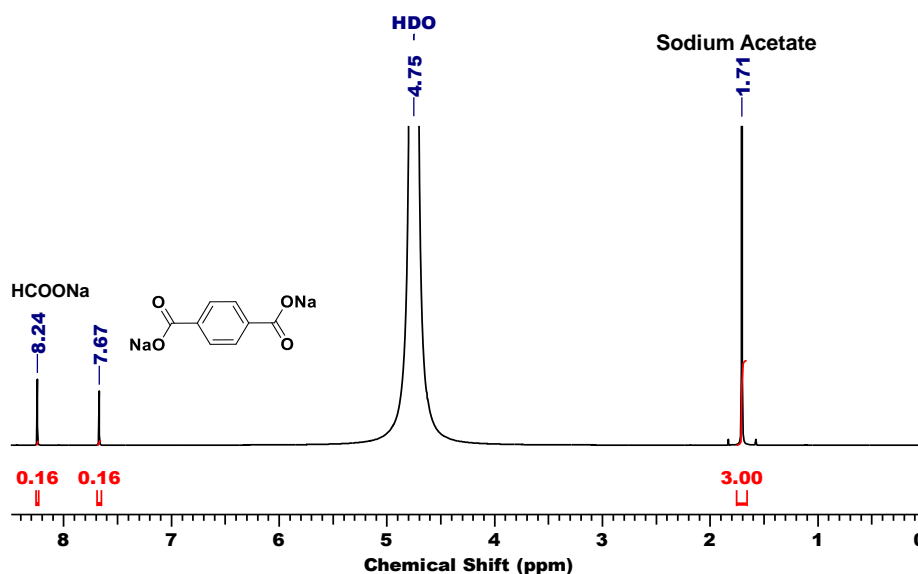


Figure 5.11. ¹H NMR spectra (in D₂O:H₂O (v/v 1:9)) of the crude reaction mixture of the catalytic dehydrogenation of BHET over the ruthenium catalyst. Reaction conditions: Ruthenium catalyst (0.1 mmol), BHET (1.0 mmol), NaOH (12 M), water (2 mL), 120 °C, and 3.5 h.

Further increase in the reaction temperature to 130-140 °C, the complete transformation of PET with the release of H₂ gas (~15 mmol/g_{PET}) and SF (~9.6 mmol/g_{PET}) is achieved in 2 h at 140 °C (Table 5.1, entries 6, 7). Altogether, we could achieve complete conversion of *t*-PET with the quantitative release of H₂ gas (~15 mmol/g_{PET}) at all the reaction temperature (120-140 °C) with an estimated activation energy of 22.3 kJ/mol (Figure 5.12).

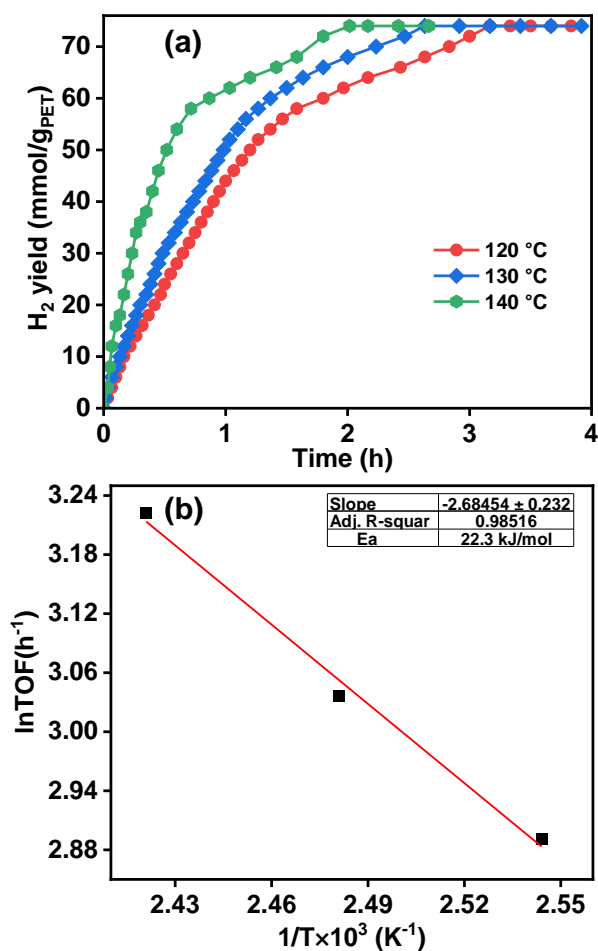


Figure 5.12. (a) Temperature-dependent plot for hydrogen gas generation from *t*-PET over the ruthenium catalyst, and the corresponding (b) Arrhenius plot of initial TOF values to calculate activation energy. Reaction conditions: Ruthenium catalyst (0.1 mmol), *t*-PET (0.192 g), NaOH (12 M), H₂O (2 mL), and 120-140 °C.

In addition to SF, we obtained purified TPA (as a white solid) in all the reactions performed over the ruthenium catalyst under varying reaction temperature. These results together demonstrated the one-pot process for the selective production of hydrogen gas from *t*-PET over the ruthenium catalyst under mild conditions with the quantified yield of Na₂TPA. It is worth mentioning here that TPA is an important monomer for the synthesis of polyester, PET-based synthetic fabrics, and beverage bottles, while SF is an important de-icer compound.^[32,33] Moreover, Na₂TPA (disodium terephthalate) and K₂TPA (dipotassium terephthalate) show excellent electrochemical properties in sodium ion batteries (NIBs) and potassium ion batteries (KIBs).^[34,35]

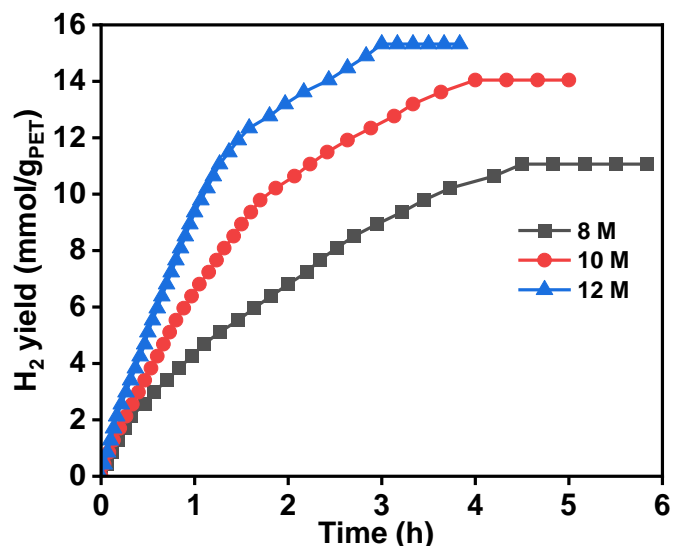


Figure 5.13. Effect of base concentration on hydrogen gas generation from *t*-PET over the ruthenium catalyst. Reaction conditions: Ruthenium catalyst (0.1 mmol), *t*-PET (0.192 g), NaOH (8 M -12 M), H₂O (2 mL), and 120 °C.

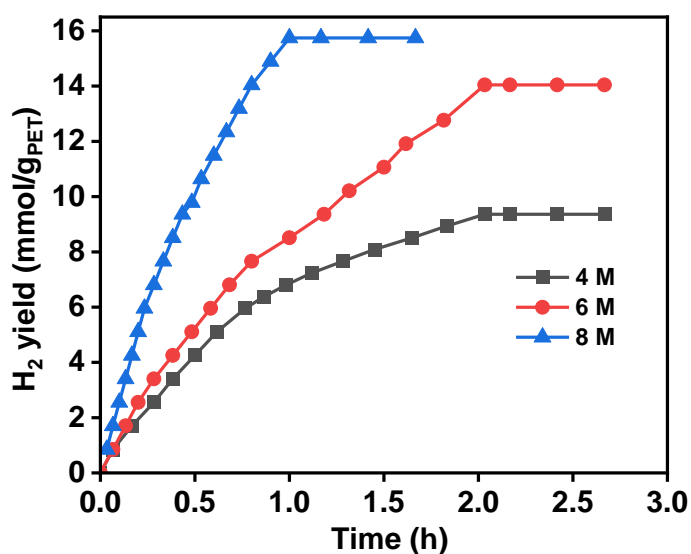


Figure 5.14. Effect of base concentration on hydrogen gas generation from *t*-PET over the ruthenium catalyst. Reaction conditions: Ruthenium catalyst (0.1 mmol), *t*-PET (0.192 g), NaOH (4 M-8 M), H₂O (2 mL), and 160 °C.

Further, varying the base concentration or the type significantly impacted the H₂ yield (Table 5.1 and Figure 5.13-5.15). In contrast to the reaction with 12 M NaOH, we observed the release of 14.5 mmol/g_{PET} of H₂ gas along with the observation of 0.8 mmol/g_{PET} of SG from *t*-PET in the presence of 10 M NaOH (Table 5.1, entry 8). On the other hand, with even

lower base concentration (8 M NaOH), the amount of SG was increased to 1.6 mmol/g_{PET} with only 11.5 mmol/g_{PET} yield of H₂ gas (Table 5.1, entry 9), which indicates the crucial role of base (NaOH) in achieving complete transformation of PET over the ruthenium catalyst (Figure 5.13). Further, we performed reactions at elevated reaction temperature (140 and 160 °C) with lower NaOH concentrations (≤ 8 M) (Table 5.1, entries 10-13, and Figure 5.14). Although complete depolymerization of *t*-PET was achieved at 140 °C with 8 M NaOH, it could not lead to the complete conversion of PET to H₂ (Table 5.1, entry 10).

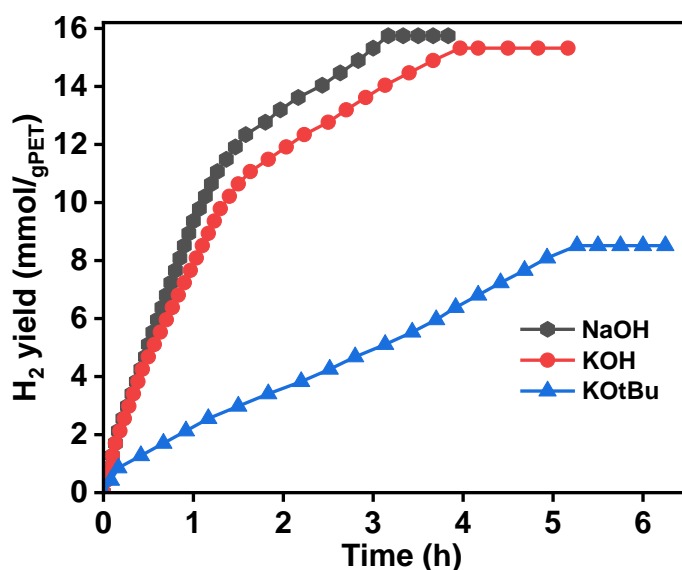


Figure 5.15. Effect of different bases: time course plot for hydrogen gas generation from *t*-PET over the ruthenium catalyst. Reaction conditions: Ruthenium catalyst (0.1 mmol), *t*-PET (0.192 g), base (12 M), H₂O (2 mL), and 120 °C.

On the other hand, *t*-PET was completely converted into H₂ (15.6 mmol/g_{PET}), SF (9.5 mmol/g_{PET}), and Na₂TPA (5.2 mmol/g_{PET}) at 160 °C in the presence of 8 M NaOH (Table 5.1, entry 11). However, with 4 M and 6 M NaOH at 160 °C, a lower yield of H₂ gas was observed, suggesting the incomplete dehydrogenation of EG (Table 5.1, entries 12-13). Analogous to NaOH, KOH also exhibited analogous activity with the release of 15.3 mmol/g_{PET} of H₂ gas along with 5.2 mmol/g_{PET} of K₂TPA, and 9.5 mmol/g_{PET} of SF (Table 5.1, entry 14). Contrary to the efficient activity observed with NaOH and KOH, moderate activity was observed with KO^tBu, while weak base (Na₂CO₃ and K₂CO₃) displayed no activity (Table 5.1, entries 15-17 and Figure 5.15).

5.3.3. Catalytic hydrogen production from different types of PET

Notably, PET-based plastic waste is available in various forms and, most often, in mixed forms. PET with different colors contain different additives (pigments), but their chemical compositions are the same. Though in some cases, PET with different other additives, such as polypropylene, polyethylene, are mixed with PET to get different grades of PET-based plastics, results inferred that alkaline hydrolysis results in the formation of purified terephthalate salt, which can be readily recovered from the aqueous solution, while filtration can remove the other additives, such as polypropylene, polyethylene.^[19] Notably, recycling of pigmented (coloured) PET is problematic as during mechanical recycling; the pigments may result in undesirable colors (often grey) when mixed with *t*-PET, making it unattractive for recycling. Further, sorting of colored PET from *t*-PET is also problematic and has negative impacts on the recycling process, resulting in the disposal of colored or mixed PET in landfills or incinerated. Therefore, it is important to have a suitable recycling process for such mixed PET waste to yield high-purity starting materials (e.g., TPA). There have been few recent reports on the depolymerization of color or mixed PET. For instance, Meester et al. reported the depolymerization of black PET to obtain purified TPA (95%) in the presence of 5-15 wt% NaOH at 50-80 °C in the ethanol-water mixture, with successful removal of carbon black additive of black PET.^[20] Petrossian et al. also studied the depolymerization of color or mixed PET under alkaline conditions (30% aqueous NaOH) at 80-110 °C to obtain purified TPA (95% yield in ethanol and 81% yield in EG), where the colored contaminants have no negative impact on the PET depolymerization process.^[19] We, therefore, explored the applicability of the developed integrated process for hydrogen production from brown-colored PET (*b*-PET), green-colored (*g*-PET) and mixed PET (*m*-PET a mixture of *t*-PET, *g*-PET, and *b*-PET flakes) obtained from various sources, such as colored beverage bottles (Figure 5.16).

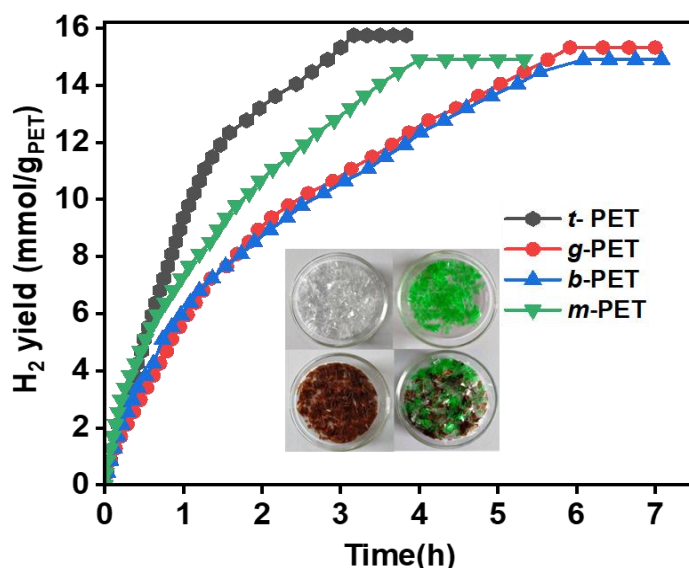


Figure 5.16. Catalytic one-pot dehydrogenation of *t*-PET, *g*-PET, *b*-PET, and *m*-PET over the ruthenium catalyst. Reaction conditions: Ruthenium catalyst (0.1 mmol), PET (0.192 g), NaOH (12 M), H₂O (2 mL), and 120 °C.

Notably, the ruthenium catalyst also displayed complete depolymerization of these PET-based plastic waste (*b*-PET and *g*-PET) with high selectivity for H₂ gas (Table 5.1, entries 18-20), analogous to that observed with *t*-PET (Figure 5.4). We observed the complete transformation of *b*-PET over the ruthenium catalyst also released over 15 mmol/g_{PET} of H₂ gas in 6 h with a yield of 5.2 mmol/g_{PET} of Na₂TPA and 9.4 mmol/g_{PET} of SF (Table 1, entry 18). The complete transformation of *g*-PET with the evolution of 15.3 mmol/g_{PET} of H₂ gas and obtained 5.2 mmol/g_{PET} of Na₂TPA and 9.6 mmol/g_{PET} of SF at 120 °C in 6 h (Table 1, entry 19). In addition, conducting the reaction with *m*-PET flakes resulted in the complete transformation of PET with the release of 15 mmol/g_{PET} of H₂ gas at 120 °C in 4 h, also with 5.2 mmol/g_{PET} of Na₂TPA and 9.4 mmol/g_{PET} of SF, highlighting the effectiveness of the developed ruthenium-catalyzed the complete one-pot transformation of PET-based plastic waste to H₂ gas (Table 5.1, entry 20, and Figure 5.17).

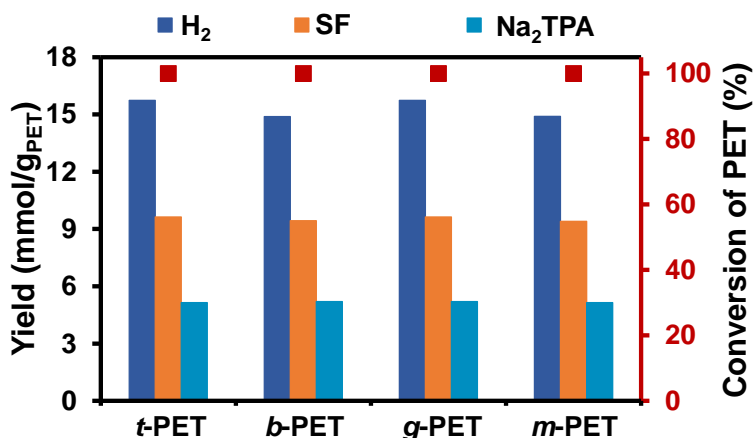


Figure 5.17. Product distribution for the catalytic one-pot dehydrogenation of *t*-PET, *g*-PET, *b*-PET, and *m*-PET over the ruthenium catalyst. Reaction conditions: Ruthenium catalyst (0.1 mmol), PET (0.192 g), NaOH (12 M), H₂O (2 mL), and 120 °C.

Further, we also performed a reaction with the catalyst loading of 0.05 mmol and observed 15.3 mmol/g_{PET} of H₂ gas along with 5.2 mmol/g_{PET} of Na₂TPA and 9.5 mmol/g_{PET} of SF (Table 5.1, entry 21). The composition of the gas evolved for all these reactions inferred the complete selectivity for H₂ gas, with no contamination of CO₂ or CO as determined by GC-TCD (Figure 5.4). It is also worth mentioning that TPA obtained (after acidification) during the catalytic depolymerization of PET (*t*-PET, *b*-PET, *g*-PET, and *m*-PET) was of high purity, as the P-XRD, FTIR, NMR, and TGA, patterns of the as-obtained TPA were consistent with those of the commercial TPA (Figures 5.18-5.22).^[22] The P-XRD pattern for the TPA obtained from different colour/mixed PET flakes (*t*-PET, *g*-PET, *b*-PET and *m*-PET) at 2θ values of 17.32°, 25.3°, and 28.0°, which is analogous to that of the commercial TPA (Figure 5.18) and matches well with the standard P-XRD pattern of TPA (ICDD PDF card 00-031-1916).^[19] Analogously, FTIR peaks at 1674 and 1276 cm⁻¹, corresponding to C=O and C-O bonds, and 1487 and 1418 cm⁻¹ for the phenyl ring of TPA (as obtained from *t*-PET, *b*-PET, and *g*-PET), also matches well with the commercial TPA (Figure 5.19). ¹H and ¹³C NMR of the spectra of the as-obtained TPA and the commercial TPA was also analogous, where peaks corresponding to the aromatic protons were obtained at 7.64 ppm (¹H NMR) and 136.2, and 126.2 ppm (¹³C NMR), while the carboxylate group appeared at 172.7 ppm in ¹³C NMR (Figures 5.20-5.21).

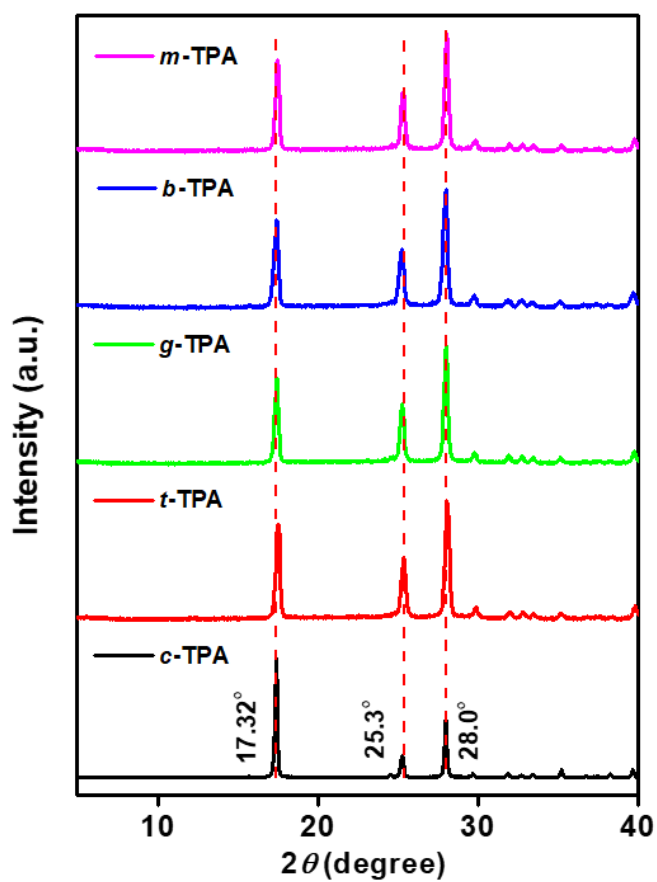


Figure 5.18. P-XRD pattern of c-TPA, along with the TPA, was produced during the catalytic dehydrogenation of t-PET, g-PET, b-PET, and m-PET. Reaction conditions: Ruthenium catalyst (0.1 mmol), PET (0.192 g), NaOH (12 M), water (2 mL), and 120 °C. (t, b, g, m, and c stands for transparent, brown, green, mixed, and commercial, respectively).

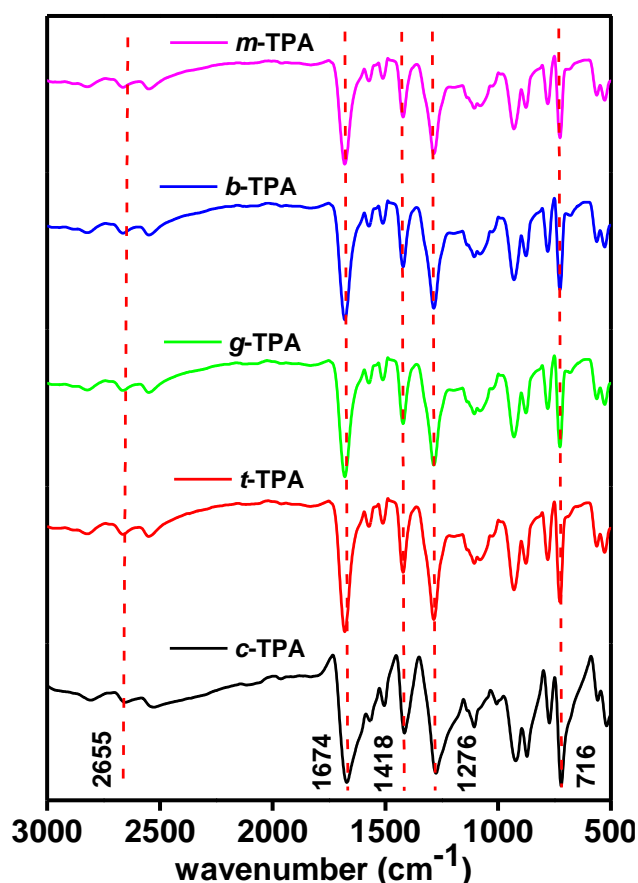


Figure 5.19. FT-IR spectra of c-TPA along with the TPA as produced during the catalytic dehydrogenation of t-PET, b-PET, g-PET, and m-PET. Reaction conditions: Ruthenium catalyst (0.1 mmol), PET (0.192 g), NaOH (12 M), water (2 mL), and 120 °C. (t, b, g, m, and c stands for transparent, brown, green, mixed, and commercial, respectively).

Therefore, our findings inferred that the developed process demonstrated a simple integrated one-pot protocol for the complete depolymerization and dehydrogenation of a wide range of PET-based plastic waste over ruthenium catalyst with selective production of H₂ gas (~15.6 mmol/g_{PET}) along with the quantitative yield of Na₂TPA (5.2 mmol/g_{PET}) and SF (9.6 mmol/g_{PET}) at low-temperature (120 °C). The observed high yield and selectivity of H₂ from PET depolymerization and dehydrogenation are significant considering the previously reported low H₂ yield from PET-based plastic waste, such as ~11 mmol/g_{PET} (by PET pyrolysis reforming/steam gasification at 700-800 °C),^[36-38] 0.238 mmol/g_{PET} (by photo-reforming of PET hydrolysate over CdS/CdO_x),^[28] and 19.97 mmol/g_{PET} (by aqueous phase

reforming over Ru-ZnO/MEC at 250 °C, ~68% H₂ selectivity).^[31] It is also evident from these reports that most of these PET depolymerization processes were either performed at a very high temperature or resulted in lower selectivity for H₂ gas.

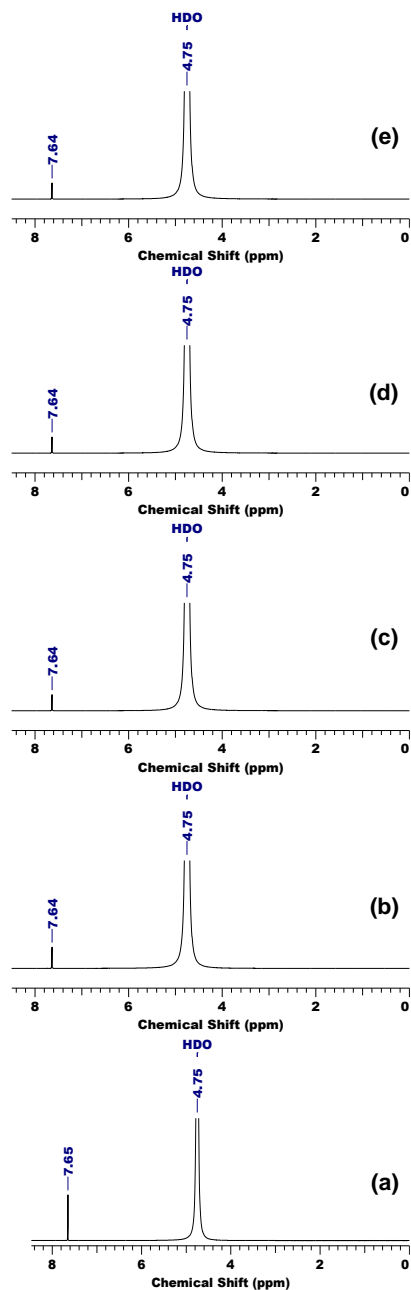


Figure 5.20. ¹H NMR spectra of (a) *c*-TPA along with the (b-e) TPA as produced during the catalytic dehydrogenation of (a) *t*-PET, (b) *g*-PET, (c) *b*-PET, and (d) *m*-PET. Reaction conditions: Ruthenium catalyst (0.1 mmol), PET (0.192 g), NaOH (12 M), water (2 mL), and 120 °C. (*t*, *b*, *g*, *m*, and *c* stands for transparent, brown, green, mixed, and commercial, respectively).

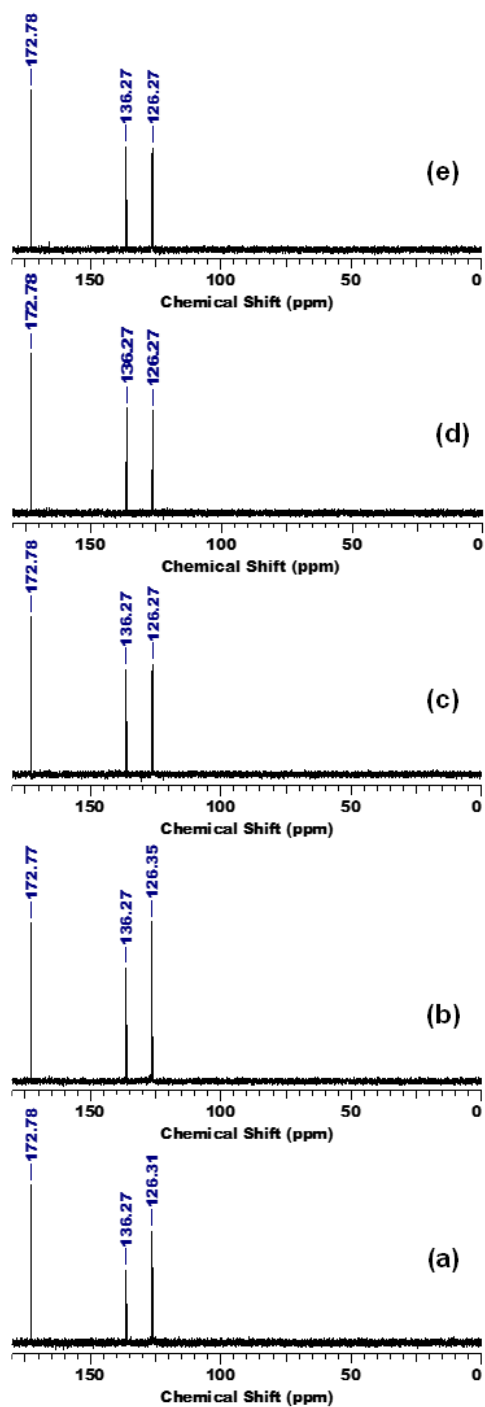


Figure 5.21. ^{13}C NMR spectra of (a) *c*-TPA along with the (b-e) TPA as produced during the catalytic dehydrogenation of (a) *t*-PET, (b) *g*-PET, (c) *b*-PET, and (d) *m*-PET. Reaction conditions: Ruthenium catalyst (0.1 mmol), PET (0.192 g), NaOH (12 M), water (2 mL), and 120 °C. (*t*, *b*, *g*, *m*, and *c* stands for transparent, brown, green, mixed, and commercial, respectively).

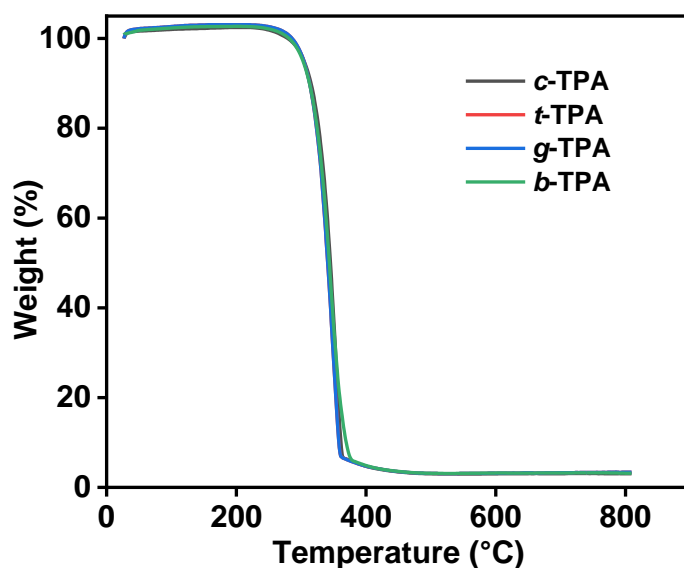


Figure 5.22. TGA analysis of the commercial (c-TPA) and synthesized TPA (t-TPA, g-TPA, and b-TPA) by one-pot depolymerization and dehydrogenation of respective PET over ruthenium catalyst. Reaction conditions: Ruthenium catalyst (0.1 mmol), PET (0.192 g), NaOH (12 M), water (2 mL), and 120 °C.

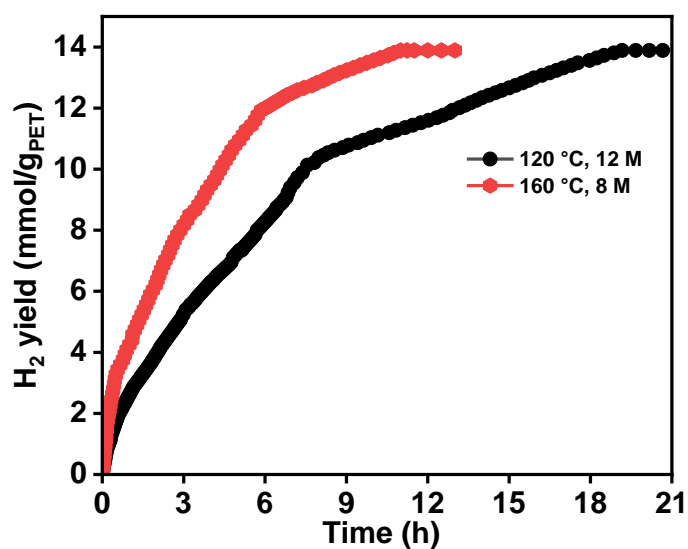


Figure 5.23. Bulk scale reaction for hydrogen production from t-PET over the ruthenium catalyst. Reaction conditions: ruthenium catalyst (0.1 mmol), t-PET (1.0 g), NaOH (12M and 8M), 120 °C and 160 °C, and H₂O (10 mL).

5.3.4. Bulk scale transformation of PET and reusability of the ruthenium catalyst

Further, the robustness and efficacy of the ruthenium catalyst for the one-pot transformation of PET for hydrogen production were investigated by conducting the catalytic reaction with bulk-scale of PET and recyclability experiments at 120 °C and 160 °C (Figure 5.23). Notably, complete depolymerization of *t*-PET (1.0 g) was achieved with the release of 340 mL of H₂ gas from 1.0 g of *t*-PET, along with 5.1 mmol/g_{PET} of Na₂TPA and 6.3 mmol/g_{PET} of SF at 120 °C in 19 h (Figure 5.23). On the other hand, the reaction performed at 160 °C using 8 M NaOH also resulted in the release of 340 mL of H₂ gas (13.9 mmol/g_{PET}) with the TPA (yield 5.2 mmol/g_{PET}) and SF (5.8 mmol/g_{PET}) in much lesser reaction time (11 h) (Figure 5.23). Moreover, complete depolymerization of *t*-PET for three consecutive catalytic runs was achieved with no significant loss in the yield of H₂ gas (~15.6 mmol/g_{PET} of H₂ gas per cycle), along with Na₂TPA and SF at 120 °C (with 12 M NaOH) and 160 °C (with 8 M NaOH) (Figure 5.24 and). The observed slight loss in the activity is attributed to the loss of catalyst during the recovery process. These results demonstrated the high stability of the ruthenium catalyst for PET dehydrogenation. Further, the reaction performed in the presence of elemental mercury could not yield any gas evolution, while complete depolymerization of PET was achieved. These findings suggest the heterogenous nature of active ruthenium catalyst involved in the dehydrogenation of in-situ produced EG during the depolymerization of PET (Figure 5.25).

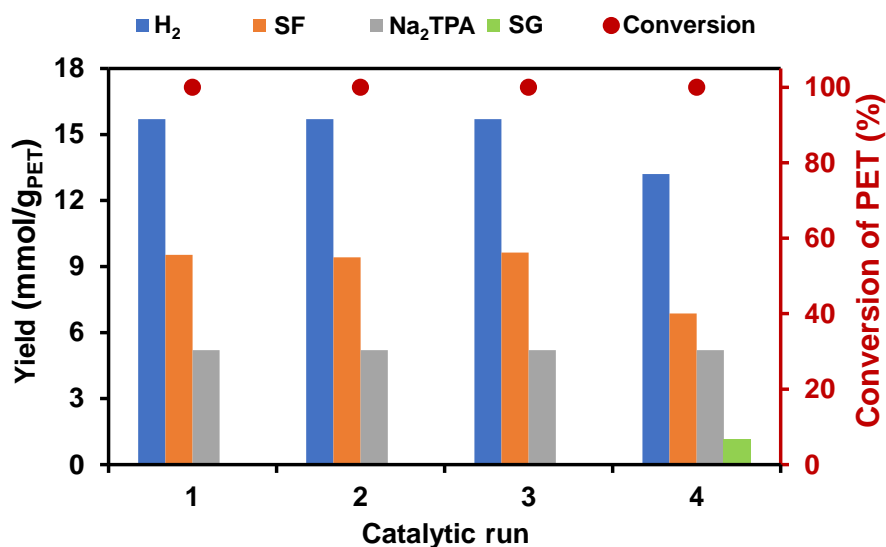


Figure 5.24. Recyclability experiment for hydrogen production from *t*-PET over the ruthenium catalyst. Reaction conditions: ruthenium catalyst (0.1 mmol), *t*-PET (0.192 g), NaOH (8 M), 160 °C, and H₂O (2 mL).

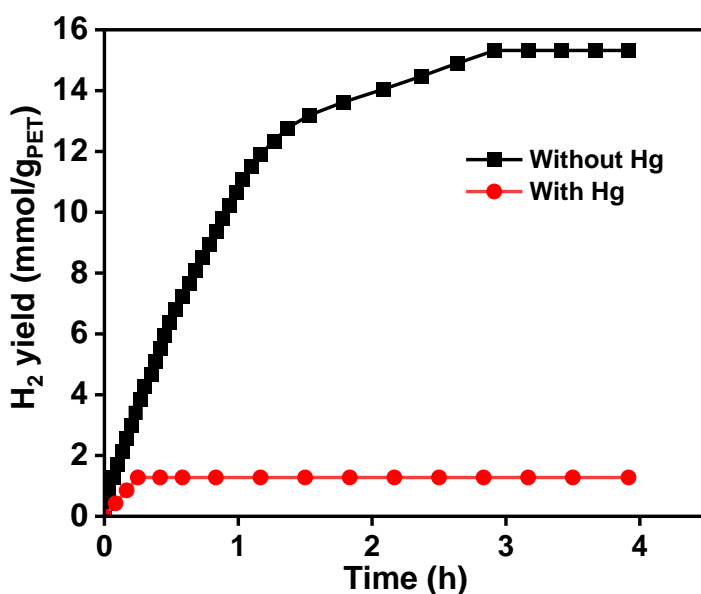


Figure 5.25. Mercury poisoning experiment performed for one-pot dehydrogenation of *t*-PET over ruthenium catalyst. Reaction conditions: Ruthenium catalyst (0.1 mmol), elemental Hg (0.3 g), PET (0.192 g), NaOH (12 M), water (2 mL), and 120 °C.

5.4. Conclusions

The present report describes a highly efficient, sustainable, and integrated protocol for the one-pot transformation of PET-based plastic waste for the large-scale and selective production of hydrogen gas over ruthenium catalyst at low temperature (120 °C) using 12 M NaOH. Moreover, by increasing the reaction temperature to 160 °C, the NaOH amount can be reduced to 8 M without any loss in the catalytic activity for PET to H₂ conversion. Ruthenium catalyst displayed high activity for PET depolymerization and dehydrogenation with H₂ yield as high as ~15.6 mmol/g_{PET} (~38,000 mLH₂/g_{Ru}). Moreover, a quantitative carbon yield (as high as 98%) was achieved with SF yield (9.6 mmol/g_{PET}). Notably, ruthenium catalyst displayed long-term stability for the bulk production of hydrogen gas, with no traces of CO and CO₂ contaminations. The developed protocol performed equally well for hydrogen production from different types of PET-based plastic waste (transparent, green, brown, and even mixed PET obtained from beverage bottles and food packets). Notably, the purified and quantitative yield of TPA (5.2 mmol/g_{PET}) was achieved for all the reactions. In contrast to the traditional processes, such as pyrolysis, steam reforming, photo-reforming, and other processes for hydrogen production from PET-based plastic waste, which are highly energy-intensive and require high-temperature, and yield poor selectivity of H₂ gas, our process is highly selective towards H₂ gas under mild condition and hence, has demonstrated the potential for application in the industrial-scale one-pot transformation of PET-based plastic waste for selective hydrogen production.

Note: The content of this chapter is published as Kumar et al., ChemCatChem, 15, e202300574 (DOI: 10.1002/cctc.202300574) and reproduced with permission from Wiley VCH with license number 5671331171239.

5.5. References

1. Plastics Europe. *Plastics the Facts* 2022. <https://plasticseurope.org/knowledge-hub/plastics-the-facts-2022/> (accessed on April 24, 2023).
2. Li H., Aguirre-Villegas H. A., Allen R. D., Bai X., Benson C. H.,

- Beckham G. T., Bradshaw S. L., Brown J. L., Brown R. C., Cecon V. S., Curley J. B., Curtzwiler G. W., Dong S., Gaddameedi S., García J. E., Hermans I., Kim M. S., Ma J., Mark L. O., Mavrikakis M., Olafasakin O. O., Osswald T. A., Papanikolaou K. G., Radhakrishnan H., Sanchez Castillo M. A., Sánchez-Rivera K. L., Tumu K. N., van Lehn R. C., Vorst K. L., Wright M. M., Wu J., Zavala V. M., Zhou P., Huber G. W. (2022), Expanding Plastics Recycling Technologies: Chemical Aspects, Technology Status and Challenges, *Green Chem.*, 24, 8899-9002 (DOI: 10.1039/d2gc02588d)
3. Garcia J. M., Robertson M. L. (2017), The Future of Plastics Recycling, *Science*, 358, 870-872 (DOI: 10.1126/science.aaq0324)
 4. Sonnendecker C., Oeser J., Richter P. K., Hille P., Zhao Z., Fischer C., Lippold H., Blázquez-Sánchez P., Engelberger F., Ramírez-Sarmiento C. A., Oeser T., Lihanova Y., Frank R., Jahnke H. G., Billig S., Abel B., Sträter N., Matysik J., Zimmermann W. (2022), Low Carbon Footprint Recycling of Post-consumer PET Plastic with a Metagenomic Polyester Hydrolase, *ChemSusChem*, 15, e2021010 (DOI: 10.1002/cssc.202101062)
 5. Smith R. L., Takkellapati S., Riegerix R. C. (2022), Recycling of Plastics in the United States: Plastic Material Flows and Polyethylene Terephthalate (PET) Recycling Processes, *ACS Sustain. Chem. Eng.*, 10, 2084-2096 (DOI: 10.1021/acssuschemeng.1c06845)
 6. Wang C., Han H., Wu Y., Astruc D. (2022), Nanocatalyzed Upcycling of the Plastic Wastes for a Circular Economy, *Coord. Chem. Rev.*, 458, 21442-214447 (DOI: 10.1016/j.ccr.2022.214422)
 7. Barnard E., Rubio Arias J. J., Thielemans W. (2021), Chemolytic Depolymerisation of PET: a review, *Green Chem.*, 23, 3765-3789 (DOI: 10.1039/d1gc00887k)
 8. Suo Q., Zi J., Bai Z., Qi S. (2017), The Glycolysis of Poly(ethylene terephthalate) Promoted by Metal-Organic Framework (MOF) Catalysts, *Catal. Letters*, 147, 240-252 (DOI: 10.1007/s10562-016-1897-0)
 9. Bohre A., Jadhao P. R., Tripathi K., Pant K. K., Saha B. (2023), Chemical Recycling Processes of Waste Polyethylene Terephthalate using Solid Catalysts, *ChemSusChem*, 16, e202300142 (DOI: 10.1002/cssc.202300142)

- 10.1002/cssc.202300142)
10. Krall E. M., Klein T. W., Andersen R. J., Nett A. J., Glasgow R. W., Reader D. S., Dauphinais B. C., McIlrath S. P., Fischer A. A., Carney M. J., Hudson D. J., Robertson N. J. (2014), Controlled Hydrogenative Depolymerization of Polyesters and Polycarbonates Catalyzed by Ruthenium(II) PNN pincer Complexes, *Chem. Commun.*, 50, 4884-4887 (DOI: 10.1039/c4cc00541d)
 11. Westhues S., Idel J., Klankermayer J. (2018), Molecular Catalyst Systems as Key Enablers for Tailored Polyesters and Polycarbonate Recycling concepts, *Sci. Adv.*, 4, 1-9 (DOI: 10.1126/sciadv.aat9669)
 12. Kratish A. Y., Li J., Liu S., Gao Y., Marks J. (2020), Polyethylene Terephthalate Deconstruction Catalyzed by a Carbon-Supported Single-Site Molybdenum-Dioxo Complex, *Angew. Chem. Int. Ed.*, 59, 19857-19861 (DOI: 10.1002/ange.202007423)
 13. Wu P., Lu G., Cai C. (2021), Cobalt–Molybdenum Synergistic Catalysis for the Hydrogenolysis of Terephthalate-based Polyesters, *Green Chem.*, 23, 8666-8672 (DOI: 10.1039/d1gc02929k)
 14. Wu Y., Wang X., Kirlikovali K. O., Gong X., Atilgan A., Ma K., Schweitzer N. M., Gianneschi N. C., Li Z., Zhang X., Farha O. K. (2022), Catalytic Degradation of Polyethylene Terephthalate Using a Phase-Transitional Zirconium-Based Metal–Organic Framework, *Angew. Chem. Int. Ed.*, e202117528 (DOI: 10.1002/anie.202117528)
 15. Jing Y., Wang Y., Furukawa S., Xia J., Sun C., Hülsey M. J., Wang H., Guo, Liu X., Yan N. (2021), Towards the Circular Economy: Converting Aromatic Plastic Waste Back to Arenes over a Ru/Nb₂O₅ Catalyst, *Angew. Chem. Int. Ed.*, 60, 5527-5535 (DOI: 10.1002/anie.202011063)
 16. Paszun D., Szychaj T. (1997), Chemical Recycling of Poly(ethylene terephthalate), *Ind. Eng. Chem. Res.*, 7, 1373-1383 (DOI: 10.1021/ie960563c)
 17. Ghosal K., Nayak C. (2022), Recent Advances in Chemical Recycling of Polyethylene Terephthalate Waste into Value added Products for Sustainable Coating Solutions—Hope vs. Hype, *Mat. Adv.*, 3, 1974-1992 (DOI: 10.1039/d1ma01112j)
 18. Karayannidis G. P., Chatziavgoustis A. P., Achilias D. S. (2002),

- Poly(ethylene terephthalate) Recycling and Recovery of Pure Terephthalic Acid by Alkaline Hydrolysis, *Adv. Polym.*, 21, 250-259 (DOI: 10.1002/adv.10029)
19. Cosimbescu L., Merkel D. R., Darsell J., Petrossian G. (2021), Simple But Tricky: Investigations of Terephthalic Acid Purity obtained from Mixed PET Waste, *Ind. Eng. Chem. Res.*, 60, 12792-12797 (DOI: 10.1021/acs.iecr.1c02604)
 20. Ügdüler S., van Geem K. M., Denolf R., Roosen M., Mys N., Ragaert K., De Meester S. (2020), Towards Closed-loop Recycling of Multilayer and Coloured PET Plastic Waste by Alkaline Hydrolysis, *Green Chem.*, 22, 5376-5394 (DOI: 10.1039/d0gc00894j)
 21. Barredo A., Asueta A., Amundarain I., Leivar J., Miguel-Fernandez R., Arnaiz S., Epelde E., Lopez-Fonseca R., Gutierrez-Ortiz J. I. (2023), Chemical Recycling of Monolayer PET Tray Waste by Alkaline Hydrolysis, *J. Environ. Chem. Eng.*, 11, 109823-109833 (DOI: 10.1016/j.jece.2023.109823)
 22. Zou Y. Q., von Wolff N., Anaby A., Xie Y., Milstein D. (2019), Ethylene glycol as an efficient and reversible liquid-organic hydrogen carrier, *Nat. Catal.*, 2, 415-422 (DOI: 10.1038/s41929-019-0265-z)
 23. Sundari R., Vaidya P. D. (2015), On the Efficacy of Ru/Al₂O₃ Catalyst for Steam Reforming of Ethylene Glycol, *Chem. Eng. Commun.*, 202, 1446-1454 (DOI: 10.1080/00986445.2014.934446)
 24. Kiadehi A. D., Taghizadeh M. (2018), Evaluation of a Micro-channel Reactor for Steam Reforming of Ethylene Glycol: A Comparative Study of Catalytic Activity of Pt or/and Ni Supported γ -Alumina Catalysts, *Int. J. Hydrog. Energy*, 43, 4826-4838 (DOI: 10.1016/j.ijhydene.2018.01.103)
 25. Mei D., Lebarbier Dagle V., Xing R., Albrecht K. O., Dagle R. A. (2016), Steam Reforming of Ethylene Glycol over MgAl₂O₄ Supported Rh, Ni, and Co Catalysts, *ACS Catal.*, 6, 315-325 (DOI: 10.1021/acscatal.5b01666)
 26. Jeon S., Park Y. M., Saravanan K., Han G. Y., Kim B. W., Lee J. B., Bae J. W. (2017), Aqueous Phase Reforming of Ethylene Glycol over Bimetallic Platinum-Cobalt on Ceria-Zirconia Mixed Oxide, *Int. J.*

- Hydrog. Energy, 42, 9892-9902 (DOI: 10.1016/j.ijhydene.2017.01.221)
27. Cesar D. V., Santori G. F., Pompeo F., Baldanza M. A., Henriques C. A., Lombardo E., Schmal M., Cornaglia L., Nichio N. N. (2016), Hydrogen Production from Ethylene Glycol Reforming Catalyzed by Ni and Ni–Pt Hydrotalcite-derived Catalysts, *Int. J. Hydrog. Energy*, 41, 22000-22008 (DOI: 10.1016/j.ijhydene.2016.07.168)
 28. Uekert T., Kuehnel M. F., Wakerley D. W., Reisner E. (2018), Plastic Waste as a Feedstock for Solar-driven H₂ Generation, *Energy Environ. Sci.*, 11, 2853-2857 (DOI: 10.1039/c8ee01408f)
 29. Gong X., Tong F., Ma F., Zhang Y., Zhou P., Wang Z., Liu Y., Wang P., Cheng H., Dai Y., Zheng Z., Huan B., (2022), Photoreforming of Plastic Waste poly(ethylene terephthalate) via in-situ derived CN-CNTs-NiMo hybrids, *Appl. Catal. B Environ.*, 307, 121143-121153 (DOI: 10.1016/j.apcatb.2022.121143)
 30. Behera S., Dinda S., Saha R., Mondal B. (2023), Quantitative Electrocatalytic Upcycling of Polyethylene Terephthalate Plastic and Its Oligomer with a Cobalt-Based One-Dimensional Coordination Polymer Having Open Metal Sites along with Coproduction of Hydrogen, *ACS Catal.*, 13, 469-474 (DOI: 10.1021/acscatal.2c05270)
 31. Su H., Hu Y., Feng H., Zhu L., Wang S. (2023), Efficient H₂ Production from PET Plastic Wastes over Mesoporous Carbon-Supported Ru-ZnO Catalysts in a Mild Pure-Water System, *ACS Sustain. Chem. Eng.*, 11, 578-586 (DOI: 10.1021/acssuschemeng.2c05062)
 32. Xiao B., Zheng M., Pang J., Jiang Y., Wang H., Sun R., Wang A., Wang X. (2015), Synthesis and Characterization of Poly(ethylene terephthalate) from Biomass-based Ethylene Glycol: Effects of Miscellaneous Diols, *Ind. Eng. Chem. Res.*, 54, 5862-5869 (DOI: 10.1021/acs.iecr.5b00487)
 33. Bang S. S., Johnston D. (1998), Environmental Effects of Sodium Acetate/Formate deicer, *Ice Shear, Contam. Toxicol.*, 35, 580-587 (DOI: 10.1007/s002449900419)
 34. Ghosh S., Makeev M. A., Qi Z., Wang H., Rajput N. N., Martha S. K., Pol V. G. (2020), Rapid Upcycling of Waste Polyethylene Terephthalate to Energy Storing Disodium Terephthalate Flowers with DFT

- Calculations, *ACS Sustain. Chem. Eng.*, 8, 6252-6262 (DOI: 10.1021/acssuschemeng.9b07684)
35. Lei K., Li F., Mu C., Wang J., Zhao Q. (2017), High K-Storage Performance Based on the Synergy of Dipotassium Terephthalate and Ether-based Electrolytes, *Energy Environ. Sci.*, 10, 552-557 (DOI: 10.1039/c6ee03185d)
36. Namioka T., Saito A., Inoue Y., Park Y., Min T. J., Roh S. A., Yoshikawa K. (2011), Hydrogen-rich Gas Production from Waste Plastics by Pyrolysis and Low-temperature Steam Reforming over a Ruthenium Catalyst, *Appl. Energy*, 88, 2019-2026 (DOI: 10.1016/j.apenergy.2010.12.053)
37. Jiang Y., Li X., Li C., Zhang L., Zhang S., Li B., Wang S. (2022), Pyrolysis of Typical Plastics and Coupled with Steam Reforming of Their Derived Volatiles for Simultaneous Production of Hydrogen-Rich Gases and Heavy Organics, *Renew. Energy*, 200, 476-491 (DOI: 10.1016/j.renene.2022.09.120)

Chapter 6

Summary and Future Scope

6.1. Summary of this thesis

In summary, during my thesis work, I aimed to design and develop ruthenium-based heterogeneous catalysts and explore them for catalytic selective hydrogen production from polyols i.e., ethylene glycol and glycerol, under milder reaction conditions in water. Different reaction parameters that influence the rate of hydrogen production and product selectivity of these reactions were studied in detail. Catalyst characterization has been performed extensively to know the structure-activity relationship and strong-metal support interaction. Controlled experiments and NMR studies were performed to gain insights into the catalytic pathway of the reactions.

In chapter 1, the current scenario of energy production, energy consumption globally, storage and production of hydrogen gas, and the development of heterogeneous catalysts for the production of hydrogen gas from polyols (ethylene glycol and glycerol) have been discussed.

In chapter 2, we synthesized a ruthenium nanoparticle catalyst using the aqueous phase chemical reduction method and characterized by various spectroscopic techniques such as P-XRD, FESEM, TEM, XPS and others. Furthermore, we explored ruthenium nanoparticle catalyst for the selective hydrogen production from glycerol in water at low temperatures in the presence of a base. Various reaction parameters, such as the effect of water concentration, base concentration, different types of bases and temperature effect, were employed to optimize the best reaction conditions where a high yield of hydrogen gas was achieved with complete conversion of glycerol. Experimental findings revealed that water and base played a crucial role in achieving a high yield of hydrogen gas (1.6 equiv. per mol of glycerol) and lactic acid (70%) with complete conversion of glycerol (>99%) at 110 °C. Controlled experiments were carried out to elucidate the reaction pathway of catalytic dehydrogenation of glycerol under optimized reaction conditions. Advantageously, our studied catalyst also exhibited high long-term stability

and generated ~ 2 L H₂/gRu/h from glycerol at 110 °C.

In chapter 3, we synthesized various supported ruthenium-based catalysts (Ru/La(OH)₃, Ru/Mg(OH)₂, Ru/ZnO, Ru/ZrO₂, Ru/TiO₂) via the wet-impregnation method followed by chemical reduction and developed an efficient catalytic system to produce H₂ gas and lactic acid (LA) from aqueous glycerol under mild reaction conditions (90-130 °C). Notably, a high yield of H₂ gas ($n(\text{H}_2)/n(\text{GLY})$ ratio of 1.4) and LA (86%) from glycerol was achieved over the Ru/La(OH)₃ catalyst. By tuning the reaction conditions like temperature, base, water concentration and choosing appropriate support materials, we substantially increased the production of both H₂ gas and LA. Various characterization techniques have been employed to understand the metal-support interaction between Ru metal and La(OH)₃ support. Several controlled experiments were carried out under optimized reaction conditions to validate the catalytic dehydrogenation pathway of glycerol, which corroborated well with experimental results. Notably, Ru/La(OH)₃ catalyst displayed remarkable performance in bulk-scale reactions with a 12 L H₂/gRu/h productivity at 130 °C. The studied Ru/La(OH)₃ based catalytic system provides new insights in exploring glycerol, ethylene glycol and other terminal diols as important substrates for selectively producing purified hydrogen gas under optimized reaction conditions.

In chapter 4, We synthesized a ruthenium catalyst by the aqueous phase chemical reduction method and characterized using P-XRD, TEM, XPS, and other techniques. We explored an efficient catalytic process to produce H₂ gas from ethylene glycol at 90-160 °C in water. We achieved a high yield of hydrogen gas (up to 3.0 $n(\text{H}_2)/n(\text{EG})$) and formic acid (85% yield) from ethylene glycol in aqueous alkaline medium at 110 °C, where the role of reaction temperature and base concentration was found to be critical in achieving a high yield of H₂ gas. The effect of base concentration and temperature greatly influenced the catalytic reaction, and it was observed that at low concentrations of base (2.1 equiv.) and high reaction temperature (160 °C), a high yield of H₂ gas and formic acid was achieved. Efforts are being made to investigate the reaction pathway during the dehydrogenation process by identifying intermediates and using them in controlled reactions under

optimized reaction conditions. Advantageously, the ruthenium catalyst exhibited appreciably high long-term stability over 70 h, generating ca. 290 L of H₂/g Ru with a yield of 1035 L of H₂/L of EG.

In chapter 5, we explored ruthenium catalyst and reported an integrated process of one-pot upcycling of PET-based plastic waste for selective hydrogen gas production in an alkaline aqueous condition at low temperatures (110-160 °C). The developed catalytic system performed equally well for hydrogen production from different colored PET-based plastic waste (transparent, green, brown, and mixed PET). Notably, purified and quantitative yield of terephthalic acid (5.2 mmol/gPET) was achieved for all the reactions. Experimental evidence suggests that during one-pot upcycling of PET-based plastics over ruthenium catalyst, initially, PET undergoes depolymerization to produce Na₂TPA and ethylene glycol in the presence of a base. Then ethylene glycol undergoes a dehydrogenation process to generate H₂ gas and formic acid. The developed catalytic system is applicable to gram-scale H₂ gas production from PET-based plastic waste with a high yield of H₂ gas (~38,000 mL H₂/gRu) without contamination of other gases (CO, CO₂ and CH₄), highlighting the potential application of the developed catalytic system.

In this thesis, attempts have been made to develop efficient catalytic systems to generate pure H₂ gas under milder reaction conditions so that pure H₂ gas can be directly utilized in fuel cell applications. However, during the recyclability experiments, we observed a significant challenge with the agglomeration of ruthenium nanoparticles which affected the long-term stability and activity of the catalyst. Addressing this issue is crucial for the advancement and practical application of these catalysts. The use of functionalized support materials can help in easy dispersion and anchoring of ruthenium nanoparticles over the supports or post-synthesis treatments such as annealing may help in addressing this issue. Additionally, it was interesting to observe that the properties of ruthenium nanoparticles can be finely tuned by using different types of support materials. Different supports with specific electronic interactions can influence the charge distribution around ruthenium nanoparticles, thereby impacting both the activity and selectivity of these catalysts. This ability to tune the properties of ruthenium nanoparticles through

support selection is a promising strategy for designing more efficient and selective catalysts for hydrogen production. In this thesis, we used the chemical reduction method to synthesize ruthenium nanoparticles. It is important to note that the method of synthesis significantly affects the properties of the ruthenium catalyst. Different synthesis techniques, such as microwave-assisted synthesis, thermal decomposition, and hydrothermal methods, can lead to variations in particle size, shape, and dispersion, which, in turn, can be used to tune the catalytic performance and stability of the nanoparticles.

6.2. Future scope

Hydrogen energy is widely recognized as a promising renewable energy alternative. Although it is naturally abundant, it doesn't exist in a free state and can be derived from sustainable sources such as biomass or water in the presence of a suitable catalyst. It serves as a clean energy carrier, generating only water as a byproduct when used in fuel cells. Most of the hydrogen is currently produced from the reforming of non-renewable resources (coal, petroleum, and natural gas). Reforming is an energy-intensive process which requires high temperatures (>250 °C), and the produced H_2 gas often has contamination of CO_2 and other gases (CO and alkanes). In this thesis, we explored the potential of Ru-based heterogeneous catalysts for hydrogen production from polyols such as ethylene glycol and glycerol extensively. However, there is significant scope for further improvement and exploration of Ru-based catalysts to advance the field of hydrogen production.

For the synthesis of ruthenium nanoparticles, various advanced synthesis techniques, such as microwave-assisted synthesis, electrochemical methods, and atomic layer deposition, could lead to better control over the size, shape, and distribution of ruthenium nanoparticles. Moreover, the use of various support materials to understand the metal-support interactions at a molecular level can help in designing more efficient catalytic systems. Detailed mechanistic investigations using in-situ spectroscopy and others can help in understanding the underlying pathways for hydrogen production. Addressing the long-term stability and reusability of Ru-based catalysts is essential for practical applications. Research should focus on developing methods to enhance the durability of the catalysts, such as by the incorporation of stabilizing agents and

evaluating their performance over extended periods and multiple reaction cycles. Alloying Ru nanoparticles with other non-noble metals can reduce the cost associated with monometallic ruthenium nanoparticles. Further, the potential of developed Ru-based catalytic systems can also be explored for selective H₂ gas production from other biomass-derived polyols such as xylitol (C-5), sorbitol (C-6) or glucose (C-6) at lower temperatures.

By addressing these research directions, we can advance the understanding and application of ruthenium-based catalysts, contributing to the development of efficient, sustainable, and economically viable hydrogen production technologies and other catalytic processes.

APPENDIX-I
(Rights and Permissions)

SPRINGER NATURE LICENSE
TERMS AND CONDITIONS

Nov 19, 2023

This Agreement between IIT Indore -- Ankit Kumar ("You") and Springer Nature ("Springer Nature") consists of your license details and the terms and conditions provided by Springer Nature and Copyright Clearance Center.

License Number	5672430374539
License date	Nov 19, 2023
Licensed Content Publisher	Springer Nature
Licensed Content Publication	Nature
Licensed Content Title	Hydrogen from catalytic reforming of biomass-derived hydrocarbons in liquid water
Licensed Content Author	R. D. Cortright et al
Licensed Content Date	Aug 29, 2002
Type of Use	Thesis/Dissertation
Requestor type	academic/university or research institute
Format	print
Portion	figures/tables/illustrations
Number of figures/tables/illustrations	1
Would you like a high resolution image with your order?	no
Will you be translating?	no
Circulation/distribution	1 - 29
Author of this Springer Nature content	no
Title of new work	Development Of ruthenium based heterogeneous catalyst for hydrogen production from polyols
Institution name	Indian Institute of Technology Indore
Expected presentation date	Mar 2024
Portions	figure 1
Requestor Location	IIT Indore IIT Indore

ELSEVIER LICENSE
TERMS AND CONDITIONS

Nov 19, 2023

This Agreement between IIT Indore -- Ankit Kumar ("You") and Elsevier ("Elsevier") consists of your license details and the terms and conditions provided by Elsevier and Copyright Clearance Center.

License Number	5672430009147
License date	Nov 19, 2023
Licensed Content Publisher	Elsevier
Licensed Content Publication	Applied Catalysis B: Environmental
Licensed Content Title	Remarkable activity and stability of Ni catalyst supported on CeO ₂ -Al ₂ O ₃ via CeAlO ₃ perovskite towards glycerol steam reforming for hydrogen production
Licensed Content Author	Krongthong Kamonsuangkasem, Supaporn Therdthianwong, Apichai Therdthianwong, Nirawat Thammajak
Licensed Content Date	Dec 5, 2017
Licensed Content Volume	218
Licensed Content Issue	n/a
Licensed Content Pages	14
Start Page	650
End Page	663
Type of Use	reuse in a thesis/dissertation
Portion	figures/tables/illustrations
Number of figures/tables/illustrations	1
Format	print
Are you the author of this Elsevier article?	No
Will you be translating?	No
Title of new work	Development Of ruthenium based heterogeneous catalyst for hydrogen production from polyols
Institution name	Indian Institute of Technology Indore

Expected presentation date	Mar 2024
Portions	scheme 1
Requestor Location	IIT Indore IIT Indore
	Indore, 453552 India Attn: IIT Indore
Publisher Tax ID	GB 494 6272 12
Total	0.00 USD

JOHN WILEY AND SONS LICENSE
TERMS AND CONDITIONS

Nov 17, 2023

This Agreement between IIT Indore -- Ankit Kumar ("You") and John Wiley and Sons ("John Wiley and Sons") consists of your license details and the terms and conditions provided by John Wiley and Sons and Copyright Clearance Center.

License Number	5671331334907
License date	Nov 17, 2023
Licensed Content Publisher	John Wiley and Sons
Licensed Content Publication	ChemCatChem
Licensed Content Title	Selective Hydrogen Production from Glycerol over Ruthenium Catalyst
Licensed Content Author	Sanjay Kumar Singh, Bhanu Priya, Mahendra Kumar Awasthi, et al
Licensed Content Date	Mar 10, 2022
Licensed Content Volume	14
Licensed Content Issue	10
Licensed Content Pages	9
Type of use	Dissertation/Thesis
Requestor type	Author of this Wiley article
Format	Print and electronic
Portion	Full article
Will you be translating?	No
Title of new work	Development Of ruthenium based heterogeneous catalyst for hydrogen production from polyols
Institution name	Indian Institute of Technology Indore
Expected presentation date	Mar 2024

Requestor Location	IIT Indore IIT Indore Indore, 453552 India Attn: IIT Indore
Publisher Tax ID	EU826007151
Total	0.00 USD



Ruthenium-Catalyzed Transformation of Ethylene Glycol for Selective Hydrogen Gas Production in Water

Author: Ankit Kumar, Bhanu Priya, Sanjay Kumar Singh

Publication: ACS Sustainable Chemistry & Engineering

Publisher: American Chemical Society

Date: Mar 1, 2023

Copyright © 2023, American Chemical Society

PERMISSION/LICENSE IS GRANTED FOR YOUR ORDER AT NO CHARGE

This type of permission/license, instead of the standard Terms and Conditions, is sent to you because no fee is being charged for your order. Please note the following:

- Permission is granted for your request in both print and electronic formats, and translations.
- If figures and/or tables were requested, they may be adapted or used in part.
- Please print this page for your records and send a copy of it to your publisher/graduate school.
- Appropriate credit for the requested material should be given as follows: "Reprinted (adapted) with permission from {COMPLETE REFERENCE CITATION}. Copyright {YEAR} American Chemical Society." Insert appropriate information in place of the capitalized words.
- One-time permission is granted only for the use specified in your RightsLink request. No additional uses are granted (such as derivative works or other editions). For any uses, please submit a new request.

If credit is given to another source for the material you requested from RightsLink, permission must be obtained from that source.

[BACK](#)

[CLOSE WINDOW](#)

JOHN WILEY AND SONS LICENSE
TERMS AND CONDITIONS

Nov 17, 2023

This Agreement between IIT Indore -- Ankit Kumar ("You") and John Wiley and Sons ("John Wiley and Sons") consists of your license details and the terms and conditions provided by John Wiley and Sons and Copyright Clearance Center.

License Number	5671331171239
License date	Nov 17, 2023
Licensed Content Publisher	John Wiley and Sons
Licensed Content Publication	ChemCatChem
Licensed Content Title	One-pot Upcycling of Waste Plastics for Selective Hydrogen Production at Low-Temperature
Licensed Content Author	Ankit Kumar, Sanjay K. Singh, Tushar A. Kharde, et al
Licensed Content Date	Jul 17, 2023
Licensed Content Volume	15
Licensed Content Issue	18
Licensed Content Pages	10
Type of use	Dissertation/Thesis
Requestor type	Author of this Wiley article
Format	Print and electronic
Portion	Full article
Will you be translating?	No
Title of new work	Development Of ruthenium based heterogeneous catalyst for hydrogen production from polyols
Institution name	Indian Institute of Technology Indore
Expected presentation date	Mar 2024
Requestor Location	IIT Indore IIT Indore Indore, 453552 India Attn: IIT Indore

Publisher Tax ID	EU826007151
Total	0.00 USD

